Reconstruction of tectonically induced vertical motions and paleo-ecological evolution of the Island of Rhodes during the Plio-Pleistocene

Dissertation

with the aim of achieving a doctoral degree

at the Faculty of Mathematics, Informatics and Natural Sciences

Department of Earth Sciences

at Universität Hamburg

submitted by

Daniela Eichner

from Mönchengladbach

Hamburg, 2024

Department of Earth Science

Date of Oral Defense:	19.09.2024
Reviewers:	Dr. Yvonne Milker
	Prof. Dr. Gerhard Schmiedl
Members of examination commission:	Dr. habil. Yvonne Milker (chair)
	Prof. Dr. Gerhard Schmiedl
	Prof. Dr. Kai Jensen
	Prof. Dr. Ulrich Riller
	Prof. Dr. Jürgen Böhner

Chair of the Subject Doctoral Committee

Earth System Science:	Prof. Dr. Hermann Held
Dean of Faculty MIN:	Prof. Dr.-Ing. Norbert Ritter

Dedicated to my parents, Klasina and Frank

Cibicidoides pseudoungerianus painted by my grandmother.

Abstract

The Island of Rhodes, located in the Eastern Mediterranean Sea and at the eastern end of the Hellenic forearc, has been a vulnerable area for tectonic and climatic processes in the past. Due to its position at the subduction zone of the African and Eurasian plate, the island experienced intense tectonic motions, including several cycles of subsidence and uplift. Marine and fossil-rich sediments of Plio- to Pleistocene age, of the so-called Lindos Bay Formation, have been uplifted and are outcropping in graben structures along the eastern coast of the island. Despite some studies on the tectonic evolution of the island, it has not been investigated whether the individual depocenters underwent similar or different vertical motions and the quantification of long- and short-term vertical motions have not yet been studied. Besides the tectonic influence, the Mediterranean Sea is sensitive to climate variability, and the sedimentary archive records orbital-driven climate changes, for example as organic-rich layers, called sapropels. An enhanced rainfall in phase with the African monsoon and Mediterranean sapropel formation has also been reported for the northern borderlands of the Eastern Mediterranean Sea. However, until now evidence for orbital-induced climate changes that affected the Island of Rhodes during the Plio-Pleistocene are missing and information on local and regional responses to global forcing as well as the effects on the near-shore environments are still limited.

The doctoral thesis follows the approach to reconstruct the tectonically induced vertical motions on the eastern coast of the Island of Rhodes, to quantify the large- and small-scale cycles of subsidence and uplift and to unravel the hydrological and climatic impact on the benthic foraminiferal assemblage during the Plio-Pleistocene. This was achieved through a detailed study of four sedimentary deposits of the Lindos Bay Formation, distributed from the northern (Cape Vagia), over the middle eastern (Agathi Beach and Lardos), and towards the southern (Plimiri) coast. The investigation of benthic foraminiferal assemblages and the analysis of stable oxygen and carbon isotopes revealed that the individual depocenters reflect orbital-driven climate changes differently. Periodic, precession-driven changes can primarily be seen in the increase of eutrophic indicator species and in the decrease of $\delta^{13}C$ values in Agathi Beach and Plimiri. Lardos and Cape Vagia on the other hand revealed long-lasting, most-likely not precession-driven, eutrophication in the Middle and Early Pleistocene, respectively. Especially the Pliocene Plimiri section suggest a strong periodicity in the assemblage composition and diversity, with thick intervals mainly dominated by eutrophic indicator species, which has been attributed to an increased primary production of the near-coastal environments. This is suggested to be triggered by enhanced

precipitation and higher river-run off. These phases are interpreted as near-coastal equivalents of deep sea sapropels of the Eastern Mediterranean Sea.

The use of a benthic foraminiferal-based transfer function, and its correction for glacio-eustatic seal level and precession-driven changes, proved to be a useful tool to quantify and better understand tectonically induced vertical motions in the Pleistocene on a much smaller scale than previously done. Apart from the long-term trend of subsidence (Agathi Beach and older part of Cape Vagia) and uplift (younger part of Cape Vagia and Lardos), each depocenter also reflects small-scale motions with rates up to 10.4 mm a^{-1}. The integration of the new data sets with previous studies, allowed to reconstruct the full cycle of subsidence (transgression) and uplift (regression) on the Island of Rhodes during the Pleistocene, lasting from 1.97 Ma to 0.47 Ma, with a maximum uplift of about 700 m in the last 1.40 Myrs. Differences in the rates of vertical motions and amplitudes are observed between individual depocenters. When comparing sedimentary sections deposited at the same time, higher rates are observed in the northern part of the island compared to the middle part. The vertical motions and differences between the individual depocenters are explained by a combination of large-scale subsidence and uplift processes and locally induced and site-specific processes on the island and in the graben structures.

Kurzfassung

Rhodos ist eine griechische Insel im östlichen Mittelmeer und liegt am östlichen Ende des Hellenischen Inselbogens, der durch die Subduktion der Afrikanischen unter der Eurasischen Platte entstanden ist. Aufgrund ihrer Lage an der Subduktionszone war die Insel intensiven tektonischen Bewegungen ausgesetzt, die mehrere Zyklen von Absenkungen und Hebungen umfassen. Dabei wurden marine und fossilreiche Sedimente der Lindos Bay Formation aus dem Plio-Pleistozän angehoben und sind heutzutage in Grabenstrukturen entlang der Ostküste der Insel aufgeschlossen. Trotz einiger Studien zur tektonischen Entwicklung der Insel wurde bisher nicht untersucht, ob die einzelnen Sedimentablagerungen in den Grabenstrukturen ähnlichen oder unterschiedlichen tektonisch bedingten Vertikalbewegungen unterworfen waren. Des Weiteren wurde noch keine Quantifizierung der lang- und kurzfristigen Vertikalbewegungen durchgeführt. Neben den tektonischen Einflüssen ist das Mittelmeer empfindlich gegenüber Klimaschwankungen, so dass sich in den Sedimentarchiven auch orbital bedingte Klimaänderungen, wie zum Beispiel Sapropele, nachweisen lassen. Eine Zunahme der Niederschläge in der nordöstlichen Randzone des östlichen Mittelmeers, die mit dem afrikanischen Monsun und der Bildung von Sapropelen in der Tiefsee im Zusammenhang stehen, wurde bereits festgestellt. Bisher fehlen jedoch Belege für den Einfluss orbitaler Klimaveränderungen auf die Insel während des Plio-Pleistozäns. Die Auswirkungen auf die küstennahe Umwelt, sowie Informationen über lokale und regionale Anpassungen des benthischen Lebens an die großräumigen Veränderungen vor Rhodos sind noch limitiert.

Die Dissertation verfolgt den Ansatz, die tektonisch induzierten Vertikalbewegungen an der Ostküste von Rhodos zu rekonstruieren, die groß- und kleinskaligen Zyklen von Absenkung und Hebung zu quantifizieren und die hydrologischen und klimatischen Auswirkungen auf die benthische Foraminiferen Vergesellschaftung während des Plio-Pleistozäns zu untersuchen. Dies wurde durch die detaillierte Untersuchung von vier Sedimentablagerungen der Lindos Bay Formation erreicht, die von der nördlichen (Cape Vagia) über die mittelöstliche (Agathi Beach, Lardos) bis hin zur südlichen Küste (Plimiri) verteilt sind. Die Untersuchung der benthischen Foraminiferen Vergesellschaftung und die Analyse der stabilen Sauerstoff- und Kohlenstoffisotope zeigten, dass die einzelnen Sedimentablagerungen der Lindos Bay Formation orbitale Klimaänderungen unterschiedlich widerspiegeln. Periodische und präzessionsbedingte Veränderungen spiegelten sich vor allem in der Zunahme eutropher Indikatorarten und in der Abnahme der $\delta^{13}C$-Werte in Agahti Beach und Plimiri wider. In Lardos und Cape Vagia hingegen deutet sich eine anhaltende Eutrophierung an, die wahrscheinlich nicht mit dem Minimum der Präzession im mittleren bis frühen Pleistozän zusammenhängt. Insbesondere die pliozänen

Sedimente des Plimiri Aufschlusses weisen eine starke Periodizität in der Zusammensetzung und Diversität der benthischen Foraminiferen Vergesellschaftung auf, mit mächtigen Intervallen, in denen hauptsächlich eutrophe Indikatorarten dominieren. Dies deutet auf eine erhöhte Primärproduktion im küstennahen Bereich vor Rhodos hin. Es wird angenommen, dass dies auf erhöhte Niederschlagsmengen und auf die damit verbundene Erhöhung der Flusseinträge zurückzuführen ist. Diese Phasen werden als küstennahe Äquivalente der Tiefsee-Sapropele im östlichen Mittelmeer interpretiert.

Die Verwendung einer auf benthischen Foraminiferen basierenden Transferfunktion, korrigiert um den Einfluss von glazialen Meeresspiegelschwankungen und Präzession, erwies sich als nützliche Methode, um tektonisch bedingte Vertikalbewegungen im Plio-Pleistozän in einer wesentlich höheren Auflösung als bisher zu quantifizieren und besser zu verstehen. Neben dem langfristigen Trend von Absenkung (Agathi Beach und älterer Abschnitt von Cape Vagia) und Hebung (jüngerer Abschnitt von Cape Vagia und Lardos) spiegeln die einzelnen Sedimentablagerungen auch kleinräumige und kurzfristige Bewegungen mit Raten von bis zu 10 mm a^{-1} wider. Durch die Integration der neuen Datensätze mit früheren Studien konnte der gesamte Zyklus von Absenkung (Transgression) und Hebung (Regression) auf der Insel Rhodos währen des Pleistozäns rekonstruiert werden, der von ca. 1.97 Ma bis 0. 47 Ma andauerte und eine maximale Hebung der Ostküste um 700 m während der letzten 1.40 Ma ergab. Die Raten und Amplituden unterscheiden sich zwischen den einzelnen Ablagerungsorten. Vergleicht man Sedimentabschnitte, die zur gleichen Zeit abgelagert wurden, so sind die Raten im nördlichen Teil der Insel höher als im südlichen Teil. Die Vertikalbewegungen und die Unterschiede zwischen den einzelnen Ablagerungen können auf eine Kombination von großräumigen Senkungs- und Hebungsprozessen und lokal induzierte und standortspezifische Prozesse auf der Insel und in den Grabenstrukturen zurückgeführt werden.

Acknowledgement

First and foremost, I would like to thank my supervisors, Dr. Yvonne Milker and Prof. Dr. Gerhard Schmiedl, for assigning me the topic of my dissertation, and especially Yvonne for coming up with the topic and the funding acquisition. I appreciate the endless support and scientific discussions during the past three years and the many opportunities for me to develop my skills in the attendance of conferences and workshops. Your guidance, encouragement and patience have been crucial to the success of this work. Thank you! I am very proud to be the first to call Yvonne my "Doktormutti"!

This doctoral thesis was improved by collaborative sampling and analysis but also by critical comments and scientific discussion by some key people:

Dr. Jürgen Titschack is thanked for providing samples, his help during the field campaign on Rhodes and for sharing his knowledge of the island. I appreciated the numerous calls and the wide-ranging discussions on results and interpretations over the years.

My fellow PhD student of the project, Malu Ferreira, is thanked for being my personal structural geologist, for always taking the time to explain and discuss and for the great company during our joint field work. Prof. Dr. Ulrich Riller is thanked for his expertise and scientific discussions during our meetings and field work, and for being part of my examination commission.

Thanks are given to Prof. Dr. Maria Triantaphyllou for the analysis of the nannofossil samples and her support and input during the publication process. Prof. Dr. Nils Andersen is thanked for the reliable and quick measurements of the stable isotope samples and scientific input to the interpretation of the results.

I would also like to thank the entire working group of micropaleontology, Nicolaas Glock, Sha Ni, Ulrich Kotthoff and my fellow PhDs Anjaly Menon and Raphaël Hubert-Huard, for creating a supportive and friendly working environment, great scientific discussions and fun times and emotional support during conferences.

For support during laboratory work, Jutta Richarz, Louisa Kanzler and Tobias Winkler are thanked.

I would like to thank the School of Integrated Climate System Science (SICSS), for the opportunity to take part in valuable lectures, workshops, and retreats. My panel chair Prof. Dr. Kai Jensen is thanked for productive meetings, critical questions, motivating words and for taking the time to be part of my examination commission.

For language editing purpose and for rephrasing single sentences of this thesis, the application DeepL Translate (www.deepl.com/translator) and DeepL Write (www.deepl.com/write) were used. No scientific content, interpretation or data was generated or edited by these tools.

This work was funded by the Deutsche Forschungsgemeinschaft (DFG).

Finally, I would like to thank my family and friends.

I owe my deepest gratitude to my parents, Klasina and Frank Eichner, who have always supported and assisted me unconditionally. Thank you for your endless understanding, kindness, and encouragement throughout my life. I could not have taken this journey without you. Thank you!

My sisters, Sarah and Isabel, are thanked for their endless support in any situation in life and for the many hours of laughter. Still so little but with such a significant impact, I would like to thank my nephew (Lenn) and niece (Lou) for bringing so much joy in my life. I am very grateful to my grandparents, Brigitte and Heinz, for life-long and unconditional support in any situation.

A special thanks also goes to Chrissi, Anne and Sabine for always motivating me to push a little further and for giving my brain a little rest in enjoyable quality time.

Last but not least, I would like to thank my partner Mike Frenken for his endless support and patients, the many hours of listening to my exciting talks on forams and for sacrificing his holiday to dig in the mud with us. Thank you calming me down, cheering me up and motivating me to reach further.

Table of Content

List of Figures

List of Tables

List of Abbreviations

a	annum (year)
B.P.	Before Present (i.e., before 1950)
BFN	Benthic Foraminiferal Number
CDW	Crete Deep Water
CNPL	Calcareous Nannofossil Zone
DEM	Digital Elevation Model
DIC	Dissolved Inorganic Carbon
EMDW	Eastern Mediterranean Deep Waters
E	East
F(C)O	First (Common) Occurrence
FBFZ	Fethiye-Burdur Fault Zone.
H_2O_2	Hydrogen Peroxide
ka	klio annum (one-thousand years)
kyr(s)	thousand year(s)
LBC	Lindos Bay Clay
LBF	Lindos Bay Formation
LCO	Lowest Common Occurrence
LDW	Levantine Deep Water
LIW	Levantine Intermediate Water
Ma	Mega annum (one-million years ago)
MAW	Modified Atlantic Water
MIS	Marine Isotope Stage
MIW	Mediterranean Intermediate Waters
Myr(s)	million year(s)
MNN	Mediterranean Neogene Nannoplankton
N	North
NN	Neogene Nannoplankton
ODP	Ocean Drilling Program
P/B	Planktic/Benthic
PLS	Partial Least Squares
PT	Pliny Trench
RMSEP	Root Mean Squared Error of Prediction
RTF	Rhodes Transform Fault
S	South
SEM	Scanning Electron Microscope
SPB	Saint Paul's Bay
TF	Transfer Function
TOC	Total organic carbon
TROX	Trophic Oxygen
VPDB	Vienna PeeDee Belemnite
W	West
WA	Weighted Averaging
WA-PLS	Weighted Averaging-Partial Least Squares
WB	Windmill Bay
WMDW	Western Mediterranean Deep Waters

I Thesis Outline and Publications

Pre-chapter II – Aims of the doctoral thesis.

In this pre-chapter an overview of the motivation and aims of the study are introduced and the main hypotheses and associated research questions are presented.

Chapter 1 – Introduction

The first chapter provides a brief introduction to the benthic foraminifera as environmental indicators, their use in the quantification of paleo-water depths and the progress that research has made over the years.

Chapter 2 – Study area

Chapter two deals with the study area of the thesis – the Mediterranean Sea. The modern climate and current oceanographic system of the Mediterranean are briefly introduced and the orbital-driven climate changes in the Mediterranean since the Neogene will be presented. The chapter will close with an introduction to the geological setting of the Eastern Mediterranean Sea and a description of the lithostratigraphy of the Island of Rhodes.

Chapter 3-5 - Publications

The cumulative doctoral thesis is compiled of three individual research articles, that have either already been published as peer-reviewed publications in different international journals or are available in manuscript form. Minor changes have been made to the articles to ensure a better overall consistency of the thesis. The numbering of chapters, sections, figures and tables, as well as the reference to the supplementary material have been adapted in accordance with the thesis structure. None of the changes affect the scientific content, interpretation, or data of the publications.

Chapter 3

Based on: **Eichner D.**, Schmiedl G., Titschack J., Triantaphyllou M., Andersen N., Forster N., Milker Y., 2024. Impact of hydrological changes and vertical motions on Pleistocene marine environments of the eastern coast of the Island

of Rhodes (Greece). Palaeogeography, Palaeoclimatology, Palaeoecology 636, 111980. doi: 10.1016/j.palaeo.2023.111980.

In this chapter the hydrological and neotectonic evolution of the middle eastern coast of the Island of Rhodes during the Pleistocene is investigated. This chapter contributes to the understanding of the long-term uplift and subsidence history of the island and shows the individual evolution with several small-scaled uplift and subsidence cycles.

Chapter 4

Based on: **Eichner D.**, Schmiedl G., Titschack J., Ferreira, M., Triantaphyllou M., Andersen N., Milker Y., 2024. Humid climate phases on the Island of Rhodes (Greece) during the Late Pliocene at times of sapropel formation. Marine Micropaleontology 187, 102341. doi: 10.1016/j.marmicro.2024.102341.

A faunal analysis of a marine Pliocene deposit of the southeastern coast of Rhodes provides evidence to a more humid climate during Northern Hemisphere summer insolation maxima by the recurrent dominance of eutrophic indicator species.

Chapter 5

Based on: **Eichner D.**, Schmiedl G., Ferreira, M., Titschack J., Andersen, N., Milker Y., in prep. Tectonically induced vertical motions on the Island of Rhodes (Greece) during the Plio-Pleistocene.

New data on the paleo-water depth evolution from a sediment section on the northeastern coast of the Island of Rhodes is combined with existing data to recognize a temporal trend in the subsidence and uplift history of the island and proposes the individual depocenters to be influenced by large-scale and locally induced and site-specific processes in order to explain different rates of short-term vertical motions.

Chapter 6- Conclusion

In chapter 6, the main findings of chapters 3-5 are summarized and discussed with regard to the hypotheses and research questions raised in the introduction.

Chapter 7- Outlook

Chapter 7 provides potential ideas for future research questions to further develop the research of this thesis.

II Aims of the doctoral thesis

The aim of the doctoral thesis is to unravel the complex hydrological and neotectonic history of the Island of Rhodes during the Plio-Pleistocene. The island is located at the collision zone between the African and Eurasian plate and is consequently influenced by tectonically induced vertical motions. Additionally, it is situated in the Eastern Mediterranean Sea, which is known to record drastic orbital-driven climate changes in the past. Marine sedimentary sequences with well-preserved and diverse microfossil assemblages' outcrop along the eastern coast of Rhodes. This makes the island an ideal model system for a better understanding of long-term and short-term tectonic events at an active convergence plate boundary and the influence of orbital-driven climate changes on the benthic ecosystem.

The doctoral thesis is therefore aiming to confirm the following two main hypotheses:

1) *Different sedimentary depocenters along the eastern coast of the Island of Rhodes underwent different tectonically induced vertical motions.*
2) *Uplift and subsidence rates of the sedimentary deposits are significantly higher than those proposed in previous publications.*

The main hypotheses should be supported and validated by the following research questions:

a) *Do the foraminiferal assemblages reflect orbital-driven cyclic changes and glacio-eustatic sea level changes that influence the accuracy of paleo-water depth reconstructions?*
b) *To what extend are the climate-corrected paleo-water depth changes related to the tectonically induced vertical motions?*
c) *Are the reconstructed rates of uplift and subsidence similar in each of the sedimentary depocenters or do they differ significantly?*

1 Introduction

1.1 Benthic foraminifera as environmental indicators

Foraminifera are single-celled eukaryotic organisms (protists) that inhabit a wide range of marine environments, from the transitional zone to the deep sea (e.g., Alve, 1999; van der Zwaan et al., 1999; Murray, 2001; Gooday, 2003; Jorissen et al., 2007), but might also be found in freshwater (Holzmann and Pawlowski, 2002) and terrestrial (e.g., Lejzerowicz et al., 2010) environments. The marine foraminifera can be divided into two groups: species living within the water column (planktic foraminifera) and species living on or in the seafloor (benthic foraminifera). The latter make up the majority with estimates of extant species that range from approximately 4,100 (Murray, 2007) to 12,000 (Boltovskoy and Wright, 1976). Although the group of foraminifera often occurs in high numbers and constitute well-diversified assemblages, individual taxa can be extremely sensitive to specific environments (Gooday, 2003; Murray, 2006). In shelf environments, for example, the benthic foraminiferal number and diversity is high, while in Oxygen Minimum Zones only specific taxa are adapted to those extreme environments, resulting in low numbers and diversity (e.g., Sen Gupta and Machain-Castillo, 1993; Den Dulk et al., 2000; Milker et al., 2009).

In deep-sea environments the most important controls on the benthic foraminiferal distribution comprise the dissolved oxygen concentration and the food availability at the seafloor (e.g. Jorissen et al., 1995; de Rijk et al., 2000; Murray, 2001). Benthic foraminifera inhabit a range of different stratified microhabitats at and below the sediment surface and are known to be able to change their microhabitat in response to the food availability and dissolved oxygen concentrations in the bottom and pore waters (e.g., Corliss, 1985; Mackensen and Douglas, 1989; Jorissen et al., 1995). The so-called TR(Trophic)OX(oxygen)-model explains the relationship of the benthic foraminiferal microhabitats and the interplay between oxygen and food supply

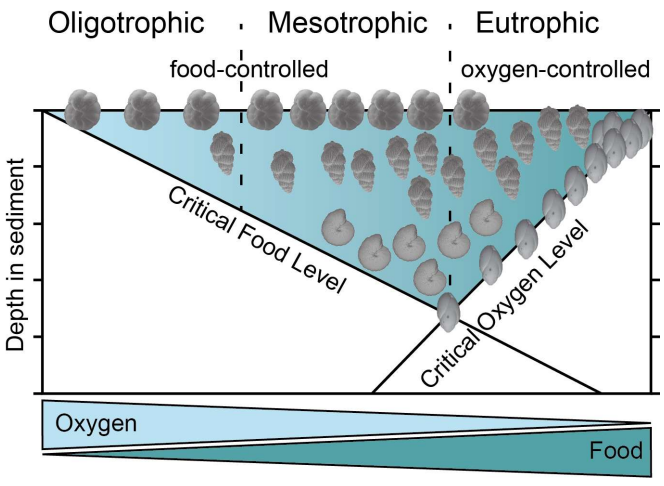

Figure 1.1. TROX-model of Jorissen et al. (1995) describing the relationship of the benthic foraminiferal microhabitat structure with food supply and oxygen content (figure modified after Jorissen et al. (2007) and Schmiedl et al. (2019)).

(Fig. 1.1; Jorissen et al., 1995). Thereafter, a foraminiferal fauna consisting of epifaunal species, low benthic foraminiferal number (BFN) and diversity, is commonly found in food-limited but well-oxygenated environments (oligotrophic conditions). Food-rich, oxygen-limited environments (eutrophic conditions) are characterized by a low-diversity fauna, consisting mainly of deep-infaunal species that are well adapted to dysoxic conditions (Fig. 1.1). Finally, the benthic foraminiferal assemblage with the highest diversity is found under mesotrophic conditions, with moderate food supply and oxygen concentration. The fauna consists of a variety of epifaunal, shallow and deep infaunal species (Fig. 1.1; Jorissen et al., 1995). In shallow marine and coastal environments, however, the benthic foraminiferal assemblage is much more variable than in the deep sea and their distribution is additionally influenced by other environmental parameters, such as temperature, light, salinity, substrate type, velocity, turbulence of surface waters and vegetation (e.g., Sen Gupta, 1999; Schönfeld, 2002; Gooday, 2003; Murray, 2006), which are in turn correlated to water depth (e.g., Horton et al., 2007; Milker et al., 2009; Rossi and Horton, 2009).

The high abundance and distribution, as well as the great preservation potential, make fossil benthic foraminifera a suitable proxy for a quantitative reconstruction of a wide range of past environmental conditions, such as relative sea level, temperature, salinity, oxygen content, current velocities and organic matter fluxes (e.g., de Vernal et al., 2006; Rohling et al., 2014; Kemp et al., 2015; Theodor et al., 2016a; García-Gallardo et al., 2017; Kranner et al., 2022).

1.1.2 Quantitative paleo-water depth reconstruction

Benthic foraminifera have been shown to be suitable relative sea level indicators, particularly in intertidal environments (Horton et al., 1999; Gehrels, 2000; Gehrels et al., 2006; Kemp et al., 2009, 2015; Leorri et al., 2010) because of their strong vertical zonation with respect to the tidal frame. They have also proven to be suitable sea level indicators in shallow marine environments (Hawkes et al., 2010; Milker et al., 2015a,b). In the latter case, however, the distribution of benthic foraminifera is not directly dependent on water depth but rather on biotic and abiotic factors that change with water depth, such as availability and quality of food, temperature, and salinity (Jorissen, 1987; de Stigter et al., 1998; de Rijk et al., 1999, 2000; Avnaim-Katav et al., 2015). First data on the bathymetric zonation of shallow water to deep-sea benthic foraminifera was provided by Bandy and Chierici (1966) and Cita and Zocchi (1978). In the Adriatic Sea and the Western Mediterranean Sea, for example, the bathymetric zonation of benthic foraminifera can be related to environmental parameters, such as substrate, water turbulence and organic matter content (Jorissen, 1987; de Stigter et al., 1998; Milker et al., 2009). De Rijk et al. (1999; 2000) postulated that the west to east shift in the zonation of shallow water to deep-sea benthic foraminifera in the Mediterranean Sea is

mainly driven by food availability. Paleo-bathymetric information is provided by both, the benthic and planktic foraminiferal assemblage.

Quantitative estimates of the paleo-water depth can be made by using a simple method: the ratio of planktic and benthic foraminifera (P/B ratio; van der Zwaan et al., 1990). Coastal and turbidity conditions are generally avoided by planktic foraminifera because they are confined to narrow salinity ranges (Schiebel and Hemleben, 2017). Therefore, the number of planktic foraminifera increases with water depth or distance from the coast. Simplified, one can say that the proportion of planktic foraminifera at the shelf break make up 50%, and decrease above and increase below (Gibson, 1989; van der Zwaan et al., 1990). Nevertheless, changes in productivity, oxygen content or shelf and slope geometry may affect the relationship (van Hinsbergen et al., 2005b). Because the infaunal benthic fauna rather relays on the oxygen content and organic matter fluxes than on water depth changes, the method has been modified by removing those species from the data set (van der Zwaan et al., 1990; van Hinsbergen et al., 2005b). Even after this modification, uncertainties remain relatively high. Apart from the environmental parameter influencing the benthic foraminifera, some planktic foraminifera are partially or fully absent in coastal and marginal seas because of the influence of brackish surface water, e.g., near river outflows (e.g., Rutherford et al., 1999; Frontalini et al., 2018). A major problem also occurs because of the preferential dissolution of the more delicate planktic foraminifera compared to the benthic foraminiferal test (Kucera, 2007; Nguyen et al., 2009; Kawahata et al., 2019), which consequently reduces the P/B ratio.

Progress has been made in quantitative past sea level reconstructions using foraminiferal-based transfer functions (TFs) (e.g., Rossi and Horton, 2009; Milker et al., 2011, 2017; Avnaim-Katav et al., 2016). Pioneering work was done by Imbrie and Kipp (1971), who used microfossil-based TFs to reconstruct past sea surface temperatures and salinities from the Late Pleistocene for the first time. Since then, marine studies applying microfossil-based TFs (e.g., by using benthic and planktic foraminifera, diatoms, or pollen) for the reconstruction of past environmental conditions, such as paleo-sea surface temperatures, paleo-salinity, paleo-productivity and paleo-sea levels, have increased. One requirement for using TFs to reconstruct the environmental conditions, is the close relationship of the modern assemblage to the variable of interest. The TF-models relate the distribution pattern of different taxa to the environmental parameter of interest. For a quantitative reconstruction the development of a modern training data set is needed, where the observed relationship between species assemblages and environmental variable are obtained (Fig. 1.2a, Juggins and Birks, 2012; Kemp and Telford, 2015). The development of a TF that generates an ecological response function using the modern data set is followed (Fig. 1.2b). This is done by

using different methods, such as Weighted Averaging (WA; Ter Braak, 1986), Partial Least Squares (PLS; Wold et al., 1984) or by using a combination of both methods (WA-PLS; Ter Braak and Juggins, 1993). Finally, the paleo-environment is reconstructed by using the TF and the fossil micropaleontological assemblage as an input (Fig. 1.2c; Kemp and Telford, 2015). Detailed reviews on the development and usage of transfer functions, the available methods and their advantages and disadvantages are provided by Juggins and Birks (2012) and Kemp and Telford (2015).

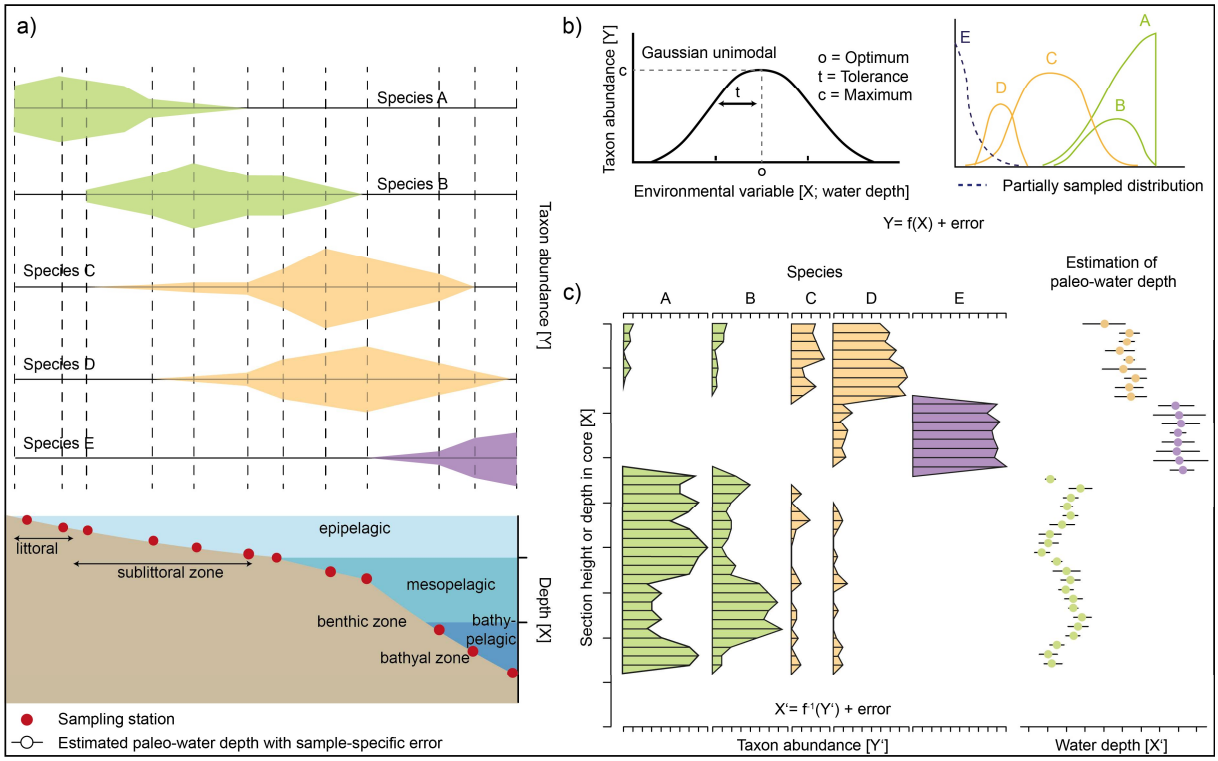

Figure 1.2. The use of transfer functions for relative sea level reconstruction by using marine microfossils. a) Development of a modern training data set, comprising modern species abundance [Y] and water depth [X] the samples were collected in. Samples are collected across the environmental gradient of interest. b) Development of a transfer function that relates Y and X by using an appropriated numerical technique. c) Application of the transfer function to the microfossil assemblages [Y'] to estimate the paleo-water depth where the assemblage was formed. For each fossil sample, a sample-specific uncertainty is generated, indicated as horizontal lines through circles (figure modified after Kemp and Telford (2015)).

Only a few studies have concentrated on quantitative paleo-water depth reconstructions in deeper marine settings, such as outer shelf and upper slope environments. For example, Milker et al. (2017) successfully developed a regional WA-PLS TF, which is based on the modern distribution of benthic foraminifera in shelf and upper slope environments of the Western Mediterranean and Adriatic Seas. The TF covers a wider range of water depths than any other previous model. Additionally, it has been shown, that paleo-water depth reconstructions up to bathyal water depths can be reliable if the modern and fossil benthic foraminiferal assemblages are not too strongly influenced by other environmental parameters, such as productivity or oxygen content (Milker et al., 2017). This TF was then applied to a Pleistocene sediment section from the Island of Rhodes

for paleo-water depth reconstruction, and derived from this, for the reconstruction of neotectonic vertical motions of the island (Milker et al., 2019).

2 Study area

The Mediterranean Sea is a land-locked and semi-enclosed sea which covers an area of 2.5 million km^2 and is located between the European and African continents (Fig. 2.1). To the west it is connected to the Atlantic Ocean through the Strait of Gibraltar and to the east to the Black Sea via the Marmara Sea. The Mediterranean Sea is divided into two, nearly equal-sized basins, the Western Mediterranean and Eastern Mediterranean Basins. The western basin is subdivided into the Alboran, Provencal, Algerian and Tyrrhenian Basins, while the eastern basin includes the Levantine Basin, Ionian Basin, Adriatic Sea and Aegean Sea. Both, the western and eastern basins, are connected via the Strait of Sicily with a maximum water depth of 500 m that limits the water-mass exchange between the basins (e.g. Pinardi et al., 2015; Rohling et al., 2015).

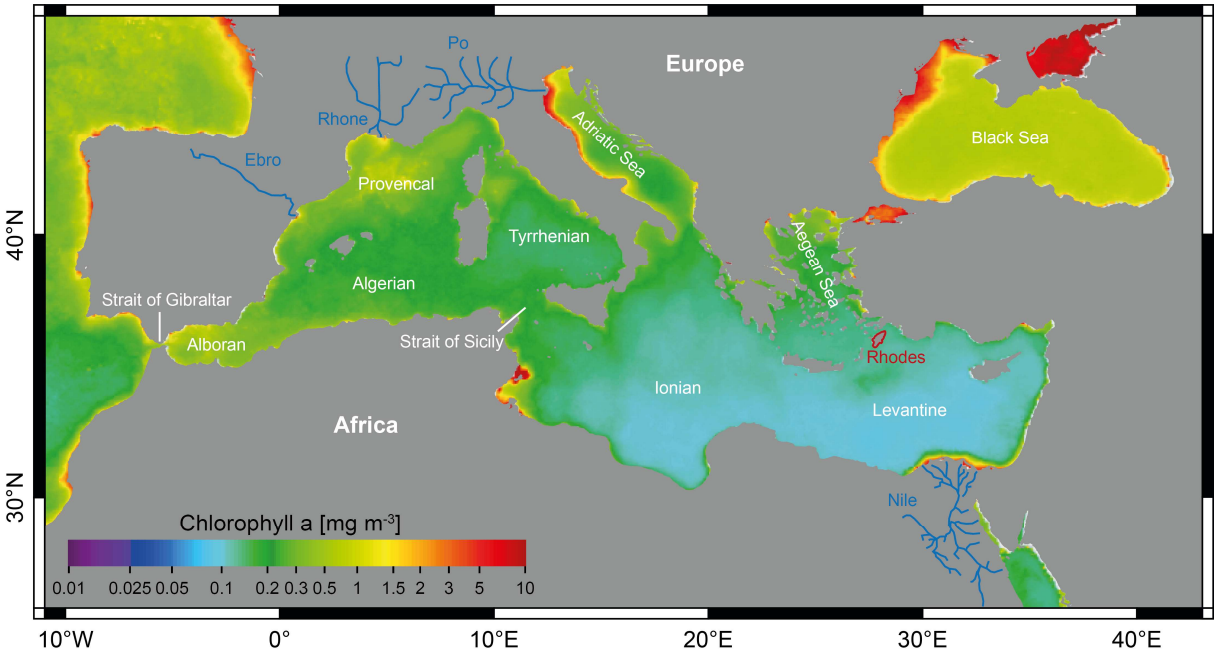

Figure 2.1 Overview of the Mediterranean Basin and its chlorophyll *a* concentration (MODIS-Aqua Chl-*a* data from European Marine Observation and Data Network (EMODnet) and Joint Research Centre (JRC)). The location of the Island of Rhodes (red), geographic regions (white) and rivers (blue) that are discussed in the text are marked (background map was created with Natural Earth (2012)).

2.1 Modern climate, circulation and productivity

The Mediterranean Sea is located in the transitional zone between two different climatic regimes: the subtropical high-pressure belt over North Africa and the temperate westerlies over central and northern Europe (e.g., Lolis et al., 2002). The modern climate is therefore characterized

by warm and dry summers, with the transition shifted northwards, and mild and wet winters, with a southward-shifted transitional zone (Lolis et al., 2002).

The Mediterranean Basin is on average a typical concentration basin, where the annual rainfall and the freshwater contribution via rivers is less than the water loss by evaporation. Thus, the total evaporation increases towards the east of the basin because enhanced evaporation occurs in areas subject to strong winds. The European topography, channels cold and dry winds, especially in winter and spring, into the Mediterranean, affecting the Gulf of Lions (Mistral), the Adriatic Sea (Bora) and the Aegean Sea (Vardar), inducing strong evaporation and cooling of the sea surface (e.g., Saaroni et al., 1996; Poulos et al., 1997; Maheras et al., 1999). The presence of relative humid Atlantic air masses in the west, causes less evaporation along the Algerian and Moroccan coast. Additionally, the overall excess of evaporation over freshwater input is lower in the northern part of the Mediterranean Sea due to freshwater inputs from the Rhone, Po and Ebro rivers and the Black Sea (Fig. 2.1), while the southern part, especially the southeastern part, shows high evaporation rates (Bethoux and Gentili, 1994). This leads to an increase in the surface salinity from the west to east across the Mediterranean Basin (e.g., Bryden and Kinder, 1991; Bethoux et al., 1999; Criado-Aldeanueva et al., 2012).

The modern Mediterranean circulation is mainly driven by atmosphere-ocean-interactions. As the total evaporation exceeds the amount of average precipitation and river run-off, the net inflow of Atlantic waters through the Strait of Gibraltar must compensate for this deficit (Bethoux et al., 1999; Cusinato et al., 2018). The inflowing Atlantic water mixes with the upwelled Mediterranean Intermediate Waters (MIW) to form a more saline Modified Atlantic Water (MAW), which flows eastward in the surface layers, across the western and eastern basins while gradually increasing in salinity due to evaporation losses (Fig. 2.2). Finally, when the MAW enters the Levantine basin, winter cooling and enhanced mixing, caused by intense dry winds, forces the MAW to sink to intermediate depths, resulting in the formation of the Levantine Intermediate Water (LIW) (Robinson et al., 1991; Pinardi et al., 2015). The LIW settles between approximately 200 and 600 m water depth (Lascaratos et al., 1999) and is separated from the overlying MAW by a distinct salinity gradient. It flows westward, crosses the Strait of Sicily with some re-circulation back into the eastern basin, and finally reaches the Strait of Gibraltar, where it then flows into the North Atlantic Ocean (Fig. 2.2). Deep water formation in the Mediterranean Sea takes place in both, the eastern and western basin. The Western Mediterranean Deep Waters (WMDW) are formed in the Gulf of Lion and the Eastern Mediterranean Deep Waters (EMDW) in the Adriatic Sea. However, some deep waters might also form in the Rhodes gyre, referred to as the Levantine Deep Water (LDW; Gertman et al., 1994) and in the Sea of Crete (CDW; Tsimplis et al., 1999)

(Fig. 2.2). In the late 1980s and early 1990s, a large change in the deep-water formation of the Eastern Mediterranean Sea, known as the Eastern Mediterranean Transient (Roether et al., 1996), caused the Aegean Sea to become a major component to the deep water formation, where previously it had only played a minor role (Wüst, 1961).

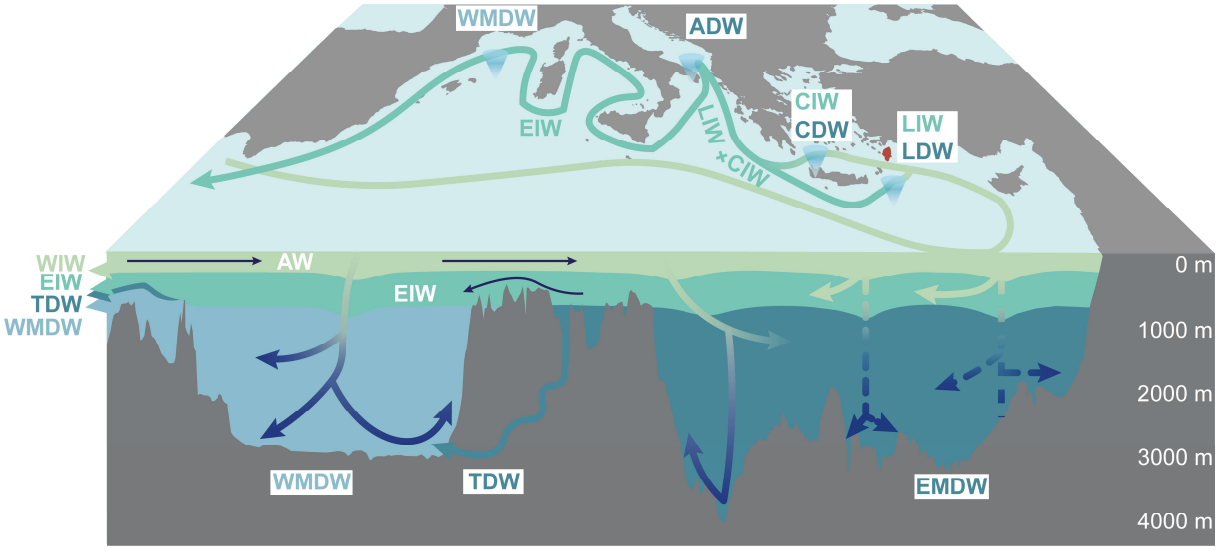

Figure 2.2. Schematic illustration of the thermohaline circulation of the Mediterranean Sea. Blue ellipses indicate the main deep water formation areas by open-sea convection. The Island of Rhodes is marked in red. AW: Atlantic Water, LIW: Levantine Intermediate Water, CIW: Cretan Intermediate Water, EIW: Eastern Mediterranean Water, WIW: Western Intermediate Water, ADW: Adriatic Deep Water, CDW: Crete Deep Water, LDW: Levantine Deep Water, EMDW: Eastern Mediterranean Deep Water; TDW: Tyrrhenian Deep Water, WMDW: Western Mediterranean Deep Water (figure modified from Millot and Taupier-Letage (2005); background map made with Natural Earth (2012); cross section of the Mediterranean Sea from Google Earth).

The trophic conditions in the Mediterranean Sea are generally oligotrophic (Tanhua et al., 2013), and the primary production is characterized by a strong contrast between the western and eastern basin. The Western Mediterranean Sea, with its strong water column mixing in the Alboran Sea and the supply of relatively nutrient rich Atlantic water, is the most productive area in the Mediterranean Sea (mean annual value of 163 $gCm^{-2}a^{-1}$; Bosc et al. (2004)), except for coastal areas with local riverine food supply (Fig. 2.1). The Eastern Mediterranean is characterized by oligotrophic conditions, especially in the Levantine Sea, where ultra-oligotrophic conditions prevail with an annual primary productivity of < 100 $gCm^{-2}a^{-1}$ (Psarra et al., 2000; Bosc et al., 2004). This is the result of a higher water column stratification in the eastern basin, leading to nearly nutrient depleted surface waters (Pujo-Pay et al., 2011). However, in the more coastal parts of the eastern basin, where rivers such as the Nile or Po Rivers supply nutrients, productivity increases remarkably (Fig. 2.1).

2.2 Orbital-driven climate changes in the Mediterranean since the Neogene

Long-term changes in the seasonal and latitudinal distribution of solar insolation on the Earth's surface are caused by periodic oscillations in the Earth's Orbit and tilt relative to the Sun. This is defined by three orbital parameters that are also known as the Milankovitch cycles: eccentricity, obliquity and precession, which are not constant but vary with different periodicities on a scale of thousands of years (Fig. 2.3; Hays et al., 1976).

Eccentricity defines the variation in the shape of the Earth's Orbit around the Sun (Fig. 2.3a). It indicates, how much the orbit of the Earth deviates from a perfect cycle and is characterized by three main periodicities at 413 kyrs, 100 kyrs and 2.3 Ma (Berger, 1978). The angle between the Earth's rotational axis and the normal to the orbital plane is defined as the obliquity (Fig. 2.3b). The largest amplitude of the obliquity component is at 41 kyrs (Berger, 1978). Finally, the precession defines the direction in which the Earth's axis of rotation is pointing (the wobble; Fig. 2.3c). The most prominent periodicities for the precession are 23 kyrs and 19 kyrs (Berger, 1978). The interaction of these orbital parameters, which determine the seasonal and latitudinal distribution of the solar radiation on the Earth' surface, influence what is known as insolation. While the eccentricity affects the global annual mean insolation, the precession impacts the seasonality of insolation. The obliquity affects different latitudes and impacts both hemispheres equally.

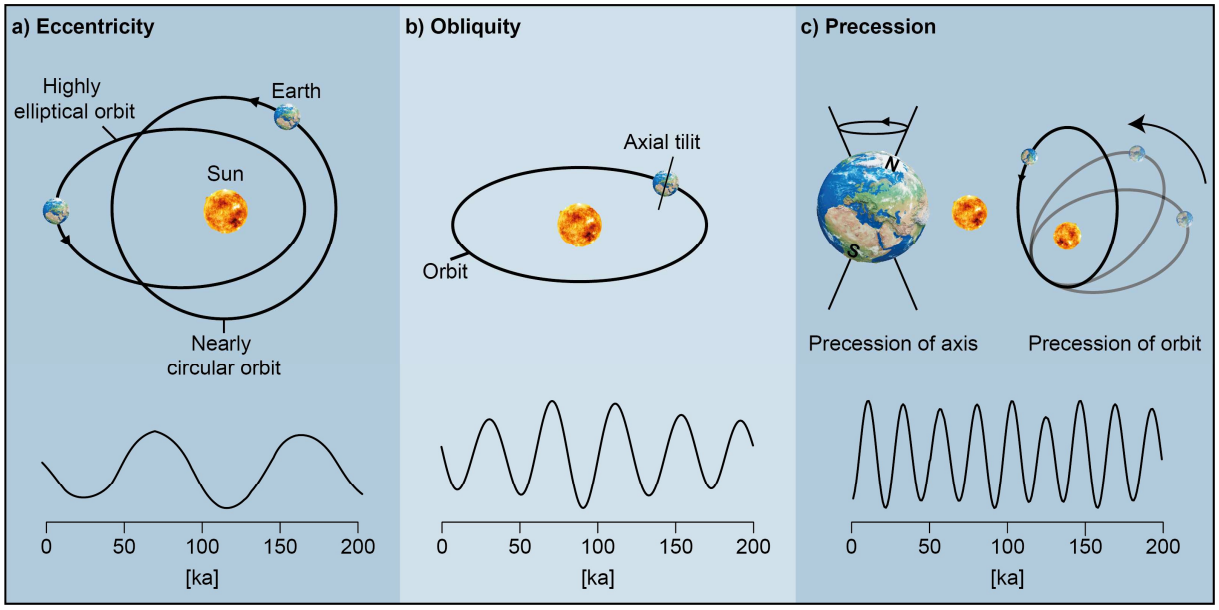

Figure 2.3. Overview of the orbital parameters and their variation through time. a) Eccentricity describes the shape of the Earth's Orbit around the Sun; b) Obliquity describes the tilt of the Earth's axis of rotation and c) Precession defines the direction in which the Earth's axis is pointing. The Earth's axis of rotation and the orbital path rotate over time and produce a cycle of ~21 ka (figure modified after Maslin (2016)).

Long-term climate changes in link with orbital forcing and their frequencies can be recognized in the sedimentary record (e.g., Hilgen et al., 1995; Lourens et al., 1996a). Local climate responses to the variations in the distribution of the solar radiation might also be tracked by changes in the chemical, physical and biological parameters of the sedimentary archive. Thereafter, the Milankovitch cycles are used to explain the glacial and interglacial cycles, with expanding and retreating ice sheets at the poles, but also for climate variations in lower latitudes, that do not influence the ice sheets. One example is the African summer monsoon that varies on precessional time scales, where maximum precipitation rates occur at times of precession minima and which is responsible for the formation of organic-rich and dark, laminated layers, so-called sapropels (e.g., Rossignol-Strick, 1983).

Sapropels are commonly found in deep-sea sedimentary sequences of the Mediterranean Sea since the Neogene (e.g., Rossignol-Strick, 1983; Kroon et al., 1998; Grant et al., 2022). Even though some organic-rich layers are also reported from the Western Mediterranean (known as Organic Rich Layers), they are much more common and with higher organic carbon contents in the Eastern Mediterranean (e.g., Emeis et al., 1991; Cramp and O'Sullivan, 1999; De Kaenel et al., 1999; Meyers and Doose, 1999; Rogerson et al., 2008). Their periodic occurrence is in close relation to the Northern Hemisphere summer insolation maxima and therefore related to minimum values in the precessional band (Rossignol-Strick et al., 1982; Rossignol-Strick, 1983; Hilgen, 1991; Lourens et al., 1996a; Kroon et al., 1998; Rohling et al., 2015). A precession-driven intensification of the African monsoon leads to an increased freshwater run-off from the Nile River and other North African rivers and consequently in a density stratification and reduction of deep-water ventilation in the Eastern Mediterranean (Rossignol-Strick et al., 1982; Rossignol-Strick, 1983; Cramp et al., 1988; Hilgen, 1991; Rohling and Hilgen, 1991; Kroon et al., 1998). There is further evidence that the deposition of past sapropel layers was characterized by an enhanced export productivity and an improved preservation of organic matter due to anoxia in the deep sea (Rohling, 1994; Emeis et al., 2000; Casford et al., 2003; Rohling et al., 2015).

2.3 Geotectonic setting

The present geotectonic setting of the Mediterranean Sea is dominated by a system of connected fold-and thrust-belts and associated foreland and backarc basins as the result of convergence processes between the relatively stable Eurasian and African continental plates, during the past 44 million years. The marine Mediterranean Basins are variably floored by remnants of the Tethyan oceanic domains (Ionian and Libyan Seas), Neogene oceanic crust (Algero-Provençal basin and

Tyrrhenian Sea), extended continental lithosphere (Alboran and Aegean Seas, Valencia Trough), and thick continental lithosphere (Adriatic Sea) (Cavazza and Wezel, 2003).

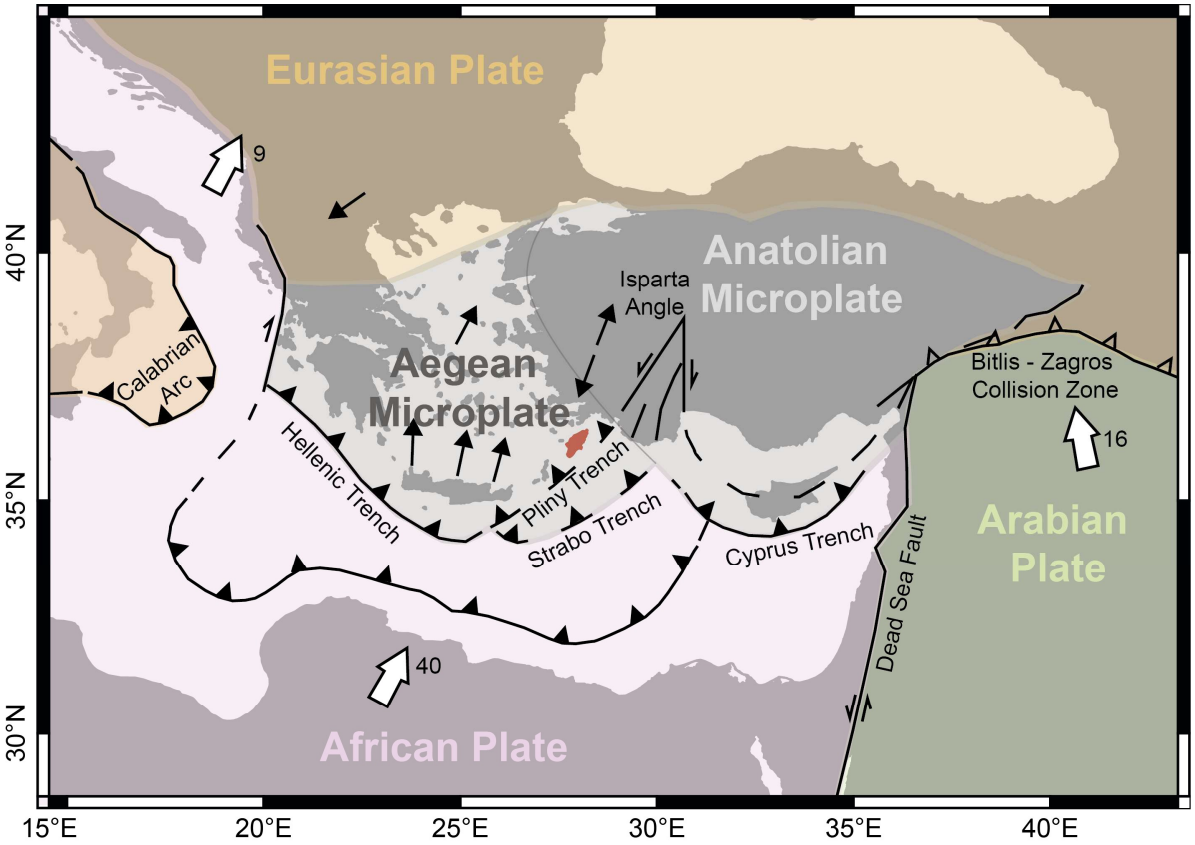

Figure 2.4. Map of the Eastern Mediterranean Sea showing the plate boundaries and major suture zones. White arrows show the direction and magnitude (mm a^{-1}) of plate convergence. Black errors mark the extension direction, and the location of the Island of Rhodes is marked in red (map modified from Dilek and Sandvol (2009); background map made with Natural Earth (2012)).

The main geotectonic features of the Eastern Mediterranean are controlled by the relative motion of the Eurasian, African and Arabian plates. The modern, about 100 km long, convergent plate boundary of the Anatolian and Aegean plates with the African plate comprises two separate arcs: the Hellenic and the Cyprian arcs (Fig. 2.4). While the Hellenic arc is characterized by a relatively steep, retreating subduction, the Cyprian arc appears to be associated with shallow subduction (e.g., Zitter et al., 2003). The intersection of these two subduction zones occurs at a sharp angle, the Isparta Angle (Fig. 2.4). The Hellenic forearc comprises a deformed stack of upper crustal nappes and ophiolites accreted on top of subducted continental and oceanic crust (Bonneau, 1984; van Hinsbergen et al., 2005a). The stacked nappes originally had a WNW-ESE trend, with only a slight curvature around the stable Eurasian margin. Since the Eocene, however, the Aegean forearc became strongly curved because of a clockwise rotation in the west and a counterclockwise rotation in the east (Morris and Robertson, 1993), in addition to large arc-normal and arc-parallel extensions in the Aegean backarc and forearc (Gautier et al., 1999; van Hinsbergen and Schmid,

2012; Philippon et al., 2014). Since the Pliocene, an increased curvature has led to stretching along the eastern part of the forearc, together with NE-SE trending strike-slip faults parallel to the Eurasian-African plate boundary (e.g., ten Veen, 2004; Tur et al., 2015; Kaymakcı et al., 2018). The so-called Rhodes Basin is a major bathymetric depression, located east of the Island of Rhodes, which forms the prolongation of the Pliny and Strabo trenches (Fig. 2.4). They are connected to the eastern part of the Hellenic subduction zone and parallel to the eastern coast of Rhodes, that is therefore exposed to the plate boundary (Howell et al., 2015). Additionally, the about 4,000 m deep Rhodes Basin started to open before approximately 6 Ma (Woodside et al., 2000; van Hinsbergen et al., 2007; Hall et al., 2009; Aksu et al., 2018), promoting sinking and uplift movements on the Island of Rhodes. During these phases, the island was subject to counterclockwise rotation, in the order of 25°, and additionally, the island was tilted southeast-ward and back to the northwest (van Hinsbergen et al., 2007). This geotectonic setting led to the deposition of Plio-Pleistocene marine sediments, that later have been uplifted and are outcropping today mainly along the east coast of the Island of Rhodes (Fig. 2.5A).

2.2.1 Lithostratigraphy of the Island of Rhodes

A series of steep horst-graben systems formed isolated basins, so-called depocenters, along the eastern coast of the Island of Rhodes, due to deformation, erosion, and multiple faulting of the Mesozoic basement (Mutti et al., 1970; Hanken et al., 1996). These basins are filled with Plio-Pleistocene sediments. However, due to their isolated locations in a tectonically active environment, changes in sedimentary facies within these depocenters are common, making a correlation of the infills difficult (Titschack et al., 2013). Since the first detailed stratigraphic description of the Plio-Pleistocene deposits along the northeastern coast of the Island of Rhodes by Hanken et al. (1996), many studies have proposed lithostratigraphic schemes (Hansen, 1999; Nelson et al., 2001; Cornée et al., 2006a, 2019; Titschack et al., 2008, 2013). Revised stratigraphic subdivisions have been proposed by Titschack et al. (2013), Quillévéré et al. (2016) and Cornée et al. (2019). Finally, five synthems have been defined (Fig. 2.5B; from bottom to top):

- Trianda Synthem, including the Damatria Formation and the Kritika Formation,
- Rhodes Synthem, which is subdivided into the Kolymbia, St. Paul's, Lindos Bay and Cape Arkhangelos Formations,
- Afandou Synthem, consisting of the Ladiko-Tsampika and Windmill Bay Formation,
- Lindos-Acropolis Synthem, including the Gialos and Kleopulu Formations, and
- Malona Synthem, which comprises the Agathi and Plimiri Formations.

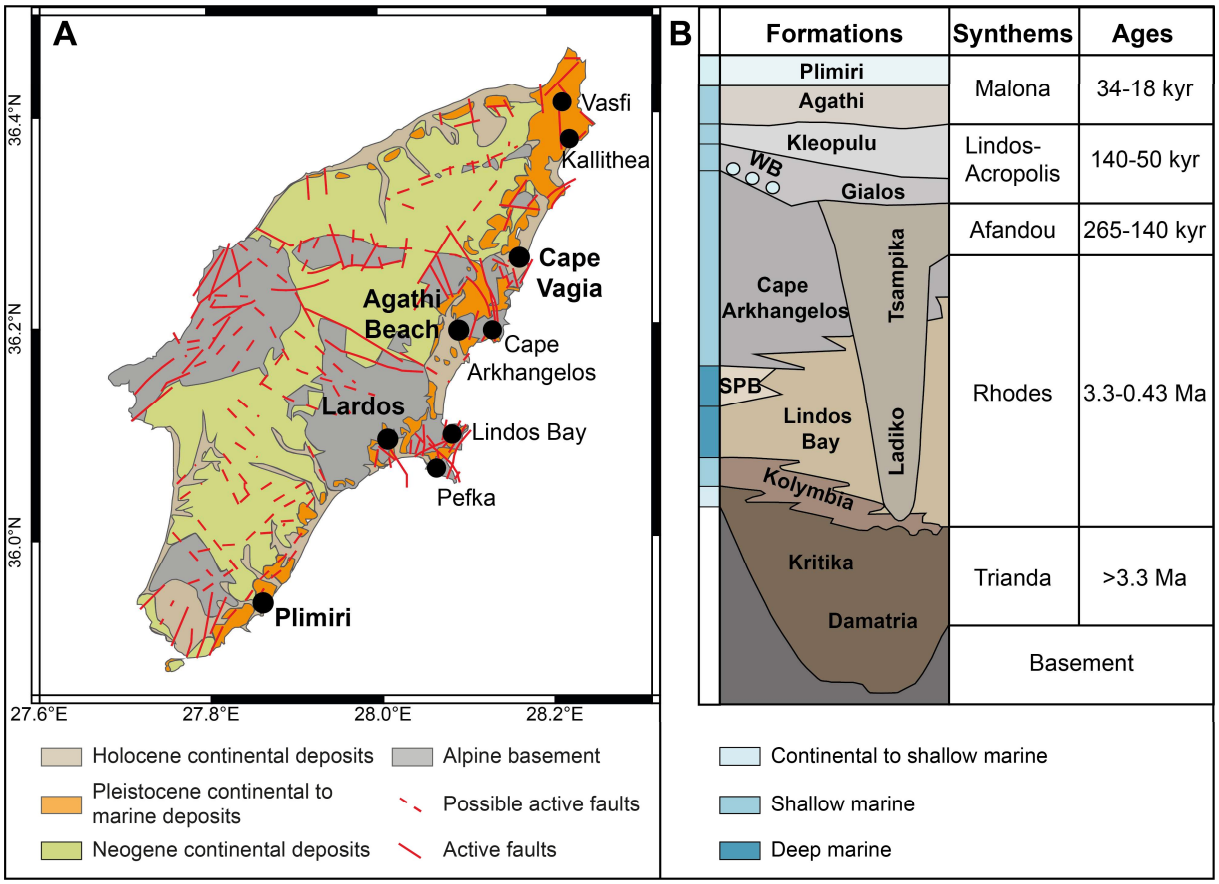

Figure 2.5. A. Simplified geological map of the Island of Rhodes with main tectonic features after Lekkas et al. (2000) and the locations of outcrops of the Lindos Bay Formation in black (figure modified after Cornée et al. (2019)). **B.** Lithostratigraphic scheme of the Plio-Pleistocene sediment deposits along the eastern coast of the Island of Rhodes and their depositional environments indicated by the colors in the left column (figure modified from Cornée et al., (2019)). SPB: Saint Paul's Bay; WB: Windmill Bay.

These synthems represent long-term transgressive and regressive sedimentary cycles (Cornée et al., 2019), among which the Rhodes Synthem, more specifically the Lindos Bay Formation (LBF), records the maximum drowning of the eastern coast, where water depths reached bathyal depths (e.g., Hanken et al., 1996, Titschack et al., 2013; Milker et al., 2019). The full-marine LBF is distributed along the eastern coast of Rhodes, with outcrops reported in scattered locations from Vasfi in the north (Meulenkamp, 1985) to Plimiri in the south (Nelson et al., 2001; Fig. 2.5A). Due to the good accessibility and the good preservation of microfossil-rich marine sediments, the LBF has been of particular interest, to better understand the complex neotectonic history of the island.

3 Impact of hydrological changes and vertical motions on Pleistocene marine environments of the eastern coast of the Island of Rhodes (Greece)

Daniela Eichner, Gerhard Schmiedl, Jürgen Titschack, Maria Triantaphyllou, Nils Andersen, Nina Forster, Yvonne Milker

Abstract

The Island of Rhodes in the Eastern Mediterranean Sea is situated in an area affected by an ongoing plate convergence, and its Pleistocene marine environments were influenced by recurring hypoxia and changes in organic matter fluxes. This makes the island an important site to study the influence of orbital-driven climate changes and tectonically induced vertical motions on the marine benthic ecosystems in near-coastal areas at local and regional scales. We investigated the Early and Late Pleistocene sediment sections at Agathi Beach and Lardos, located on the middle eastern coast of the island. Our results show variations in oxygen and food levels at the seafloor, including transient phases of enhanced fresh-water and nutrient input to near-coastal environments. These phases occurred at times of Northern Hemisphere summer insolation maxima, simultaneously to the formation of sapropels in the deep-sea basins of the Eastern Mediterranean Sea. The application of a benthic foraminiferal transfer function revealed that both sections were influenced by tectonic-driven long-term and short-term vertical motions with higher rates than expected on the Island of Rhodes. While Agathi Beach underwent two short-term cycles of uplift and subsidence, Lardos indicates at least three cycles with average rates of vertical motion as high as 8.6 mm/a.

This chapter is published as peer reviewed article in *Palaeogeography, Palaeoclimatology, Palaeoecology* (doi: 10.1016/j.palaeo.2023.111980) and is a slightly modified version.

3.1 Introduction

The eastern coast of the Island of Rhodes is a unique place to study easily accessible and microfossil-rich marine sedimentary sequences of Pleistocene age. The island experienced intensive tectonic motions during the Pleistocene with phases of uplift and subsidence. These motions were related to alternating southeastward and northwestward tilting of the island (Hanken et al., 1996; van Hinsbergen et al., 2007), resulting in a major long-term transgression-regression cycle and the deposition of brackish to marine sediments along the eastern coast of Rhodes (Hanken et al., 1996; Cornée et al., 2006a; Titschack et al., 2013). Today, these sediments are exposed at various locations along the eastern coast of the Island of Rhodes in graben or micro-graben structures (Hanken et al., 1996). The sediments contain a rich benthic foraminiferal fauna, which allows a detailed reconstruction of regional paleoenvironmental changes and neotectonic motions.

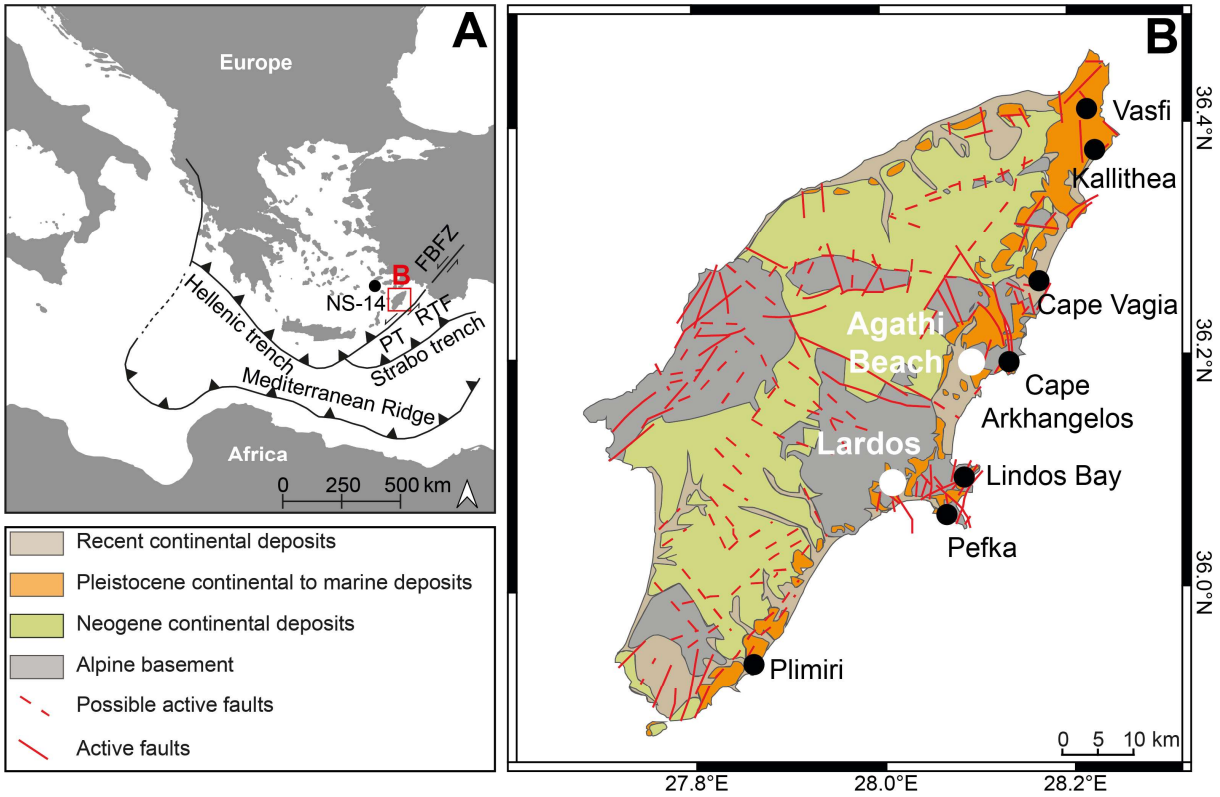

Figure 3.1. A. Simplified overview of the Eastern Mediterranean region and the main tectonic features after Dilek and Sanvol (2009) and Görgun et al. (2014) and the position of the core NS-14. RTF: Rhodes transform fault; PT: Pliny trench; FBFZ: Fethiye-Burdur fault zone. **B.** Simplified geological map of Rhodes showing the Alpine basement, Neogene and recent continental deposits and Pleistocene continental and marine deposits. Displayed in red are the potential active faults (dotted lines) and the active faults after Lekkas et al. (2000) (figure modified after Cornee et al. (2019)). The map also shows the investigated locations in white and additional locations of Lindos Bay Clay outcrops in black (Map created with Q GIS 3.26.1).

The modern Eastern Mediterranean Sea is characterized by oligotrophic conditions (Antoine et al., 1995; de Rijk et al., 2000). In contrast, studies from the southern coast (Milker et al., 2019) and from the northeastern coast of Rhodes (Fig. 3.1; Rasmussen and Thomsen, 2005) indicate rather mesotrophic conditions during the Pleistocene. However, it is largely unknown whether these conditions were local or whether the whole region around the Island of Rhodes was affected. To gain a better understanding of the trophic conditions off the Island of Rhodes during the Pleistocene, we aim to unravel the complex depositional history at the seafloor. By adding new benthic foraminiferal data from two sediment sections, located at the middle eastern coast of Rhodes, and by comparing them with other studies covering different time intervals, we will be able to answer the question of whether the mesotrophic bottom water conditions persisted during the Pleistocene, and whether these conditions were primarily affected by local conditions, such as riverine influence.

The so-called sapropels, a type of organic-rich layer, have been formed periodically, particularly in the Eastern Mediterranean Sea (Rossignol-Strick, 1983; Hilgen, 1991; Lourens et al., 1996a; Kroon et al., 1998). Multiple studies revealed a close relation of sapropel formation to orbital changes in the precessional band (e.g. Rossignol-Strick et al., 1982; Rossignol-Strick, 1983; Hilgen, 1991; Kroon et al., 1998; Rohling et al., 2015). Their timing is influenced by the Northern Hemisphere summer insolation maxima (Hilgen, 1991; Lourens et al., 1996a). As a result, the African monsoon intensified, leading to an increased river run-off and strengthened primary production in the Eastern Mediterranean Sea. Likewise, an increased precipitation and a more humid climate during times of sapropel formation were also reported from the northern borderlands of the Eastern Mediterranean Sea (Shaw and Evans, 1984; Rossignol-Strick, 1987; Wijmstra et al., 1990; Gogou et al., 2007; Kotthoff et al., 2008a,b; Geraga et al., 2010; Triantaphyllou et al., 2016). These climatic conditions resulted in a density stratification of the water column, a reduction of deep-water ventilation, and the formation of anoxic conditions at the sea bottom as indicated by the absence of benthic foraminifera in deep-water sapropels (Schmiedl et al., 2003, 2010; Kuhnt et al., 2008). Shallow water sapropels have rarely been described. The shallowest sapropel deposit was reported from the Aegean Sea by Perissoratis and Piper (1992) at a water depth of 125 m, whereas several relatively shallow sapropels have been analyzed, e.g., in the southeastern Aegean Sea at 505 m water depth (Triantaphyllou et al., 2009) and in the northeastern Aegean Sea at 216 m water depth (Triantaphyllou et al., 2016). Rasmussen and Thomsen (2005) found sapropel-like deposits in the Kallithea section, northeastern Rhodes (Fig. 3.1), at a reconstructed water depth of ~75 m and interpreted these as shallow-water extensions of strong sapropel events in the Eastern Mediterranean Sea. However, how and to what

extent sapropel forming events in the Eastern Mediterranean Sea resulted in a change of near-shore bottom water conditions along the middle and southeastern coast of Rhodes during the Pleistocene is largely unknown. The identification of low-oxygen events in sediments from the middle eastern coast of Rhodes provides a great opportunity to better understand the impact of orbital-driven climate changes on the near-coastal environments along Rhodes and whether these events had a similar or different influence on benthic foraminiferal assemblages, depending on time and region.

A first attempt for a more detailed quantitative reconstruction of tectonically induced water depth changes was made by Milker et al. (2019), who applied a regional transfer function based on modern benthic foraminiferal assemblages to the fossil assemblages in the Pefka E section at the southeastern coast of Rhodes, and by Quillévéré et al. (2019), who used the planktic/benthic ratio of foraminiferal assemblages in the Lindos section at the middle eastern coast of Rhodes (Fig. 3.1). Both studies suggest that the neotectonic vertical motions during the Pleistocene were more complex than previously thought. Besides the long-term vertical motions described by for example Hanken et al. (1996) and Cornée et al. (2006a), the other studies also identified short-term paleo-water depth fluctuations. Milker et al. (2017) found up to four cycles of transgression and regression between 1656 ka and 1278 ka and Quillévéré et al. (2019) noticed three short-term cycles during the time period of 1100 ka to 850 ka. The question whether individual depocenters underwent different vertical motions and to what extend short-term cycles are also exposed in other locations remains unclear. By using the transfer function from Milker et al. (2019) for paleo-water depth reconstructions in the studied sections, we aim to better understand the vertical motions that influenced the middle eastern coast of Rhodes during the Pleistocene.

3.2 Study area

The Island of Rhodes is situated on the eastern end of the Hellenic sedimentary forearc and is mainly composed of Mesozoic and Tertiary bed rocks, deformed during the Alpine orogeny (Meulenkamp et al., 1972). Major N 70° trending sinistral strike-slip faults, as well as anticlockwise rotation and vertical motions influenced the island since the Pliocene (Hanken et al., 1996; Cornée et al., 2006a; van Hinsbergen et al., 2007). Due to deformation, erosion and multiple faulting of the Mesozoic basement, a series of steep horst and graben systems formed isolated basins, which later influenced the deposition and distribution of Pleistocene marine and continental deposits (Mutti et al., 1970; Hanken et al., 1996). The tectonically induced vertical motions uplifted the isolated basins, filled with Pleistocene marine sediment sequences, which are now outcropping along the eastern coast of Rhodes. However, sedimentary facies changes within these separated depocenters are common and a correlation of the infillings of the different depocenters is hard to establish

(Titschack et al., 2013). The Pleistocene marine deposits, reflecting major and minor tectonically controlled sea level changes, were classified as the Rhodes Synthem, which can further be subdivided into three transgressive formations, Kolymbia, Lindos Bay and St. Paul's Formation, and one regressive formation, Cape Arkhangelos Formation (Titschack et al., 2013; Cornée et al., 2019). The here studied Lindos Bay Formation (LBF; also known as Lindos Bay Clay, LBC) is distributed along the eastern coast of the island and outcrops are documented in scattered locations from Vasfi in the north (Meulenkamp et al., 1972) to Plimiri in the south of Rhodes (Fig. 3.1; Nelson et al., 2001). Nevertheless, only a limited number of outcrops comprise the lower LBF-Kolymbia Formation boundary (e.g., at Cape Vagia, Cape Arkhangelos, Lindos Bay, Pefka and Plimiri; Fig. 3.1). The age of the mostly erosive upper boundary (LBF - Cape Arkhangelos) varies considerably from section to section, making a chronological correlation of the LBF upper boundary from different locations difficult (Titschack et al., 2013; Quillévéré et al., 2016).

3.2.1 Studied sedimentary sections

This work focuses on two sedimentary sections from Agathi Beach and Lardos (Fig. 3.1). The Agathi Beach section outcrops along the road connecting the main road with Agathi Beach (36◦10'51.90"N; 28◦5'21.66"E). The about 4.7-m-thick marly succession of the LBF shows a distinct layer of volcanoclastic sediments approximately 2.5 m above the base. This layer was dated to 1.89 ± 0.09 Ma by Cornée et al. (2006b). Additionally, within a laminated layer with sharp boundaries between 1.3 and 1.5 m, plenty of fish remains were identified and at approximately 4 m section height a red layer (red marker horizon) was defined (Fig. 3.2). The LBF at the Agathi Beach location is overlain by a recent terrace.

The Lardos section is located in the Lardos Valley, a N-S orientated depression at the middle eastern coast of Rhodes (36◦5'18.48"N; 28◦0'35.59"E) approximately 16 km south of the Agathi Beach section and is composed of about 9.3 m of sediments from the LBF (Fig. 3.3). The section is characterized by marly deposits with grain sizes ranging from muddy silt to muddy fine sand with a slight upward coarsening (Titschack et al., 2013). Some layers within the LBF contain randomly orientated fossils and show a sharp or erosive base (Titschack et al., 2013). Additionally, Titschack et al. (2013) identified five layers as debris flow deposits (Fig. 3.3). Cold-water corals from two samples between 1.49 and 1.7 m and one sample between 3.68 and 3.72 m section height were $^{234}U/^{238}U$ dated to 756 ± 17.5 ka, 755.2 ± 16 ka and 688.9 ± 15.5 ka (Titschack et al., 2013).

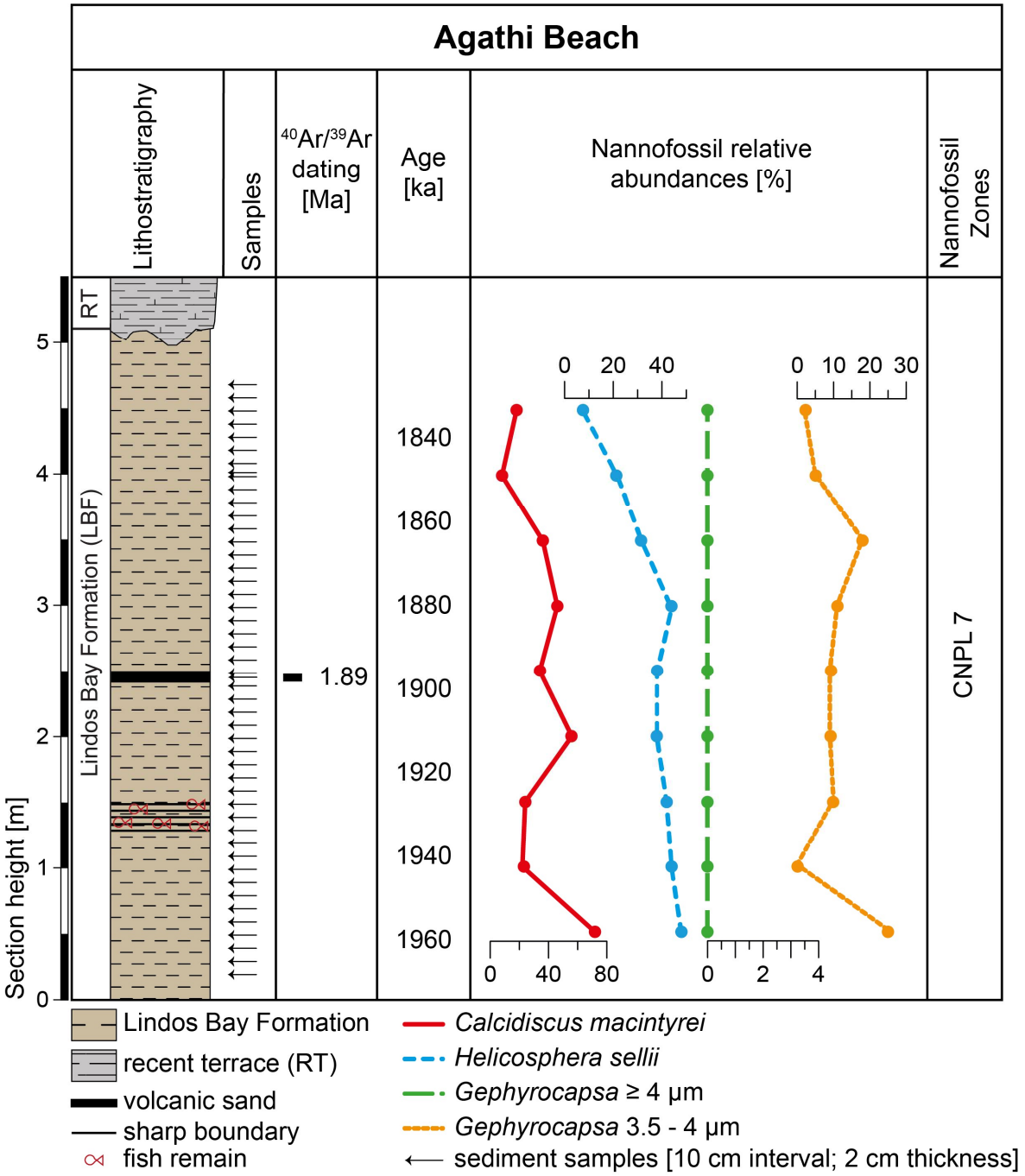

Figure 3.2. Simplified lithology of Agathi Beach and nannofossil abundances and zones. $^{40}Ar/^{39}Ar$ dating of the volcanic sand resulted in an age of 1.89 ± 0.09 Ma after Cornée et al. (2006b). Ages resulting from the cyclostratigraphic analysis. The nannofossil zone refers to Calcareous Nannofossil (CNPL) biozone 7 (1.93-1.71 Ma).

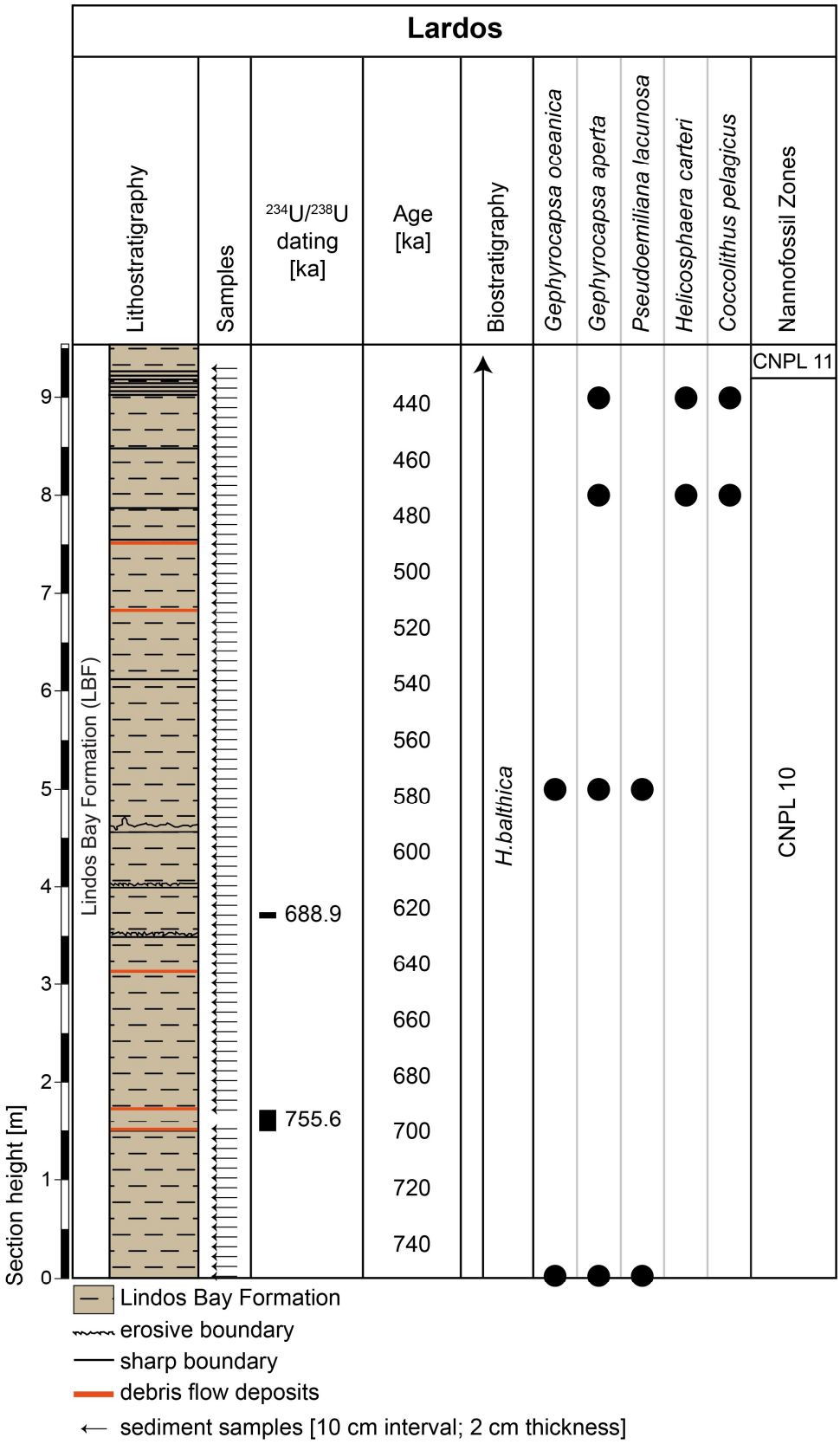

Figure 3.3. Simplified lithology of Lardos. $^{234}U/^{238}U$ dating resulted in ages of 756 ± 17.5 ka, 755.2 ± 16 ka and 688.9 ± 15.5 ka (Titschack et al., 2013). Ages resulting from the cyclostratigraphic analysis. Biostratigraphy is based on the lowest common occurrence (LCO) of *Hyalinea balthica* and nannofossil analysis after Titschack et al. (2013). The nannofossil zone of the lower part of the section refers to CNPL 10 (1.06-0.43 Ma) and the upper part to CNPL 11 (0.43-0.00 Ma). Debris flow samples, identified in Titschack et al. (2013) are marked in orange.

3.3 Methods

3.3.1 Chronostratigraphic framework and stable isotope measurements

The stratigraphic framework of the sections is based on a combination of biostratigraphic information, radiometric ages, and stable oxygen isotope stratigraphy. We have investigated the distribution of calcareous nannofossils in nine sediment samples taken at 50 cm resolution for Agathi Beach. The preparation of samples followed the standard smear slide techniques for calcareous nannofossil analysis (Perch-Nielsen, 1985; Bown and Young, 1998). All samples were routinely examined at 1250×, using a LEICA DMLSP light microscope. Frequencies of index species have been established according to the methodology of Rio et al. (1990), by counting the index species vs. a fixed number of taxonomically related forms. This method involves the monitoring of index species relative to a predetermined number of a reference group and is considered as independent of preservation state, dilution and paleoecological exclusion (Rio et al., 1990). More specifically, for the presence of *Gephyrocapsa* 3.5–4 μm there have been counted the *Gephyrocapsa* specimens in 100 placoliths, for *Calcidiscus macintyrei* the species specimens in 100 coccoliths of genus *Calcidiscus* and for *Helicosphaera sellii*, the species specimens in 100 helicoliths of genus *Helicosphaera*.

Further biostratigraphic information was obtained from the lowest common occurrence (LCO) of the planktic foraminifera *Neogloboquadrina pachyderma* sinistral (1.79 Ma; Zijderveld et al., 1991; Lourens et al., 1996a,b; Lourens and Hilgen, 1997) and the benthic foraminifer *Hyalinea balthica* (1.492 Ma; Lourens et al., 1998). For the Agathi Beach section, the absolute age of an ash layer, dated to 1.89 ± 0.09 Ma was available (Cornée et al., 2006b).

We refined the age model for the Lardos section implied by Titschack et al. (2013), who used the available $^{234}U/^{238}U$ ages as tie points for the graphical correlation of the planktic $\delta^{18}O$ record with the oxygen isotope curve of ODP hole 967 (Kroon et al., 1998), suggesting an age of ~900 to 300 ka B.P. for the section. The planktic $\delta^{18}O$ record is less suitable for correlation with the global standard isotope record due to the stronger influence of salinity and temperature fluctuations in the surface water and strong biological effects of symbiont-bearing planktic foraminifera (Rohling and Cooke, 1999). Therefore, the stratigraphy was refined by a graphical correlation of the epibenthic $\delta^{18}O$ records of the sections with the benthic LR04 stack of Lisiecki and Raymo (2005) (Supplement 3.1), and by using the absolute $^{234}U/^{238}U$ ages from reworked cold-water corals provided in Titschack et al. (2013). Further, the relative abundance of eutrophic/low oxygen tolerant indicator species of the Lardos section was used for the uppermost fix point, as no $\delta^{18}O$ data were available for this interval but the eutrophic/low oxygen tolerant indicator species

mirror orbital changes (Table 3.1). Correlations were performed with the software AnalySeries 2.0 (Paillard et al., 1996).

Table 3.1. Fixpoints used for the generation of the age models for the Agathi Beach and Lardos sediment sections. Age model development is mainly based on the graphical correlation of the epibenthic $\delta^{18}O$ records of Agathi Beach and Lardos with the LR04 stack (Lisiecki and Raymo, 2005).

Agathi Beach		Lardos	
Section height [cm]	Age [ka]	Section height [cm]	Age [ka]
461	1830.06	921	431
403.5	1847.65	771	490.85
361	1866.04	491	584.5
221	1905.72	341	626.5
91	1946.15	171	690.44
		71	718.22
		11	746.09

Benthic foraminiferal stable oxygen and carbon isotope composition was measured in all 48 sediment samples from the Agathi Beach section. Three clean specimens of the epibenthic foraminifer *Cibicidoides pseudoungerianus* from the 250–355 µm fraction were picked from each sample. In one sample at 1.4 m section height of the Agathi Beach section, only two specimens of *C. pseudoungerianus* were found in the 250–355 µm fraction, so that two additional specimens were picked in the size fraction <250 µm. The tests were soaked in ethanol and cleaned in the ultrasonic bath for five to eight seconds. The composition of stable oxygen and carbonate isotopes were measured at the Leibniz-Laboratory for Radiometric Dating and Stable Isotope Research at the University Kiel. The measurements were performed using a Thermo Finnigan MAT 253 mass spectrometer connected to a Kiel IV carbonate preparation device and the analytical precision (standard external error) was better than ±0.08 ‰ for $\delta^{18}O$ values and ± 0.05 ‰ for $\delta^{13}C$ values. Results are reported in per mil with respect to the Vienna PeeDee Belemnite (VPDB) scale. In 80 samples of the Lardos section, four to five specimens of the epibenthic *Cibicidoides pachyderma* were picked from the fraction >250 µm. Prior to cleaning in ethanol and in the ultrasonic bath, the shells were crushed between two glasses to remove the sediment from the test chambers. The stable oxygen and carbon isotope measurements were carried out in the Geochemical Laboratory of the GeoZentrum Nordbayern, Germany (Titschack et al., 2013).

3.3.2 Foraminiferal investigations

Sediment samples, each of 2 cm thickness, were sampled every 10 cm in the investigated sections during two field surveys in 2001 and 2003. A total of 48 samples were taken from the 4.7 m-long Agathi Beach section and a total of 93 samples from the 9.3 m-long Lardos section. Two additional samples, at 2.42 and 4.03 m, were taken in Agathi Beach due to visual anomalies, such as an ash

layer and a red marker horizon, in the section (Fig. 3.2). Prior to sampling, the weathered material was removed to access fresh material. Sample preparation for the Agathi Beach section took place in the laboratories of the University of Hamburg, while the samples of the Lardos section were prepared in the laboratories of GeoZentrum Nordbayern, in 2006 (Titschack et al., 2013) and were provided as already picked benthic foraminifera, with at least 250 individuals in a representative split of the >125 µm fraction. Each sample of Agathi Beach, with a weight of approximately 50 g, was treated with 10% hydrogen peroxide (H_2O_2) for one hour to disaggregate the sediment and subsequently washed over a 63 µm mesh screen. Highly compacted samples of the Agathi Beach section were further soaked in a solution containing 50% Rewoquat W3690 and 50% Ethanol (96%) for one hour. If necessary, the step was repeated, and samples were soaked again for half an hour with the Rewoquat-Ethanol solution. Afterwards the samples were washed over a 63 µm mesh screen, dried at 40°C and subsequently dry-sieved over a 125 µm mesh screen. The pretreatment of compacted sediment samples with H_2O_2 in a variety of concentration is a common technique for foraminiferal investigations (e.g., Feldmeijer et al., 2013; Jones, 2013). Feldmeijer et al. (2013) studied the effect of a one-hour sample pretreatment with 10% H_2O_2 on the foraminiferal abundance, shell fragmentation, Mg/Ca and stable carbon and oxygen isotope composition and found no significant influence on the taxa or the geochemical shell signals. Rewoquat is commonly used for cleaning fossils and less commonly to disaggregate organic-rich rocks for micropaleontological purposes (Jarochowska et al., 2013). Nevertheless, Jarochowska et al. (2013) reported a good recovery and preservation of organic-walled and calcareous microfossils, even after soaking for multiple days.

In the Agathi Beach section, foraminiferal investigations were carried out on representative splits (using a microsplitter), of the >125 µm-fraction. For the identification on species level, we used Jones (1994), Rasmussen (2005) and Milker and Schmiedl (2012). Whenever the identification on species level was not possible, individual species were grouped into their genus. Photographs of the most dominant taxa were made by using a scanning electron microscope (SEM; HITACHI TM4000Plus) at the University of Hamburg. Further, the species (grouped to their genus-level) were categorized into eutrophic and oligotrophic taxa, based on their morphological features and the presence or absence of fine pores following Corliss and Chen (1988) and Milker et al. (2019) (Supplement 3.2). The diversity of the fauna was calculated after the Shannon-Wiener biodiversity index H (Shannon and Weaver, 1949), by using the software Past 4.07 (Hammer et al., 2001).

3.3.3 Paleo-water depth reconstructions

For the paleo-water depth reconstructions, the relative abundance of benthic foraminifera in the >150 µm-fraction was used for Agathi Beach (method after Milker et al., 2017). The >150 µm-fraction was used for a better accuracy in the reconstruction because this fraction was also analyzed in the modern data set, to develop the transfer function (Milker et al., 2017). For this, the representative splits were further sieved using a 150 µm mesh screen. The split contained at least 250 individuals in the >150 µm-fraction. For Lardos, the reconstruction is based on the >125 µm-fraction since no data for the >150 µm fraction is available. After Weinkauf and Milker (2018), general trends of paleo-ecological reconstructions are comparable between data sets counted in the fractions >125 µm and >150 µm, even though the data might differ in detail. The paleo-water depth reconstructions were made with an existing transfer function, which used modern Mediterranean benthic foraminiferal assemblages from the Adriatic Sea and the Western Mediterranean Sea shelf as a training data set and the Weighted Averaging-Partial Least Square (WA-PLS) method (Ter Braak and Juggins, 1993) and cross validation (bootstrap, N = 1000) for transfer function development (Milker et al., 2017). Further explanations and supporting material on the chosen method is provided in the supplementary information 3.3 (modified version in Appendix D). The robustness and significance of the paleo-water depth estimates is evaluated by applying a set of statistical tests (i.e., goodness-of-fit statistics (Birks, 1998; Simpson and Hall, 2012) and random TF (transfer function)-test (Telford and Birks, 2011)). To identify the final component of the transfer function we choose the component with an RMSEP (Root Mean Squared Error of Prediction) >5% better than the previous component and a statistically significant improvement (t-test; Kemp and Telford, 2015). For the paleo-water depth reconstructions, samples with a high relative abundance of eutrophic/low oxygen tolerant taxa in the sediment sections were excluded from the fossil data set since the foraminiferal assemblages in these parts are influenced by trophic conditions rather than by water depth (see chapter 3.5.3). All estimations and evaluations were made with the software R 4.2.0 (R Core Team, 2022) and R packages "PalaeoSig" (Telford and Trachsel, 2019), "rioja" (Juggins, 2020) and "vegan" (Oksanen et al., 2022).

To extract the tectonic component of the paleo-water depth fluctuations, we corrected the estimates for the effect of glacio-eustatic sea level changes by using the data of Bintanja and van de Wal (2008). Because the paleo-water depth estimates and the benthic foraminiferal assemblage are also influenced by precession-driven changes in the paleo-productivity, this component was filtered out to avoid a distortion of the tectonic component. Any precession signal found in the reconstructed paleo-water depth was removed and the record was subsequently smoothed. This

was done using a moving average smoothing with a calculated mean precession period of 20.5 ka and by using the software R and the package "smooth" (Svetunkov, 2023).

3.4 Results

3.4.1 Biostratigraphy

The sediments from Agathi Beach cover the time period from 1968 to 1827 ka B.P. (Fig. 3.2). Sedimentation rates vary between 2.3 cm kyr^{-1} and 3.5 cm kyr^{-1}, with a mean sedimentation rate of 3.1 cm kyr^{-1} (Fig. 3.4A). The age model is in consistency with the absence of *Hyalinea balthica* (1.492 Ma; Lourens et al., 1998) and *Neogloboquadrina pachyderma* sinistral (1.79 Ma; Zijderveld et al., 1991; Lourens et al., 1996a,b; Lourens and Hilgen, 1997). Further support comes from the nannofossil analysis (Supplement 3.4). This analysis revealed the presence of *Gephyrocapsa* 3.5–4 μm with up to 25 specimens in 100 placoliths, *Calcidiscus macintyrei* with up to 72 individuals in 100 *Calcidiscus* and *Helicosphera sellii* showing up to 48 individuals in 100 *Helicosphera*. *Gephyrocapsa* ≥ 4 μm, however, were absent in any sample and, thus, Agathi Beach is assigned to Calcareous Nannofossil Zone (CNPL) 7 (Backman et al., 2012) that covers an interval between 1.93 and 1.71 Ma in the Early Pleistocene (Gelasian-Calabrian boundary; Fig. 3.2) and is correlated with the lower part of Neogene Nannoplankton (NN) 19 (Martini, 1971) biozone and Mediterranean Neogene Nannoplankton (MNN) 19a (Rio et al., 1990). Additionally, there is no particular sign of reworking in the samples of Agathi Beach.

According to the revised age model (see chapter 3.3.1) the sediments of Lardos cover the time period from 751 ka to 427 ka B.P. (Fig. 3.3). Sedimentation rates vary between 2.2 cm kyr^{-1} and 3.6 cm kyr^{-1} with an average rate of 2.9 cm kyr^{-1}, while the higher rates are restricted to the middle part of the section (Fig. 3.4B). Further support comes from *Hyalinea balthica*, which is present in the entire Lardos section, indicating an age younger than 1.492 Ma (Lourens et al., 1998). The two lower most nannofossil samples of Titschack et al. (2013) contain, among others, *Gephyrocapsa oceanica*, *Gephyrocapsa aperta*, and *Pseudoemiliania lacunosa*, while the two upper most samples consist of *G. aperta*, *Helicosphaera carteri* and *Coccolithus pelagicus*. Thus, the nannofossil analysis published by Titschack et al. (2013) assigns the lower part of the section to CNPL 10 (1.06–0.43 Ma; Backman et al., 2012) and the upper part to CNPL 11 (0.43–0.00 Ma; Backman et al., 2012).

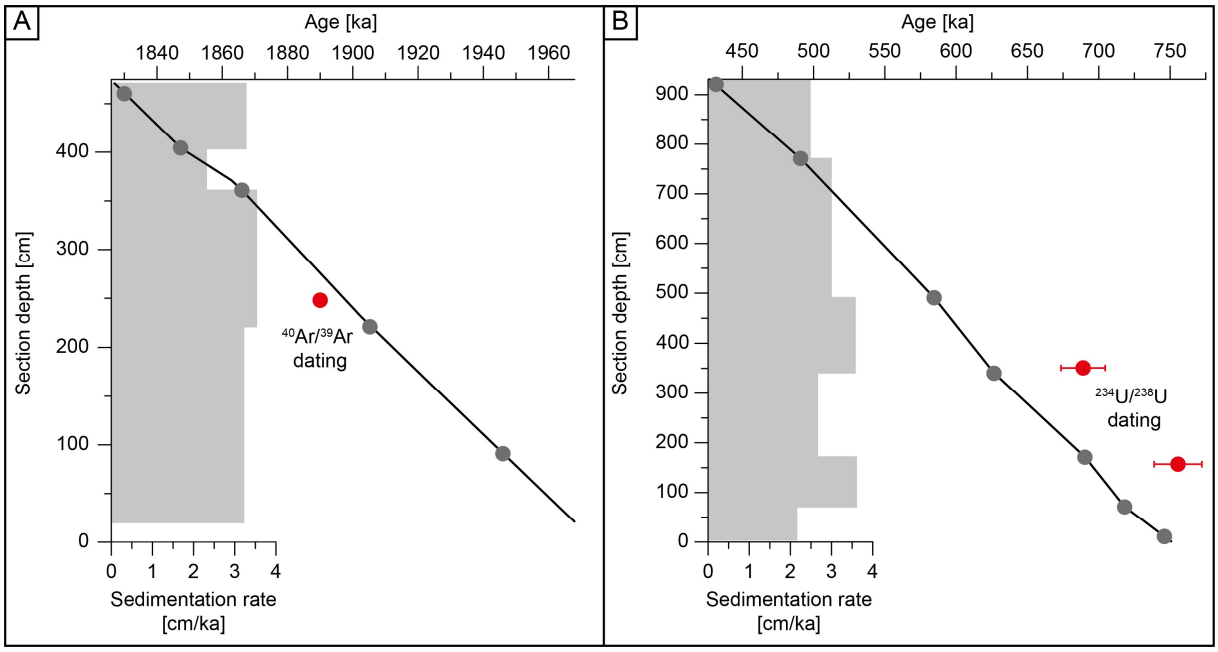

Figure 3.4. Age-depth plot with calculated sedimentation rates for **A.** Agathi Beach and **B.** Lardos. Tie points for the chronostratigraphic approach is based on already published absolute ages by Cornée et al. (2006b) and Titschack et al. (2013), indicated by red dots. Error bars of the $^{234}U/^{238}U$ dating are shown, while the error of the $^{40}Ar/^{39}Ar$ dating (±90 ka) is extending the figure and is therefore not shown. Fix points used for the correlation with the LR04 stack after Lisiecki and Raymo (2005) are marked in grey dots.

3.4.2 Benthic foraminiferal assemblages in the sections

3.4.2.1 Agathi Beach section

A total of 250 different taxa were identified in the Agathi Beach section, ranging between 46 and 89 taxa in individual samples. The most dominant species of the Agathi Beach section, with a relative abundance of ≥10% in at least one sample, comprise *Bulimina striata* (0–21%), *Bulimina marginata* (0–11%), *Cassidulina carinata* s.l. (1–14%), *Cibicidoides mundulus* (0–10%), *Cibicidoides pseudoungerianus* (0–33%), *Globocassidulina subglobosa* (0–15%), *Oridorsalis umbonatus* (0–14%), *Rectuvigerina phlegeri* (0–10%), *Uvigerina auberiana* (0–15%) and *Uvigerina peregrina* (1–18%) (Figs. 3.5 and 3.6; complete census counts in Supplement 3.5).

Cibicidoides pseudoungerianus is the most dominant species in the Agathi Beach section with an average abundance of about 17%. Together with *C. carinata* s.l., *C. mundulus* and *G. subglobosa* it occurs in the entire section with high to medium abundances. *Oridorsalis umbonatus* also occurs in the entire section but its abundance decreases towards the top of the section. At 1931–1928 ka and 1889–1886 ka, the abundances of these taxa decrease drastically to 0–4%, while *B. striata*, *B. marginata* and *R. phlegeri* show their highest occurrences with 20, 11 and 10%, respectively. *Uvigerina auberiana* and *U. peregrina* occur in the entire section with medium abundances of an average of 5–6%. Both show higher abundances in the middle and upper part of the section, compared to the lower part.

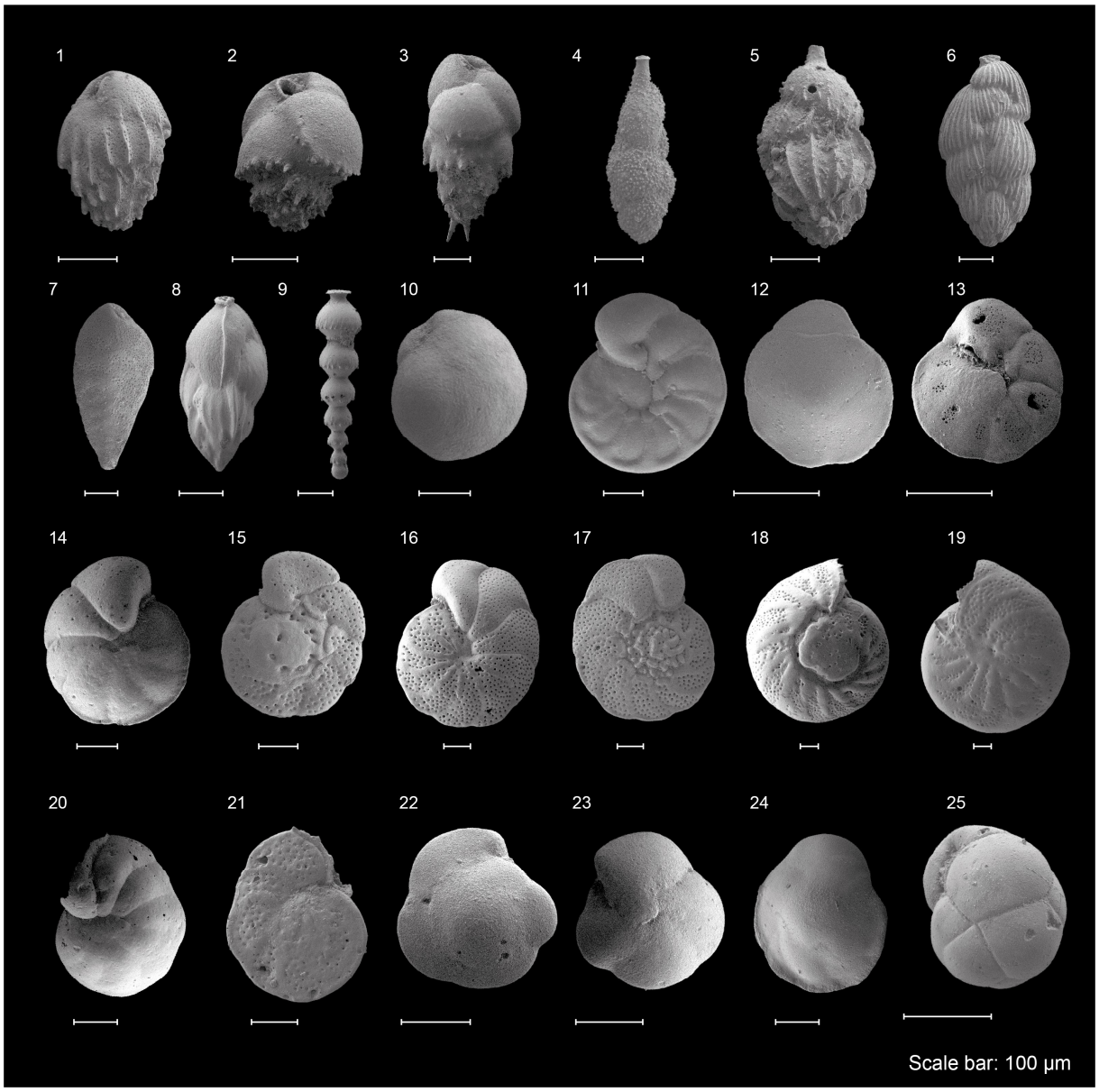

Figure 3.5. Most dominant benthic foraminifera of the Agathi and Lardos section. 1 *Bulimina striata*, 2 *Bulimina marginata*, 3 *Bulimina aculeata*, 4 *Uvigerina auberiana*, 5 *Uvigerina peregrina*, 6 *Rectuvigerina phlegeri*, 7 *Brizalina spathulata*, 8 *Trifarina angulosa*, 9 *Stilostomella lepidula*, 10 *Globocassidulina subglobulosa*, 11 *Hyalinea balthica*, 12-13 *Gavelinopsis praegeri*, 14-15 *Cibicidoides pseudoungerianus*, 16-17 *Cibicidoides mundulus*, 18-19 *Cibicidoides pachyderma*, 20-21 *Cibicides pseudolobatulus*, 22-23 *Oridorsalis umbonatus*, 24 *Cassidulina carinata* s.l., 25 *Cassidulina obtusa.*

The Agathi Beach samples contain between 27 and 72% eutrophic/low oxygen tolerant indicator species and between 19 and 51% oligotrophic taxa (Fig. 3.6). Eutrophic/low oxygen tolerant indicator species reach their peak values at 1931 ka and 1886 ka, whereas the oligotrophic taxa decrease in relative abundance. Likewise, the oligotrophic taxa show a decreasing long-term trend towards the top of the section.

The diversity, expressed by the Shannon-Wiener-Index (H), ranges between 2.8 and 3.7 and fluctuates throughout the section, with the lowest diversity of 2.8 at 1915 ka and the highest of 3.7 at 1842 ka (Fig. 3.6).

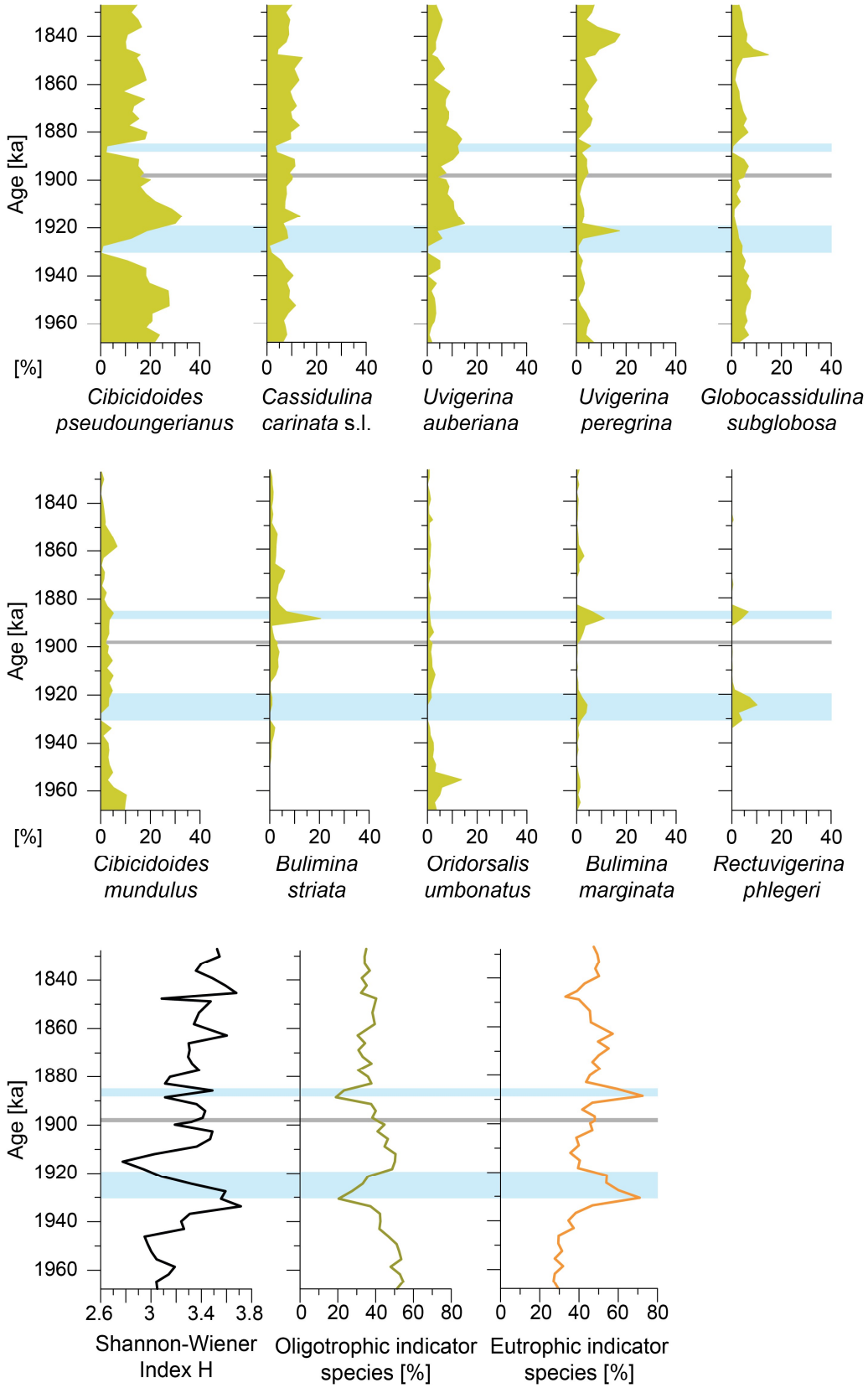

Figure 3.6. Relative abundance of most dominant foraminifera of the Agathi Beach section, with relative abundance of ≥ 10% in at least one sample of the > 125 µm fraction plotted against age. Shannon-Wiener-Index (H) and relative abundance of oligotrophic and eutrophic/low oxygen tolerant indicator species are presented below. Highlighted in grey is the position of the tephra layer, blue bars indicate a strong increase in eutrophic taxa.

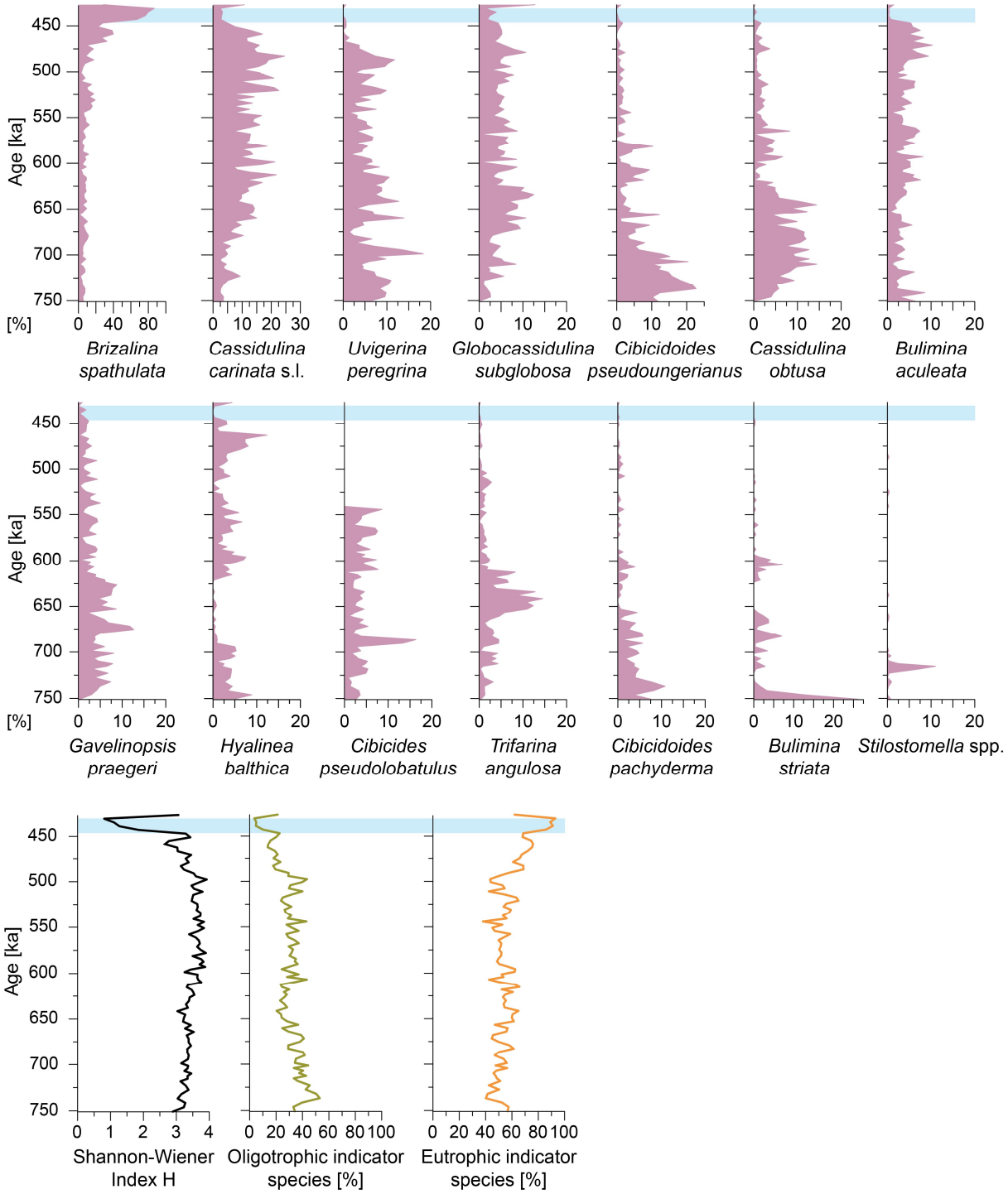

Figure 3.7. Relative abundance of most dominant foraminifera of the Lardos section, with relative abundance of ≥ 10% in at least one sample of the > 125 µm fraction plotted against age. Shannon-Wiener-Index (H) and relative abundance of oligotrophic and eutrophic/low oxygen tolerant indicator species are presented below. Blue bars indicate a strong increase in eutrophic taxa.

3.4.2.2 Lardos section

In the Lardos section, a total of 224 taxa were observed (complete census counts in Supplement 3.6). The most dominant species comprise *Brizalina spathulata* (1–87%), *Bulimina aculeata* (0–10%), *Bulimina striata* (0–26%), *Cassidulina obtusa* (0–14%), *Cassidulina carinata* s.l. (2–25%), *Cibicides pseudolobatulus* (0–16%), *Cibicidoides pseudoungerianus* (0–23%), *Cibicidoides pachyderma* (0-11%), *Gavelinopsis praegeri* (0–13%), *Globocassidulina subglobosa* (0–13%), *Hyalinea balthica* (0–12%), *Stilostomella* spp. (0–11%), *Trifarina angulosa* (0–15%) and *Uvigerina peregrina* (0–18%) (Figs. 3.5 and 3.7).

Brizalina spathulata is present throughout the section in most cases with an abundance of <20%. Its abundance drastically increases to 87% between 467 and 431 ka. *Cassidulina carinata* s.l. is present throughout the entire section with an increasing trend towards the top, followed by a decline. *Cibicidoides pseudoungerianus*, *C. pachyderma*, *C. pseudolobatulus*, *C. obtusa*, *B. striata* and *T. angulosa* on the contrary, show their highest occurrences in the lower part of the section, while their relative abundance decreases towards the top. *Cibicides pseudolobatulus* is absent from 544 ka on. *Uvigerina peregrina*, *G. subglobosa*, *B. aculeata*, *G. praegeri* and *H. balthica* occur in the entire section with average abundances between 2 and 6%. *Stilostomella* spp. has only one high occurrence at 715 ka and is absent or nearly absent in the rest of the section.

Eutrophic/low oxygen tolerant taxa range between 38% and 93%. They show an increasing long-term trend towards the top of the section while the oligotrophic taxa, which have a relative abundance between 4% and 53%, show a decreasing trend (Fig. 3.7). The Shannon-Wiener diversity ranges between 0.81 and 3.06. The diversity is slightly increasing towards the top, followed by a sudden drop between 439 and 431 ka (Fig. 3.7).

3.4.3 Paleo-water depth reconstructions

We selected the third component of the final transfer function model because the RMSEP (Root Mean Squared Error of Prediction) of 49.06 m is >5% better than that of the second component and this improvement is statistically significant (t-test, $p < 0.001$) (Table 3.2; Kemp and Telford, 2015). The cross-validated coefficient of determination (R^2) between the observed and estimated water depths in the combined modern data is 0.95 for the third component (Table 3.2). For the validation of the reconstructions, the goodness-of-fit statistics was applied to determine, whether the fossil samples have a good fit to the water depth. At Agathi Beach, 12 samples (29%) show a good fit to water depth, 9 samples (21%) a poor fit, 15 samples (36%) a very poor fit, and 6 samples (14%) have an extremely poor fit. A total of 44 samples (53%) of the Lardos section show a good fit to the water depth, whereas 19 samples (22%) have a poor fit, 12 samples (15%) a very poor fit,

and 8 samples (10%) are extremely poor fitting (Supplement 3.3; Appendix D). Further, the random TF-test was applied to test the significance of the reconstructions. The results reveal that none of the reconstructions are significant at the 95% confidence level (Supplement 3.3; Appendix D). The poor fit to water depth is likely attributed to the fact that some species of the fossil record occur in higher abundances compared to the modern record and some modern species do not occur in the fossil record at all (list of modern and fossil species, is available in Supplement 3.3; Appendix D).

Table 3.2 Transfer function performance. Shown is the cross-validated root mean squared error of prediction (RMSEP), the cross-validated coefficient of determination (R^2_{boot}) between the estimated and observed water depth of the modern data set, improvement of the RMSEP from one to the next component (%change) and the significance of the component fitting increase according to a randomized t-test. Chosen component is marked.

	RMSEP	R^2	% change	*p*
Comp01	98.69	0.8	53.57	0.001
Comp02	54.27	0.94	45.01	0.001
Comp03	**49.06**	**0.95**	**9.6**	**0.001**
Comp04	46.75	0.96	4.7	0.017
Comp05	45.12	0.96	3.48	0.047

The uncorrected reconstructed paleo-water depths range between 110 ± 50 m and 391 ± 49 m for the Agathi Beach section with a trend to deeper water depths towards the top of the section. The corrected paleo-water depth estimates range between 138 m and 301 m. After the correction for the precession-influenced and relative global sea level changes, the water depths of Agathi Beach show a general deepening trend towards the top of the section (Fig. 3.8; Supplement 3.3; Appendix D). Apart from the long-term depth increase of about 120 m, the section indicates two small-scale cycles of shallowing and deepening between 1957 ka and 1944 ka and from 1944 ka to 1827 ka.

In the Lardos section, the uncorrected reconstructed paleo-water depths range between 99 ± 58 m and 476 ± 86 m, with a general shallowing trend of about 377 m from the bottom to the top of the section and relatively large fluctuations in the entire section (Fig. 3.8; Supplement 3.3; Appendix D). The corrected water depth estimates vary between 46 m and 394 m with a long-term shallowing of ~156 m (Fig. 3.8). Further, three short-term paleo-water depth changes were detected between 751 and 705 ka, 705 and 647 ka and between 647 ka and 505 ka in the corrected estimates.

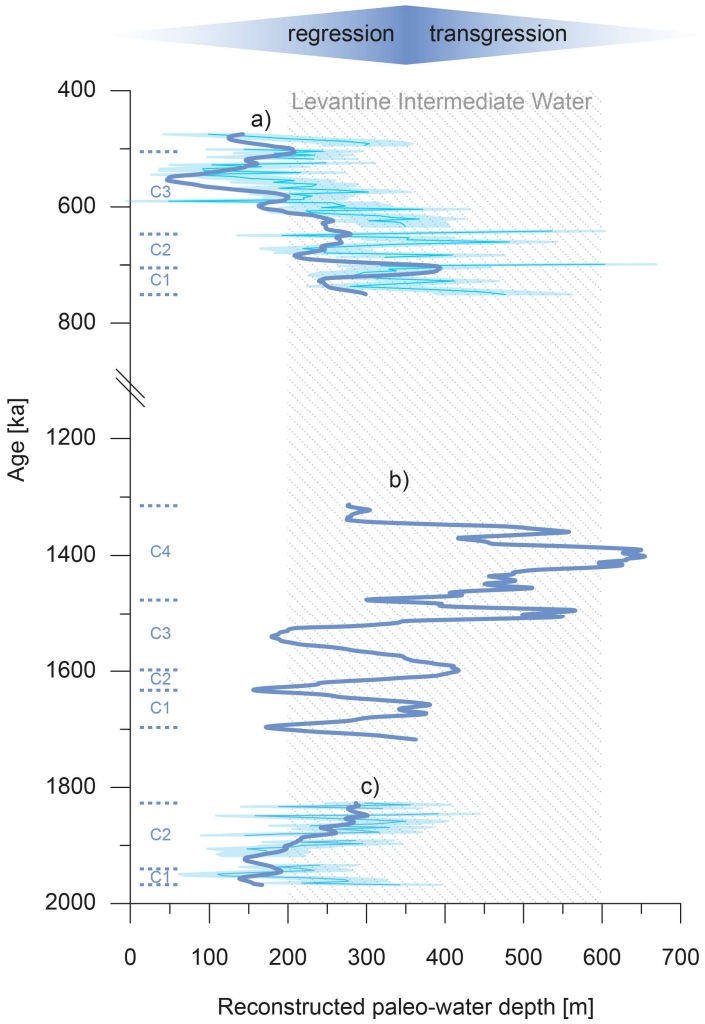

Figure 3.8. Estimated uncorrected paleo-water depths (light blue) including an average sample specific error and paleo-water depth corrected for the effects of relative, glacio-eustatic sea-level changes and for precession-influenced changes (dark blue) for a) Lardos, b) Pefkos after Milker et al. (2019) and c) Agathi Beach. Identified short-term cycles (C) of vertical motions are shown, and the depth limits of the modern Levantine Intermediate Water (LIW) after Lascaratos et al. (1999).

3.4.4 Oxygen and carbon stable isotopes

In the Agathi Beach section, $\delta^{18}O$ values of the epibenthic foraminifera *C. pseudoungerianus* range between 0.32‰ and 2.80‰ with a slight trend towards lower values from the middle part to the top of the section (Fig. 3.9). Two peaks with 2.08‰ and 1.90‰ can be identified at 1903 ka and 1858 ka. The $\delta^{13}C$ values are fluctuating between -1.09‰ and 1.13‰, with the lowest value at 1886 ka, and show a general decreasing trend towards the top of the section (Fig. 3.9). In Lardos, $\delta^{18}O$ values of the epibenthic foraminifera *C. pachyderma* range between -0.31‰ and 2.81‰ and $\delta^{13}C$ values between -0.28‰ and 1.69‰ (Fig. 3.10). Both records reveal substantial fluctuations throughout the sediment record and follow a similar trend with decreasing values towards the top of the section.

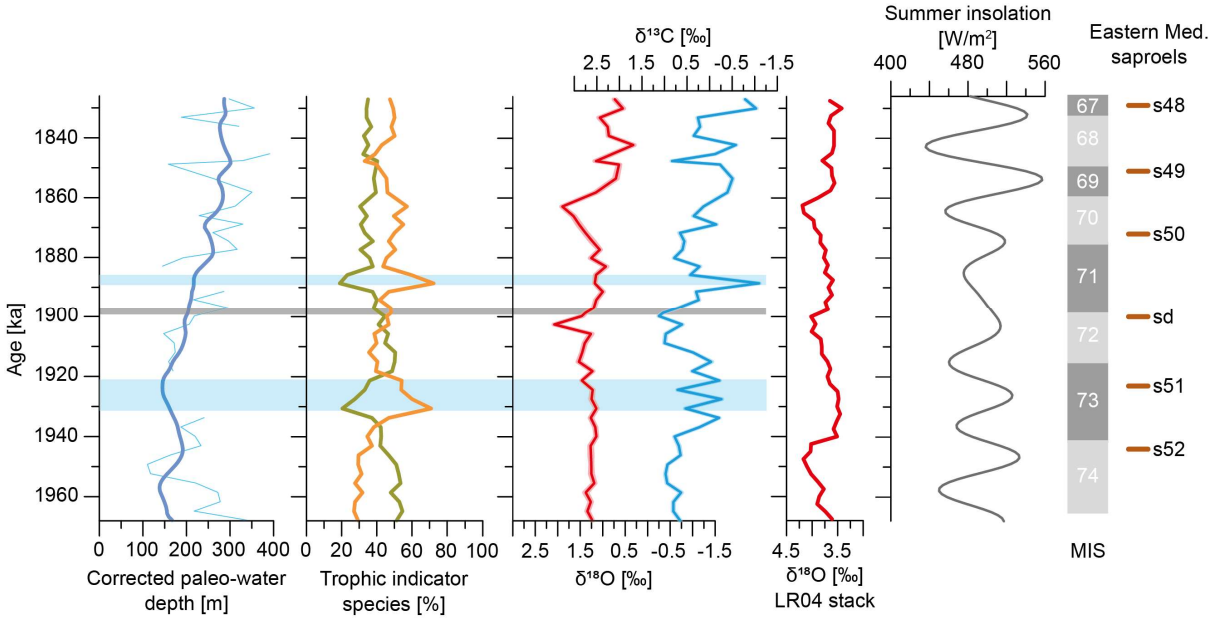

Figure 3.9. Agathi Beach: Corrected paleo-water depth and for reference uncorrected paleo-water depth in thin line. Relative abundance of eutrophic/low oxygen tolerant taxa (orange) and oligotrophic taxa (green). Values for $\delta^{18}O$ and $\delta^{13}C$, measured on the epibenthic foraminifera *C. pseudoungerianus*, are presented in red and light blue with specific error shown in pale color. Highlighted in grey is the position of the tephra layer, blue bars indicate a strong increase in eutrophic taxa. $\delta^{18}O$ values of the LR04 stack (Lisiecki and Raymo, 2005) and the Northern Hemisphere summer insolation are plotted against age. Marine isotope stages as published by Lisiecki and Raymo (2005) are marked with dark grey for warm stages and light grey for cold stages. Brown lines indicate sapropels from the eastern Mediterranean Sea after Kroon et al. (1998).

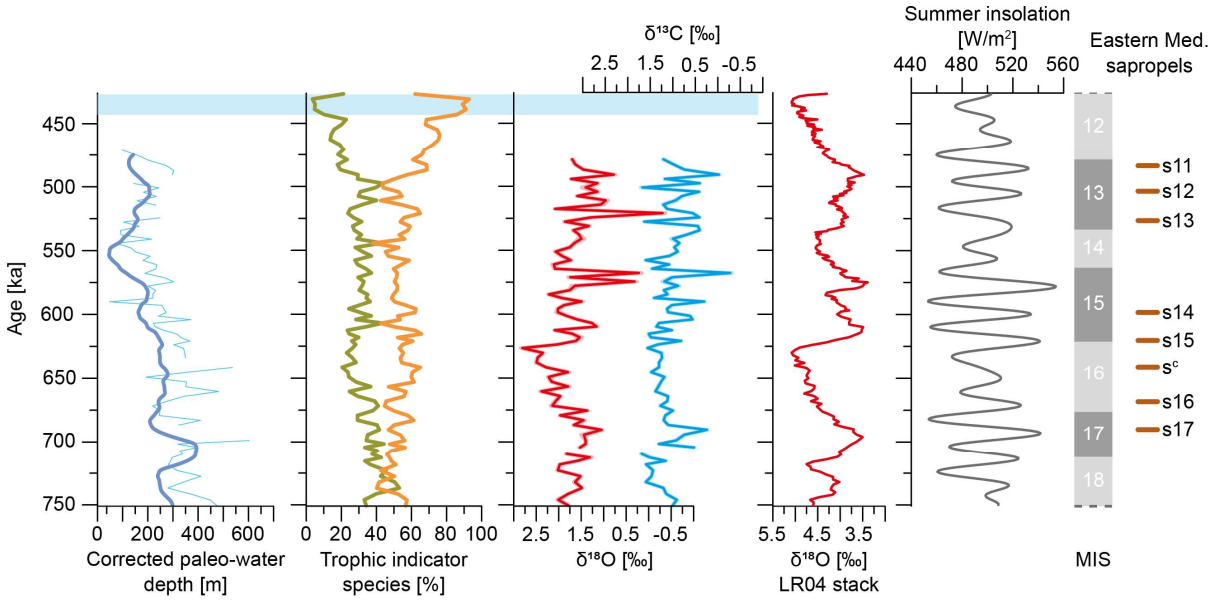

Figure 3.10. Lardos: Corrected paleo-water depth and for reference uncorrected paleo-water depth in thin line. Relative abundance of eutrophic/low oxygen tolerant taxa (orange) and oligotrophic taxa (green). Values for $\delta^{18}O$ and $\delta^{13}C$, measured on the epibenthic foraminifera *C. pachyderma*, are presented in red and light blue with specific error shown in pale color. Highlighted in grey is the position of the tephra layer, blue bars indicate a strong increase in eutrophic taxa. $\delta^{18}O$ values of the LR04 stack (Lisiecki and Raymo, 2005) and the Northern Hemisphere summer insolation are plotted against age. Marine isotope stages as published by Lisiecki and Raymo (2005) are marked with dark grey for warm stages and light grey for cold stages. Brown lines indicate sapropels from the eastern Mediterranean Sea after Kroon et al. (1998).

3.5 Discussion

3.5.1 Chronology of the Lindos Bay Formation along the eastern coast of the Island of Rhodes

The age models for the studied sections mainly rely on the correlation of the epibenthic $\delta^{18}O$ record with the LR04 standard isotope record (Lisiecki and Raymo, 2005). Although there is a possibility of inaccuracies in the peak-to-peak correlations, the biostratigraphic information further supported the validity of our age models (see chapter 3.4.1 and Titschack et al., 2013). The coral ages, used as tie points for the revised age model of the Lardos section, are approximately 60 ka older than the surrounding sediments. The nearly constant age offset may be mainly because the $^{234}U/^{238}U$ dating did not meet the necessary criteria and an open system could have biased the coral ages to systematically older ages (Andersen et al., 2009).

The age position of the LBF has been discussed over the past years, suggesting diachronous lower and upper boundaries (Fig. 3.11; Cornée et al., 2006a,b; Titschack et al., 2013; Quillévéré et al., 2016; Milker et al., 2019, and references therein). The lower boundary of the LBF to the Kolymbia Formation, was dated between ~1945 ka and >1120 ka, the upper erosive boundary to the Cape Arkhangelos Formation to 1314 ka and > 960 ka (Thomsen et al., 2001; Quillévéré et al., 2016; Milker et al., 2017). The documented sedimentation rates range between 4.4 cm kyr^{-1} (Milker et al., 2017) and 19.8 cm kyr^{-1} (Quillévéré et al., 2019). The section studied in this work therefore belong to one of the oldest (Agathi Beach) and most likely the youngest (Lardos) deposits of the LBF exposed along the eastern coast of Rhodes, both without exposed over- or underlying boundary (Fig. 3.11). Likewise, our average sedimentation rates, of ~3.1 cm ky^{-1} (Agathi Beach) and ~2.91 cm kyr^{-1} (Lardos), are lower than other findings from LBF deposits along the eastern coast of the island. Titschack et al. (2013) emphasized the high degree of diachroneity of the lithostratigraphic units and suggested that each regional depocenter along the eastern coast of the Island of Rhodes should be evaluated separately, to unravel the complex depositional history. Also, Cornée et al. (2019) reported a high variability of the maximal drowning and their amplitudes from different LBF deposits on Rhodes and suggested an individual development of different parts of the island, which is also indicated by the high variation of sedimentation rates along the eastern coast.

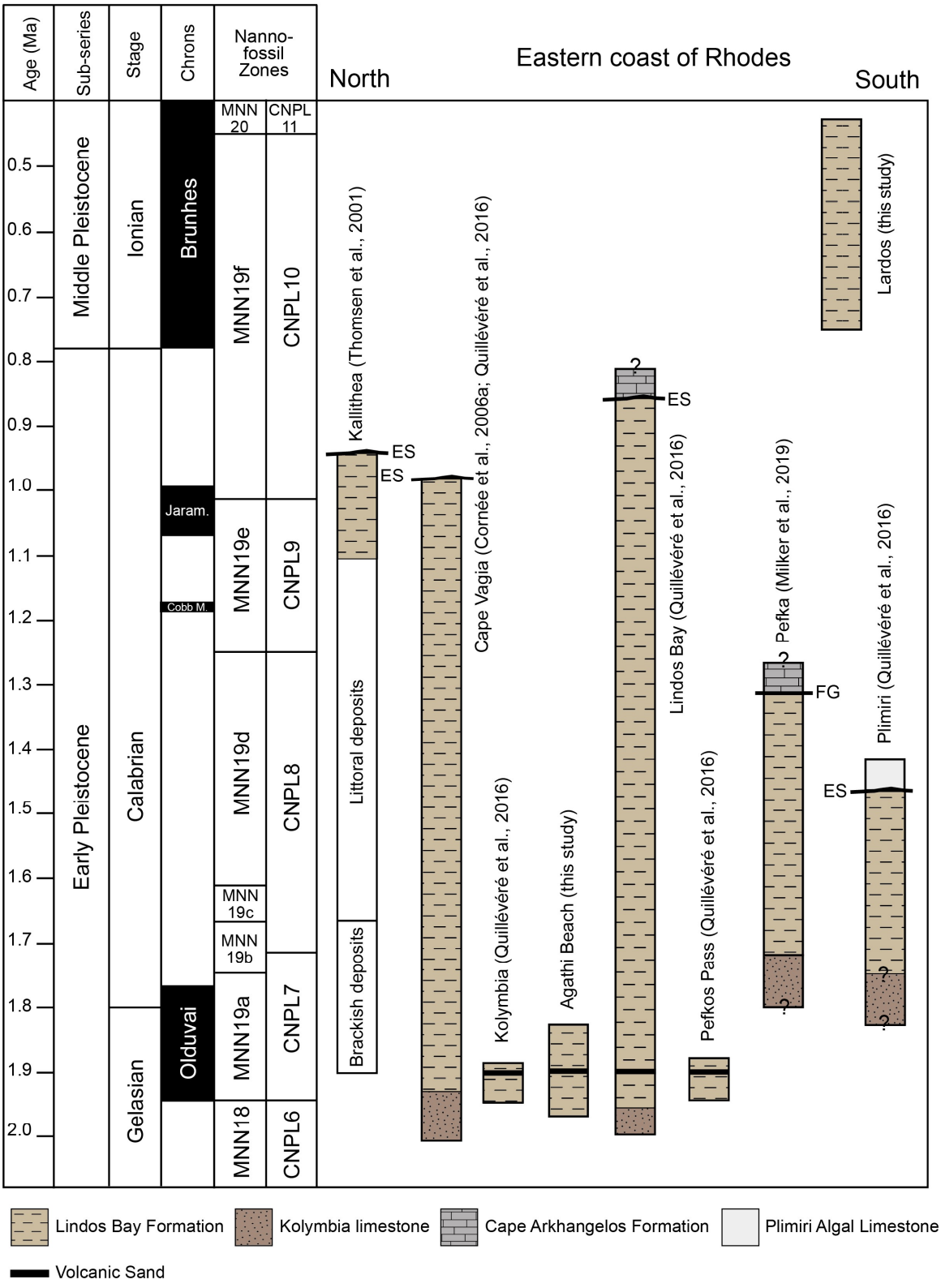

Figure 3.11. Overview of available chronostratigraphic data of the Lindos Bay Formation, outcropping along the eastern coast of the Island of Rhodes (figure modified and updated after Quillévéré et al. (2016)), showing the temporal duration of the stratigraphic sections and exposed upper and lower boundaries. The ages of the volcanic sands of sediment sections of Kolymbia, Lindos Bay and Pefkos Pass have been modified to fit with the shifted age of the volcanic sand of Agathi Beach to follow the interpretation of Quillévéré et al. (2016) that the ashes mirror the same event.

3.5.2 Paleoecology of benthic foraminiferal faunas

We observed general high proportions of eutrophic/low oxygen tolerant indicator species with average percentages of 44% for Agathi Beach and 57% for Lardos, which point to rather mesotrophic conditions off the Island of Rhodes during the Pleistocene. Although there is no data available for the modern benthic foraminiferal faunas from the outer shelf and upper slope environments of Rhodes, the Late Holocene data from the nearby sediment core NS-14, recovered from a water depth of 505 m, show the co-occurrence of the shallow and intermediate infaunal *Uvigerina mediterranea*, *Melonis barleeanum* together with *Planulina arimininensis*, and *Bulimina marginata*. This core exhibits an average percentage of 55% for eutrophic/low oxygen tolerant indicator species and 26% for oligotrophic indicator species indicating mesotrophic to eutrophic conditions after approximately 4 ka B.P. (Triantaphyllou et al., 2009). The Pleistocene faunas suggest a regional eutrophication of near-coastal marine environments of Rhodes. Trophic conditions in two sediment sections from the north- and middle eastern coast of the Island of Rhodes (Kallithea and Pefka E; Fig. 3.1) have also been described as rather mesotrophic during the Pleistocene (Rasmussen and Thomsen, 2005; Milker et al., 2019). Thereafter the Eastern Mediterranean Sea surrounding the island was dominated by species such as *C. pseudoungerianus*, *U. peregrina*, *C. carinata* s.l., *C. obtusa* and *G. subglobosa* (Figs. 3.5-3.7; Rasmussen and Thomsen, 2005; Milker et al., 2019).

It is widely accepted that the most important factors controlling the benthic foraminiferal distributions are the flux of organic matter and the dissolved oxygen content at the seafloor and in pore waters (e.g., de Rijk et al., 2000; Jorissen et al., 2007). The so-called TR(trophic)OX(oxygen) model (Fig. 1.1) suggests that mesotrophic environments are characterized by the highest diversity with the co-occurrence of epifaunal to deep infaunal taxa (Jorissen et al., 1995; de Rijk et al., 2000; Jorissen et al., 2007). The Agathi Beach and Lardos sections show a high mean diversity of H = 3.3 (Figs. 3.6 and 3.7). For comparison, the diversity in the Pefka E section shows similar values between H = 2.0 and 3.3 (Milker et al., 2019). Mean diversity in the modern mesotrophic Gulf of Lions (Western Mediterranean) is comparable with H between 2.3 and 2.4 (Schmiedl et al., 2000). Thereafter, mesotrophic conditions in the abovementioned studies are characterized by diversity values between H = 2 to 3.3.

The Pleistocene records further show a co-occurrence of epifaunal and infaunal taxa, indicative of oligotrophic/high oxygen and eutrophic/low oxygen conditions, respectively. The most dominant species in the studied sections comprise *C. pseudoungerianus*, *C. carinata* s.l., *U. auberiana*, *U. peregrina*, *G. subglobosa*, *C. obtusa*, *B. aculeata*, *H. balthica*, *G. praegeri*, *C. mundulus*, and

B. striata (Figs. 3.6 and 3.7). Oligotrophic and high oxygen indicator species include *C. pseudoungerianus*, *G. subglobosa*, *G. praegeri* and *C. mundulus* (van der Zwaan, 1982; Jorissen, 1987; Kaiho, 1994; Schmiedl et al., 1997; Altenbach et al., 1999, 2003; Den Dulk et al., 2000; Singh and Gupta, 2010) while as eutrophic and low oxygen indicator species *C. carinata* s.l., *U. auberiana*, *U. peregrina*, *C. obtusa*, *B. aculeata*, *H. balthica* and *B. striata* were classified (Lutze and Coulbourn, 1984; Rathburn and Corliss, 1994; Schmiedl et al., 1997, 2000; de Rijk et al., 2000). On average, the benthic fauna of Agathi Beach includes 44% eutrophic and 38% oligotrophic taxa and Lardos represents 57% eutrophic and 30% oligotrophic taxa. Milker et al. (2019) found a similar faunal distribution with an average of 50% eutrophic/low oxygen tolerant taxa and 43% oligotrophic taxa in the Pefka E section on Rhodes.

Especially high abundances of *C. carinata* s.l., *H. balthica* and *Bulimina* species in the sections may indicate relatively higher food levels compared to similar environments of the modern Eastern Mediterranean Sea, where these species are nearly absent at comparable water depths (de Rijk et al., 1999, 2000). These species are known to be sensitive to pulses of fresh organic matter (e.g., Schmiedl et al., 1997, 2000; Fontanier et al., 2003; Bartels-Jónsdóttir et al., 2006). The relative abundance of these species as well as the high amount of eutrophic/low oxygen tolerant indicator species in Agathi Beach and Lardos might be indicative for an enhanced food supply due to increasing river discharge from the Island of Rhodes and the bordering mainland and can be compared to the modern mesotrophic Adriatic Sea. Most of the dominant species studied here, recently occur in the central and southern Adriatic Sea (Jorissen, 1987). The higher primary production in the Adriatic Sea compared to the Eastern Mediterranean Sea can be explained by the supply of nutrients from the discharge of the Po River and an anticlockwise circulation, which transports these nutrients southwards (Revelante and Gilmartin, 1976). A similar fauna like those of Agathi Beach and Lardos was also observed in the Kallithea and Pefka E sections (Rasmussen and Thomsen, 2005; Milker et al., 2019). The similar benthic faunal distribution of these studies and our observations imply that the trophic conditions in upper slope and outer shelf environments off the Island of Rhodes were mesotrophic during large parts of the Pleistocene. Likewise, it is concluded, that those conditions were regionally distributed along the entire eastern coast of the island.

3.5.3 Response of paleo-bottom water ecosystems to climate and oceanographic changes

The long-term increase of the $\delta^{18}O$ values at Agathi Beach show an opposite trend to water depth (Fig. 3.9), while the long-term decrease of $\delta^{18}O$ values at Lardos parallels the decrease of the paleo-water depth (Fig. 3.10). The latter, agrees well with Tanhua et al. (2013) who found a decrease of

~0.5–0.7 ◦C temperature per 100 m in the modern Mediterranean Sea, which equals an increase of 0.1‰ per 100 m water depth change (Epstein et al., 1953). Assuming similar conditions during the Early Pleistocene, this would result in lighter $\delta^{18}O$ values with shallowing water depth that is also indicated in Lardos. The $\delta^{18}O$ record of Agathi Beach however, follows the opposite trend. One explanation might be, that the environmental conditions of Agathi Beach were not only influenced by precessional changes but also by orbital fluctuations in the obliquity band. Accordingly, warm conditions and associated lower $\delta^{18}O$ values are superimposed on the influence of water depth. Both, $\delta^{18}O$ records reveal orbital variations similar to those of the LR04 stack (Lisiecki and Raymo, 2005), although the absolute $\delta^{18}O$ values are lower and the glacial-interglacial amplitudes are higher than in the LR04 stack (Supplement 3.1; Appendix C). This is interpreted to reflect relatively warm temperatures of shelf and intermediate waters in the Mediterranean Sea and high sensitivity of Eastern Mediterranean Sea surface water salinity to orbital hydrological changes (Rohling et al., 2015). Spectral analysis of the Agathi Beach and Lardos $\delta^{18}O$ records reveal peaks at 44 ka and 8 ka and at 139 ka, 42 ka and 8 ka, respectively, indicating the influence especially by obliquity related orbital fluctuations on the isotope record (Supplement 3.7).

In both sections, the faunal distribution is highly influenced by bathymetric effects, which are caused by tectonically induced vertical motions (see chapter 3.5.4). In Agathi Beach, the shallower and older sediments are dominated by *C. pseudoungerianus*, a species indicating well-ventilated waters and a moderate supply of organic material (van der Zwaan, 1982; Den Dulk et al., 2000; Singh and Gupta, 2010). Towards deeper waters this species is replaced by a more infaunal assemblage, dominated by *U. peregrina*, *C. carinata* s.l., and *G. subglobosa*. Similar bathymetric effects are also noticeable in Lardos. At this location, sediments from deeper water depths are dominated by *C. pseudoungerianus*, *U. peregrina*, and *C. pachyderma*, while the assemblage shifts towards a combination of infauna and shelf fauna, such as *C. carinata* s.l., *U. peregrina*, and *A. mamilla* (see Supplement 3.6), together with a shallowing of the water depth. The intensive shallowing of the Lardos section results in an increasing eutrophication of the bottom waters, explaining the increasing infauna. Why both sediment sections follow an opposite trend remains unclear. One explanation might be, that the depositional environment of the Agathi Beach section reached the Levantine Intermediate Water (LIW), contained less oxygen, favoring the infaunal preservation of organic matter in the sediment and the generation of niches. The reconstructed paleo-water depths of Lardos, however, show very shallow water depth of <100 m, so that riverine input of the island likely had a larger effect on the deposition of the section. Additionally, Lardos was deposited approximately 1 Ma after Agathi Beach, so that the ventilation and characteristics of the surface and intermediate waters might have been changed over time.

Periodic fluctuations in eutrophic/low oxygen tolerant and oligotrophic species, and to some extend in the most dominant taxa, is observed in both, the Agathi Beach and Lardos sections. A strong increase of eutrophic/low oxygen tolerant indicator species at Agathi Beach of up to 72% between 1931 and 1921 ka and 1889 to 1886 ka and at Lardos of up to 93% between 443 and 431 ka are noticeable (Figs. 3.9 and 3.10). The most prominent taxa in these time intervals comprise *B. spathulata* (at Lardos), *R. phlegeri*, *B. marginata* and *B. striata* (at Agathi Beach). In greater detail, *R. phlegeri* occurs at Agathi Beach only during periods with the highest abundance of eutrophic/low oxygen tolerant indicator species (Fig. 3.6). This species is a shallow to intermediate infaunal species that prefers environments with a relatively high organic matter content and is typical for poorly oxygenated sediments (Guimerans and Currado, 1999; Bartels-Jónsdóttir et al., 2006). In the Western Mediterranean Sea and in sediments close to the Tagus River (Portugal), *R. phlegeri* shows increased abundance in ecosystems influenced by river plumes and its abundance increases during times of high river run-off (Bartels-Jónsdóttir et al., 2006; Frezza and Carboni, 2009; Milker et al., 2009; Mojtahid et al., 2009). Likewise, the occasional occurrence of *B. marginata* indicates changing environmental conditions at the sea bottom. This species also prefers a high and steady organic matter flux and is tolerant to low oxygen conditions (Lutze and Coulbourn, 1984; Alavi, 1988; Sen Gupta and Machain-Castillo, 1993; Gooday, 1994). *Brizalina spathulata*, which occurs with up to 87% in the upper part of the Lardos section, is an indicator for a high organic matter influx, often in combination with dysoxic conditions (Gooday, 1994; Bernhard and Sen Gupta, 1999; Jorissen, 1999). This species is associated with sapropel formation and has been reported to be the last species disappearing before the total oxygen deficiency in Pliocene sapropels was reached (Jonkers, 1984).

The strong dominance of *B. spathulata* in the upper part of the Lardos section clearly indicates an oxygen depletion as a result of increased surface production. Titschack et al. (2013) found evidence of delta toe deposits within this potentially dysoxic layer in the uppermost part of the Lardos section. This high amount of riverine input caused most likely an increase in productivity and a resulting oxygen consumption at the sediment-water-interface. According to our age model, the sediments of the upper part of the Lardos section were deposited during glacial MIS 12. The eustatic sea level lowering of up to 126 m after Bintanja and van de Wal (2008) (see also Rohling et al., 1998, 2014; Siddall et al., 2003; Bintanja et al., 2005; Lisiecki and Raymo, 2005) in combination with the ongoing tectonic uplift gradually led to increasingly restricted conditions prone to local eutrophication. The recovery of the oxygen content is indicated by the re-occurrence of some species such as *Globocassidulina subglobosa*, *Cassidulina carinata* s.l. and *Hyalinea balthica* at the uppermost top of the section.

The two low-oxygen intervals in Agathi Beach are indicated by the strong increase in eutrophic/low oxygen tolerant indicator species. Additionally, the older of these layers at approximately 1931 ka contains several, well-preserved fish remains (Fig. 3.2), suggesting the temporal presence of at least dysoxic conditions. Apart from the dominant taxa (Fig. 3.6), the benthic foraminiferal assemblage within the sapropels comprises species such as *Elphidium complanatum*, *Elphidium complanatum thyrreanum*, *Globobulimina affinis* and others (Supplement 3.5), which are absent or nearly absent in other parts of the section. The sudden presence of typical shelf fauna like the genera *Elphidium* provides evidence that reworked shelf sediments were transported towards deeper waters. We argue that the transportation was mainly due to strong river run-off from the island caused by a humid climate during this time period. The subsequent oxygen depletion due to increased productivity is visible in the sharp increase in eutrophic/low oxygen tolerant taxa and in decreased diversity of the benthic foraminiferal fauna. The sudden increase of the relative abundance of *R. phlegeri* in both layers supports a riverine-influenced nutrient input. Nevertheless, even in the layer where fish remains were prominent and a strong depletion of oxygen is most likely, oligotrophic indicator species still occur with relative abundances of ~20%. Kroon et al. (1998) identified the sapropel event s51 in the ODP Leg 967 from the Eastern Mediterranean Sea at 1923 ka that correlates with the older sapropelic layer shown in our Agathi Beach record (Fig. 3.9). The ODP Leg 967 record, however, does not show a corresponding deep-water sapropel for the younger event starting at ~1889 ka. Due to the strong signal shown in the fauna and in the $\delta^{13}C$ values, we believe this event to be related to the sapropel s50 (1.872 Ma). An inaccuracy in the peak-to-peak correlation of our age model could be responsible for the offset in time. The elevated proportion of eutrophic/low-oxygen-tolerant taxa is generally associated with decreased epibenthic $\delta^{13}C$ values, particularly at Agathi Beach (Fig. 3.9). Various studies have shown that the dissolved inorganic carbon of both surface and sub-surface water masses decreased during humid intervals of sapropel formation, due to riverine influx of ^{13}C-depleted freshwater and stagnation of intermediate and deep-water masses (Casford et al., 2002; Grimm et al., 2015). In the near coastal ecosystems of Rhodes, epibenthic $\delta^{13}C$ values can be further depleted by locally enhanced productivity and related addition of ^{12}C due to remineralization of organic matter at the seafloor (Casford et al., 2002; Kuhnt et al., 2008; Ní Fhlaithearta et al., 2010).

The timing of the formation of low-oxygen deposits in near-coastal areas along the Island of Rhodes is in relation to the sapropel formation in the Eastern Mediterranean Sea. However, the deposition of the sapropelic layers is mainly influenced by local conditions, such as increased river run-off, resulting in higher productivity. Higher precipitation in the northern borderlands of the Eastern Mediterranean Sea during times of sapropel formation have already been shown by various

studies (Shaw and Evans, 1984; Rossignol-Strick, 1987; Wijmstra et al., 1990; Gogou et al., 2007; Kotthoff et al., 2008a,b; Triantaphyllou et al., 2016). The deeper environments off Rhodes were likely additionally influenced by the inflow of oxygen-depleted intermediate water masses from the Levantine and Aegean Seas (Zirks et al., 2019) but given the relatively shallow water depths, largely ranging between 50 and 400 m (Fig. 3.8), local eutrophication processes likely played a dominant role.

3.5.4 Paleo-water depth trends and tectonically induced vertical motions

The paleo-water depth estimates at Agathi Beach indicate a regressive trend at the base of the section followed by a general transgressive trend, while the Lardos section rather shows a long-term shallowing upward trend (Fig. 3.8). Global orbital-scale sea level changes at times of the deposition of the sections were estimated to a maximum amplitude of ~62 m between 1967.8 and 1827 ka and ~ 128 m between 750.7 and 427 ka (Bintanja and van de Wal, 2008). The maximum fluctuations in the uncorrected paleo-water depth estimates were noticeably higher with approximately 280 m and 560 m for Agathi Beach and Lardos, respectively (Fig. 3.8). This suggests that besides glacio-eustatic sea level fluctuations also vertical tectonic movements are recorded in our sediment sections.

Due to the position of Rhodes at a major plate boundary, changes in paleo-water depth, detected in the Pleistocene deposits, are dominated by tectonically induced vertical motions (Fig. 3.1). The LBF is known to represent the transition from a major (long-term) transgressive to a regressive phase during the Pleistocene with a maximum submergence of the eastern part of the island to bathyal depths (Hanken et al., 1996; Cornée et al., 2006; Titschack et al., 2013; Quillévéré et al., 2016). We show that the Agathi Beach section records the long-term transgressional phase, with a deepening of ~120 m between 1968 ka and 1827 ka (Fig. 3.8). Lardos represents the subsequent long-term regressional phase of the LBF, where the water depth shallows by ~156 m between 751 ka to 475 ka (Fig. 3.8). Titschack et al. (2013) found a similar shallowing for the Lardos section, based on the known depth distribution of for example corals, scaphopods and brachiopods. They concluded that the lower part of the section was deposited at water depths of ~320 m and the upper part around ~90 m. Cornée et al. (2019) showed that the eastern coast of Rhodes experienced two episodes of subsidence (2000 ka to 800 ka; 260 ka to 140 ka) and uplift (800 to 400 ka; since 33 ka) and already stated, that rates of vertical motions were rather high and comparable to forearc settings. Both, the findings from Agathi Beach and Lardos, are in agreement with the general timing of vertical motions suggested by Cornée et al. (2019).

Besides the long-term trends, both sections indicate short-term movements. The corrected paleo-water depth estimates of Agathi Beach clearly indicate two transitions from regression to transgression (Fig. 3.8), while the Lardos section indicate at least three cycles of uplift and subsidence (Fig. 3.8). Short-term vertical movements, recorded in the LBF, have also been described by Milker et al. (2019) and Quillévéré et al. (2019). Milker et al. (2019) assumed up to four cycles of transgression and regression in the Pefka E section with uplift- and subsidence rates between 4.2 mm a^{-1} and 10.3 mm a^{-1} (1.630–1.390 Ma; Fig. 3.8), and Quillévéré et al. (2019) observed three short-term cycles of uplift and subsidence with minimum rates of 6 mm a^{-1} in the younger sediments (1.10–0.850 Ma) of the northern Lindos Bay section. While Quillévéré et al. (2019) concluded that their rates are fairly overestimated, Milker et al. (2019) explained the high rates by the repeated occurrence of abrupt vertical motions, as a result of earthquakes. Even though the cause of the high rates of vertical motion is still a matter of debate, similar rates have been found elsewhere in the Eastern Mediterranean Sea. In southern Turkey, short-term uplift rates have been found and estimated to 3.2–3.4 mm a^{-1} (Öğretmen et al., 2018), while another study from the western coast of the island of Crete found short-term subsidence rates of 2.6–3.2 mm a^{-1} (42 ka to 23 ka), followed by uplift rates as high as 7.7 mm a^{-1} (23 ka to present; Tiberti et al., 2014). Since vertical motions with similar rates have also been reconstructed from different areas of the Eastern Mediterranean, we consider our rates as plausible. The wide range of rates at different locations along the eastern coast of Rhodes, however, provides further evidence, that the individual depocenters of Rhodes experienced differential vertical motion histories.

3.6 Conclusion

We investigated two marine sediment successions of Early and Middle Pleistocene age from the middle eastern coast of the Island of Rhodes. The benthic foraminiferal, and stable isotope data suggest the influence of regional and local hydrological and trophic changes on the benthic ecosystems. The paleo-water depth reconstructions imply regional tectonic motions at the middle eastern coast during the Pleistocene. Our main findings can be concluded as followed:

- The combined bio- and isotope stratigraphy revealed that the Agathi Beach section was deposited between 1968 ka and 1827 ka B.P. and represents one of the older LBF deposits outcropping on Rhodes. Lardos can be interpreted as the so far youngest LBF section representing an age between 751 ka and 427 ka B.P.
- We identified intervals of low-oxygen to dysoxic conditions in both, Agathi Beach and Lardos, sections. The two intervals in the Agathi Beach section co-occur with the sapropel-forming events s51 and possibly s50 in the Eastern Mediterranean Sea. The relatively

shallow water depths, make a direct impact of oxygen depleted deep waters from the Eastern Mediterranean Sea unlikely. The local occurrence of the sapropelic layers is rather influenced by local climatic conditions. The inferred temporal increase of river-run off and resulting rise in productivity and oxygen consumption can be related to a more humid climate linked to insolation-driven changes of precipitation in the Eastern Mediterranean. The prominent dysoxic environment in the Lardos section reflects a restricted depositional environment, particularly prone to riverine nutrient and related organic matter input.

- Long-term tectonic vertical motions were identified in both sections. While the reconstruction of Agathi Beach reflects a long-term transgressive phase of ~120 m, Lardos shows a long-term regressive trend of ~156 m. Additionally, Agathi Beach indicates two short-term cycles and Lardos reveals up to three short-term cycles of uplift and subsidence with an average uplift rate of 2.5 mm a^{-1} and 4.3 mm a^{-1}, respectively and average subsidence rates of 2.8 mm a^{-1} and 4.0 mm a^{-1}, possibly triggered by earthquakes. The identification of short-term vertical motions proves that the middle eastern coast of the island of Rhodes has been affected in a much more dynamic way than previous reconstructions of uplift and subsidence rates have suggested.

Acknowledgements

Sampling of both sections were performed in two field campaigns in 2001 and 2003 funded by the Deutsche Forschungsgemeinschaft (DFG) project Fr 1134/7. Tsampikos Athanasas from Lardos, R.G. Bromley and U. Asgaard (both Copenhagen) are gratefully acknowledged for their support during the field campaigns on the Island of Rhodes. Edith Maier and Jutta Richarz for her technical support during laboratory work and the MSc student Gerassimos Diamantis is thanked for his contribution in the calcareous nannofossil analyses. The Deutsche Forschungsgemeinschaft (DFG) financially supported the study of Yvonne Milker (MI 1508/9-1) and Gerhard Schmiedl (Schm 1180/25-1). The study is a contribution to the "Center for Earth System Research and Sustainability (CEN)" of Universität Hamburg. Sampling took place with the permission of the Director of the Institute of Geology and Mineral Exploration, Athens, Greece.

Data availability:

Supplementary material referred to in this chapter was published together with the manuscript and is available at *Palaeogeography, Palaeoclimatology, Palaeoecology* (doi: 10.1016/j.palaeo.2023.111980):

Supplement 3.1: Correlation of $\delta^{18}O$ and $\delta^{13}C$ values of Agathi Beach and Lardos with the benthic LR04 stack of Lisiecki and Raymo (2005). Modified version available in Appenix C of this work.

Supplement 3.2: Genera grouped into eutrophic or oligotrophic taxa after Corliss and Chen (1988) and Milker et al. (2019).

Supplement 3.3: Evaluation of transfer function. Modified version available in Appenix D of this work.

Supplement 3.4: Relative abundance of nannofossils in the Agathi Beach section

Supplement 3.5: Census counts of Agathi Beach

Supplement 3.6: Census counts of Lardos

Supplement 3.7: Methods and Results of spectral analysis

Appendix B: Carbon and oxygen stable isotope data.

4 Humid climate phases on the Island of Rhodes (Greece) during the late Pliocene at times of sapropel formation

Daniela Eichner, Gerhard Schmiedl, Jürgen Titschack, Malu Ferreira, Maria Triantaphyllou, Nils Andersen, Yvonne Milker

Abstract

The Island of Rhodes, located in the Eastern Mediterranean Sea, is affected by an active convergent plate boundary. In this context, marine sediments of Plio-Pleistocene age have been uplifted and are outcropping along the eastern coast of Rhodes. These archives provide an excellent opportunity to unravel the hydrological and climatic changes of the region during the late Pliocene. Our results provide new evidence for a more humid climate and an increased precipitation on the island during times of Northern Hemisphere summer insolation maxima and related sapropel formation in the Mediterranean deep sea. The periodic occurrence of eutrophic conditions at the shelf and upper slope off Rhodes is indicated by the recurrent dominance of eutrophic indicator species (of the genera *Bolivina*, *Eubuliminella* and *Rectuvigerina*), simultaneously with a decline in diversity and oligotrophic indicator species. These conditions resulted from higher primary productivity, triggered by local effects, such as enhanced precipitation and river run-off, which consequently favors the appearance of eutrophic taxa. The $\Delta\delta^{13}C$ records of the epibenthic foraminifera *Cibicidoides pseudoungerianus* and the shallow infaunal species *Uvigerina peregrina* indicate a slight productivity decrease towards younger times.

This chapter is published as peer reviewed article in *Marine Micropaleontology* (doi: j.marmicro.2024.102341) and is a slightly modified version.

4.1 Introduction

The Island of Rhodes is a unique place to study marine sediments of Plio-Pleistocene age that have been uplifted and are outcropping at scattered locations along the eastern coast of the island (Fig. 4.1). The good accessibility as well as the good preservation of the microfossil-rich marine sediments provide an excellent opportunity to study the influence of hydrological and climatic changes on near-coastal benthic ecosystems.

The analysis of fossil benthic foraminiferal assemblages is a commonly used proxy for paleo-ecological and environmental reconstructions (e.g., Gooday, 2003; Jorissen et al., 2007; Schmiedl et al., 2023) as they are found in the entire marine realm, with individual taxa sensitive to specific conditions at the seafloor. The amount and quality of food, arriving at the seafloor in deep-sea environments, and oxygen are considered being the most important factors, controlling the foraminiferal assemblage (e.g., Corliss, 1985; Murray, 1991; Jorissen et al., 1995; Schmiedl et al., 2023). The benthic foraminiferal distribution can be characterized by the so-called TR(Trophic)OX(Oxygen)-model of Jorissen et al. (1995) (Fig. 1.1). According to this model, epifaunal species are rather found in food-limited and oxic environments, while a high occurrence of infaunal species is characteristic for eutrophic and oxygen-limited conditions at the seafloor (Jorissen et al., 1995). The distribution, diversity and density of benthic foraminifera in shallow-water habitats can additionally be influenced by other factors, such as substrate, current velocity, turbulence of surface waters, vegetation, temperature and salinity (e.g. Sen Gupta, 1999; Schönfeld, 2002; Gooday, 2003; Murray, 2006).

The stable isotope composition of benthic foraminifera is a widely used proxy to reconstruct paleoceanographic changes. While the $\delta^{18}O$ signal is commonly used for isotope stratigraphy and for the estimation of past ice volume changes (e.g., Shackleton and Opdyke, 1973; Adkins et al., 2002; Marchitto et al., 2014), the $\delta^{13}C$ signal is used as a tool to reconstruct changes in the deep-sea circulation, bottom-water oxygen concentration and organic carbon fluxes to the seafloor (e.g., Curry and Lohmann, 1982; Zahn et al., 1986; McCorkle and Emerson, 1988; Schmiedl and Mackensen, 2006; Kuhnt et al., 2008). The epifaunal $\delta^{13}C$ values represent the $\delta^{13}C$ signal of the dissolved inorganic carbon (DIC) of the ambient bottom water (Duplessy et al., 1984; Zahn et al., 1986; Gottschalk et al., 2016; Schmittner et al., 2017; Mackensen and Schmiedl, 2019), while the shallow infaunal $\delta^{13}C$ values are rather reflecting the $\delta^{13}C$ signal of pore water DIC (McCorkle et al., 1990; Mackensen and Licari, 2004). Therefore, the offset between epifaunal and infaunal $\delta^{13}C$ signals has been used as a proxy for the estimation of organic-matter fluxes and remineralization (Hoogakker et al., 2015; Gottschalk et al., 2016; Theodor et al., 2016a; Penaud et

al., 2022). Also, Zahn et al. (1986) stated a close relation of the $\Delta\delta^{13}C$ fluctuations with the accumulation rates of organic carbon and highlighted its great potential to document the paleo-productivity changes in the ocean.

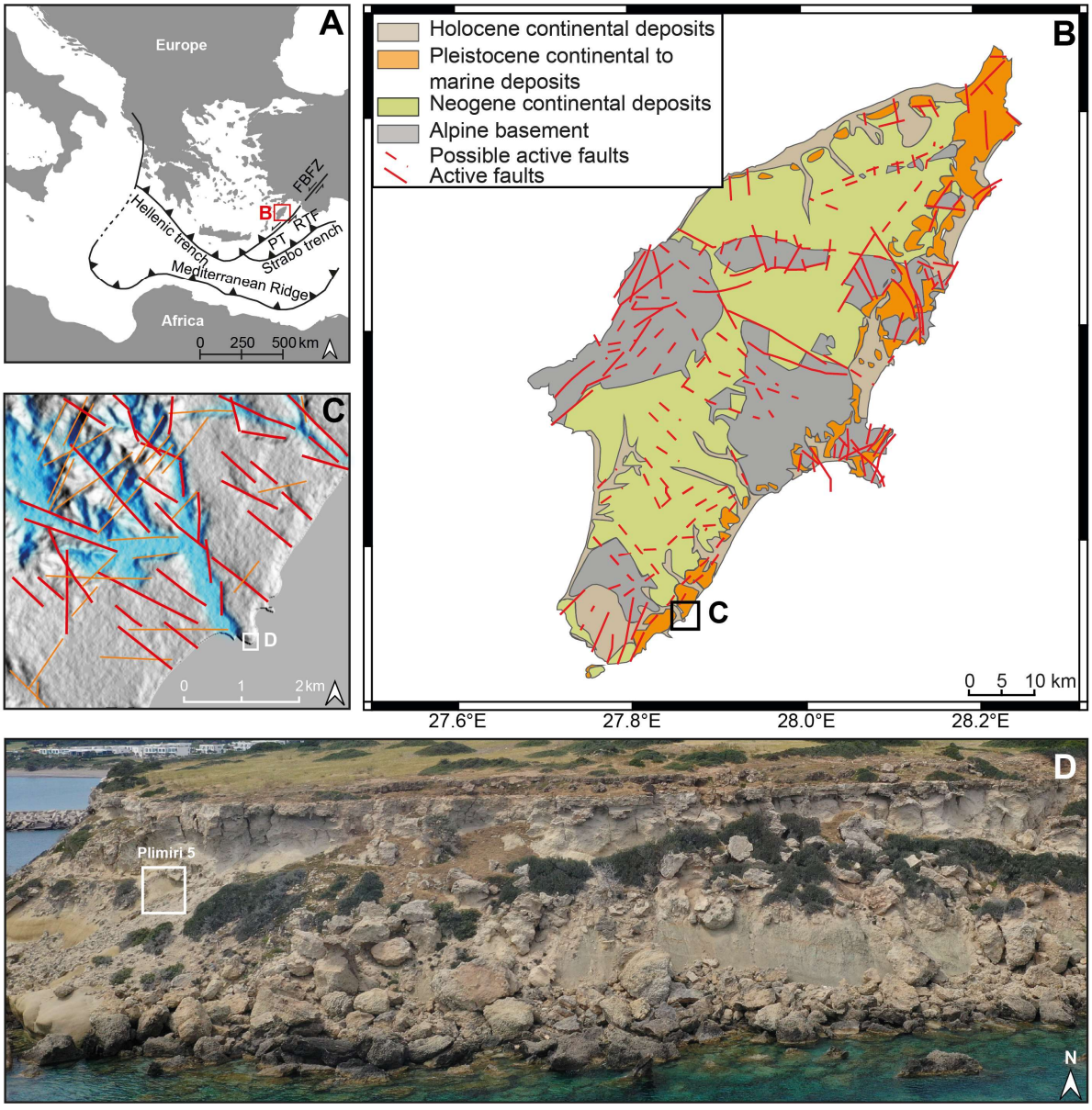

Figure 4.1. A. Overview of the Eastern Mediterranean region with its main tectonic features after Dilek and Sanvol (2009) and Görgun et al. (2014). FBFZ: Fethiye-Burdur fault zone; PT: Pliny trench; RTF: Rhodes transform fault. **B.** Simplified geological map of the Island of Rhodes with its main tectonic features after Lekkas et al. (2000) (figure modified after Cornée et al. (2019); Map created with Q GIS 3.26.1). **C.** Digital Elevation Model (DEM) of the Plimiri area. Red lines show the north-west orientated lineaments, orange lines the north-east orientated lineaments. Indicated in blue is the recent river system. **D.** Overview photo of the Plimiri headland. The white box marks the position of the Lindos Bay Formation of the Plimiri 5 section.

In the Eastern Mediterranean Sea, organic-rich layers, so-called sapropels, formed periodically since the Neogene (e.g., Rossignol-Strick, 1983; Hilgen, 1991; Lourens et al., 1996a; Kroon et al., 1998; Grant et al., 2022). Their occurrence is in close relation to the Northern

Hemisphere summer insolation maxima (Hilgen, 1991; Lourens et al., 1996a) and is, thus, related to the minimum values in the precessional band (e.g., Rossignol-Strick et al., 1982; Rossignol-Strick, 1983; Hilgen, 1991; Kroon et al., 1998; Rohling et al., 2015). At times of summer insolation maxima, the African monsoon is intensified, leading to an increased river run-off of the Nile River, and other North African and Mediterranean rivers (Rossignol-Strick et al., 1982; Rossignol-Strick, 1983; Cramp et al., 1988; Hilgen, 1991; Rohling and Hilgen, 1991; Kroon et al., 1998). The enhanced addition of freshwater to the Mediterranean Sea results in a density stratification, and reduction of deep-water ventilation. The sapropel formation in the past is believed to result from a combination of anoxic conditions at the deep seafloor and increased primary production (e.g. Rohling, 1991; Passier et al., 1999; Emeis et al., 2000), resulting in the increment of organic matter preservation. However, the general pattern of sapropel deposition might differ due to water depth and variations in site-specific environments such as productivity (Rohling et al., 2015).

Enhanced winter rainfall in phase with the African monsoon and Mediterranean sapropel formation has also been reported for the northern borderlands of the Eastern Mediterranean Sea (e.g., Rohling et al., 2002; Casford et al., 2003; Gogou et al., 2007; Marino, 2008; Wagner et al., 2019). Especially for the depositional period of the most recent sapropel S1, various studies indicate a warmer and more humid climate for the Aegean Sea (e.g., Kotthoff et al., 2008b; Triantaphyllou et al., 2009, 2016; Geraga et al., 2010), the Cilicia Basin (Shaw and Evans, 1984) and for the Libyan Sea (Triantaphyllou et al., 2010). The processes of Pliocene sapropel formation, such as their timing, intensity and preservation, have been studied on outcrops in Italy (e.g., Lourens et al., 1992, 1996a; Rio et al., 1997; Sgarrella et al., 2012) and on the island of Cyprus (e.g., Athanasiou et al., 2015, 2017), but also in deep-sea cores of the Eastern Mediterranean Sea (e.g., Emeis et al., 2000; Grant et al., 2022).

On the northeastern coast of the Island of Rhodes, Rasmussen and Thomsen (2005) found laminated units, containing a benthic fauna which is mainly associated with dysoxic conditions. These layers correspond to sapropel units of the Early Pleistocene. The authors concluded that these units were deposited during a warm and humid climate and represent shallow-bathyal sapropel-extensions from strong deep-sea sapropel events. Likewise, Milker et al. (2019) and Eichner et al. (2024a) found periodic changes in Early Pleistocene benthic foraminiferal assemblages at the middle eastern coast of the Island of Rhodes during times of Northern Hemisphere summer insolation maxima and attributed these changes to transient phases of enhanced freshwater and nutrient input.

Until now, evidence for orbital-induced climate changes that affected Rhodes during the Pliocene is missing and information on local and regional responses to global orbital forcing and the effects on near-shore environments are still limited. To fill this gap, we present information about strong local hydrological and climatic changes during times of Pliocene sapropel formations in near-shore environments at the southern part of the Island of Rhodes. Specifically, we explore the response of the benthic foraminiferal assemblages and diversity to local variations in surface-water eutrophication and related organic matter fluxes to the seafloor.

4.2 Study area

The Island of Rhodes is located at the eastern end of the Hellenic forearc (Fig. 4.1A). Its proximity to an active subduction zone between the African and the Eurasian plates, has shaped the island including extensive tectonic motions (Meulenkamp et al., 1972). Multiple faulting and erosion of the basement led to the formation of steep horst-graben systems, which formed isolated basins along the eastern coast of the island (Mutti et al., 1970; Hanken et al., 1996). Additionally, tectonically driven vertical motions led to multiple phases of uplift and subsidence of the eastern coast of Rhodes. These movements are mainly related to a southward and northward tilting of the island and consequently resulted in a major long-term cycle of transgression and regression during the Plio-Pleistocene (Hanken et al., 1996; Cornée et al., 2006a; van Hinsbergen et al., 2007; Titschack et al., 2013). During these vertical motions, brackish to marine sediments deposited in isolated basins, formed by the horst-graben systems, reflect major and minor tectonically driven relative sea level changes. These sediments have finally been uplifted and are now outcropping in scattered locations along the eastern coast of the Island of Rhodes. They have been classified as the Rhodes Synthem and are subdivided into three transgressive formations (Kolymbia, Lindos Bay and St. Paul's Formation) and one regressive formation (Cape Arkhangelos Formation) (Titschack et al., 2013; Cornée et al., 2019).

The here studied marine sediments of the Lindos Bay Formation (LBF) outcrop along the eastern coast of Rhodes at various locations and provide a well-preserved fossil record. These sediments capture a major transgression-regression cycle (Titschack et al., 2013; Milker et al., 2017; Cornée et al., 2019), as well as several small-scale cycles of transgression and regression (Milker et al., 2019; Quillévéré et al., 2019; Eichner et al., 2024a). The southernmost, and here studied, outcrop of the LBF on Rhodes is located at a prominent headland east of the Plimiri settlement (Fig. 4.1B and D). The studied section (35°55'47"N; 27°51'43"E) comprises 6.7 m of the LBF, referred to as Plimiri 5 by Nelson et al. (2001). The LBF is characterized by blue-grey calcareous marls, with up to three interbedded coarse-grained carbonate layers of up to 110 cm thickness (Fig. 4.2). Any

laminated, dark sediment layers are not visible in the outcrop. The section further records the transition from the underlying Kolymbia Formation into the basal LBF in the lowermost part, while the erosive top of the section is overlain by the Lindos Acropolis Synthem (Nelson et al., 2001; Titschack et al., 2008; Fig. 4.2).

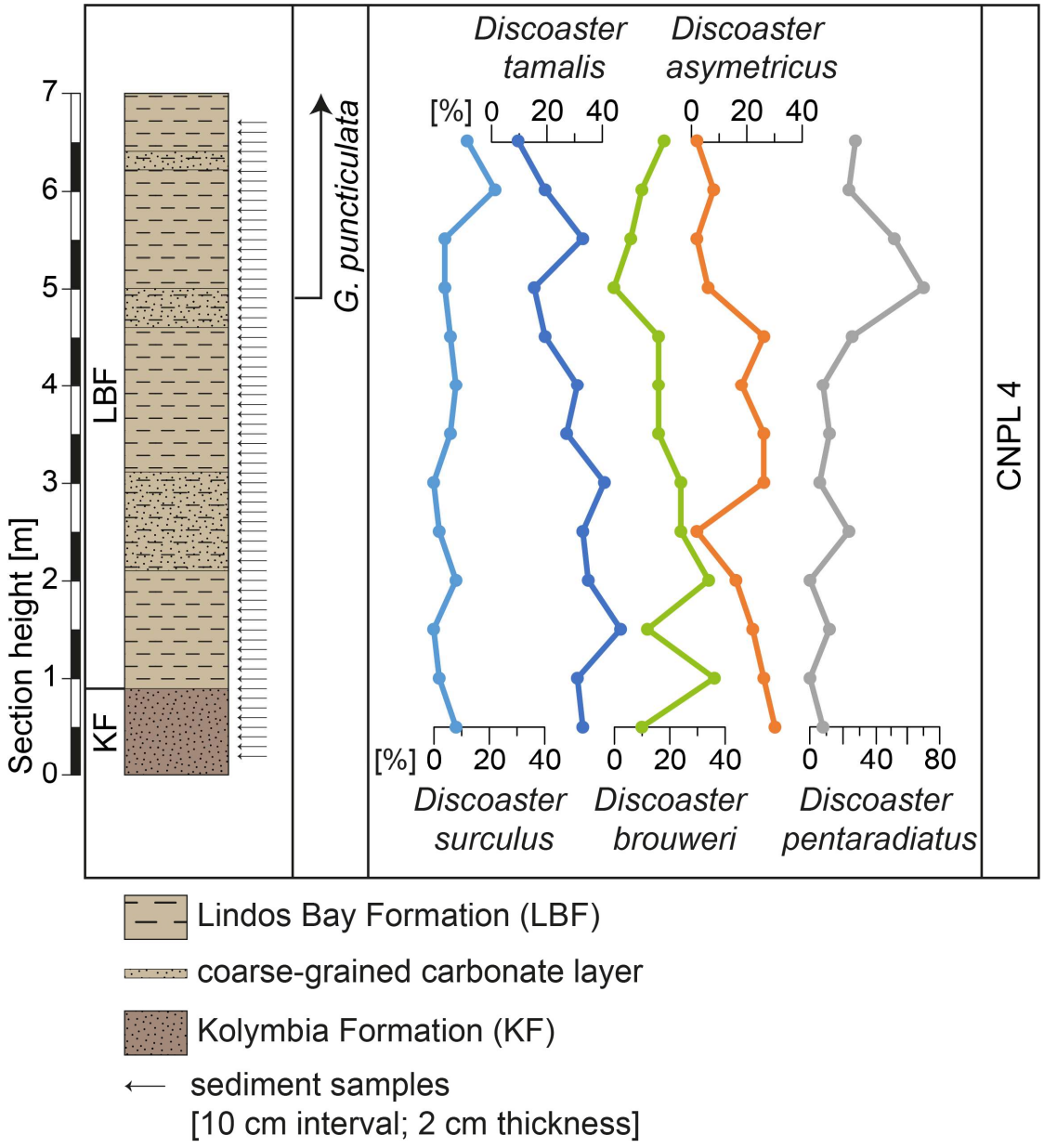

Figure 4.2. Simplified lithology of the Plimiri 5 sediment section, the first re-occurrence of the planktonic foraminifera *Globoconella puncticulata* (3.31 Ma; Lourens et al., 1996a) and relative abundances of calcareous nannofossils.

4.3 Methods

4.3.1 Chronostratigraphic framework

The stratigraphic framework is based on a combination of biostratigraphic information and a cyclostratigraphic approach. Biostratigraphic information was obtained from the distribution of calcareous nannofossils in a total of 13 samples taken at 50 cm resolution (Fig. 4.2), following the standard smear slide techniques for calcareous nannofossil analysis (Perch-Nielsen, 1985; Bown and Young, 1998). The samples were examined by using a LEICA DMLSP light microscope and 1250× magnification.

Further biostratigraphic information was obtained from the re-occurrence of the planktic foraminifer *Globoconella puncticulata* at 3.31 Ma (Lourens et al., 1996b; Fig. 4.2). As *G. puncticulata*/*G. bononiensis* disappear and re-occur several times between 3.31 and 2.9 Ma (Lourens et al., 1996b; Sprovieri et al., 2006), we further validated our age model by checking the samples for *Sphaeroidinellopsis* spp. which has its last occurrence at 3.21 Ma (Sprovieri et al., 2006). Specimens of the *Sphaeroidinellopsis* group were recorded in various samples across the entire section, so that we are confident to use the tie point of 3.31 Ma for *G. puncticulata*. Using the first re-occurrence of *G. puncticulata* as a basis, the filtered time series of the combined relative abundance of the eutrophic indicator benthic foraminifera was correlated to the Northern Hemisphere (65°N) summer insolation (June 21; Laskar et al., 2004). Blackman-Tukey spectral analyses revealed a dominant period of 222.22 cm, which is assumed to represent the precession cycle (23-ka- cycle). For the comparison of the filtered precessional component of the Northern Hemisphere summer insolation, a Gaussian band pass filter, centered at 222.22 cm, was applied. The maxima of the combined relative abundance of the eutrophic indicator species was then correlated to the maxima of the Northern Hemisphere summer insolation, using the re-occurrence of *G. puncticulata* as a tie point and the software AnalySeries 2.0 (Paillard et al., 1996) for the correlations (Supplement 4.1A and Appendix C).

4.3.2 Foraminiferal investigations

During a field survey in 2001, a total of 67 sediment samples of the Plimiri 5 section were taken, each of 2 cm thickness and in 10 cm resolution. Prior to sampling, weathered material was removed from the surface to access fresh material. Sample preparation took place in 2022. Approximately 50 g of each sample was soaked in 10% hydrogen peroxide (H_2O_2) for one hour and subsequently wet-sieved over a 63 µm sieve. Five samples of the Plimiri 5 section were additionally soaked in a solution containing 50% Rewoquat W3690 and 50% Ethanol (96%) for one hour to break up these highly compacted samples and were subsequently wet sieved over a 63 µm sieve. Feldmeijer et al.

(2013) analyzed the effects of the H_2O_2 (10%) pretreatment to the isotopic composition of the foraminiferal test calcite and Jarochowska et al. (2013) studied the preservation of a Rewoquat pretreatment. Both did not find any significant influence on the foraminiferal test geochemistry and preservation, respectively. Afterwards all samples were dried at 40°C and dry-sieved over a 125 µm sieve.

The foraminiferal analysis was carried out on a representative split, using a micro-splitter, containing at least 300 benthic individuals. Jonkers (1984), Jones (1994), Rasmussen (2005) and Milker and Schmiedl (2012) were used for the identification on species level. For the case that the identification on species level was not possible, individual species were grouped into their genus. Species were further grouped (on genus-level) into eutrophic and oligotrophic taxa following Corliss and Chen (1988) and Milker et al. (2019) (see supplements of Milker et al., 2019 or Eichner et al., 2024a). The most dominant species were photographed with a scanning electron microscope (SEM; HITACHI TM4000Plus). The Shannon-Wiener biodiversity index H (Shannon and Weaver, 1949) of each sample was calculated with the software Past 4.07b (Hammer et al., 2001).

4.3.3 Oxygen and carbon stable isotope measurements

The stable oxygen and carbon isotope compositions were measured in a total of 42 samples of the epibenthic foraminifera *Cibicidoides pseudoungerianus* and in 66 samples of the infaunal species *Uvigerina peregrina*. Three specimens of *C. pseudoungerianus* and five specimens of *U. peregrina* were picked in the 250–355 µm fraction to avoid ontogenetic effects on the isotopic signal (Schmiedl et al., 2004; Theodor et al., 2016b). If samples were lacking enough specimens of the required size, additional tests from the fraction <250 µm were picked. All tests were soaked in ethanol and cleaned in the ultrasonic bath for five to eight seconds. Measurements were conducted at the Leibniz-Laboratory for Radiometric Dating and Stable Isotope Research at the University Kiel by using a Thermo Finnigan MAT 253 mass spectrometer connected to a Kiel IV carbonate preparation device. The analytical precision (standard external error) was better than ±0.08 ‰ for $\delta^{18}O$ values and ± 0.05 ‰ for $\delta^{13}C$ values and results are reported in per mil with respect to the Vienna Pee Dee Belemnite (VPDB) scale.

Because the isotopic values of tests in samples retrieved from an outcrop might have been altered by meteoric diagenesis, such as carbonate dissolution and/or precipitation by secondary calcite, the reliability of the isotopic compositions was checked by comparing the obtained data with data of other outcrop and soil carbonate data from Rhodes and marine sediment core data from the Eastern Mediterranean Sea of synchronously deposited sediments in carbon vs. oxygen

isotope cross plots (Supplement 4.1.B). The comparison exhibited no indication for any diagenetic influence.

As a proxy for paleo-productivity, the deviation between *C. pseudoungerianus* $\delta^{13}C$ and *U. peregrina* $\delta^{13}C$ (referred to as $\Delta\delta^{13}C$) is used. For a better visualization, the $\Delta\delta^{13}C$ data set has subsequently been smoothed by using a LOESS regression and by using the software Past 4.07b (Hammer et al., 2001).

4.4 Results

4.4.1 Bio- and cyclostratigraphy

The Plimiri 5 nannofossil sediment samples are characterized by the presence of common *Discoaster tamalis* (up to 48%) and *Discoaster pentaradiatus* (up to 70%), as well as the presence of *Discoaster asymmetricus* (up to 30%; Fig. 4.2). Based on this assemblage the entire section is assigned to the Neogene Nannoplankton (NN) 16 biozone of Martini (1971), which correlates to the Calcareous Nannofossil Zone (CNPL) 4 (3.81 Ma to 2.76 Ma) of Backman et al. (2012). Several samples also contain reworked specimens from the Oligocene and Early Miocene such as *Reticulofenestra hillae*, *Reticulofenestra floridana*, *Furcatolithus predistentus*, and *Sphenolithus belemnos*.

In the Plimiri 5 section, the planktic foraminifer *Globoconella puncticulata* firstly occurs at a section height of 4.9 m (Figs. 4.2 and 4.3), indicating the re-appearance of this species at 3.31 Ma (Lourens et al., 1996a) which was used as a tie point for the cyclostratigraphical correlation. According to the combined bio- and cyclostratigraphic information, the sediment section covers a time span of 67 kyrs, lasting from 3.36 Ma to 3.29 Ma B.P. (Supplement 4.1.A), covering approximately Marine Isotope Stages MG3 to M2 (Lisiecki and Raymo, 2005). The Plimiri 5 sediment section is therefore the oldest known outcrop of the LBF on the island and its base is considerably older than previously believed (Quillévéré et al., 2016; Eichner et al., 2024b). However, the great thickness of the layers with high abundances of eutrophic species may have resulted in uncertainties in the peak-to-peak correlation. Likewise, the age model does not take into account, that some layers might have experienced higher sedimentation rates than others, so that minor errors in the relative age assignment cannot be excluded. The $\delta^{18}O$ values of the infaunal species *Uvigerina peregrina* possibly allows to shift the age model towards one older precession cycle (see also chapter 4.5.2). However, an adjustment to the isotopic values would result in an offset of the reported re-appearance of *G. puncticulata* date of approximately 22 ka, which seems to be unrealistic.

According to our age model, sedimentation rates were 10.32 cm kyr^{-1} in the lower part and 9.07 cm kyr^{-1} in the upper part of the section (Supplement 4.1.A). Nelson et al. (2001) noted a deposition of the sediment in the outcrop with a dip of 15°NE, suggesting a slight overestimation of the sedimentation rates.

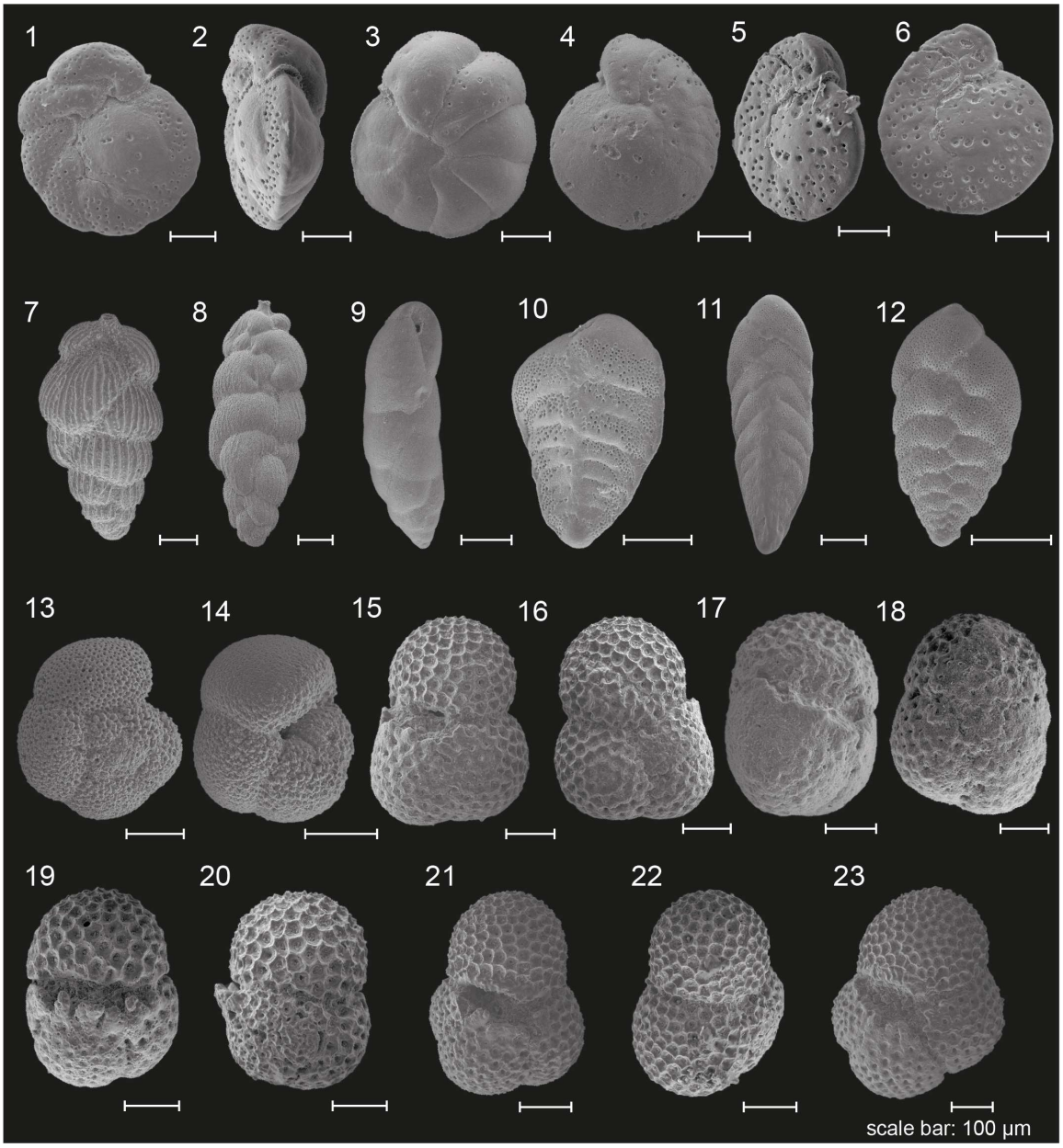

Figure 4.3. SEM photos of the most dominant benthic species and planktonic species used as age markers. 1-3 *Cibicidoides pseudoungerianus*, 4-6 *Cibicidoides* sp., 7 *Uvigerina peregrina*, 8 *Rectuvigerina bononiensis*, 9 *Eubuliminella exilis*, 10 *Bolivina spathulata*, 11 *Bolivina* cf. *antiqua*, 12 *Bolivina* sp. 1, 13-14 *Globoconella puncticulata*, 16-23 *Sphaeroidinellopsis* spp.

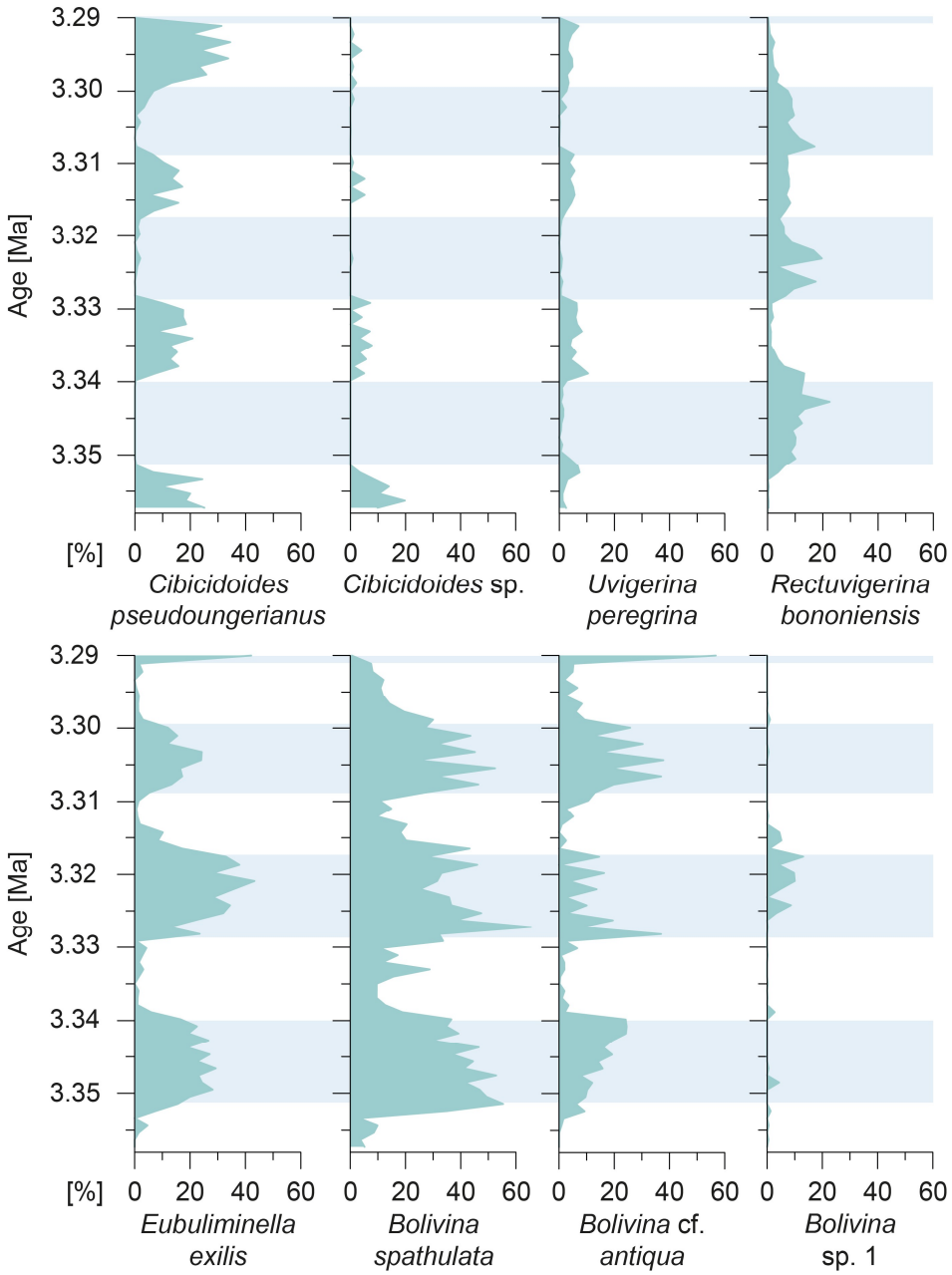

Figure 4.4. Relative abundances of most dominant species in the Plimiri 5 sediment sections against age. Blue bars indicate layers with high relative abundance of eutrophic species.

4.4.2 Foraminiferal assemblages

The 6.7 m long Plimiri 5 section contains a rich benthic foraminiferal fauna with a total of 146 taxa. The number of taxa varies between 6 and 57 taxa in individual samples. The most dominant species include *Bolivina spathulata* (1–66%), *Eubuliminella exilis* (0–43%), *Bolivina* cf. *antiqua* (0–57%), *Cibicidoides pseudoungerianus* (0–35%), *Rectuvigerina bononiensis* (0–23%), *Uvigerina peregrina* (0–11%), *Cibicidoides* sp. (0–20%) and *Bolivina* sp. 1 (0–10%) (Figs. 4.3 and 4.4; complete census counts in Supplement 4.2). *Bolivina spathulata*, *E. exilis* and *B.* cf. *antiqua* show high abundances of up to 66% within three intervals at approximately 3.35 Ma and 3.34 Ma (81 to 201 cm), 3.33 Ma to 3.32 Ma

(321 to 431 cm) and 3.31 Ma to 3.30 Ma (511 to 591 cm). Their abundances decrease drastically in the other parts of the section. *Eubuliminella exilis* and *B.* cf. *antiqua* also reach high abundances at the uppermost sample of the section, with 57% and 42% respectively. *Cibicidoides pseudoungerianus*, *U. peregrina* and *Cibicidoides* sp. are present with high abundances in intervals ranging from approximately 3.36 Ma to 3.35 Ma (21 to 71 cm), 3.34 Ma to 3.33 Ma (211 to 311 cm), 3.32 Ma to 3.31 Ma (441 to 501 cm) and 3.30 Ma to 3.29 Ma (601 to 661 cm) and are absent or only occur in low abundances in-between. *Rectuvigerina bononiensis* shows a low relative abundance until 3.35 Ma (71 cm) and between 3.33 Ma and 3.32 Ma (251 cm and 311 cm) and occurs with medium to high abundances between 5 and 20% in the other parts of the section. *Bolivina* sp. 1 only occurs in low abundance throughout the section, except in the interval 3.32 Ma to 3.31 Ma (351 to 451 cm), where it reaches its highest abundance of 10%.

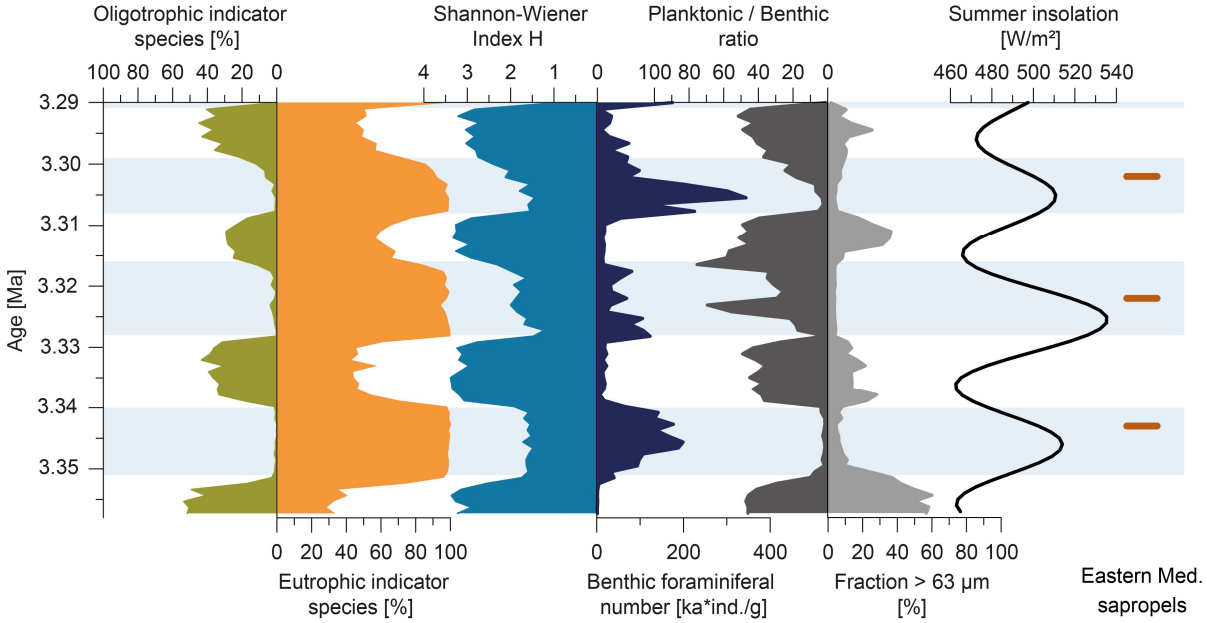

Figure 4.5. Relative abundances of oligotrophic (inverse axis) and eutrophic indicator species, diversity (inverse axis) and benthic foraminiferal number, planktonic/benthic ratio (inverse axis) and relative proportion of the fraction > 63µm of the sediment section and Northern Hemisphere summer insolation after Laskar et al. (2004). Blue bars mark the strong increase in eutrophic taxa and brown lines show the occurrence of Eastern Mediterranean sapropels after Emeis et al. (2000) and Athanasiou et al. (2017).

The relative abundance of eutrophic indicator species (e.g., *B. spathulata*, *E. exilis*, *B.* cf. *antiqua* and *R. bononiensis*) varies periodically across the section, with values ranging from 29% to 100% and highest abundances between 3.35 Ma and 3.34 Ma (81 and 201 cm), 3.32 Ma and 3.31 Ma (321and 431 cm) and 3.31 Ma and 3.30 Ma (511 and 591 cm) (Fig. 4.5). Oligotrophic indicator species (e.g., *C. pseudoungerianus* and *Cibicidoides* sp.) follow the opposite trend with relative abundances ranging from 0% to 54% (Fig. 4.5). The Shannon-Wiener Index has values between 0.88 and 3.39, while the trend follows that of the oligotrophic indicator species. The lowest value

of 0.88 is found at 3.29 Ma (671 cm) and the highest value of 3.39 at 3.33 Ma (251 cm). Benthic foraminiferal number (BFN) ranges between 1508 and 344,199 individuals per gram and fluctuate strongly within the section (Fig. 4.5). Highest numbers are generally reached simultaneously with the maximum relative abundance of eutrophic indicator species (Fig. 4.5).

4.4.3 Oxygen and carbon isotopes

The $\delta^{18}O$ values of the Plimiri 5 section range between 0.13‰ and 1.20‰ for the epifaunal foraminifer *C. pseudoungerianus* and between 0.35‰ and 2.26‰ for the shallow infaunal species *U. peregrina*. Highest values are reached at 3.32 Ma (441 cm) and 3.31 Ma (501 cm), respectively, while the lowest values are reached at 3.35 Ma (51 cm) and 3.34 Ma (161 cm) (Fig. 4.6). In average, $\delta^{18}O$ values of *U. peregrina* are approximately 0.76‰ higher than those of *C. pseudoungerianus*.

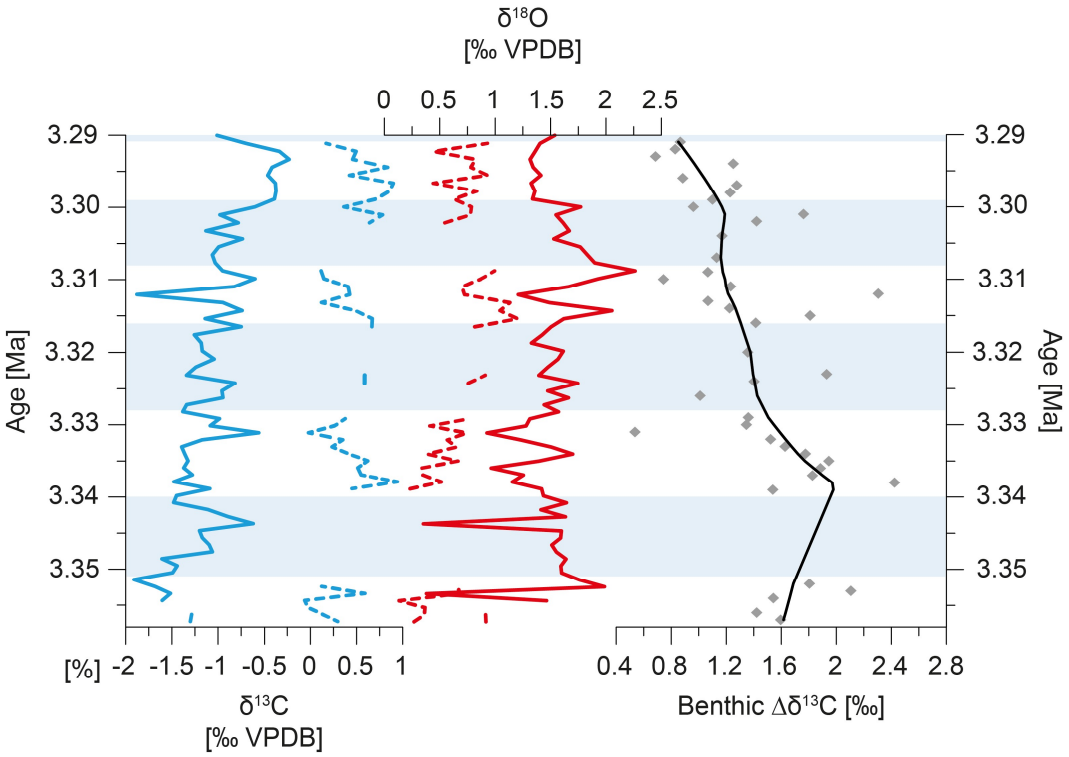

Figure 4.6. Stable isotopes ($\delta^{13}C$ and $\delta^{18}O$) of the shallow infaunal foraminifera Uvigerina peregrina (solid line) and epibenthic foraminifera Cibicidoides pseudoungerianus (dotted line). The benthic $\Delta\delta^{13}C$ is displayed as grey diamonds, black line is the smoothed data set, calculated by using a LOESS regression (using past 4.07b). Blue bars mark the strong increase in eutrophic taxa.

The $\delta^{13}C$ values range between -0.06‰ (3.35 Ma; 51 cm) and 0.94‰ (3.34 Ma; 221 cm) for *C. pseudoungerianus* and between -1.91‰ (3.35 Ma, 81 cm) and -0.23‰ (3.29 Ma; 641 cm) for *U. peregrina* (Fig. 4.6). Both $\delta^{13}C$ records show a trend towards higher values towards the top of the section. Opposite to the $\delta^{18}O$ record, the $\delta^{13}C$ values of *C. pseudoungerianus* are on average 1.40‰

higher than those of *U. peregrina*, whereas the difference between the $\delta^{13}C$ values of both species is slightly higher in the older parts of the section and then decreases towards younger times (Fig. 4.6).

4.5 Discussion

4.5.1 Benthic indicators of humid phases on the Island of Rhodes during times of Pliocene sapropel formation

The Plimiri 5 section is characterized by a recurrent and strong dominance of eutrophic indicator species, simultaneously with an increase of the benthic foraminiferal number and a decline in foraminiferal diversity and oligotrophic indicator species (Figs. 4.4 and 4.5). The most dominant species in these layers comprise *B. spatulata*, *E. exilis*, *B.* cf. *antiqua* and *R. bononiensis* (Fig. 4.4). These species are (shallow) infaunal benthic taxa that are indicative for high organic matter fluxes and are adapted to low oxygen conditions (Jonkers, 1984; Corliss, 1985; Jorissen, 1999; Fontanier et al., 2003; Bartels-Jónsdóttir et al., 2006). *Eubuliminella exilis* is abundant in a range of settings such as oxygen minimum zones, upwelling sites and sapropels (e.g. Jonkers, 1984; Caralp, 1989; Jannink et al., 1998; Jorissen, 1999; McKay et al., 2015). It is considered as an indicator for fresh organic matter input under low oxygen conditions (Jonkers, 1984; Caralp, 1989) and is used for the reconstruction of changes in the bottom-water oxygenation (McKay et al., 2015; Tetard et al., 2021). *Bolivina spathulata* and *B.* cf. *antiqua* can withstand a variety of conditions from well-oxygenated to oxygen-deficient (Jonkers, 1984; Rasmussen, 2005). Additionally, these species have been described in sediments that are rich in organic compounds (e.g., Hess et al., 2005; Duros et al., 2012). They have also been found in close relation to sapropel forming events, which resulted in dysoxic bottom waters in the Sea of Marmara (e.g., Jonkers, 1984; Alavi, 1988; Çağatay et al., 2000). *Rectuvigerina bononiensis* has been described in Pliocene deposits from the Eastern Mediterranean Sea where it was interpreted, together with *B. spathulata* and *E. exilis*, as an indicator for a high degree of bottom water stagnation (Jonkers, 1984). In summary, the foraminiferal composition in the Plimiri 5 section suggests periodic increases in nutrient supply and near-coastal primary production due to enhanced riverine input, triggered by elevated precipitation and/or by increased weathering on land. Likewise, the sedimentation rates of up to 10.32 cm kyr^{-1} of the Plimiri 5 section are higher than those reported from other LBF outcrops along the eastern coast of the Island of Rhodes (e.g., Milker et al., 2017; Eichner et al., 2024a), and may only be comparable to those calculated in the Lindos Bay section with ~8.6 cm kyr^{-1} to 10.2 cm kyr^{-1} (Quillévéré et al., 2019). The observed high sedimentation rates support our interpretation that the Plimiri 5 sediment section experienced periods of higher fluvial inputs when compared to sediment sections further north. The distinct periodicity of the eutrophic species suggests a close relation to precessional-

induced climate changes, and to the occurrence of sapropels in the deep basin of the Eastern Mediterranean Sea (Fig. 4.5). Although relative ages of Pliocene sapropels are rare, Emeis et al. (2000) identified three sapropels at 3.343 Ma, 3.322 Ma, and 3.302 Ma at ODP Site 966 (sapropel numbers u, 33, and 34, respectively), and red intervals at ODP Sites 969 and 964 at the same time. Likewise, the astronomically calibrated sapropel cycles 89 to 91 (Lourens et al., 1996a), also recorded by Athanasiou et al. (2017) at Pissouri outcrop on the island of Cyprus, correlates well with the layers with a high relative abundance of eutrophic species of the Plimiri 5 outcrop (Fig. 4.5) and with those found in Emeis et al. (2000).

Paleo-water depth reconstructions, based on an existing transfer function of Milker et al. (2017), suggest a sediment deposition at Plimiri in shelf to upper slope environments with water depths between 90 m ±48 m and 335 m ± 57 m (Supplement 4.1.C). Therefore, a direct influence of oxygen-depleted intermediate and deep waters in the study area during times of sapropel formation is highly unlikely and local effects appear more plausible. Proxy data and model results, covering periods of sapropel formation in the Neogene and Quaternary, document increased winter precipitation over the Eastern Mediterranean region during phases with enhanced North African summer monsoon (Kotthoff et al., 2008b; Triantaphyllou et al., 2009, 2016; Wagner et al., 2019; Grant et al., 2022). Accordingly, we assume that during times of Pliocene sapropel formation in the deep Eastern Mediterranean basin, the southern part of the Island of Rhodes experienced a more humid climate. The amplified precipitation led to enhanced river run-off, evidenced by the high sedimentation rates, and the deposition of terrestrial organic material in a depocenter in near-coastal shelf environments. The increased input of riverine nutrients is responsible for a strengthened primary productivity and together with the enhanced terrestrial organic matter, fine-grained detrital input resulted in a reduction of the oxygen content in the surface sediment and favored the occurrence of a low- diverse fauna dominated by eutrophic taxa of the genera *Bolivina*, *Eubuliminella* and *Rectuvigerina* (Figs. 4.4, 4.5, 4.7). This assumption is supported by the near absence of planktic foraminifera within these layers. The high nutrient input and the resulting turbidity, just as the very low salinity of the riverine fresh water, are detrimental for planktic foraminifera (Fig. 4.5; e.g., Bijma et al., 1990; Kucera, 2007; Bhadra and Saraswat, 2021). A stratification of the water column and the development of anoxic conditions at the sediment-water interface, however, seems unrealistic because the high benthic foraminiferal numbers rather indicate increased eutrophication. In addition, the sediments of the outcrop did not show any laminated and dark layers which would be typical for anoxic conditions. Comparing the very low diversity of the foraminiferal assemblage of the Marmara Sea (Shannon-Wiener diversity of <1), where modern dysoxia prevail (Fontanier

et al., 2018), with the relatively high diversity of >1.5 (Fig. 4.5) provides a further indication for non-dysoxic bottom waters off the Island of Rhodes.

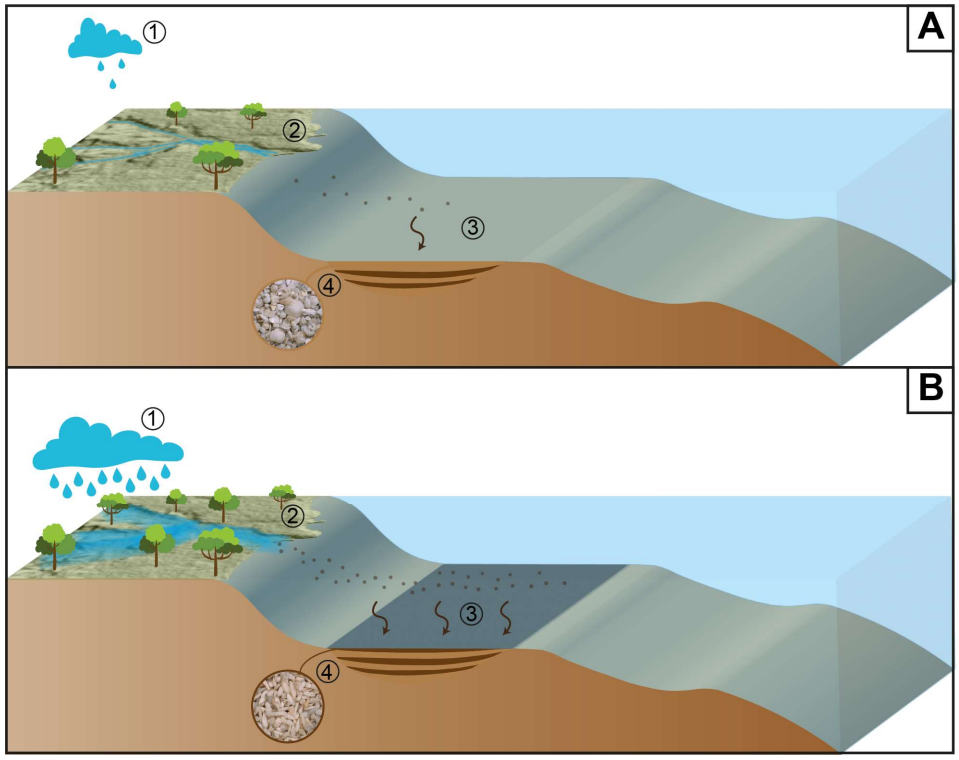

Figure 4.7. A. Schematic illustration of the processes during times of Northern Hemisphere summer insolation minima, where moderate precipitation (1) and river run-off (2) favors mesotrophic conditions at the near-coastal seafloor (3) off the Island of Rhodes. This results in a diverse benthic foraminiferal assemblage (4). **B.** Schematic illustration of the processes during times of Northern Hemisphere summer insolation maxima. (1) Increased precipitation leads to an (2) enhanced river run-off. (3) Input of terrestrial organic material supplies nutrients and results in a strengthened primary productivity in the surface water. (4) The enhanced food supply results in an increasing eutrophication of near-coastal areas and favors the occurrence of eutrophic taxa.

Even though other sapropelic layers within the LBF have been observed at the middle and northeastern coast of the Island of Rhodes (Rasmussen and Thomsen, 2005; Milker et al., 2019; Eichner et al., 2024a), none of them are as prominent and distinctive as the layers in the Plimiri 5 section. One possible factor might be, that the eutrophic layers in this study are much older than the Pleistocene deposits of the middle and northeastern coast. Various studies showed that the highest peaks of organic carbon were reached in Pliocene sapropels with up to 30% total organic carbon (TOC; e.g., van Os et al., 1994; Rullkötter et al., 1998; Bouloubassi et al., 1999; Nijenhuis and Lange, 2000; Arnaboldi and Meyers, 2006). Nijenhuis and Lange (2000) suggested that the very high TOC content is reached by a combination of an increased export productivity during precession minima and an improved preservation under anoxic condition. Rullkötter et al. (1998) proposed the deposition of the Pliocene sapropels under hotter and wetter conditions compared to Pleistocene sapropels, resulting in the deposition of particularly organic carbon-rich sapropels and Bouloubassi et al. (1999) states that their occurrence was more frequent and independent of

water depth before the onset of the Northern Hemisphere glaciation. On the contrary, Grant et al. (2022), postulate that the organic burial intensified after 3.2 Ma due to an increased sediment load from the African continent.

Another reason for the prominent deposition and thickness of the sapropel-like layers at the Plimiri 5 section might be the proximity to a river system (Fig. 4.1C), which by itself could lead to a stronger continental influence during sedimentation. The modern drainage pattern in the Plimiri 5 locality, formed by rivers and associated streams, is a combination of rectangular and parallel patterns (Feldman et al., 1968), indicating a strong tectonic control in the area, as both drainage patterns are associated with faulting processes (Marghany, 2022). These geomorphological aspects are characteristic for the southeastern coast as they were not identified or are not as typical in middle and northeastern coast of the Island of Rhodes, where less dominant sapropel- like layers were observed. Fluvial conglomerates of Pliocene age have also been observed approximately 2 km south of Plimiri at Cape Vigli (Schneider et al., 2023) as well as in underlying deposits in the Plimiri section (Nelson et al., 2001). Further, the separation of Rhodes from the Turkish mainland probably occurred no earlier than the earliest Pleistocene (Meulenkamp, 1985), so that the drainage area was considerably larger than during the Pleistocene. Likewise, the hinterland geology of the island is characterized by easily erodible siliciclastic rocks in the south, whereas the northern part is rather characterized by carbonate rocks (Mutti et al., 1970).

From the modern drainage pattern, it is also possible to identify a NW-SE and a NE-SW set of lineaments (Fig. 4.1C), the first of which is the most notable as it is related to the main rivers. The NW-SE trending lineaments were previously classified as normal faults in different locations on the island (ten Veen and Kleinspehn, 2002), which leads to the assumption that they have a similar kinematics at the Plimiri region. As a result of the fault activity, spaces for sediment deposition might have been created structures such as grabens and half-grabens, which could then serve as discrete depocenters for the riverine input (Fig. 4.7). The sediments deposited in these sites would be in a more isolated environment in relation to sediments deposited in regular marine slopes.

4.5.2 Long-term trends in paleo-productivity and –climate as indicated by stable isotope record

The stable isotope values and observed species-specific offsets are comparable to those from the modern Mediterranean Sea, suggesting that the environmental and microhabitat effects are well preserved and not blurred by diagenetic alteration (e.g., Schmiedl et al., 2004; Theodor et al., 2016a).

An alteration of the primary $\delta^{13}C$ and $\delta^{18}O$ signals by meteoric diagenesis could not be detected (see Supplement 4.1.B).

The Plimiri 5 $\delta^{13}C$ values for both, the shallow infaunal and epifaunal microhabitats, record a trend towards higher values through time. The trend is more prominent for *U. peregrina*, so that the deviation between $\delta^{13}C$ of *U. peregrina* and *C. pseudoungerianus* reduces towards younger times (Fig. 4.6). High $\Delta\delta^{13}C$ values, in the lower part of the section (Fig. 4.6), are indicative for high remineralization rates and associated release of isotopically light ^{12}C to the pore waters of the uppermost surface sediment (McCorkle and Emerson, 1988; Gehlen et al., 1999; Theodor et al., 2016a). The gradual trend to lower $\Delta\delta^{13}C$ values towards the top of the section, therefore, is indicative for a long-term decrease in organic matter supply to the seafloor, resulting from a trend towards drier conditions and consequently decreasing continental run-off. This might also explain the decrease in the thickness of the layers with high proportion of eutrophic indicator species through time (Fig. 4.5).

An increased aridification has also been identified for the Gulf of Aden in northeast Africa between 3.3 Ma to 3.0 Ma (Liddy et al., 2016) and in the Alboran Sea (Western Mediterranean Sea) after 3.5 Ma (Khélifi et al., 2009). Likewise, Grant et al. (2022) reported about larger climate changes to more arid conditions after 3.2 Ma in the Eastern Mediterranean. The epibenthic $\delta^{18}O$ record of the Plimiri 5 section shows a long-term trend towards higher values (Fig. 4.6; dotted red line), which indicates either slightly decreasing temperatures and/or increasing salinities of shelf water masses. Bottom water salinities in the Western Mediterranean Sea increased between 3.5 Ma and 3.3 Ma, while the bottom water temperature remained constant (Khélifi et al., 2009). Similarly, the prominent M2 cooling of the northern hemisphere has been found to occur earlier in the Mediterranean records compared to the global scale (Athanasiou et al., 2017). The $\delta^{18}O$ values of *U. peregrina* show two high values at 3.31 Ma and 3.35 Ma, which are possibly correlating with the Marine Isotope Stages MG2 and MG4, respectively. In summary, $\Delta\delta^{13}C$ values suggest a decline in marine primary- production towards younger times, which is caused by a progressively aridification and related reduced nutrient input by rivers, while the $\delta^{18}O$ data is reflecting long-term global changes.

4.6 Conclusion

Changes in the diversity and assemblage of the benthic foraminiferal fauna in a Late Pliocene sediment section from the southeastern coast of the Island of Rhodes provide indications for the periodic occurrence of eutrophic conditions at the seafloor. Periods of strongly enhanced food

fluxes are indicated by the recurrent dominance of eutrophic indicator species of the genera *Bolivina*, *Eubuliminella* and *Rectuvigerina*. Due to the periodic occurrence, the eutrophic intervals are interpreted as near- coastal equivalents of sapropels of the deep Eastern Mediterranean Sea. The near-coastal depositional shelf environment, however, makes the direct influence of oxygen-depleted intermediate and deep-waters from the Eastern Mediterranean basin very unlikely. Instead, the documented phases of increased primary productivity of near-coastal environments are attributed to local effects, such as increased precipitation on the island and associated riverine nutrient fluxes. $\Delta\delta^{13}C$ values of the epibenthic foraminifera *C. pseudoungerianus* and the shallow infaunal species *U. peregrina* provide indications of generally decreasing paleo-productivity towards younger times, suggesting a trend towards drier conditions.

Acknowledgements

Sampling of the section was performed in a field campaign in 2001 and was funded by the Deutsche Forschungsgemeinschaft (DFG) project Fr 1134/7. Tsampikos Athanasas from Lardos, Richard G. Bromley and Ulla Asgaard (both Copenhagen) are gratefully acknowledged for their support during the field campaign on the Island of Rhodes. Edith Maier and Jutta Richarz are thanked for their technical support during laboratory work. Louisa Kanzler is thanked for the processing of the samples, Tobias Winkler for his contribution in some of the counting and Gerassimos Diamantis for his contribution in the calcareous nannofossil analyses. Antje Voelker is acknowledged for her advice in the identification of planktic foraminifera. We further thank Christophe Fontanier and one anonymous reviewer for the constructive reviews, which helped to improve the manuscript, and the editor Valeria Luciani is thanked for the smooth handling of the review process. This study was financially supported by the Deutsche Forschungsgemeinschaft (DFG) by grants to Yvonne Milker (MI 1508/9-1) and Gerhard Schmiedl (Schm 1180/25-1). The study is a contribution to the "Center for Earth System Research and Sustainability (CEN)" of Universität Hamburg. Sampling took place with the permission of the Director of the Institute of Geology and Mineral Exploration, Athens, Greece.

Data availability:

Supplementary material referred to in this chapter was published together with the manuscript and is available at *Marine Micropaleontology* (doi: j.marmicro.2024.102341):

Supplementary note 4.1.	A. Age Model (modified version available in Appendix C) B. Evaluation of isotopic data; C. Reconstruction of paleo-water depth
Supplement 4.2:	Complete census counts of Plimiri 5
Appendix B:	Carbon and oxygen stable isotope data.

5 Tectonically induced vertical motions on the Island of Rhodes (Greece) during the Plio-Pleistocene

Daniela Eichner, Gerhard Schmiedl, Malu Ferreira, Jürgen Titschack, Nils Andersen, Yvonne Milker

Abstract

The Island of Rhodes is located in the Eastern Mediterranean Sea, at the eastern end of the Hellenic fore-arc and experienced intensive tectonic motions during the Plio-Pleistocene. Marine sediments of Plio-Pleistocene age, of the so-called Lindos Bay Formation, were uplifted and are outcropping today along the eastern coast of the island. The easy access and the well-preserved fossil record make the Lindos Bay Formation a unique opportunity to study in detail the neotectonic motions and paleoenvironmental evolution of Rhodes. Here we present new insights on the neotectonic evolution of the island by reconstructing past tectonically induced vertical motions and by identifying the large- and small-scale differences between individual sedimentary depocenter. To do so, an existing transfer function for paleo-water depth reconstruction was applied to the fossil benthic foraminiferal assemblage of the Cape Vagia section at the northeastern coast of the island. The reconstruction revealed that the marine sediments were influenced by tectonically induced long- and short-term and high- and low-amplitude vertical motions and it captured the transition from the transgressive to the regressive phase. Long-term average subsidence and uplift rates were estimated to ~2.2 mm a^{-1} and ~1 mm a^{-1}, respectively and short-term rates were as high as ~10.4 mm a^{-1}. By combining already existing and new data, we were able to reconstruct the full cycle of transgression and regression lasting from 1.97 to 0.47 Ma. A maximum uplift of ~700 m from the Early Pleistocene until today is proposed and differences in the rates and timing of vertical motions are revealed. It is hypothesized that the short-term cycles of uplift and subsidence are the result of an accretionary wedge that causes uplift due to the continuous sediment supply (underplating) and subsidence due to internal deformation to reach a state of stability. Differences in the rates, timing, and amplitudes of vertical motions are explained by a combination of large-scale uplift and subsidence processes and locally induced and site-specific processes in the graben structures.

This chapter has been prepared as a manuscript for submission in a peer-reviewed journal and is a slightly modified version.

5.1 Introduction

The Island of Rhodes is well known for its exposed and microfossil-rich marine deposits of Pliocene to Pleistocene age, such as the Lindos Bay Formation, that outcrop at scattered locations along the eastern coast of the island (Hanken et al., 1996; Cornée et al., 2006a; Titschack et al., 2013; Quillévéré et al., 2016; Milker et al., 2019). Due to its location at the active convergence plate boundary of the African and Eurasian plates, tectonic motions influenced the island (Fig. 5.1A; e.g., Woodside et al., 2000; van Hinsbergen et al., 2007; Howell et al., 2017). These motions led to major transgressive-regressive cycles and to the deposition of brackish to deep marine sediments in graben structures, so called depocenters, along the eastern coast of Rhodes (Hanken et al., 1996; Cornée et al., 2006; Titschack et al., 2013). It is still a matter of debate to what extent the individual depocenters experienced similar or different vertical motions (Cornée et al., 2019; Milker et al., 2019; Quillévéré et al., 2019). The quantification of small-scale vertical motion of each depocenter is therefore fundamental to gain a better understanding of the complex neotectonic history of the island and to better understand subduction processes in the Eastern Mediterranean Sea.

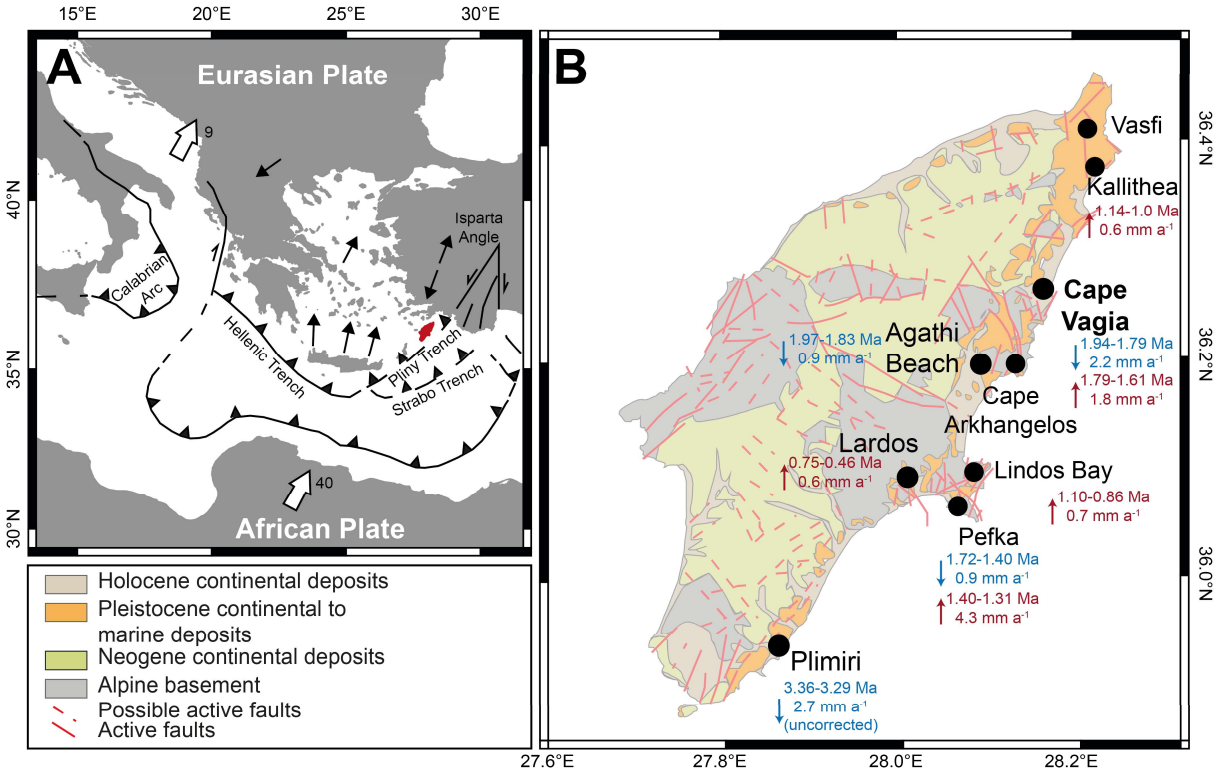

Figure 5.1. A. Overview of the Eastern Mediterranean region and its tectonic features after Dilek and Sandvol (2009). White arrows indicate the direction and magnitude (mm a^{-1}) of plate convergence. Black errors mark the extension direction and the location of the Island of Rhodes is indicated in red. **B.** Simplified geological map of the Island of Rhodes with its main tectonic features after Lekkas et al. (2000) (figure modified after Cornee et al. (2019)) and the long-term subsidence (blue) and uplift (red) rates of individual LBF sediment sections after Rasmussen and Thomsen (2005), Milker et al. (2019), Quillévéré et al. (2019), Eichner et al. (2024a,b) and this study.

The Island of Rhodes is located at the eastern end of the Hellenic forearc, which has been formed by the subduction of the African beneath the Eurasian plate (Fig. 5.1A; e.g., Jolivet et al., 2013). It experienced intense tectonic motions, such as large-scale NE-SW stretching in the eastern forearc that influenced the upper crust of Rhodes, including counterclockwise rotation and repeated tilting of the island (Kontogianni et al., 2002; Howell et al., 2015; Cornée et al., 2019). The opening of the ~4 km deep Rhodes Basin, SE of the island, before ~6 Ma, contributed to subsidence and uplift movements of the eastern coast of Rhodes. A large escarpment that borders the Rhodes Basin, and runs parallel to the eastern coast of Rhodes, is often interpreted as a reverse or thrust fault that additionally contributed to the vertical movements (Kontogianni et al., 2002; Howell et al., 2015; Howell et al., 2017; Cornée et al., 2019). During the early Pleistocene Rhodes experienced a counterclockwise rotation, simultaneously with a tilting of Rhodes to the SE around a NNE-SSW orientated horizontal axis and the subsidence of eastern part of Rhodes (Kontogianni et al., 2002; Cornée et al., 2019). The subsequent uplift of the crust, underlying Rhodes, and the NW tilting of the island was synchronous with a second counterclockwise rotation (Cornée et al., 2019). Tectonic-driven vertical motions were responsible for multiple phases of uplift and subsidence during the Plio- Pleistocene (Hanken et al., 1996; Woodside et al., 2000; Cornée et al., 2006a; van Hinsbergen et al., 2007; Titschack et al., 2013; Aksu et al., 2018). The deformation, erosion and multiple faulting of the Mesozoic basement led to the development of a series of steep NW-SE-striking horst and graben systems along the eastern coast of Rhodes. The graben formed isolated basins which later influenced the deposition and distribution of marine and continental deposits (Mutti et al., 1970; Hanken et al., 1996), that were uplifted and are outcropping in scattered locations along the eastern coast of Rhodes (Fig. 5.1B). Consequently, these sedimentary deposits record major and minor tectonically driven relative sea-level changes.

Benthic foraminifera have proven to be a suitable tool for the quantitative reconstruction of paleo-water depths on different time scales and over a wide bathymetric range, and for the reconstruction of paleo-elevations in intertidal settings by using transfer functions (TFs; e.g., Horton, 1999; Hawkes et al., 2010; Kemp et al., 2015; Milker et al., 2015a,b, 2017). The use of foraminiferal-based TFs was also successfully applied to reconstruct tectonic- and earthquake-induced vertical motions along the US-Pacific coast (e.g., Hawkes et al., 2010; Milker et al., 2016). More recently, this knowledge was used for a more detailed reconstruction of tectonically induced vertical motions by Milker et al. (2017) who developed and applied a regional benthic foraminiferal-based TF to a Pleistocene sediment section on Rhodes, nearby Pefka (Fig. 5.1B). Likewise, Quillévéré et al. (2019) used the ratio of planktic and benthic foraminifera for the reconstruction of vertical motions of the Lindos section, approximately 5 km north of Pefka (Fig. 5.1B). Both

studies corrected the estimates for glacio-eustatic sea-level changes and Milker et al. (2019) additionally for precession-driven influences. Both concluded that apart from the well-known long-term cycle of transgression and regression (e.g., Hanken et al., 1996; Cornée et al., 2006a; Titschack et al., 2013) also small-scale vertical motions influenced the eastern coast of the island, that have not been recorded before. A follow-up study was conducted by Eichner et al. (2024a), who additionally found small-scaled vertical motions at Agathi Beach and Lardos (Fig. 5.1B), on the middle eastern coast.

This study aims to answer the question of whether the individual depocenters record similar or different tectonically induced vertical motions and aims to quantify and explain the small-scale motions. For the first time, the compilation of available paleo-water depth reconstructions is used to recognize a temporal trend in the subsidence and uplift history of the island. The new data, in combination with already existing data, will also contribute to the question of how much the island has been uplifted since the Pleistocene.

5.2 The Lindos Bay Formation at Cape Vagia

The Plio-Pleistocene marine deposits were classified as the Rhodes Synthem with a maximum thickness of ~420 m (Cornée et al., 2019). The Synthem is further subdivided into three transgressive formations, Kolymbia, Lindos Bay and St. Paul's Formation and one regressive formation, Cape Arkhangelos Formation (Titschack et al., 2013; Cornée et al., 2019). Sedimentary outcrops of the Rhodes Synthem are distributed along the eastern coast of the island from Vasfi in the north (Meulenkamp et al., 1972) to Plimiri in the south (Fig. 5.1B; Nelson et al., 2001). The marine and microfossil-rich sediments of the Lindos Bay Formation (LBF), which are the focus of this study, are known to record a major transgression-regression cycle (Titschack et al., 2013; Cornée et al., 2019; Milker et al., 2019), as well as various small-scale cycles (Milker et al., 2019; Quillévéré et al., 2019; Eichner et al., 2024a).

The herein studied Cape Vagia sediment section is located close to the Kolymbia settlement at the northeastern coast of Rhodes (36°15'0.38"N; 28°10'7.60"E) and has been subject of several previous studies (Løvlie et al., 1989; Moissette and Spjeldnæs, 1995; Spjeldnæs and Moissette, 1997; Cornée et al., 2006a; Steinthorsdottir et al., 2006; Boyd, 2009; Quillévéré et al., 2016). It comprises of approximately 20 m LBF, which is underlain by the Kolymbia Formation and uncomfortably overlain by a strongly altered limestone (Fig. 5.2). The massive grey clay shows some bluish laminated layers about 1 m above the base (Fig. 5.2a) and a prominent red layer ~8 m above the

base (Fig. 2b), including some inclusions of gypsum. Approximately 10 m above the base, the signs of the trace fossil *Zoophycos* were found (Fig. 5.2c).

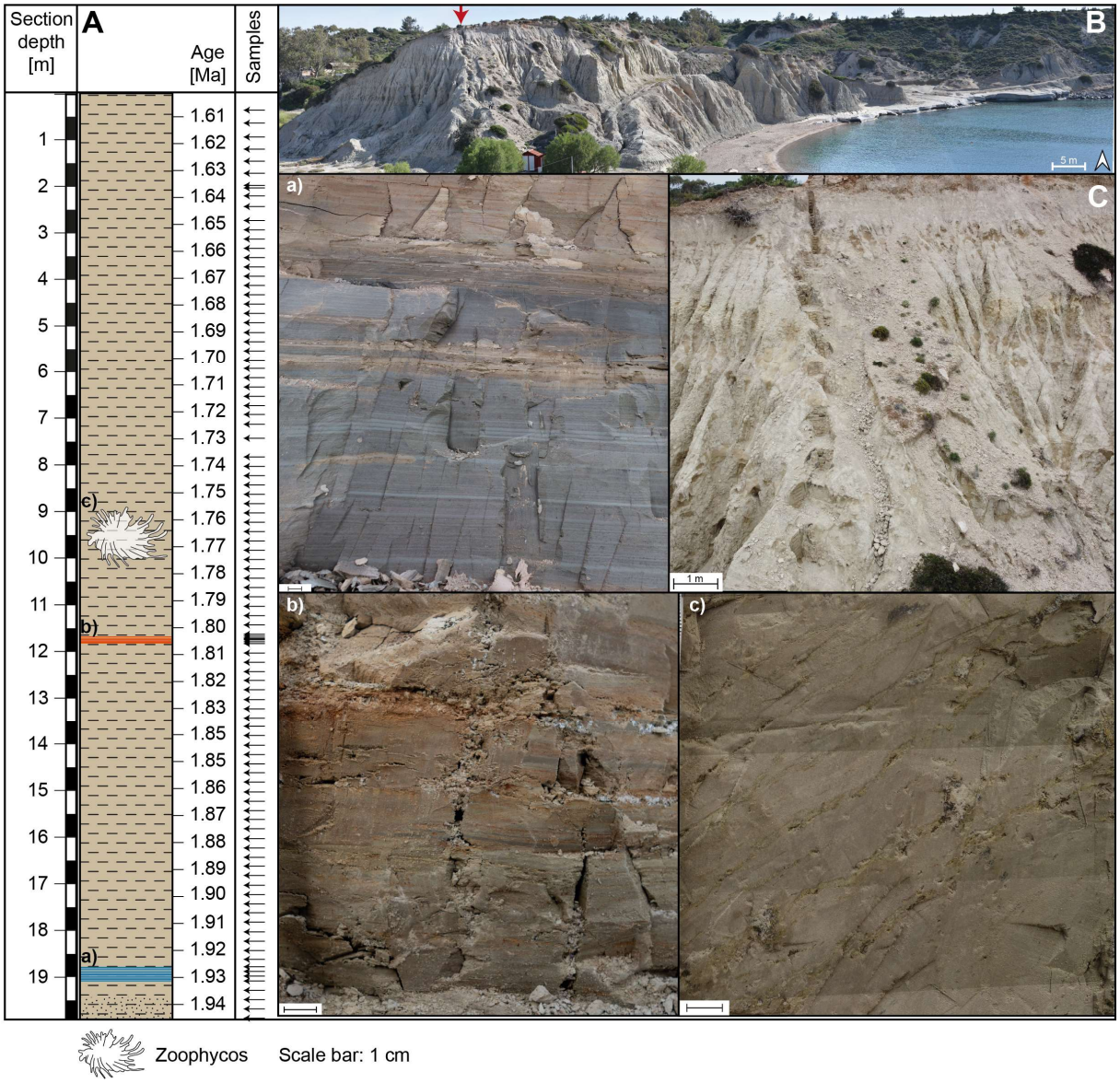

Figure 5.2. A. Simplified lithology of Cape Vagia and position of sampling. **B.** Overview photo of Cape Vagia Bay, red arrow indicates the position of sediment section. **C.** Overview of sampling location. a-c) Photos taken of anomalies in the outcrop. a) greyish-blue layering, b) red layer with inclusion of gypsum. c) traces of the trace fossil *Zoophycos*.

5.3 Methods

5.3.1 Chronostratigraphic framework

The chronostratigraphic framework of the section is based on the first common occurrence (FCO) of the planktic foraminifer *Neogloboquadrina pachyderma* sinistral in the Mediterranean Sea at 1.79 Ma (Zijderveld et al., 1991; Lourens et al., 1996b; Lourens and Hilgen, 1997). For this, the relative abundance of the left coiled *N. pachyderma* was calculated (Fig. 5.3). The FCO was placed where the relative abundance of *N. pachyderma* sinistral shifted to approximately 8% for the first

time. This is in accordance with Zijderveld et al. (1991) and Lourens et al. (1996b) who placed the FCO approximately where the relative abundance of left coiled *Neogloboquadrina* spp. excided 5-8% in their records. Previous studies revealed different age estimations for the Cape Vagia section. For example, Løvlie et al. (1989) applied a paleomagnetic polarity stratigraphy to the sediment section. They found the benthic foraminifera *Hyalinea balthica* approximately 5 m above a layer of volcanic ash and concluded the section to be deposited between 3.5 Ma and 0.97 Ma. Cornée et al. (2006a), however, did not find a volcanic ash nor the FO of *H. balthica* or a significant number of sinistral coiled *N. pachyderma*. The authors used magnetostratigraphy and proposed the section to be deposit in the Olduvai subchron (1.942-1.785 Ma). Quillévéré et al. (2016), on the other hand, reports the FO of *H. balthica* approximately 7 m above the Kolymbia Formation-LBF boundary and the FCO of the planktic foraminifer *N. pachyderma* sinistral at about 3 m above the boundary, indicating an age of the section between 1.95 Ma and approximately 0.95 Ma.

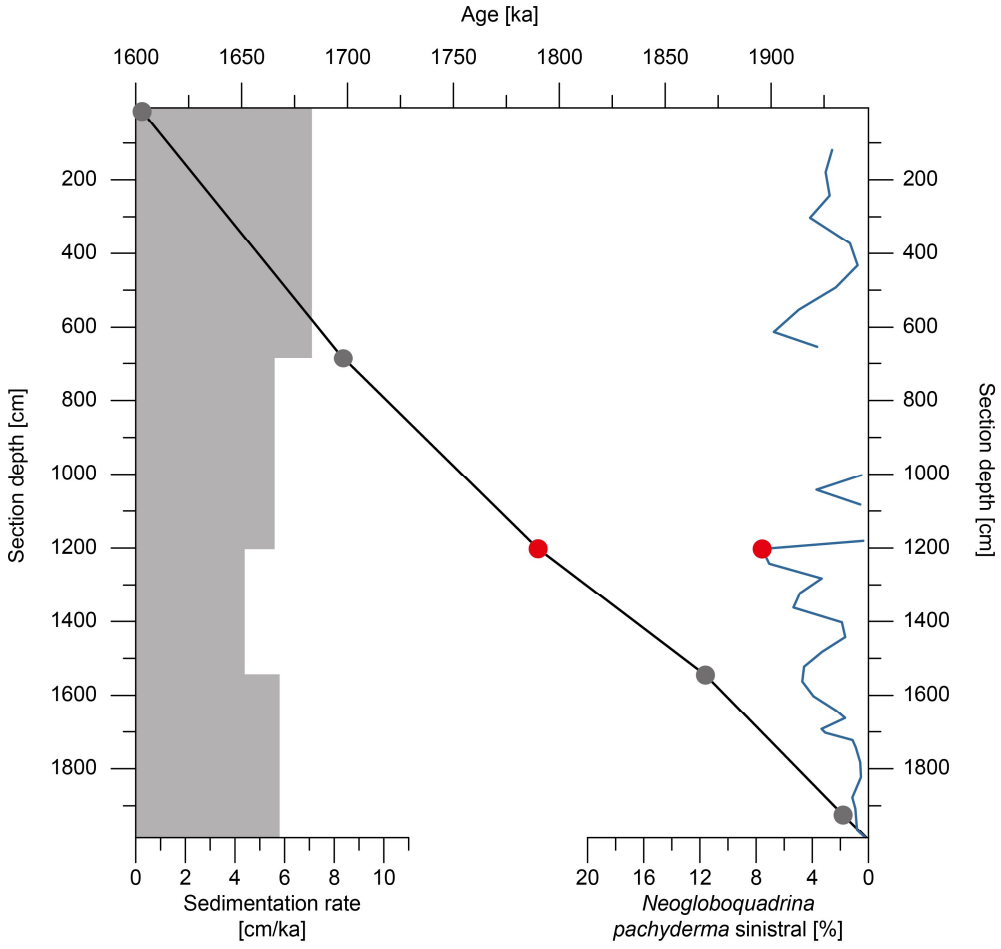

Figure 5.3. Age-depth plot with calculated sedimentation rates and relative abundance of the planktic species *N. pachyderma* sinistral. The first common occurrence of the species in the Mediterranean Sea after Zijderveld et al. (1991) and Lourens et al. (1996b) is marked as red dot. Grey dots indicate the fix points used for the correlation to the LR04 stack of Lisiecki and Raymo (2005).

However, the FO of *H. balthica* is not recorded in the LBF sediment section sampled at Cape Vagia for this study, so it must be assumed that the section covers less time than suggested by Løvlie et al. (1989) or Quillévéré et al. (2016) and is older than 1.49 Ma. For the lower limit, we follow the age estimation of Cornée et al. (2006a). This and the FCO of *N. pachyderma* were then used as tie points for the stable oxygen isotope stratigraphy, where the LR04 stack of Lisiecki and Raymo (2005) was graphically correlated to the infaunal $\delta^{18}O$ record of the Cape Vagia section by using the software AnalySeries 2.0 (Paillard et al., 1996) (Appendix C). The infaunal $\delta^{18}O$ record was used because both, the epifaunal and infaunal record, followed the same trend, but the infaunal record made a correlation with the LR04 stack easier.

5.3.2 Stable isotope measurements

Benthic foraminiferal stable oxygen and carbon isotope compositions were measured on 140 samples of the epibenthic foraminifer *Cibicidoides pseudoungerianus* and on 137 samples of the infaunal species *Uvigerina peregrina*. Three specimens of the epibenthic foraminifer and five specimens of the infaunal foraminifer were picked from the fraction between 250-355 µm in order to avoid ontogenetic effects on the isotopic signal (Schmiedl et al., 2004; Theodor et al., 2016b). If the samples were lacking enough specimens of the required size, additional individuals were picked from the fraction <250 µm. For cleaning, the samples were soaked in ethanol and cleaned in an ultrasonic bath for five to eight seconds. The measurements were performed at the Leibniz-Laboratory for Radiometric Dating and Stable Isotope Research at the University Kiel by using a Thermo Finnigan MAT 253 mass spectrometer connected to a Kiel IV carbonate preparation device. The analytical precision (standard external error) was better than ± 0.05‰ for $\delta^{13}C$ values and ± 0.08‰ for $\delta^{18}O$ values. Results are reported in per mil with respect to the Vienna Pee Dee Belemnite (VPDB) scale. The deviation between $\delta^{13}C$ of *C. pseudoungerianus* and *U. peregrina* ($\Delta\delta^{13}C$) was used as a proxy for paleo-productivity. The data set was smoothed by using the LOESS regression and the software past 4.07b (Hammer et al., 2001).

5.3.3 Foraminiferal investigations

Sediment samples for foraminiferal investigations, each of 2 cm thickness, were sampled during a field campaign in April 2022. Samples were taken every approximately 10 to 20 cm. Additional samples were taken where lithological anomalies were visible in the outcrop (Fig. 5.2). Up to 1 m of the weathered surface was removed prior to sampling to have access to fresh material (Fig. 5.2C). Sample preparation was carried out in the laboratories of the Universität Hamburg. A total of 102 raw samples, each of approximately 50 g and in 20 cm resolution, were soaked for one hour in hydrogen peroxide (H_2O_2), to disaggregate the compacted samples and subsequently wet

sieved over 63 µm and 125 µm mash screens. After washing, the fraction >125 µm of highly compacted samples were additionally soaked in a solution containing 50% Rewoquat W3690 and 50% ethanol (96%) for one hour. These samples were again washed over a 63 µm and 125 µm sieves. Where necessary the Rewoquat-Ethanol step was repeated. All samples were dried at 40°C in a drying cabinet. Pretreatments of samples for micropaleontological analysis with H_2O_2 is a common technique (e.g., Feldmeijer et al., 2013; Jones, 2013). A study on the effects of a 10% H_2O_2 (1h) pretreatment on the shell fragmentation, foraminiferal abundance, Mg/Ca and stable carbon and oxygen isotope composition, revealed no clear influence on the taxa or its geochemical signals (Feldmeijer et al., 2013). The usage of Rewoquat for micropaleontological purposes is less common, however Jarochowska et al. (2013) reported a good preservation and recovery of calcareous and organic-walled microfossils, even after soaking for multiple days. About 42% of the samples did not fully dissolve after the pretreatment, so that the weights of the fractions are not representative. Nevertheless, in this study only the relative abundances are worked with, so that the poor dissolution is not affecting the data.

A representative split of the fraction >125 µm, containing at least 100 benthic foraminifera, were used for foraminiferal investigation. For identification on species level the illustrations and descriptions of Jones (1994), Rasmussen (2005) and Milker and Schmiedl (2012) were used. If an identification on species level was not possible, taxa were grouped into their genus. Photographs of the dominant species were taken with a scanning electron microscope (SEM; HITACHI TM4000Plus). By following Corliss and Chen (1988) and Milker et al. (2019), the species were further categorized into eutrophic and oligotrophic taxa, based on their morphological features and the presence or absence of fine pores (List of genera in the supplements of Milker et al. (2019) or Eichner et al. (2024a)). The diversity was calculated using the Shannon-Wiener biodiversity index H (Shannon and Weaver, 1949) and the software Past 4.07b (Hammer et al., 2001).

5.3.4 Paleo-water depth reconstruction

The paleo-water depth reconstruction for the Cape Vagia section is based on the benthic foraminiferal assemblage of the fraction >150 µm (method after Milker et al. (2017)). Each representative split (see above) was further dry sieved through a 150 µm mash screen and contained at least 250 individuals of the fraction >150 µm. Samples with less individuals per sample were excluded for analysis. Paleo-water depths were calculated by using an existing transfer function (Milker et al., 2017). The Weighted Averaging-Partial Least Square (WA-PLS) method (Ter Braak and Juggins, 1993) and a cross validation (bootstrapping, N = 1000) for TF development was used. To test the robustness and significance of the paleo-water depth estimates, a set of statistical tests

were applied, i.e., the goodness-of-fit statistics (Birks, 1998; Simpson and Hall, 2012) and the random TF-test (Telford and Birks, 2011). The final component of the TF was identified by choosing the component with a Root Mean Squared Error of Prediction (RMSEP) which was >5% better than the previous component and had a statistically significant improvement (t-test) (Kemp and Telford, 2015). 34 of 102 samples were excluded from the analysis because they either did not contain a sufficient number of benthic foraminifera, the relative abundance of eutrophic indicator species exceeded 80%, or less than 50% of the fossil species were present in the modern assemblage. The paleo-water depth estimations and evaluations were made by using an existing R code, the software R 4.2.3 (R Core Team, 2023) and R packages "PalaeoSig" (Telford and Trachsel, 2023), "rioja" (Juggins, 2022) and "vegan" (Oksanen et al., 2022).

The paleo-water depth estimates were corrected for the effect of glacio-eustatic sea-level changes by using the data of Bintanja and van de Wal (2008), to extract the tectonic component of the paleo-water depth fluctuations. Since the benthic foraminiferal assemblages are influenced by precession-driven changes in paleo-productivity (Appendix D), which potentially affects the paleo-water depth estimates, the precession-driven changes were filtered out to avoid a distortion of the tectonic component. For this a moving average smoothing with a calculated mean precession period of 20.5 ka was used. Corrections were made in R using the package "smooth" (Svetunkov, 2023).

5.4 Results

5.4.1 Chronostratigraphic framework

The FCO of *N. pachyderma* sinistral was placed at a section depth of 1203 cm, indicating an age of 1.79 Ma. Because *H. balthica* was not found in the entire section, we concluded that the section has to be older than 1.49 Ma. According to the graphical correlation of the LR04 stack of Lisiecki and Raymo (2005) to the infaunal $\delta^{18}O$ records of Cape Vagia (Appendix C), the section covers a time span of about 343 kyrs, lasting from 1.95 to 1.60 Ma, and, hence, sediments were deposited between MIS 74 and 55 (Lisiecki and Raymo, 2005). The sedimentation rates vary between 4.4 cm kyr^{-1} in the middle part and 7.1 cm kyr^{-1} at the top of the section (Fig. 5.3). Because of potential uncertainties in the correlation with the LR04 stack of Lisiecki and Raymo (2005) and a gap of almost 5 m in the isotopic data due to missing benthic foraminifera and/or poor preservation, the age model might include certain errors.

5.4.2 Stable isotope

The $\delta^{18}O$ values of the epifaunal *C. pseudoungerianus* range from 0.71 ‰ (1.70 Ma) to 2.6 ‰ (1.65 Ma) and the $\delta^{18}O$ values of the infaunal species *U. peregrina* range from 0.75 ‰ (1.60 Ma) to 2.82 ‰ (1.85 Ma). Both records are following the same trend, whereas the infaunal record exhibits generally heavier values (Fig. 5.4A).

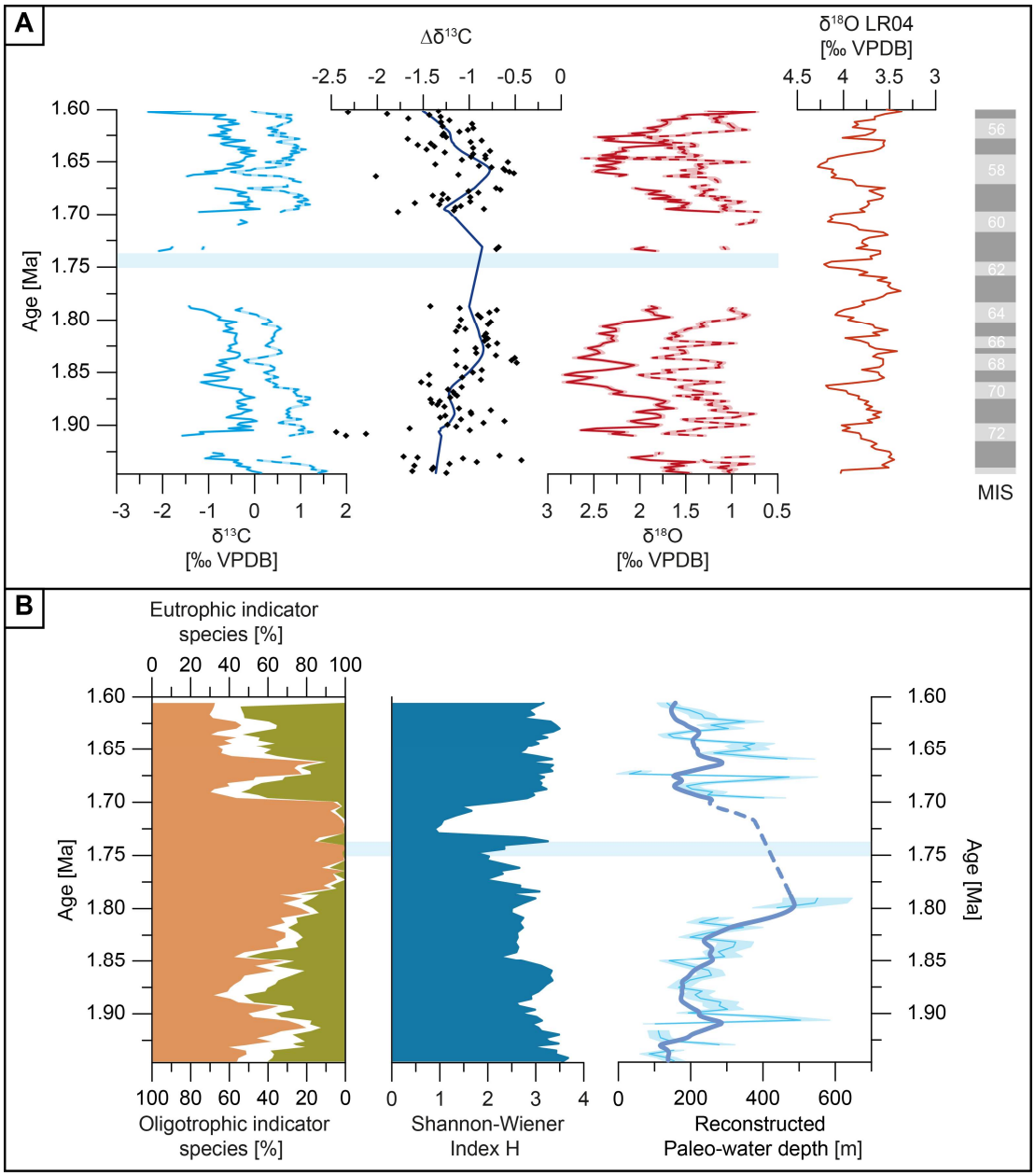

Figure 5.4. A. $\delta^{13}C$ and $\delta^{18}O$ stable isotopes of the shallow infaunal foraminifera *U. peregrina* (solid line) and the epibenthic foraminifera *C. pseudoungerianus* (dotted line). Black diamonds indicate the benthic $\Delta\delta^{13}C$ and dark blue line is the smoothed data set, by using the LOESS regression. The $\delta^{18}O$ LR04 stack and the Marine Isotope Stages of Lisiecki and Raymo (2005) are shown as a reference. **B.** Relative abundance of oligotrophic indicator species (invers axis) and eutrophic indicator species, and the Shannon-Wiener diversity index. Reconstructed uncorrected paleo-water depths are shown in light blue, including the sample specific error. Paleo-water depths corrected for the effects of relative, glacio-eustatic sea level changes and for precession-influenced changes are marked in dark blue. Blue bar in A and B indicates the position of *Zoophycos* traces.

The $\delta^{13}C$ values of *Cibicidoides pseudoungerianus* range from -1.13 ‰ (1.73 Ma) to 1.56 ‰ (1.94 Ma), while *U. peregrina* has its lowest value of -2.31 ‰ at 1.60 Ma and its highest value of 0.14 ‰ at the bottom of the section (1.95 Ma). In general, both records follow the same trend (Fig. 5.4A). However, the values of the epifaunal record are on average more than 1 ‰ heavier than those the record of *U. peregrina*. The difference between the $\delta^{13}C$ values of both species slightly increases in the lower part of the section and decreases in the younger part (Fig. 5.4A).

5.4.3 Foraminiferal investigations

The Cape Vagia sediment section contains a rich benthic fauna with 160 different taxa, ranging from 14 (1.70 Ma) to 71 (1.86 Ma) taxa per individual samples. Five of 102 samples were excluded for further investigations, because they contained less than 100 benthic individuals (1175, 1173, 1143, 1103, 1023 cm; full census counts in Appendix E).

The Cape Vagia samples contain between 0% and 54% oligotrophic indicator species and between 30% and 100% eutrophic indicator species (Fig. 5.4B). The relative abundance of the eutrophic (oligotrophic) indicator species reached their maximum (minimum) at 1.72 Ma. And their minimum (maximum) at ~1.61 Ma. The Shannon-Wiener diversity ranges from 0.89 to 3.67 and decreases from the bottom (maximum value at 1.94 Ma) until 1.73 Ma, where it reaches its minimum, and then increases again towards the top (Fig. 5.4B).

We defined the most dominant species as those occurring in at least two samples with more than 10% relative abundance. In the Cape Vagia section, the most dominant species comprise *Cassidulina carinata* s.l., *Cibicidoides pseudoungerianus*, *Bulimina marginata* s.l., *Bolivina spathulata*, *Uvigerina peregrina*, *Sphaeroidina bulloides*, *Gyroidina* spp., *Uvigerina auberiana*, *Bolivina seminuda*, *Valvulineria bradyana*, *Haynesina depressula*, *Bulimina elongata*, *Ammonia beccarii*, *Cassidulinoides bradyi*, and *Astrononion* sp. (Fig. 5.5 and 5.6).

Cassidulina carinata s.l. is the most abundant species of Cape Vagia, with abundances fluctuating throughout the section and ranging between 1% (1.79 Ma) and 76% (1.73 Ma). *Bolivina spathulata* and *Bulimina marginata* s.l. show high abundances between 1.91-1.89 Ma, 1.86-1.79 Ma, 1.73-1.70 Ma and 1.67-1.65 Ma and decrease drastically in relative abundance in between. Relative abundances range from 0% to 34% and 0% to 28%, respectively. *Cibicidoides pseudoungerianus* (0-43%) occurs with medium to high abundances and varies throughout the section. *Uvigerina peregrina* fluctuates throughout the sediment section, with its highest peak at 1.80 Ma. *Uvigerina auberiana* is absent or nearly absent between 1.85 Ma and 1.70 Ma but is present with varying abundances (0-16%) in the rest of the section. *Gyroidina* spp. (0-19%) and *S. bulloides* (0-13%) are present in the whole section and abundances vary from low to medium. *Valvulineria bradyana* occurs in low

abundances in the sediments of Cape Vagia except for two peaks at 1.79 Ma (11%) and 1.71-1.70 Ma (11-19%). *C. bradyi* only shows high occurrences in the lower part of the section with up to 32 % and it is absent or only occurs in very low abundance in the younger part of the section. *Bulimina elongata* has four occurrences at 1.93-1.91, 1.83-1.79, 1.78-1.73 and 1.67-1.66 Ma and reaches its highest occurrence with 13 % at 1.76 Ma. *Haynesina depressula* has its highest occurrence (17%) at 1.70 Ma and occurs with medium abundances between 1.78 and 1.73 Ma and 1.67 and 1.66 Ma. It is absent or only occurs in low abundances in the lower part of the sediment section. *Bolivina seminuda* and *A. beccarii* only show one high occurrence at 1.79-1.78 Ma and 1.77-1.74 Ma, respectively and almost absent in the lower and upper part of the section. *Astrononion* sp. is absent in the lower part of the section and firstly occurs at 1.76 Ma with its highest abundance of 19%. In the upper part it appears only in low abundance, except for another peak at 1.70 Ma.

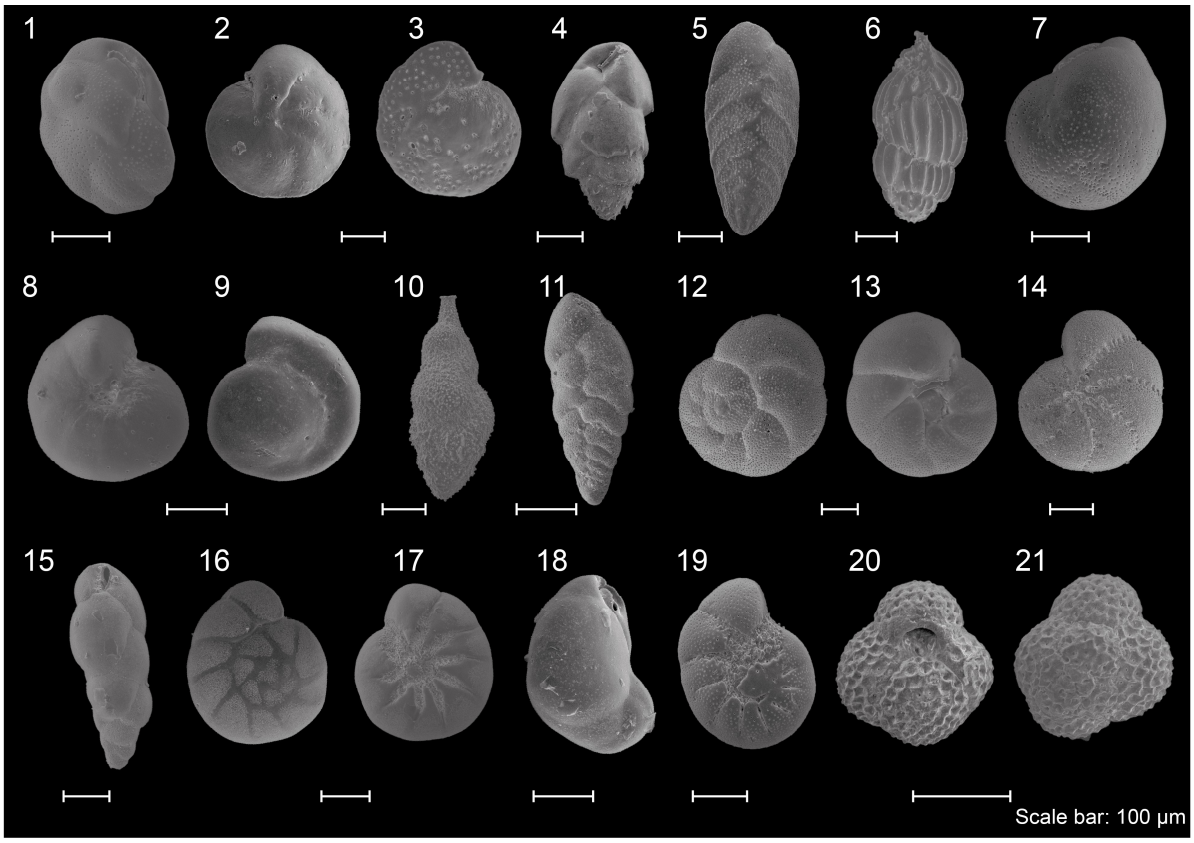

Figure 5.5. Most dominant benthic foraminifera of the Cape Vagia section and planktic species *N. pachyderma* sinistral used as age marker. 1 *Cassidulina carinata* s.l., 2-3 *Cibicidoides pseudoungerianus*, 4 *Bulimina marginata* s.l., 5 *Bolivina spathulata*, 6 *Uvigerina peregrina*, 7 *Sphaeroidina bulloides*, 8-9 *Gyroidina* sp., 10 *Uvigerina auberiana*, 11 *Bolivina seminuda*, 12-13 *Valvulineria bradyana*, 14 *Haynesina depressula*, 15 *Bulimina elongata*, 16-17 *Ammonia beccarii*, 18 *Cassidulinoides bradyi*, 19 *Astrononion* sp., 20-21 *Neogloboquadrina pachyderma* sinistral.

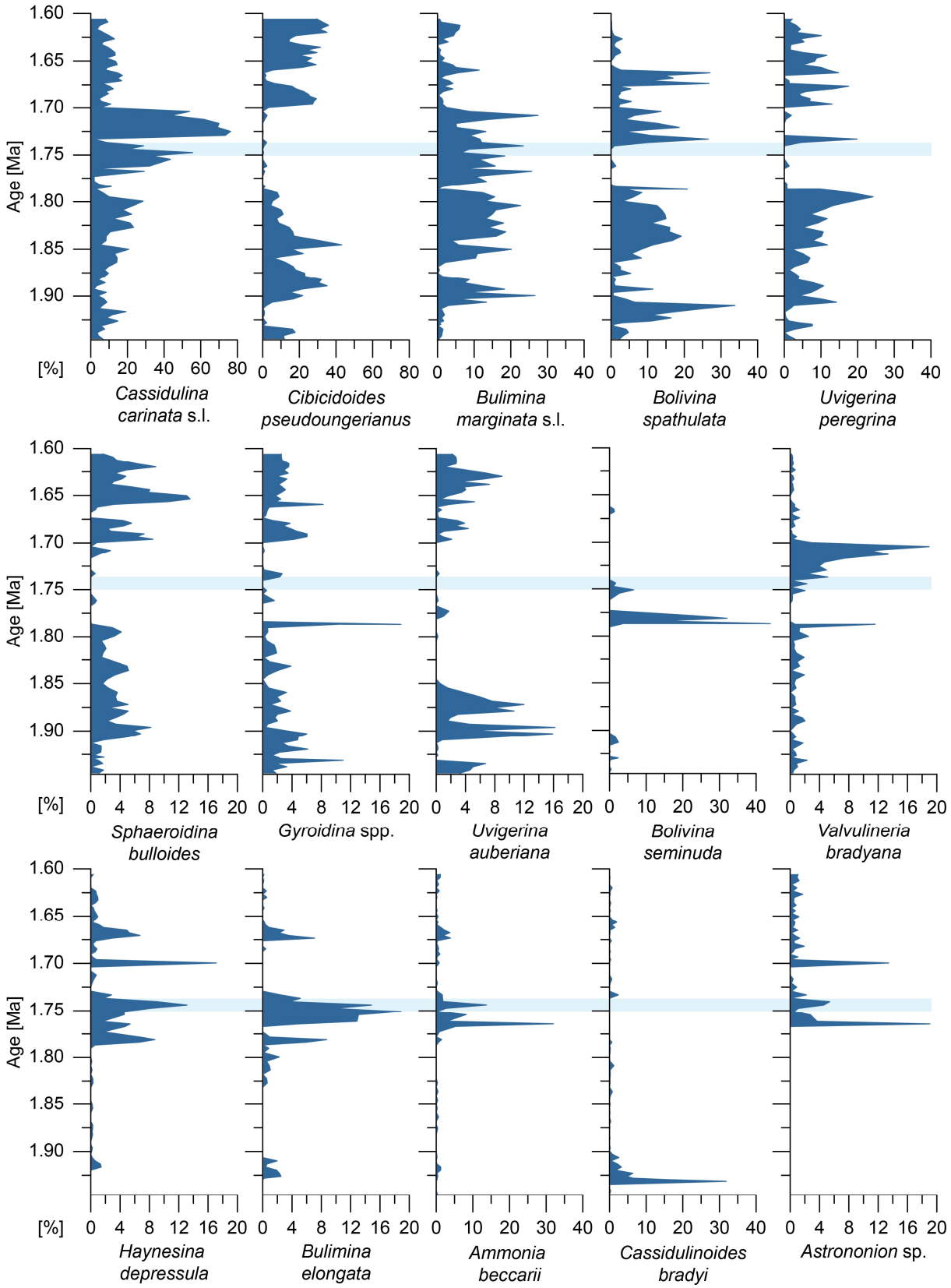

Figure 5.6. Relative abundance of most dominant species in the Cape Vagia sediment section. Blue bar indicates the position of *Zoophycos* traces.

5.4.5 Paleo-water depth estimates

We selected the third component of the final TF model due to the RMSEP of 28.91 m which is > 5% better than the previous component and is a statistically significant improvement (t-test; $p < 0.001$; Table 5.1). At Cape Vagia 12 samples (18%) have a good fit, 13 samples (19%) a poor fit, 15 samples (22%) a very poor fit and 28 samples (41%) have an extremely poor fit to water depth (Appendix D). To test the significance of the reconstructions, the random TF-test (Telford and Birks, 2011) was applied. Thereafter, the reconstruction is not significant at the 95% confident level. An evaluation of the reconstruction is presented in the Appendix D.

For the paleo-water depth reconstruction, 34 of 102 samples had to be excluded from the analysis due to the criteria described in chapter 5.3.4. Uncorrected estimates in the Cape Vagia section range from 30 m ± 35 m at 1.67 Ma to 551 m ± 96 m at 1.79 Ma (Fig. 5.4B). In the lower part of the section (1.95-1.79 Ma) a trend towards deeper waters is indicated with a deepening of approximately 400 m. In the upper part of the section from 1.70-1.61 Ma paleo-water depth estimates decrease in water depth by about 270 m. After the correction for the relative global sea-level and precession-influenced changes, paleo-water depths are estimated between 116 m (1.93 Ma) and 487 m (1.80 Ma) with a deepening trend at the bottom of about 340 m and a shallowing of about 100 m at the top (Fig. 5.4B). Additionally, at least three small-scale cycles of deepening and shallowing are recorded at 1.93 - 1.89 Ma, 1.89 - 1.68 Ma and 1.68 - 1.62 Ma (Fig. 5.4B).

Table 5.1. Transfer function performance. Shown is the cross-validated root mean squared error of prediction (RMSEP), the cross-validated coefficient of determination (R^2_{boot}) between the estimated and observed water depth of the modern data set, improvement of the RMSEP from one to the next component (%change) and the significance of the component fitting increase according to a randomized t-test. Chosen component is marked.

	RMSEP	R^2	% change	p
Comp01	55.08	0.71	44.14	0.001
Comp02	33.05	0.92	40.00	0.001
Comp03	**28.91**	**0.94**	**12.54**	**0.001**
Comp04	26.76	0.95	7.42	0.002
Comp05	26	0.95	2.84	0.044

5.5 Discussion

5.5.1 Paleo-ecological evolution of NE Rhodes during the Pleistocene

The benthic foraminiferal assemblage of the Cape Vagia section is characterized by a relatively high abundance (average of 59%) of eutrophic indicator species, and the Shannon-Wiener diversity ranges between 0.89 (1.73 Ma) and 3.67 (1.94 Ma; Fig. 5.4B). These values are in the same

range of earlier findings on the Island of Rhodes, for which it was concluded that the shelf to upper slope environments around Rhodes were characterized by rather mesotrophic conditions during the Pleistocene (Rasmussen and Thomsen, 2005; Milker et al., 2019; Eichner et al., 2024a). Our results from Cape Vagia sediment section also support this interpretation.

The assemblage is dominated by the shallow infaunal species *Cassidulina carinata* s.l., with an especially high occurrence that reaches up to 76% between 1.73 and 1.71 Ma (Fig. 5.6). Higher abundances of *Cassidulina carinata* s.l. are associated with deeper reconstructed water depths. In the modern Western Mediterranean Sea it occurs at water depths between approximately 50 and 250 m (Milker et al., 2017), but in the Gulf of Naples they have also been observed in water depths down to 700 m (Sgarella and Moncharmont-Zei, 1993). Simultaneously with *C. carinata* s.l., *V. bradyana* increases to its highest occurrence of approximately 19%, and only shows low abundances in the rest of the section. Both are opportunistic species (Fontanier et al., 2003; Frezza et al., 2005), are known to occur in areas with high export productivity and are common in river-influenced assemblages (e.g., Carboni et al., 2000, 2004; Goineau et al., 2011). *Bolivina seminuda*, *H. depressula*, *B. elongata*, *A. beccarii* and *Astrononion* sp. all have their highest occurrences between 1.79-1.73 Ma, where diversity reaches its minimum. All of these species are commonly found in environments with high export productivity (Barmawidjaja et al., 1992, 1995; Sen Gupta and Machain-Castillo, 1993; Alve and Murray, 1995; Altenbach et al., 1999), and the latter four occur in shallow-water depths in the modern Mediterranean Sea (Sgarella and Moncharmont-Zei, 1993). A visible anomaly in the outcrop is winding, dark-colored tubes between 1.75 and 1.73 Ma that were interpreted as the remains of *Zoophycos* and point to bioturbation (Fig. 5.2c). Within the Kolymbia limestone of the Cape Vagia section, Bromley and Hanken (2003) also identified and described multiple individuals of *Zoophycos*. Several studies agree, that *Zoophycos* is built in conjunction with high and strongly seasonal organic-matter deposition on the seafloor, so that the trace fossil can be used as an indicator for increased accumulation of organic matter (e.g., Wetzel, 2010; Rodríguez-Tovar et al., 2015; Dorador et al., 2016). Likewise, up until 1.70 Ma, the relative abundance of eutrophic indicator species increases to nearly 100%. An increased eutrophication and an increased export productivity are therefore not only indicated by the benthic foraminiferal assemblage but also by the traces of *Zoophycos*.

Apart from *C. carinata* s.l. and *V. bradyana*, the infaunal species *B. marginata* s.l., *B. spathulata*, *U. auberiana* and *U. peregrina* are also dominant and fluctuate throughout the section. While the latter shows an opportunistic behavior (e.g., Corliss, 1991; Schmiedl et al., 2000; Altenbach et al., 2003; Fontanier et al., 2003), all other species are indicators for high organic matter fluxes and are known to tolerate low oxygen conditions (e.g., Sen Gupta and Machain-Castillo, 1993; Gooday, 1994;

Bernhard and Sen Gupta, 1999; Schmiedl et al., 2000). Likewise, *Sphaeroidina bulloides*, which occurs in medium relative abundance in the Cape Vagia section, is a shallow infaunal species which is commonly found in high primary productivity areas with seasonal variation in the food supply (Jorissen et al., 1998; Loubere and Fariduddin, 1999; Licari and Mackensen, 2005). In contrast, *C. pseudoungerianus* is an epifaunal species, adapted to high oxygen and low organic carbon conditions (van der Zwaan, 1982; Den Dulk et al., 2000; Singh and Gupta, 2010), and consequently have a higher relative abundance when the infaunal species are less abundant. *Gyroidina* species are abundant almost in the whole sediment section but peaks at 1.79 Ma. They have been found dominating the first recolonizing faunas after sapropel deposition in the eastern Mediterranean Sea and are therefore suggested to be related to quick re-oxygenation of the benthic ecosystem (Abu-Zied et al., 2008). Together with *Gyroidina* spp., *B. seminuda*, *B. spathulata* and *V. bradyana* also occur with high abundances in the same samples at ~1.79 Ma. While *V. bradyana* has been shown to positively correlating with well oxygenated clayey sediments (Goineau et al., 2011), *B. spathulata* can withstand a variety of conditions from well-oxygenated to oxygen-deficiency (Jonkers, 1984; Rasmussen, 2005) and *B. seminuda* is known to be a dominant species in Oxygen Minimum Zones (e.g., Glock et al., 2013).

The benthic assemblages, suggest a high export productivity and meso- to eutrophic conditions at the sea floor, which is also reflected by the offset between epifaunal and infaunal $\delta^{13}C$ signals ($\Delta\delta^{13}C$) of the Cape Vagia section (Fig. 5.4A). The $\delta^{13}C$ signal of the dissolved inorganic carbon (DIC) of the ambient bottom water is represented by the epifaunal $\delta^{13}C$ values (Duplessy et al., 1984; Zahn et al., 1986; Gottschalk et al., 2016; Schmittner et al., 2017; Mackensen and Schmiedl, 2019), while the infaunal $\delta^{13}C$ values reflect the $\delta^{13}C$ signal of the pore water DIC (McCorkle et al., 1990; Mackensen and Licari, 2004). The $\Delta\delta^{13}C$ of the epifaunal and infaunal values is therefore used as a proxy for the estimation of past organic matter fluxes and remineralization, as well as to document paleo-export productivity changes in the ocean (Zahn et al., 1986; Hoogakker et al., 2015; Gottschalk et al., 2016; Theodor et al., 2016a; Penaud et al., 2022). Following these interpretations, the paleo-export productivity is increasing from the bottom towards the middle of the section and generally decreases afterwards, interrupted by a strong increase of $\Delta\delta^{13}C$ between 1.68 Ma and 1.65 Ma, together with an increase in the relative abundance of eutrophic indicator species that reach almost 90% (Fig 5.4B). Directly above the traces of the *Zoophycos*, where the benthic foraminiferal diversity reaches its minimum, $\delta^{13}C$ values are especially low. During humid periods, it has been shown that the dissolved inorganic carbon of the surface and sub-surface water masses is decreasing, due to riverine influx of ^{13}C-depleted freshwater (Casford et al., 2002; Grimm et al., 2015), but low $\delta^{13}C$ values might also be related to

remineralization of organic matter at the sea floor (e.g., Casford et al., 2002). In summary, both, the benthic foraminiferal assemblages and the epi- and infaunal $\delta^{13}C$ records indicate an increasing eutrophication of the near coastal areas until approximately 1.70 Ma, possibly induced by freshwater input at certain intervals, as indicated by some benthic species and the low $\delta^{13}C$ values.

5.5.2 Tectonic-induced vertical motions of the NE coast of Rhodes

The uncorrected paleo-water depth estimates reconstructed in this study range between 30 m ± 35 m and 551 m ± 96 m (Fig. 5.4B). The maximum drowning agrees well with paleo-water depth estimates (approx. 300-600 m) of Moissette and Spjeldnæs (1995), which were based on bryozoans at Cape Vagia, and those of van Hinsbergen et al. (2007), who suggested maximum water depths between 500 and 600 m at Cape Vagia (there referred to as Kolymbia). The Island of Rhodes underwent multiple phases of uplift and subsidence, which finally led to the deposition of the LBF in isolated graben structures along the eastern coast (e.g., Hanken et al., 1996; Cornée et al., 2006a; van Hinsbergen et al., 2007; Titschack et al., 2013). A long-term transgressional phase is associated with the transformation from the shallow-marine to brackish Kolymbia Formation to the full-marine LBF. The boundary has been dated to the late Gelasian (approx. 2 Ma) at Lindos Bay (Quillévéré et al., 2016; Quillévéré et al., 2019) and at Cape Vagia (Fig. 5.7; this study; Cornée et al., 2006a; Quillévéré et al., 2016). At Pefka, the boundary was set at about 1.71 Ma (Milker et al., 2019) and more recently Eichner et al. (2024b) reported LBF deposits at Plimiri in the south of the island, underlain by the Kolymbia Formation of Pliocene age (3.36 to 3.29 Ma), suggesting that the onset of LBF deposition was much earlier there than previously thought (Fig. 5.7). The upper and often erosive boundary of the LBF is associated with the shallow marine deposits of the Cape Arkhangelos Formation. However, up until now only the Pefka (Milker et al., 2019) and the Cape Vagia (this study) sections possibly show the shift from increasing to decreasing paleo-water depths. At Cape Vagia the maximum paleo-water depths were reached at ~1.79 Ma, while at Pefka it was found at ~1.40 Ma (Fig. 5.8; Milker et al., 2019).

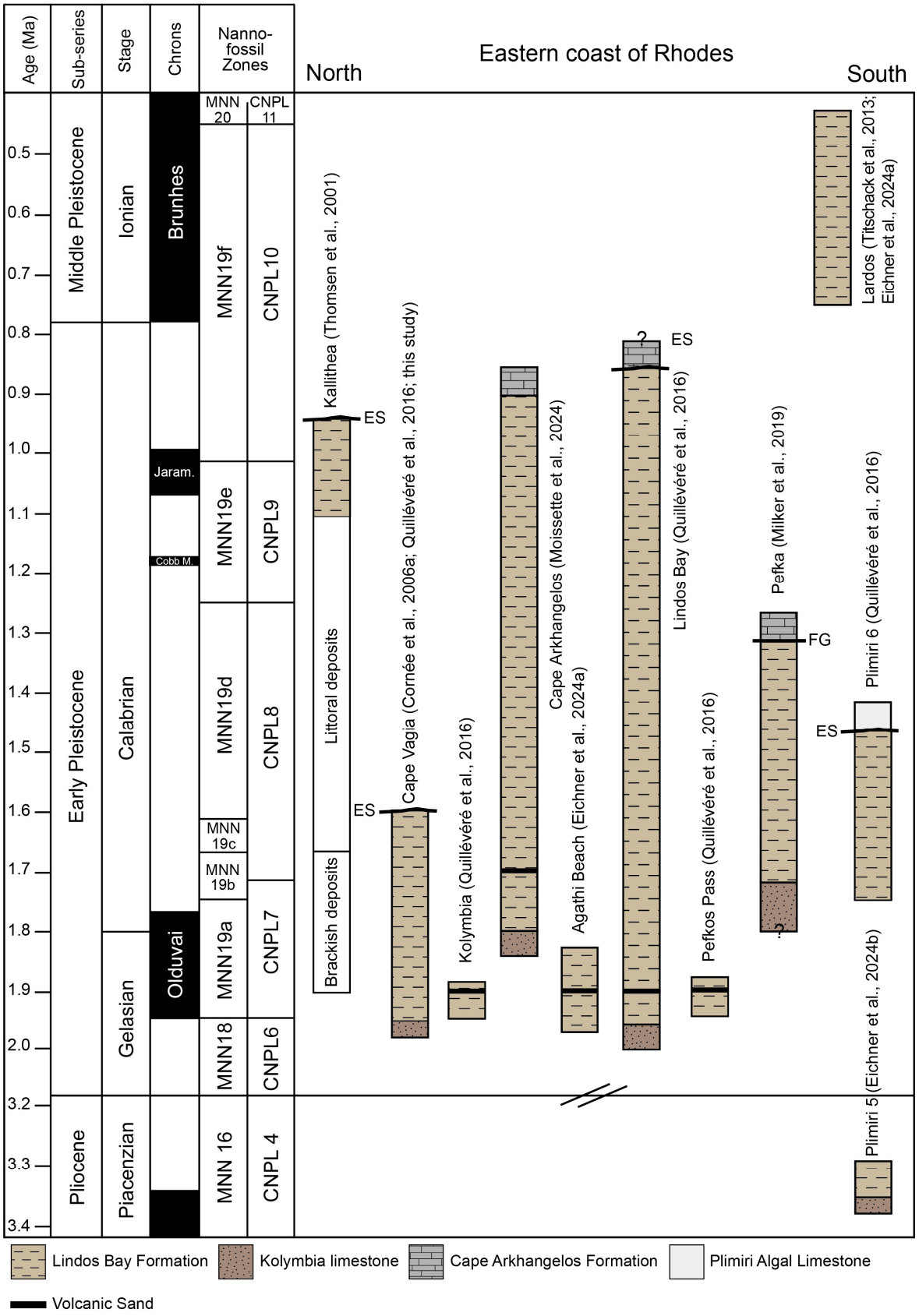

Figure 5.7. Updated overview of available chronostratigraphic data of the LBF along the eastern coast of the Island of Rhodes (figure modified after Quillévéré et al. (2016) and Eichner et al. (2024a)). Figure shows the temporal duration of the stratigraphic sections and exposed upper and lower boundaries.

5.5.2.1 Long-term vertical motions

The diachronous deposition of the LBF (Titschack et al., 2013; Quillévéré et al., 2016; Cornée et al., 2019) might be influenced by the tectonically induced vertical motions, the sediment discharge or/and the relative position of the depocenters to each other. However, sedimentation rates in the LBF are similar along the eastern coast of Rhodes and range between 2.9 and 19.8 cm kyr^{-1} (Milker et al., 2019; Quillévéré et al., 2019; Eichner et al., 2024a,b; Moissette et al., 2024) and do not show significant changes. This suggest that the influence of sedimentary input to the relative paleo-water depths and differences between the depocenters, should be minor. Additionally, deposits in more distal settings are more likely to cover longer time periods, as suggested by Pefka, Lindos Bay and Cape Vagia which are located at the modern coastline, compared to depocenters in higher altitudes (Titschack et al., 2013). Nevertheless, these two factors should not significantly influence the relative paleo-water depths estimates but it is proposed that each depocenter at the eastern coast of Rhodes developed individually and underwent site-specific vertical motions. This can also be noticed when calculating average long-term rates of subsidence and uplift (Fig. 5.1B). A tectonically induced deepening is recorded, from north to south: at Kallithea with an estimated subsidence rate of 0.6 mm a^{-1} (~1.14-1.0 Ma; Rasmussen and Thomsen, 2005), at Cape Vagia (1.94-1.79 Ma) with an average subsidence rate of 2.2 mm a^{-1}, at Agathi Beach (1.97-1.83 Ma; Eichner et al., 2024a) and at Pefka (1.72-1.40 Ma; Milker et al., 2019) both with a rate of 0.9 mm a^{-1}, and at Plimiri with a rate of 2.7 mm a^{-1} (3.36-3.29 Ma; Eichner et al., 2024b). However, it should be noted that the latter reconstruction has not been corrected for glacio-eustatic sea-level changes and calculations might therefore be overestimated. The rates agree with the estimated mean subsidence rates by Cornée et al. (2019) of 0.32-2.4 mm a^{-1} from Pefka Beach, Cape Vagia and Faliraki Road for the Rhodes Synthem. On the other hand, a long-term uplift is recorded at Cape Vagia (1.79-1.61 Ma) with an average uplift rate of 1.8 mm a^{-1}, at Lindos Bay (1.10 Ma-0.86 Ma; Quillévéré et al., 2019) with a rate of 0.7 mm a^{-1}, at Pefkos (1.40-1.31 Ma; Milker et al., 2019) with 4.3 mm a^{-1} and at Lardos with an average uplift rate of 0.6 mm a^{-1} (0.75-0.48 Ma; Fig. 5.1B; Eichner et al., 2024a). These examples illustrate well that different sedimentary deposits not only vary in time but also in their amounts of subsidence and uplift.

The timing of the maximum drowning potentially differs from Cape Vagia, in the northern part of the island, to the Pefka sediment section located at the middle eastern coast of Rhodes, where the transition from the transgressional to the regression phase is set approximately 390 kyrs later. However, we did not detect the Cape Arkhangelos Formation at Cape Vagia, but the section is topped by a strongly weathered limestone. Therefore, it is only assumed that the maximum paleo-

water depths of Cape Vagia reflect the maximum drowning of the LBF, because reconstructions reveal a general shallowing trend afterwards (Fig. 5.8).

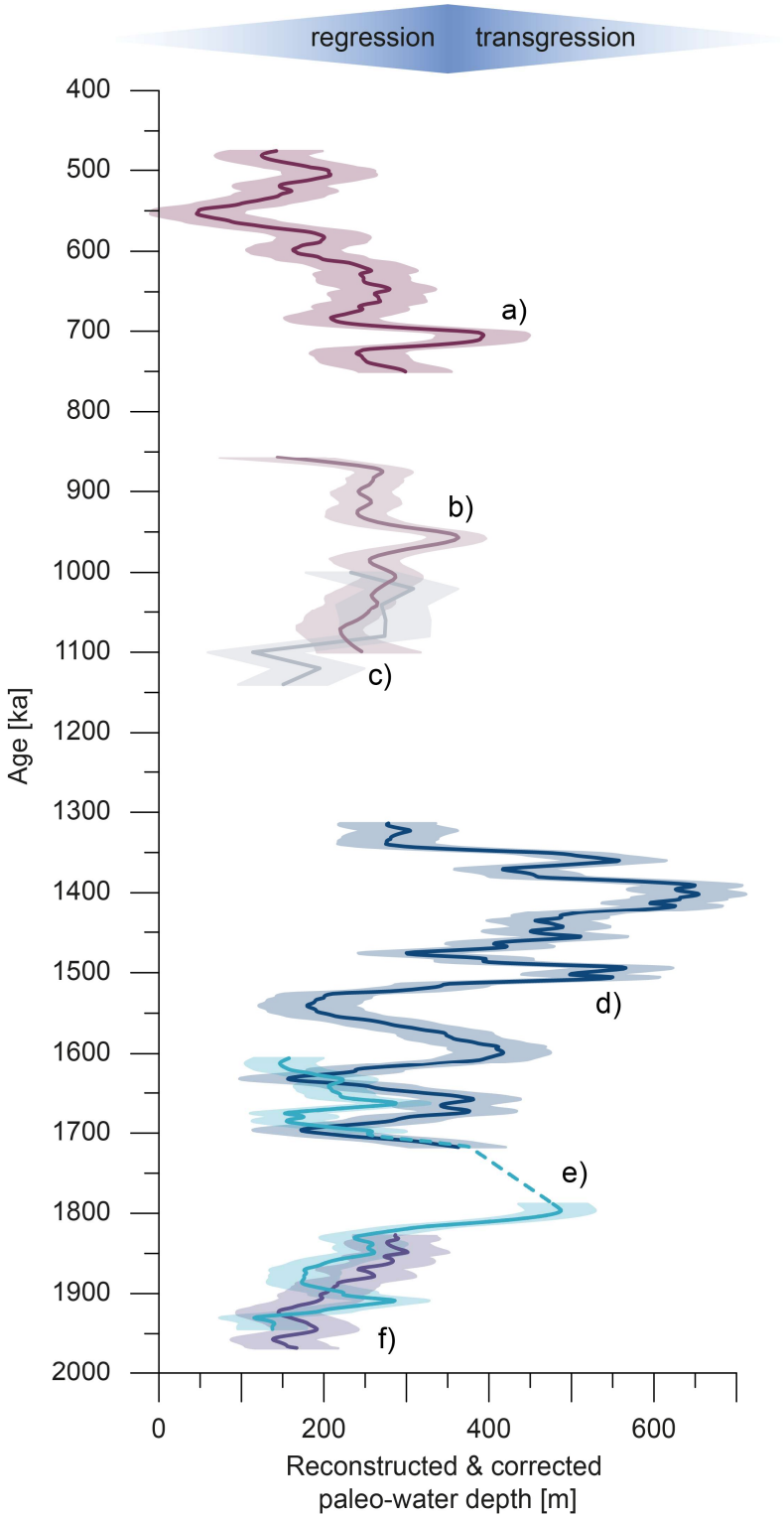

Figure 5.8. Available corrected paleo-water depth estimations of the LBF along the eastern coast of Rhodes plotted against age. The mean sample specific error of each sediment section is shown in pale color. For Lindos pale color indicates the bootstrapped 95% confidence interval. a) Lardos (Eichner et al., 2024a), b) Lindos (Quillévéré et al., 2019), c) Kallithea (data from Rasmussen and Thomsen, 2005), d) Pefka (Milker et al., 2019) e) Cape Vagia (this study), f) Agathi Beach (Eichner et al., 2024a).

Various studies have shown that the uplift gradient of eastern Rhodes increases from the south to the north during the Holocene (Pirazzoli et al., 1989; Howell et al., 2015; Triantafyllou and Papadopoulos, 2022), and observations of uplifted terraces on the island indicate a similar setting (Cornée et al., 2006a; Howell et al., 2015). Taking this into account, similar conditions during the Pleistocene seem to be possible, where the northern part was influenced by the uplift to an earlier and higher rate than the central part of the island, resulting in different ages for the onset of the long-term uplift. When comparing the rates of subsidence at Cape Vagia and Agathi Beach during the time interval of simultaneous deposition (1.93 and 1.91 Ma), the rate of Cape Vagia (~0.95 mm a^{-1}) is approximately 20% higher than those of Agathi Beach (~0.81 mm a^{-1}), which is in the same range as reported by Triantafyllou and Papadopoulos (2022) for Lindos and Tsampika for the Holocene. Another explanation for the offset of maximal drowning of about 390 kyrs might be, that the LBF did not experienced one large-scale maximal drowning, as suggested before (e.g., Titschack et al., 2013; Cornée et al., 2019) but two to three events of maximum drowning at approx. 1.8 Ma, 1.4 Ma and 0.7 Ma (Fig. 5.8), as the paleo-water depths trends during simultaneous deposition (Agathi Beach, Cape Vagia, Pefka; Kallithea, Lindos) match very well. Nevertheless, the combined data suggest, that generally the eastern coast of the island was uplifted approximately 700 m in the past 1.40 Myrs.

Due to the proximity to an active subduction zone, the tectonically induced vertical motions on Rhodes can be related to multiple causes. One factor is the long-term subsidence and subsequent uplift of the island as a result of an eastward and westward tilting around a NNE-SSW-trending horizontal axis of the island (e.g., Hanken et al., 1996; van Hinsbergen et al., 2007). In the Hellenic subduction zone an aseismic slip on fault planes (accumulation of tectonic loading through a slow slip) seems to be responsible for the major fraction of the vertical motion, while seismic slip rates, related to earthquakes, only account for a small fraction (e.g., Jackson and McKenzie, 1988; Papadopoulos, 1989; Shaw and Jackson, 2010; Howell et al., 2015). It has also been suggested that the uplift of coastlines close to the subduction zone is because of the accumulation of sedimentary material on the overriding plate by underplating (Angelier et al., 1982; Howell et al., 2015, 2017). Triantafyllou and Papadopoulos (2022) did not find evidence for an aseismic slip or underplating on the island, at least not for the late-Holocene, but attributed nearly half of the total coastal uplift of ~6 m in the last 2.3 ka to a major earthquake (M≥7.7). They suggested that the rest was uplifted by smaller but still large earthquakes (M≥7.0). Shaw et al. (2008) showed the interplay of aseismic (taking up the largest part of uplift) and seismic slip near southwest Crete and concluded that this might also be true along the rest of the Hellenic subduction zone. Variations in the subsidence and uplift gradient along the eastern coast of Rhodes might therefore be the result of an interplay

between continuous slow and abrupt vertical motions. Pirazzoli et al. (1989) proposed that the vertical motions of the island did not affect the whole island evenly but individual blocks that resulted in different Holocene notch elevations along the coast of Rhodes. Kontogianni et al. (2002), however, argued that it seems unlikely that an earthquake can affect a long fault segment, including several meters of uplift, without affecting nearby segments. They suggest that the tectonics at the island are dominated by a main compressional fault zone offshore, sub-parallel to the eastern coast of Rhodes with normal faults inland. They indicated a rather complex pattern of small uplifts alternating with major uplifts and subsidence because of the reactivation of different faults of one fault zone. It is proposed that areas previously uplifted will be submerged if the fault activity shifts away from the footwall of a reactivated fault. They further stated that small variations in the uplift or subsidence along a fault strike are usual, for example due to segmentation of faults or variations of fault slip along strike (Kontogianni et al., 2002).

5.5.2.2 Short-term vertical motions

Apart from the long-term vertical motions, the LBF sedimentary deposits in Agathi Beach, Lindos Bay, Lardos and Pefka are known to additionally record individual small-scale motions (Fig. 5.8; Milker et al., 2019; Quillévéré et al., 2019; Eichner et al., 2024a). Likewise, the corrected paleo-water depth estimates of the Cape Vagia section indicate three small-scale cycles of transgression and regression, with subsidence rates of 7.9 mm a^{-1} (1.93-1.91 Ma), 3.1 mm a^{-1} (1.89-1.79 Ma) and 10.4 mm a^{-1} (1.68-1.66 Ma), and subsequent uplifts at rates of 5.0 mm a^{-1} (1.91-1.89 Ma), 2.9 mm a^{-1} (1.79-1.68 Ma) and 2.8 mm a^{-1} (1.66-1.61 Ma). Those rates are in the range of other small-scale vertical motions on the Island of Rhodes which range between 1.5 to 10.3 mm a^{-1} (Milker et al., 2019; Quillévéré et al., 2019; Eichner et al., 2024a).

The marine sediments of the LBF are known to be deposited in individual graben structures (e.g., Hanken et al., 1996; van Hinsbergen et al., 2007), which are subject to local subsidence processes. Kanzler (2022), Szuba (2024) and Grolms (2024), revealed that these graben systems were formed due to a NE-SW horizontal extension (Szuba, 2024; Grolms, 2024), parallel to the plate-boundary, before and throughout the Pleistocene, mainly by reactivation of NW-trending faults (Kanzler, 2022; Szuba, 2024). The movement on one individual fault can cause small vertical displacement (< 20 m) but is unlikely to cause a great amount of vertical displacement, in the order of ~200 m for example, in one simple event (Ragan, 2009). However, considering that faults occur in sets and not isolated (Ramsay et al., 1987), each fault would then account for only a fraction of the total vertical displacement (Ragan, 2009), that accumulate over time. However, amplitudes of these short-term motions are rather high and might reach up to 300 m relative water depth change

within a short period of time (Fig. 5.8). In order to explain the great amplitudes of relative sea level change in the sections greater forces would be needed than the local displacement on the island. It has been proposed that the Hellenic subduction zone is influenced by increasing thickness of sedimentary material on the overriding plate by underplating, leading to an uplift of coastlines close to the subduction zone, such as Crete and possibly Rhodes (Angelier et al., 1982; Howell et al., 2015, 2017). The formation of an accretionary wedge by underplating, might explain the vertical motions observed in the sediment sections on the Island of Rhodes. An accretionary wedge aims to remain stable and will internally deform until it reaches a stable configuration (Platt, 1986). Therefore, we hypothesize that the general uplift, due to the underplating process, will continue until the stable configuration of the accretionary wedge is no longer established because of continuous supply of sediments and the resulting change in the slope (Fig. 5.9; Platt, 1986). To restore the stability, the wedge will deform internally, resulting in a shallower slope and in the subsidence of the overriding plate (Fig. 5.9). Additionally, one can notice that the frequency of the short-term sea-level fluctuations has decreased in the sections younger than approx. 1.4 Ma, compared to the older ones (Fig. 5.8). This could be an indication that the regime may have changed during the deposition of the LBF.

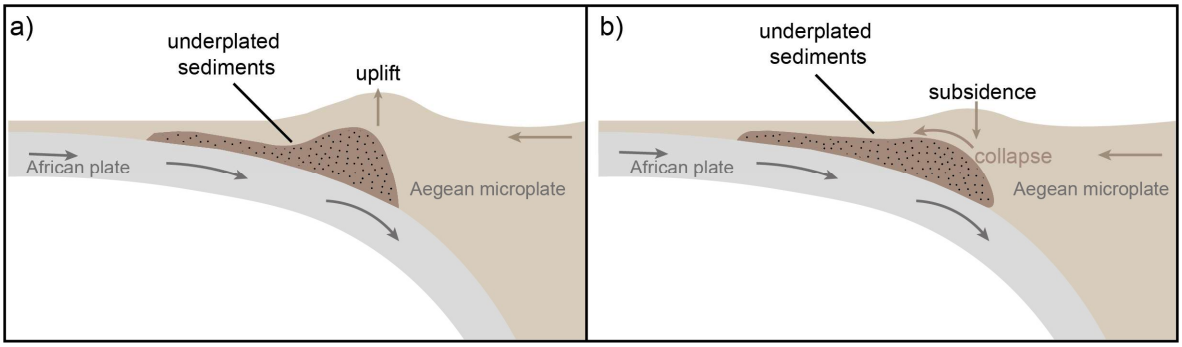

Figure 5.9. Hypothetical schematic illustration of the processes responsible for the high amplitudes of short-term uplift and subsidence processes. a) Formation of an accretionary wedge by underplating due to the subduction of the African under the Aegean microplate results in an uplift of the overlying crust (stable configuration). b) When the stability of the wedge is no longer established, it will undergo an internal deformation in order to reach the stable configuration, leading to subsidence processes.

When comparing the short-term tectonically induced vertical motions during simultaneously deposited sediment sections (Agathi Beach, Cape Vagia, Pefkos; Kallithea, Lindos) the general trends are well-fitting, however they do differ in their amplitudes (Fig. 5.8). Therefore, the small-scale vertical motions seen in the reconstructed and corrected paleo-water depths might be a combination of large-scale processes (as described above), of uplift and subsidence, and locally induced and site-specific processes that are responsible for additional minor vertical motions in individual depocenter. Vertical displacement due to normal faults between two depocenters,

account for some of vertical motions, e.g. Block B is uplifted (Fig. 5.10B). Together with the general drowning (Fig. 5.10B) and subsequent uplift (Fig. 5.10C) of the eastern coast of the island, this results in greater water depths at deposition in Block A, compared to Block B. The subsidence processes in the graben structures also account for individual motions generating further differences between individual depocenters.

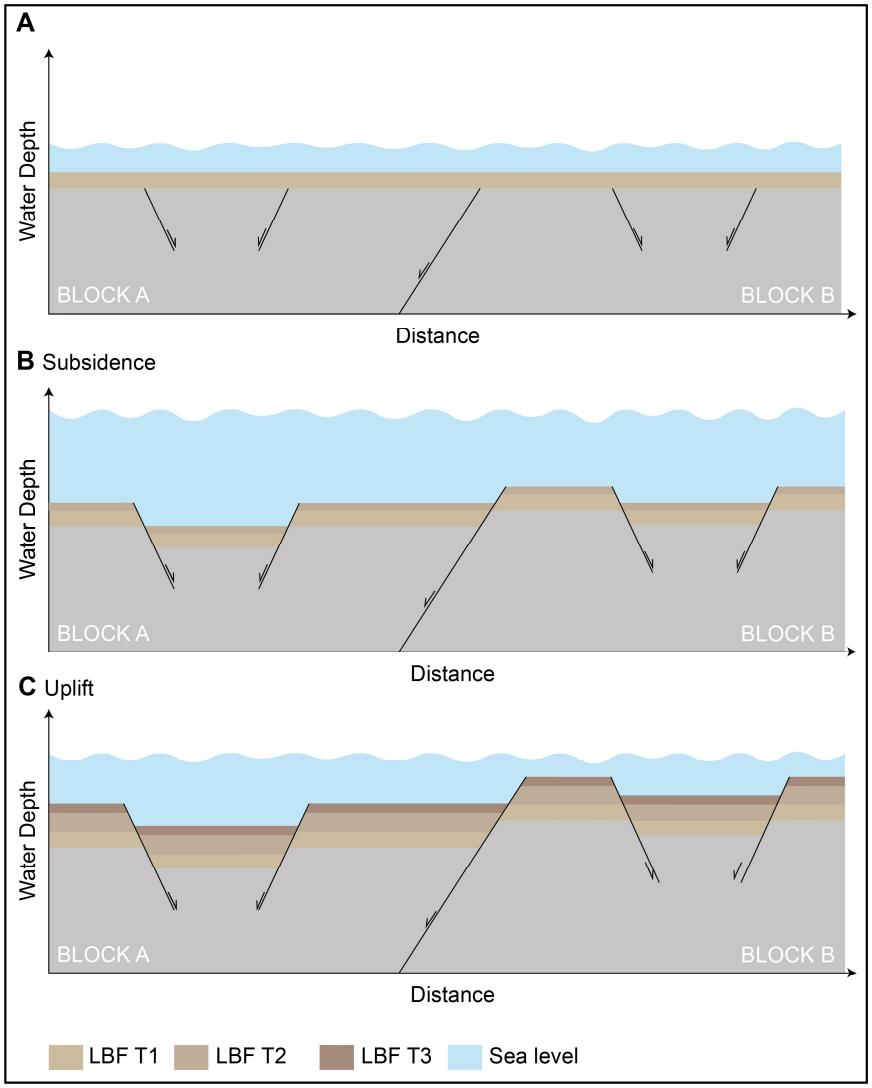

Figure 5.10. Schematic illustration of the geological features influencing the deposition of the LBF in individual depocenter along the eastern coast of Rhodes. **A.** Indicates the onset of the LBF (T1) deposition, with no tectonic interruption. **B.** Stage of island-wide subsidence, coupled with the interruption of LBF T1 by the vertical displacement of Block A and B and additional subsidence of graben structures with individual rates. After displacement, LBF T2 is deposited horizontally. **C.** Stage of island-wide uplift, where LBF T1 and T2 are displaced. LBF T3 is deposited horizontal after vertical motions.

5.6 Conclusion

The reconstruction of tectonically induced vertical motions by using benthic foraminiferal assemblages has been proven to be a valuable proxy in adding knowledge to the complex depositional history of the LBF and the neotectonic setting during the Plio-Pleistocene. The reconstruction of the Cape Vagia section revealed that the marine sediments were influenced by tectonically induced long- and short-term vertical motions and it is proposed that it also captures the transition from the transgressive to the regressive phase. Long-term average subsidence and uplift rates were estimated to ~2.2 mm a^{-1} and ~1.8 mm a^{-1}, respectively and short-term rates were as high as ~10.4 mm a^{-1}. By combining this with already existing data, we were able to reconstruct the full cycle of transgression and regression, lasting from ~1.97 Ma to 0.47 Ma with a maximum uplift of ~700 m from the Early Pleistocene until today. It is proposed that the short-term cycles of uplift and subsidence might be the result of an accretionary wedge causing uplift due to the continuous sediment supply (underplating) and subsidence because of internal deformation to gain a state of stability. Differences in the rates, timing and amplitudes of vertical motions are explained by a combination of large-scale processes of uplift and subsidence and locally induced and site-specific processes in the graben structures.

The benthic foraminiferal assemblage further reveals an increasing eutrophication off the Island of Rhodes during the deposition of the Cape Vagia sediment section in the Pleistocene, which is indicated by the high numbers of eutrophic indicator species in the sediments.

Acknowledgements

We thank Jutta Richarz for her technical support during laboratory work. Louisa Kanzler and Tobias Winkler are thanked for the processing of some samples and Mike Frenken is thanked for his help during sampling. Sampling took place with the permission of the Director of the Institute of Geology and Mineral Exploration, Athens, Greece. Further, we thank Tine Rasmussen for providing the counting data of the Kallithea section. This study was financially supported by the Deutsche Forschungsgemeinschaft (DFG) by grants to Yvonne Milker (MI 1508/9-1) and Gerhard Schmiedl (Schm 1180/25-1). The study is a contribution to the "Center for Earth System Research and Sustainability (CEN)" of Universität Hamburg. Sampling took place with the permission of the Director of the Institute of Geology and Mineral Exploration, Athens, Greece.

Data availability:

Supplementary material referred to in this chapter are available as Appendix in this thesis:

Appendix B: Carbon and oxygen stable isotope data.

Appendix C: Correlation of $\delta^{18}O$ infaunal and epifaunal data of the Cape Vagia sediment section with the benthic LR04 stack.

Appendix D: Evaluation and estimates of paleo-water depth reconstruction.

Appendix E: Complete census counts of the Cape Vagia sediment section.

6 Conclusion

In this doctoral thesis, the analysis of benthic foraminiferal assemblages of four marine sediment sections was used to quantify the neotectonic history of the Island of Rhodes to attempt a better understanding of the long- and short-term tectonic motions on the island and, thus, to help to better understand subduction processes in the Eastern Mediterranean Sea in the frame of the Alpine Orogeny. In this context, the doctoral thesis aimed to test the hypotheses, that *different sedimentary depocenters along the eastern coast of the Island of Rhodes underwent different tectonically induced vertical motions* and that *uplift and subsidence rates of the sedimentary deposits are significantly higher than those proposed in previous publications*. To do so, conclusions are drawn by answering the research questions raised in the introduction:

a) *Do the foraminiferal assemblages reflect orbital-driven cyclic changes and glacio-eustatic sea level changes that influence the accuracy of paleo-water depth reconstructions?*

   The benthic foraminiferal assemblages studied from different depocenters along the eastern coast of Rhodes reflect orbital-driven climate changes to different degrees. These changes can primarily be identified by the increase of eutrophic indicator species and in some cases by decreased $\delta^{13}C$ values of the epibenthic and/or infaunal foraminifera. For example, the Agathi Beach sediment section situated at the middle east coast of Rhodes reveals two strong increases in eutrophic indicator species, which co-occur with the Mediterranean sapropels s51 and s50 after Kroon et al. (1998), indicating a precessional-driven influence on the assemblage. By contrast, the foraminiferal assemblages of the Lardos section, also situated at the middle eastern part of Rhodes, seem not to react as strong to orbital-driven changes but indicate a strong and long-lasting eutrophication during the Middle Pleistocene. The benthic foraminiferal assemblages of the Cape Vagia section, situated in the northeastern part of the island, likewise indicate an eutrophication in the Early Pleistocene, which seems to be related to higher (seasonal) organic fluxes to the seafloor. However, the assemblages seem not to be strongly influenced by precession-driven but might rather be influenced by obliquity-driven changes. Finally, the Pliocene Plimiri 5 section, situated in the southeastern part of the island, suggests an extreme periodicity in diversity and assemblage composition, with thick intervals clearly dominated by eutrophic indicator species. Due to its periodicity, these intervals have been interpreted as near-coastal equivalents of Eastern Mediterranean deep sea sapropels, indicating a more

humid climate around the Island of Rhodes during times of sapropel formation in the Late Pliocene. These phases have been attributed to an increased primary production of the near-coastal environments, triggered by an enhanced precipitation and resulting in higher river run-off.

The differences in the reflection of orbital-driven productivity changes in the individual depocenters along the eastern coast of Rhodes might best be explained by two factors: location and time. The Plimiri section is thought to be close to a larger river system, indicated by a modern drainage pattern that has not been observed to this extent at other depocenter locations. Additionally, the Plimiri section is much older than any other, yet-known, deposit of the Lindos Bay Formation, and various studies suggest that the highest fluxes of organic carbon to the sea floor and an improved preservation of the organic carbon were reached during the deposition of Pliocene sapropels under warmer and wetter conditions compared to Pleistocene and Holocene sapropels (van Os et al., 1994; Rullkötter et al., 1998; Bouloubassi et al., 1999; Nijenhuis and Lange, 2000; Arnaboldi and Meyers, 2006).

Consequently, the benthic foraminiferal assemblages, especially of the Agathi Beach and Plimiri sediment sections, strongly reflect precession-driven climate changes that influence the accuracy of the paleo-water depth reconstructions. During these periods the relatively high proportions of eutrophic indicator species are indicative for an increased food supply and potentially changing oxygen contents on the sea bottom and pore waters (e.g., Gooday, 1994; Bernhard and Sen Gupta, 1999; Schönfeld, 2001), and hence, any bathymetric reconstructions are overprinted by environmental influences and had to be excluded for paleo-water depth reconstructions. Further, spectral analysis of the paleo-water depth reconstructions reveal a precessional influence, even if not clearly reflected in the assemblages (Appendix D). To remove a precession-controlled influence on the paleo-water depth reconstructions, this effected was filtered out. In the case of the Plimiri sediment section, the climate-driven influence on the benthic foraminiferal assemblage was so strong that this section could not be used to reconstruct tectonically driven vertical motions from southern Rhodes.

b) To what extend are the climate-corrected paleo-water depth changes related to the tectonically induced vertical motions?

The paleo-water depth reconstructions in the here studied sediment sections reflect long- and short-term paleo-water depth changes. The maximum fluctuations in the uncorrected paleo-water depth estimates exceed those of global orbital-scale sea level changes (Bintanja and van de Wal, 2008), which has been filtered out. It is assumed that the remaining proportion of reconstructed sea level changes is subject of tectonically induced vertical motions. The tectonic motions calculated during the thesis are comparable to those found in other studies (Cornée et al., 2019; Milker et al., 2019; Quillévéré et al., 2019). However, some limitations need to be pointed out in order to interpret the rates of vertical motions. For once the development of a robust chronostratigraphic framework is needed, to extract the tectonic component from the uncorrected paleo-water depth. The chronostratigraphic framework for the Plio-Pleistocene deposits on the Island of Rhodes mainly rely on the first occurrence of planktic and/or benthic foraminifera which can be used as a tie point for the correlation with stable isotope data from the sediment sections and the global LR04 stack (Lisiecki and Raymo, 2005). However, there is only a limited number of ages for first or last occurrences of foraminifera in the Mediterranean Sea (Lourens et al., 1996b; 2004), which consequently need to be captured in the sedimentary record to be used and due to the sampling with a resolution of 10 to 20 cm, certain errors cannot be ruled out.

The combination and comparison of the paleo-water depth reconstructions, however, proves that the long-term paleo-water depth evolution is in line with those suggested by the stratigraphy (Titschack et al., 2013; Cornée et al., 2019), and paleo-water depths are comparable with estimates of studies using other methods (Moissette and Spjeldnæs, 1995; van Hinsbergen et al., 2007). Apart from the long-term trend, short-term vertical motions are observable in all sedimentary records, and because environmental parameters that could have influenced the benthic assemblage were fitted out, this thesis suggests that the short-term vertical motions are tectonically induced.

c) Are the reconstructed rates of uplift and subsidence similar in each of the sedimentary depocenters or do they differ significantly?

When comparing the paleo-water depth changes of the studied sedimentary deposits on the Island of Rhodes with each other and already existing data, differences are seen especially in the rates of vertical motions. Chronostratigraphic overlaps of reconstructed

vertical motions provide evidence that the general trends of uplift or subsidence in both, long- and short-term, are similar but vary in amplitudes (Fig. 6.1). Comparing the reconstructions from Agathi Beach (middle eastern coast) and Cape Vagia (northeastern coast), which were partly deposited simultaneously, it is noticeable, that the long-term subsidence rates of Agathi Beach were approximately 20% lower than those of Cape Vagia in the same time frame. Triantafyllou and Papadopoulos (2022) found a similar pattern during the Holocene, with the southeastern coast to be less effected by tectonic uplift than the northern part. The comparison of the reconstruction for Cape Vagia and Pefka on the other hand, reveals that short-term vertical motions seem to be similar but with greater differences in the amplitudes. For example, between 1.70 Ma and 1.63 Ma a short-term cycle of subsidence and uplift is indicated in the Pefka data, which translates to a subsidence of 5.5 mm a^{-1} and a subsequent uplift of 8.8 mm a^{-1}. At Cape Vagia this cycle is also recorded, but there with a subsidence of 10.4 mm a^{-1} and a lower uplift of 2.8 mm a^{-1} and, hence, subsidence is approximately 50% higher in Cape Vagia, while uplift is about 30% lower than in Pefka. Although some uncertainties may be expected, for example in the chronology, the example nicely illustrates the differences between individual depocenter.

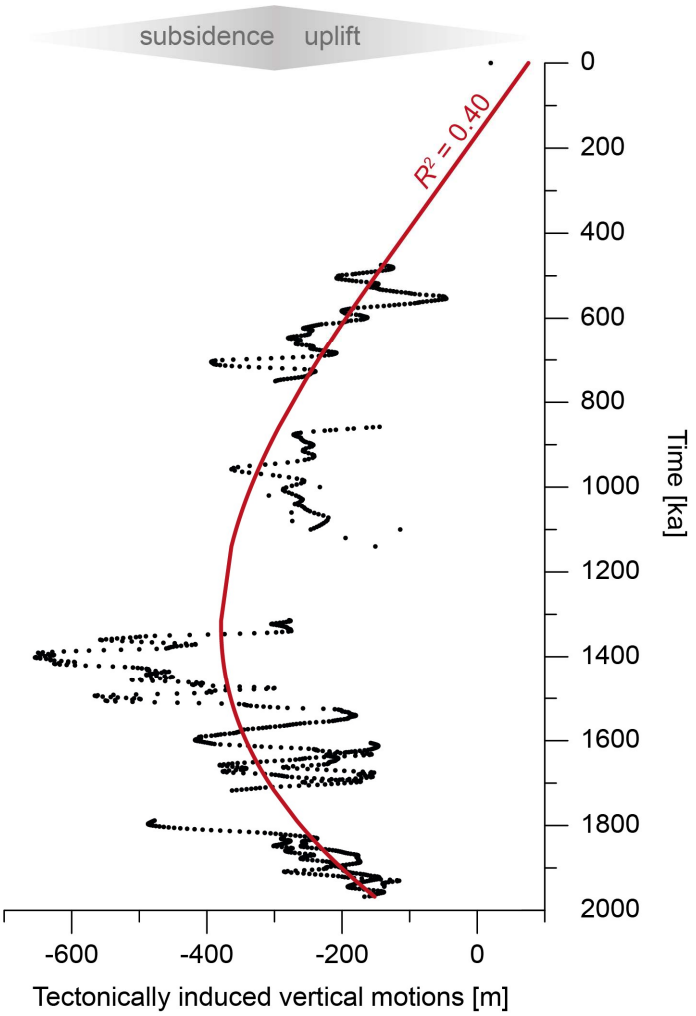

Figure 6.1 Reconstructed tectonically induced vertical motions in relation to the modern sea level, against time. Red line represents the polynomial of 2nd degree model ($p<0.001$). Both, the observed motions and the polynomial fit represent the cycle of subsidence and uplift. Modern data was obtained during field work in 2022.

The great differences between the individual depocenters are also shown by the chronostratigraphy of the LBF and the differences in contacts to the upper and lower

boundaries (chapter 5). The youngest outcropped boundary to the underlying Kolymbia Formation was deposited at about 1.71 Ma at Pefka, while the Plimiri 5 sediment section revealed a surprisingly old age for the lower boundary of ~3.35 Ma. It remains unclear, how such a setting is possible but illustrates well how individually these deposits developed.

In conclusion, the individual depocenters along the eastern coast of the Island of Rhodes were subject to different tectonically induced vertical motions, some of which may influence the whole subduction zone, some island-wide and some regional movements. Therefore, only limited conclusion can be drawn from one depocenter to another and each depocenter needs to be evaluated separately. Through a detailed study of four sedimentary deposits of the Plio-Pleistocene Lindos Bay Formation, this work quantified the long- and short-term vertical tectonic motions and provides more evidence for a highly complex tectonic evolution of the island. Finally, the results of this thesis in combination with already existing data, could be used to reconstruct the full cycle of subsidence and uplift on the Island of Rhodes during the Plio-Pleistocene, lasting from 1.97 Ma to 0.47 Ma with an uplift of ~700 m ± 42 m in the last 1.40 Myrs (Fig. 6.1), suggesting a rate of ~0.5 mm a^{-1} in the middle eastern coast. The northeastern coast, due to its earlier onset of uplift, revealed an uplift of approximately 500 m ± 51 m in the last 1.80 Myrs. This doctoral thesis can therefore confirm that *different sedimentary depocenters underwent different tectonically induced vertical motions.*

The application of a benthic foraminiferal-based transfer function enabled high-resolution paleo-water depth reconstructions, and derived from this, the quantification of tectonically induced vertical motions that not only captures the well-known large scale vertical motions, but also smaller scaled tectonic cycles with rates ranging from 1.5 to 10.4 mm a^{-1} that have not been quantified so far. In order to explain the high amplitudes, it has been proposed that these vertical motions are the result of larger processes, influencing the Hellenic subduction zone. Therefore, it is concluded that the *uplift and subsidence rates of the sedimentary deposits* during the Plio-Pleistocene *are significantly higher than those proposed in previous publications.*

7 Outlook

This doctoral thesis has proven, that the reconstruction of long- and small-scaled vertical motions by using benthic foraminiferal transfer functions can be of great benefit to better understand the subduction-related tectonic forces in the Eastern Mediterranean region and by identifying the impact of changing climate on the benthic foraminiferal assemblages in the Plio-Pleistocene may be useful in assessing future impacts and risks of climate change on modern benthic assemblages.

By adapting the benthic foraminiferal transfer function to other islands along the Hellenic subduction zone and by comparing those results with the Island of Rhodes, would help to answer the question whether the observed short-term vertical motions on Rhodes are a local phenomenon or if they can also be observed and quantified elsewhere. This would help to provide further evidence for the hypothesis proposed in this thesis that the high-amplitude short-term motions are subject to large processes that affect most of the Hellenic Arc. Multiple islands in the Eastern Mediterranean provide outcrops of marine sedimentary records from the Neogene to Quaternary (e.g., Meulenkamp et al., 1994; Hilgen et al., 1995; Athanasiou et al., 2015) and are located in different regions of the subduction zone. The Islands of Crete and Gavdos, for example, form the southernmost exposed part of the Hellenic Arc, whereas the Island of Rhodes is located at its eastern end (Fig. 2.4). Tiberti et al. (2014) found high amounts of small-scale vertical motions on the Island of Crete based on the analysis of Late Pleistocene to Holocene paleo-shorelines, and the question arises whether these small-scale motions would also be identifiable in the older sediment sections from this island. Another possible study area could be the Island of Cyprus, which is part of the Cyprian Arc, a northward-dipping subduction zone, at the northern margin of the African Plate (Fig. 2.4; Payne and Robertson, 1995; Harrison et al., 2004). Due to the different positions of the islands along the subduction zone of the African and Eurasian plates, they are exposed to different tectonic forces and the comparison of large- and small-scaled vertical motions would be of great interest to better understand subduction-zone related kinematics. Further, all the mentioned islands inhabit outcrops mainly from the Miocene. For example, the Kalamavka Formation on Crete is known to be deposited at the beginning of the break-up stage of the Aegean microplate (Drinia et al., 2013), and on Gavdos the Metochia section was deposited before the Messinian evaporitic deposition (Hilgen et al., 1995), which provides a great opportunity to not only compare different regions in in the Hellenic subduction zone, but also their temporal

development, for example, are the short-term cycles common throughout the Neogene or can an onset be noticed?

To improve the accuracy of the benthic foraminiferal based transfer function and related paleo-water depth estimates, the collection of modern samples in the Eastern Mediterranean Sea from various water depths and the documentation of the environmental parameters would be of great benefit. Especially modern samples from deeper regions of the Mediterranean Sea are lacking but would be critical for the application of the TF to sediments deposited in deep-sea settings, as suggested for example on Gavdos by Meulenkamp et al. (1994) who estimated water depths up to 1,200 m in the Late Miocene.

References

Abu-Zied, R.H., Rohling, E.J., Jorissen, F.J., Fontanier, C., Casford, J.S., Cooke, S., 2008. Benthic foraminiferal response to changes in bottom-water oxygenation and organic carbon flux in the eastern Mediterranean during LGM to Recent times. Marine Micropaleontology 67 (1-2), 46–68. doi: 10.1016/j.marmicro.2007.08.006.

Adkins, J.F., McIntyre, K., Schrag, D.P., 2002. The salinity, temperature, and delta^{18}O of the glacial deep ocean. Science (New York, N.Y.) 298 (5599), 1769–1773. doi: 10.1126/science.1076252.

Aksu, A.E., Hiscott, R.N., Kostylev, V.E., Yaltırak, C., 2018. Organized patches of bioherm growth where the Strait of Dardanelles enters the Marmara Sea, Turkey. Palaeogeography, Palaeoclimatology, Palaeoecology 490, 325–346. doi: 10.1016/j.palaeo.2017.11.010.

Alavi, S.N., 1988. Late Holocene deep-sea benthic foraminifera from the Sea of Marmara. Marine Micropaleontology 13 (3), 213–237. doi: 10.1016/0377-8398(88)90004-7.

Altenbach, A.V., Lutze, G.F., Schiebel, R., Schönfeld, J., 2003. Impact of interrelated and interdependent ecological controls on benthic foraminifera: an example from the Gulf of Guinea. Palaeogeography, Palaeoclimatology, Palaeoecology 197 (3-4), 213–238. doi: 10.1016/S0031-0182(03)00463-2.

Altenbach, A.V., Pflaumann, U., Schiebel, R., Thies, A., Timm, S., Trauth, M., 1999. Scaling percentages and distributional patterns of benthic Foraminifera with flux rates of organic carbon. Journal of Foraminiferal Research 29 (3), 173–185.

Alve, E., 1999. Colonization of new habitats by benthic foraminifera: a review. Earth-Science Reviews 46 (1-4), 167–185. doi: 10.1016/S0012-8252(99)00016-1.

Alve, E., Murray, J.W., 1995. Benthic foraminiferal distribution and abundance changes in Skagerrak surface sediments: 1937 (Höglund) and 1992/1993 data compared. Marine Micropaleontology 25 (4), 269–288. doi: 10.1016/0377-8398(95)00026-7.

Andersen, M.B., Gallup, C.D., Scholz, D., Stirling, C.H., Thompson, W.G., 2009. U-series dating of fossil coral reefs: Consensus and controversy. PAGES news 17 (2), 54–56. doi: 10.22498/pages.17.2.54.

Angelier, J., Lybéris, N., Le Pichon, X., Barrier, E., Huchon, P., 1982. The tectonic development of the hellenic arc and the sea of crete: A synthesis. Tectonophysics 86 (1-3), 159–196. doi: 10.1016/0040-1951(82)90066-X.

Antoine, D., Morel, A., André, J.-M., 1995. Algal pigment distribution and primary production in the eastern Mediterranean as derived from coastal zone color scanner observations. Journal of Geophysical Research 100 (C8), 16193. doi: 10.1029/95JC00466.

Arnaboldi, M., Meyers, P.A., 2006. Patterns of organic carbon and nitrogen isotopic compositions of latest Pliocene sapropels from six locations across the Mediterranean Sea. Palaeogeography, Palaeoclimatology, Palaeoecology 235 (1-3), 149–167. doi: 10.1016/j.palaeo.2005.09.027.

Athanasiou, M., Bouloubassi, I., Gogou, A., Klein, V., Dimiza, M.D., Parinos, C., Skampa, E., Triantaphyllou, M.V., 2017. Sea surface temperatures and environmental conditions during the "warm Pliocene" interval (~ 4.1–3.2 Ma) in the Eastern Mediterranean (Cyprus). Global and Planetary Change 150, 46–57. doi: 10.1016/j.gloplacha.2017.01.008.

Athanasiou, M., Triantaphyllou, M.V., Dimiza, M.D., Gogou, A., Theodorou, G., 2015. Zanclean/Piacenzian transition on Cyprus (SE Mediterranean): calcareous nannofossil evidence of sapropel formation. Geo-Marine Letters 35 (5), 367–385. doi: 10.1007/s00367-015-0414-6.

Avnaim-Katav, S., Hyams-Kaphzan, O., Milker, Y., Almogi-Labin, A., 2015. Bathymetric zonation of modern shelf benthic foraminifera in the Levantine Basin, eastern Mediterranean Sea. Journal of Sea Research 99, 97–106. doi: 10.1016/j.seares.2015.02.006.

Avnaim-Katav, S., Milker, Y., Schmiedl, G., Sivan, D., Hyams-Kaphzan, O., Sandler, A., Almogi-Labin, A., 2016. Impact of eustatic and tectonic processes on the southeastern Mediterranean shelf during the last one million years: Quantitative reconstructions using a foraminiferal transfer function. Marine Geology 376, 26–38. doi: 10.1016/j.margeo.2016.03.010.

Backman, J., Raffi, I., Rio, D., Fornaciari, E., Pälike, H., 2012. Biozonation and biochronology of Miocene through Pleistocene calcareous nannofossils from low and middle latitudes. Newsletters on Stratigraphy 45 (3), 221–244. doi: 10.1127/0078-0421/2012/0022.

Bandy, O.L., Chierici, M.A., 1966. Depth-temperature evaluation of selected California and Mediterranean bathyal foraminifera. Marine Geology 4 (4), 259–271. doi: 10.1016/0025-3227(66)90045-4.

Barmawidjaja, D.M., Jorissen, F.J., Puskaric, S., van der Zwaan, G.J., 1992. Microhabitat selection by benthic Foraminifera in the northern Adriatic Sea. Journal of Foraminiferal Research 22 (4), 297–317. doi: 10.2113/gsjfr.22.4.297.

Barmawidjaja, D.M., van der Zwaan, G.J., Jorissen, F.J., Puskaric, S., 1995. 150 years of eutrophication in the northern Adriatic Sea: Evidence from a benthic foraminiferal record. Marine Geology 122 (4), 367–384. doi: 10.1016/0025-3227(94)00121-Z.

Bartels-Jónsdóttir, H.B., Knudsen, K.L., Abrantes, F., Lebreiro, S., Eiríksson, J., 2006. Climate variability during the last 2000 years in the Tagus Prodelta, western Iberian Margin: Benthic foraminifera and stable isotopes. Marine Micropaleontology 59 (2), 83–103. doi: 10.1016/j.marmicro.2006.01.002.

Berger, A., 1978. Long-term variations of daily insolation and quaternary climatic changes. Journal of Atmospheric Science 35 (12), 2362–2367. doi: 10.1175/1520-0469(1978)035<2362:LTVODI>2.0.CO;2.

Bernhard, J.M., Sen Gupta, B.K., 1999. Foraminifera of oxygen-depleted environments, in: Sen Gupta, B.K. (Ed.), Modern Foraminifera. Springer Netherlands, Secaucus, 201–216. doi: 10.1007/0-306-48104-9_12.

Bethoux, J., Gentili, B., Morin, P., Nicolas, E., Pierre, C., Ruiz-Pino, D., 1999. The Mediterranean Sea: a miniature ocean for climatic and environmental studies and a key for the climatic functioning of the North Atlantic. Progress in Oceanography 44 (1-3), 131–146. doi: 10.1016/S0079-6611(99)00023-3.

Bethoux, J.P., Gentili, B., 1994. The Mediterranean Sea, a Test Area for Marine and Climatic Interactions, in: Malanotte-Rizzoli, P., Robinson, A.R. (Eds.), Ocean Processes in Climate Dynamics: Global and Mediterranean Examples. Springer Netherlands, Dordrecht, 239–254. doi: 10.1007/978-94-011-0870-6_11.

Bhadra, S.R., Saraswat, R., 2021. Assessing the effect of riverine discharge on planktic foraminifera: A case study from the marginal marine regions of the western Bay of Bengal. Deep Sea Research Part II: Topical Studies in Oceanography 183, 104927. doi: 10.1016/j.dsr2.2021.104927.

Bijma, J., Faber, W.W., Hemleben, C., 1990. Temperature and salinity limits for growth and survival of some planktonic foraminifers in laboratory cultures. Journal of Foraminiferal Research 20 (2), 95–116.

Bintanja, R., van de Wal, R.S.W., 2008. North American ice-sheet dynamics and the onset of 100,000-year glacial cycles. Nature 454 (7206), 869–872. doi: 10.1038/nature07158.

Bintanja, R., van de Wal, R.S.W., Oerlemans, J., 2005. Modelled atmospheric temperatures and global sea levels over the past million years. Nature 437 (7055), 125–128. doi: 10.1038/nature03975.

Birks, H., 1998. Numerical tools in palaeolimnology – Progress, potentialities, and problems. Journal of paleolimnology 20, 307–332. doi: 10.1023/A:1008038808690.

Boltovskoy, E., Wright, R., 1976. Recent Foraminifera. Springer Netherlands, Dordrecht.

Bonneau, M., 1984. Correlation of the Hellenide nappes in the south-east Aegean and their tectonic reconstruction. Geological Society, London, Special Publications 17 (1), 517–527. doi: 10.1144/GSL.SP.1984.017.01.38.

Bosc, E., Bricaud, A., Antoine, D., 2004. Seasonal and interannual variability in algal biomass and primary production in the Mediterranean Sea, as derived from 4 years of SeaWiFS observations. Global Biogeochemical Cycles 18 (1). doi: 10.1029/2003GB002034.

Bouloubassi, I., Rullkötter, J., Meyers, P.A., 1999. Origin and transformation of organic matter in Pliocene–Pleistocene Mediterranean sapropels: organic geochemical evidence reviewed. Marine Geology 153 (1-4), 177–197. doi: 10.1016/S0025-3227(98)00082-6.

Bown, P.R., Young, J.R., 1998. Techniques, in: Bown, P.R. (Ed.), Calcareous Nannofossil Biostratigraphy. Chapman and Hall, Kluwer Academic, 16–28.

Boyd, A., 2009. Relict conifers from the mid-Pleistocene of Rhodes, Greece. Historical Biology 21 (1-2), 1–15. doi: 10.1080/08912960903033301.

Bromley, R.G., Hanken, N.-M., 2003. Structure and function of large, lobed *Zoophycos*, Pliocene of Rhodes, Greece. Palaeogeography, Palaeoclimatology, Palaeoecology 192 (1-4), 79–100. doi: 10.1016/S0031-0182(02)00680-6.

Bryden, H.L., Kinder, T.H., 1991. Steady two-layer exchange through the Strait of Gibraltar. Deep Sea Research Part A. Oceanographic Research Papers 38, 445-463. doi: 10.1016/S0198-0149(12)80020-3.

Çağatay, M.N., Görür, N., Algan, O., Eastoe, C., Tchapalyga, A., Ongan, D., Kuhn, T., Kuşcu, I., 2000. Late Glacial–Holocene palaeoceanography of the Sea of Marmara: timing of connections with the Mediterranean and the Black Seas. Marine Geology 167 (3-4), 191–206. doi: 10.1016/S0025-3227(00)00031-1.

Caralp, M.H., 1989. Abundance of *Bulimina exilis* and *Melonis barleeanum*: Relationship to the quality of marine organic matter. Geo-Marine Letters 9 (1), 37–43. doi: 10.1007/BF02262816.

Carboni, M.G., Bellotti, P., Bergamin, L., Di Bella, L., Matteucci, R., 2000. Benthic foraminiferal assemblages from the Ombrone and Tiber deltas (Central Tyrrhenian Sea): a premiminary comparison. Géologie Méditerranéenne 27 (1-2), 3–13.

Carboni, M.G., Frezza, V., Bergamin, L., 2004. Distribution of Recent benthic foraminifers in the Ombrone River Basin (Tuscany Continental Shelf, Tyrrhenian Sea, Italy): Relations with fluvial run-off, in: Coccioni, R., Galeotti, S., Lirer, F. (Eds.), Proceedings of the First Italian Meeting on Environmental Micropaleontology, vol. 9. Grzybowski Foundation Special Publication, 7–16.

Casford, J., Rohling, E.J., Abu-Zied, R., Fontanier, C., Jorissen, F.J., Leng, M., Schmiedl, G., Thomson, J., 2003. A dynamic concept for eastern Mediterranean circulation and oxygenation during sapropel formation. Palaeogeography, Palaeoclimatology, Palaeoecology 190, 103–119. doi: 10.1016/S0031-0182(02)00601-6.

Casford, J.S.L., Rohling, E.J., Abu-Zied, R., Cooke, S., Fontanier, C., Leng, M., Lykousis, V., 2002. Circulation changes and nutrient concentrations in the late Quaternary Aegean Sea: A nonsteady state concept for sapropel formation. Paleoceanography 17 (2), 14-1-14-11. doi: 10.1029/2000PA000601.

Cavazza, W., Wezel, F.C., 2003. The Mediterranean region—a geological primer. Episodes 26 (3), 160–168. doi: 10.18814/epiiugs/2003/v26i3/002.

Cita, M.B., Zocchi, M., 1978. Distribution patterns of benthic foraminifera on floor of Mediterranean Sea. Oceanologica Acta 1 (4), 445–462.

Corliss, B.H., 1985. Microhabitats of benthic foraminifera within deep-sea sediments. Nature 314 (6010), 435–438. doi: 10.1038/314435a0.

Corliss, B.H., 1991. Morphology and microhabitat preferences of benthic foraminifera from the northwest Atlantic Ocean. Marine Micropaleontology 17 (3-4), 195–236. doi: 10.1016/0377-8398(91)90014-W.

Corliss, B.H., Chen, C., 1988. Morphotype patterns of Norwegian Sea deep-sea benthic foraminifera and ecological implications. Geology 16 (8), 716. doi: 10.1130/0091-7613(1988)016<0716:MPONSD>2.3.CO;2.

Cornée, J.-J., Moissette, P., Joannin, S., Suc, J.-P., Quillévéré, F., Krijgsman, W., Hilgen, F.J., Koskeridou, E., Münch, P., Lécuyer, C., Desvignes, P., 2006a. Tectonic and climatic controls on coastal sedimentation: The Late Pliocene–Middle Pleistocene of northeastern Rhodes, Greece. Sedimentary Geology 187 (3-4), 159–181. doi: 10.1016/j.sedgeo.2005.12.026.

Cornée, J.-J., Münch, P., Quillévéré, F., Moissette, P., Vasiliev, I., Krijgsman, W., Verati, C., Lécuyer, C., 2006b. Timing of Late Pliocene to Middle Pleistocene tectonic events in Rhodes (Greece) inferred from magneto-biostratigraphy and $^{40}Ar/^{39}Ar$ dating of a volcaniclastic layer. Earth and Planetary Science Letters 250 (1-2), 281–291. doi: 10.1016/j.epsl.2006.07.045.

Cornée, J.-J., Quillévéré, F., Moissette, P., Fietzke, J., López-Otálvaro, G.E., Melinte-Dobrinescu, M.C., Philippon, M., van Hinsbergen, D.J., Agiadi, K., Koskeridou, E., Münch, P., 2019. Tectonic motion in oblique subduction forearcs: insights from the revisited Middle and Upper Pleistocene deposits of Rhodes, Greece. Journal of the Geological Society 176 (1), 78–96. doi: 10.1144/jgs2018-090.

Cramp, A., Collins, M., West, R., 1988. Late pleistocene-holocene sedimentation in the NW Aegean Sea: A palaeoclimatic palaeoceanographic reconstruction. Palaeogeography, Palaeoclimatology, Palaeoecology 68 (1), 61–77. doi: 10.1016/0031-0182(88)90017-X.

Cramp, A., O'Sullivan, G., 1999. Neogene sapropels in the Mediterranean: a review. Marine Geology 153 (1-4), 11–28. doi: 10.1016/S0025-3227(98)00092-9.

Criado-Aldeanueva, F., Soto-Navarro, F.J., García-Lafuente, J., 2012. Seasonal and interannual variability of surface heat and freshwater fluxes in the Mediterranean Sea: budgets and exchange through the Strait of Gibraltar. International Journal of Climatology 32 (2), 286–302. doi: 10.1002/joc.2268.

Curry, W.B., Lohmann, G.P., 1982. Carbon Isotopic Changes in Benthic Foraminifera from the Western South Atlantic: Reconstruction of Glacial Abyssal Circulation Patterns. Quaternary Research 18 (2), 218–235. doi: 10.1016/0033-5894(82)90071-0.

Cusinato, E., Zanchettin, D., Sannino, G., Rubino, A., 2018. Mediterranean thermohaline response to large-scale winter atmospheric forcing in a high-resolution ocean model simulation. Pure and Applied Geophysics 175 (11), 4083–4110. doi: 10.1007/s00024-018-1859-0.

De Kaenel, E., Siesser, W.G., Murat, A., 1999. Pleistocene calcareous nannofossil biostratig- raphy and the western Mediterranean sapropels, sites 974 to 977 and 979, in: Zahn, R., Comas, M.C., Klaus, A. (Eds.), Proceedings of the Ocean Drilling Program, Scientific Results, 159–183.

de Rijk, S., Jorissen, F.J., Rohling, E.J., Troelstra, S.R., 2000. Organic flux control on bathymetric zonation of Mediterranean benthic foraminifera. Marine Micropaleontology 40 (3), 151–166. doi: 10.1016/S0377-8398(00)00037-2.

de Rijk, S., Troelstra, S.R., Rohling, E.J., 1999. Benthic foraminiferal distribution in the Mediterranean Sea. Journal of Foraminiferal Research 29 (2), 93–103. doi: 10.2113/gsjfr.29.2.93.

de Stigter, H.C., Jorissen, F.J., van der Zwaan, G.J., 1998. Bathymetric distribution and microhabitat partitioning of live (Rose Bengal stained) benthic Foraminifera along a shelf to bathyal transect in the southern Adriatic Sea. Journal of Foraminiferal Research 28 (1), 40–65.

de Vernal, A., Rosell-Melé, A., Kucera, M., Hillaire-Marcel, C., Eynaud, F., Weinelt, M., Dokken, T., Kageyama, M., 2006. Comparing proxies for the reconstruction of LGM sea-surface conditions in the northern North Atlantic. Quaternary Science Reviews 25 (21-22), 2820–2834. doi: 10.1016/j.quascirev.2006.06.006.

Den Dulk, M., Reichart, G., van Heyst, S., Zachariasse, W.J., van der Zwaan, G.J., 2000. Benthic foraminifera as proxies of organic matter flux and bottom water oxygenation? A case history from the northern Arabian Sea. Palaeogeography, Palaeoclimatology, Palaeoecology 161 (3-4), 337–359. doi: 10.1016/S0031-0182(00)00074-2.

Dilek, Y., Sandvol, E., 2009. Seismic structure, crustal architecture and tectonic evolution of the Anatolian-African Plate Boundary and the Cenozoic Orogenic Belts in the Eastern Mediterranean Region. Geological Society, London, Special Publications 327 (1), 127–160. doi: 10.1144/SP327.8.

Dorador, J., Wetzel, A., Rodríguez-Tovar, F.J., 2016. *Zoophycos* in deep-sea sediments indicates high and seasonal primary productivity: Ichnology as a proxy in palaeoceanography during glacial–interglacial variations. Terra Nova 28 (5), 323–328. doi: 10.1111/ter.12224.

Drinia, H., Antonarakou, A., Louvari, M.A., 2013. Foraminiferal biostratigraphy and palaeoenvironmental analysis of the basal part of Kalamavka formation (Late Miocene, Ierapetra Basin, Eastern Crete). Bulletin of the Geological Society of Greece 47 (1), 102. doi: 10.12681/bgsg.10908.

Duplessy, J.-C., Shackleton, N.J., Matthews, R.K., Prell, W., Ruddiman, W.F., Caralp, M., Hendy, C.H., 1984. ^{13}C record of benthic foraminifera in the Last Interglacial ocean: Implications for the carbon cycle and the global deep water circulation. Quaternary Research 21 (2), 225–243. doi: 10.1016/0033-5894(84)90099-1.

Duros, P., Fontanier, C., Stigter, H.C. de, Cesbron, F., Metzger, E., Jorissen, F.J., 2012. Live and dead benthic foraminiferal faunas from Whittard Canyon (NE Atlantic): Focus on taphonomic processes and paleo-environmental applications. Marine Micropaleontology 94-95, 25–44. doi: 10.1016/j.marmicro.2012.05.004.

Eichner, D., Schmiedl, G., Titschack, J., Triantaphyllou, M., Andersen, N., Forster, N., Milker, Y., 2024a. Impact of hydrological changes and vertical motions on Pleistocene marine environments of the eastern coast of the island of Rhodes (Greece). Palaeogeography, Palaeoclimatology, Palaeoecology 636, 111980. doi: 10.1016/j.palaeo.2023.111980.

Eichner, D., Schmiedl, G., Titschack, J., Ferreira, M., Triantaphyllou, M., Andersen, N., Milker, Y., 2024b. Humid climate phases on the Island of Rhodes (Greece) during the late Pliocene at times of sapropel formation. Marine Micropaleontology 187, 102341. doi: 10.1016/j.marmicro.2024.102341.

Emeis, K.-C., Camerlenghi, A., McKenzie, J.A., Rio, D., Sprovieri, R., 1991. The occurrence and significance of Pleistocene and Upper Pliocene sapropels in the Tyrrhenian Sea. Marine Geology 100 (1-4), 155–182. doi: 10.1016/0025-3227(91)90231-R.

Emeis, K.-C., Sakamoto, T., Wehausen, R., Brumsack, H.-J., 2000. The sapropel record of the eastern Mediterranean Sea — results of Ocean Drilling Program Leg 160. Palaeogeography, Palaeoclimatology, Palaeoecology 158 (3-4), 371–395. doi: 10.1016/S0031-0182(00)00059-6.

Epstein, S., Buchsbaum, R., Lowenstam, H.A., Urey, H.C., 1953. Revised carbonate-water isotopic temperature scale. Geological Society of America Bulletin 64 (11), 1315. doi: 10.1130/0016-7606(1953)64[1315:RCITS]2.0.CO;2.

Feldman, S., Harris, S.A., Fairbridge, R.W., 1968. Drainage patterns, in: Fairbridge, R.W. (Ed.), Geomorphology. Encyclopedia of Earth Science. Kluwer Academic Publishers, Dordrecht, 284–291. doi: 10.1007/3-540-31060-6_96.

Feldmeijer, W., Metcalfe, B., Scussolini, P., Arthur, K., 2013. The effect of chemical pretreatment of sediment upon foraminiferal-based proxies. Geochemistry, Geophysics, Geosystems14 (10), 3996–4014. doi: 10.1002/ggge.20233.

Fontanier, C., Dissard, D., Ruffine, L., Mamo, B., Ponzevera, E., Pelleter, E., Baudin, F., Roubi, A., Chéron, S., Boissier, A., Gayet, N., Bermell-Fleury, S., Pitel, M., Guyader, V., Lesongeur, F., Savignac, F., 2018. Living (stained) deep-sea foraminifera from the Sea of Marmara: A preliminary study. Deep Sea Research Part II: Topical Studies in Oceanography 153, 61–78. doi: 10.1016/j.dsr2.2017.12.011.

Fontanier, C., Jorissen, F.J., Chaillou, G., David, C., Anschutz, P., Lafon, V., 2003. Seasonal and interannual variability of benthic foraminiferal faunas at 550 m depth in the Bay of Biscay. Deep Sea Research Part I: Oceanographic Research Papers 50 (4), 457–494. doi: 10.1016/s0967-0637(02)00167-x.

Frezza, V., Bergamin, L., Di Bella, L., 2005. Opportunistic benthic foraminifera as indicators of eutrophicated environments. Actualistic study and comparison with the Santernian middle Tiber Valley (Central Italy). Bollettino della Società Paleontologica Italiana 44 (3), 193–201.

Frezza, V., Carboni, M.G., 2009. Distribution of recent foraminiferal assemblages near the Ombrone River mouth (Northern Tyrrhenian Sea, Italy). Revue de Micropaléontologie 52 (1), 43–66. doi: 10.1016/j.revmic.2007.08.007.

Frontalini, F., Kaminski, M.A., Coccioni, R., Kowalewsk, M., 2018. Agglutinated vs. calcareous foraminiferal assemblages as bathymetric proxies. Micropaleontology 64 (5/6), 403–415.

García-Gallardo, Á., Grunert, P., Voelker, A.H., Mendes, I., Piller, W.E., 2017. Re-evaluation of the "elevated epifauna" as indicator of Mediterranean Outflow Water in the Gulf of Cadiz using stable isotopes ($\delta^{13}C$, $\delta^{18}O$). Global and Planetary Change 155, 78–97. doi: 10.1016/j.gloplacha.2017.06.005.

Gautier, P., Brun, J.-P., Moriceau, R., Sokoutis, D., Martinod, J., Jolivet, L., 1999. Timing, kinematics and cause of Aegean extension: a scenario based on a comparison with simple analogue experiments. Tectonophysics 315 (1-4), 31–72. doi: 10.1016/S0040-1951(99)00281-4.

Gehlen, M., Mucci, A., Boudreau, B., 1999. Modelling the distribution of stable carbon isotopes in porewaters of deep-sea sediments. Geochimica et Cosmochimica Acta 63 (18), 2763–2773. doi: 10.1016/s0016-7037(99)00214-8.

Gehrels, W.R., 2000. Using foraminiferal transfer functions to produce high-resolution sea-level records from salt-marsh deposits, Maine, USA. The Holocene 10 (3), 367–376. doi: 10.1191/095968300670746884.

Gehrels, W.R., Marshall, W.A., Gehrels, M.J., Larsen, G., Kirby, J.R., Eiríksson, J., Heinemeier, J., Shimmield, T., 2006. Rapid sea-level rise in the North Atlantic Ocean since the first half of the nineteenth century. The Holocene 16 (7), 949–965. doi: 10.1177/0959683606hl986rp.

Geraga, M., Ioakim, C., Lykousis, V., Tsaila-Monopolis, S., Mylona, G., 2010. The high-resolution palaeoclimatic and palaeoceanographic history of the last 24,000 years in the central Aegean Sea, Greece. Palaeogeography, Palaeoclimatology, Palaeoecology 287 (1-4), 101–115. doi: 10.1016/j.palaeo.2010.01.023.

Gertman, I.F., Ovchinnikov, I.M., Popov, Y.I., 1994. Deep convection in the eastern basin of the Mediterranean Sea. Oceanology 34, 19–25.

Gibson, T.G., 1989. Planktonic benthonic foraminiferal ratios: Modern patterns and Tertiary applicability. Marine Micropaleontology 15 (1-2), 29–52. doi: 10.1016/0377-8398(89)90003-0.

Glock, N., Schönfeld, J., Eisenhauer, A., Hensen, C., Mallon, J., Sommer, S., 2013. The role of benthic foraminifera in the benthic nitrogen cycle of the Peruvian oxygen minimum zone. Biogeosciences 10 (7), 4767–4783. doi: 10.5194/bg-10-4767-2013.

Gogou, A., Bouloubassi, I., Lykousis, V., Arnaboldi, M., Gaitani, P., Meyers, P.A., 2007. Organic geochemical evidence of Late Glacial–Holocene climate instability in the North Aegean Sea. Palaeogeography, Palaeoclimatology, Palaeoecology 256 (1-2), 1–20. doi: 10.1016/j.palaeo.2007.08.002.

Goineau, A., Fontanier, C., Jorissen, F.J., Lansard, B., Buscail, R., Mouret, A., Kerhervé, P., Zaragosi, S., Ernoult, E., Artéro, C., Anschutz, P., Metzger, E., Rabouille, C., 2011. Live (stained) benthic foraminifera from the Rhône prodelta (Gulf of Lion, NW Mediterranean): Environmental controls on a river-dominated shelf. Journal of Sea Research 65 (1), 58–75. doi: 10.1016/j.seares.2010.07.007.

Gooday, A.J., 1994. The biology of deep-sea foraminifera: A review of some advances and their applications in paleoceanography. PALAIOS 9 (1), 14–31. doi: 10.2307/3515075.

Gooday, A.J., 2003. Benthic foraminifera (Protista) as tools in deep-water palaeoceanography: environmental influences on faunal characteristics. Advances in marine biology 46, 1–90. doi: 10.1016/S0065-2881(03)46002-1.

Görgün, E., Zang, A., Kalafat, D., Kekovalı, K., 2014. The 10 June 2012 Fethiye Mw 6.0 aftershock sequence and its relation to the 24–25 April 1957 Ms 6.9–7.1 earthquakes in SW Anatolia, Turkey. Journal of Asian Earth Sciences 93, 102–112. doi: 10.1016/j.jseaes.2014.07.008.

Gottschalk, J., Vázquez Riveiros, N., Waelbroeck, C., Skinner, L.C., Michel, E., Duplessy, J.-C., Hodell, D., Mackensen, A., 2016. Carbon isotope offsets between benthic foraminifer species of the genus *Cibicides* (*Cibicidoides*) in the glacial sub-Antarctic Atlantic. Paleoceanography 31 (12), 1583–1602. doi: 10.1002/2016PA003029.

Grant, K.M., Amarathunga, U., Amies, J.D., Hu, P., Qian, Y., Penny, T., Rodriguez-Sanz, L., Zhao, X., Heslop, D., Liebrand, D., Hennekam, R., Westerhold, T., Gilmore, S., Lourens, L.J., Roberts, A.P., Rohling, E.J., 2022. Organic carbon burial in Mediterranean sapropels intensified during Green Sahara Periods since 3.2 Myr ago. Communications Earth & Environment 3 (1). doi: 10.1038/s43247-021-00339-9.

Grimm, R., Maier-Reimer, E., Mikolajewicz, U., Schmiedl, G., Müller-Navarra, K., Adloff, F., Grant, K.M., Ziegler, M., Lourens, L.J., Emeis, K.-C., 2015. Late glacial initiation of Holocene eastern Mediterranean sapropel formation. Nature communications 6, 7099. doi: 10.1038/ncomms8099.

Grolms, N., 2024. Variation of principial strain directions inferred from kinematic analysis of post-Pliocene brittle shear faults, Island of Rhodes, Greece. Bachelor thesis, Hamburg.

Guimerans, P.V., Currado, J.L., 1999. The recent uvigerinids (benthic foraminifera) in the northeastern Gulf of Cadiz. Boletín del Instituto Español de Oceanografía 15, 191–202.

Hall, J., Aksu, A.E., Yaltırak, C., Winsor, J.D., 2009. Structural architecture of the Rhodes Basin: A deep depocentre that evolved since the Pliocene at the junction of Hellenic and Cyprus Arcs, eastern Mediterranean. Marine Geology 258 (1-4), 1–23. doi: 10.1016/j.margeo.2008.02.007.

Hammer, Ø., Harper, D., Ryan, P.D., 2001. PAST: Paleontological statistics software package for education and data analysis. Palaeontologia Electronica 4 (1), 9.

Hanken, N.-M., Bromley, R.G., Miller, J., 1996. Plio-Pleistocene sedimentation in coastal grabens, north-east Rhodes, Greece. Geological Journal 31 (4), 393–418. doi: 10.1002/(SICI)1099-1034(199612)31:4<393::AID-GJ712>3.0.CO;2-H.

Hansen, K.S., 1999. Development of a prograding carbonate wedge during sea level fall: Lower Pleistocene of Rhodes, Greece. Sedimentology 46 (3), 559–576. doi: 10.1046/j.1365-3091.1999.00238.x.

Harrison, R.W., Newell, W.L., Batıhanlı, H., Panayides, I., McGeehin, J.P., Mahan, S.A., Őzhűr, A., Tsiolakis, E., Necdet, M., 2004. Tectonic framework and Late Cenozoic tectonic history of the northern part of Cyprus: implications for earthquake hazards and regional tectonics. Journal of Asian Earth Sciences 23 (2), 191–210. doi: 10.1016/S1367-9120(03)00095-6.

Hawkes, A.D., Horton, B.P., Nelson, A.R., Hill, D.F., 2010. The application of intertidal foraminifera to reconstruct coastal subsidence during the giant Cascadia earthquake of AD 1700 in Oregon, USA. Quaternary International 221 (1-2), 116–140. doi: 10.1016/j.quaint.2009.09.019.

Hays, J.D., Imbrie, J., Shackleton, N.J., 1976. Variations in the Earth's Orbit: Pacemaker of the Ice Ages. Science (New York, N.Y.) 194 (4270), 1121–1132. doi: 10.1126/science.194.4270.1121.

Hess, S., Jorissen, F.J., Venet, V., Abu-Zied, R., 2005. Benthic Foraminiferal recovery after recent turbidite deposition in Cap Breton Canyon, Bay of Biscay. Journal of Foraminiferal Research 35 (2), 114–129. doi: 10.2113/35.2.114.

Hilgen, F.J., 1991. Astronomical calibration of Gauss to Matuyama sapropels in the Mediterranean and implication for the Geomagnetic Polarity Time Scale. Earth and Planetary Science Letters 104 (2-4), 226–244. doi: 10.1016/0012-821X(91)90206-W.

Hilgen, F.J., Krijgsman, W., Langereis, C.G., Lourens, L.J., Santarelli, A., Zachariasse, W.J., 1995. Extending the astronomical (polarity) time scale into the Miocene. Earth and Planetary Science Letters 136 (3-4), 495–510. doi: 10.1016/0012-821X(95)00207-S.

Holzmann, M., Pawlowski, J., 2002. Freshwater foraminiferas from Lake Geneva: past and present. Journal of Foraminiferal Research 32 (4), 344–350. doi: 10.2113/0320344.

Hoogakker, B.A.A., Elderfield, H., Schmiedl, G., McCave, I.N., Rickaby, R.E.M., 2015. Glacial–interglacial changes in bottom-water oxygen content on the Portuguese margin. Nature Geoscience 8 (1), 40–43. doi: 10.1038/NGEO2317.

Horton, B.P., 1999. The distribution of contemporary intertidal foraminifera at Cowpen Marsh, Tees Estuary, UK: implications for studies of Holocene sea-level changes. Palaeogeography, Palaeoclimatology, Palaeoecology 149 (1-4), 127–149. doi: 10.1016/S0031-0182(98)00197-7.

Horton, B.P., Culver, S.J., Hardbattle, M.I.J., Larcombe, P., Milne, G.A., Morigi, C., Whittaker, J.E., Woodroffe, S.A., 2007. Reconstructing holocene sea-level change for the central Great Barrier Reef (Australia) using subtidal foraminifera. Journal of Foraminiferal Research 37 (4), 327–343. doi: 10.2113/gsjfr.37.4.327.

Horton, B.P., Edwards, R.J., Lloyd, J.M., 1999. A foraminiferal-based transfer function: Implications for sea-level studies. Journal of Foraminiferal Research 29 (2), 117–129. doi: 10.2113/gsjfr.29.2.117.

Howell, A., Jackson, J., Copley, A., McKenzie, D., Nissen, E., 2017. Subduction and vertical coastal motions in the eastern Mediterranean. Geophysical Journal International 211 (1), 593–620. doi: 10.1093/gji/ggx307.

Howell, A., Jackson, J., England, P., Higham, T., Synolakis, C., 2015. Late Holocene uplift of Rhodes, Greece: evidence for a large tsunamigenic earthquake and the implications for the tectonics of the eastern Hellenic Trench System. Geophysical Journal International 203 (1), 459–474. doi: 10.1093/gji/ggv307.

Hutson, W.H., 1977. Transfer functions under no-analog conditions: Experiments with indian ocean planktonic foraminifera. Quaternary Research 8 (3), 355–367. doi: 10.1016/0033-5894(77)90077-1.

Imbrie, J., Kipp, N.G., 1971. A new micropaleontological method for quantitative paleoclimatology: application to a Late Pleistocene Caribbean core., in: Turekian, K.K. (Ed.), The Late Cenozoic Glacial Ages, New Haven, 71–181.

Jackson, J., McKenzie, D., 1988. The relationship between plate motions and seismic moment tensors, and the rates of active deformation in the Mediterranean and Middle East. Geophysical Journal International 93 (1), 45–73. doi: 10.1111/j.1365-246X.1988.tb01387.x.

Jannink, N.T., Zachariasse, W.J., van der Zwaan, G.J., 1998. Living (Rose Bengal stained) benthic foraminifera from the Pakistan continental margin (northern Arabian Sea). Deep Sea Research Part I: Oceanographic Research Papers 45 (9), 1483–1513. doi: 10.1016/S0967-0637(98)00027-2.

Jarochowska, E., Tonarová, P., Munnecke, A., Ferrová, L., Sklenář, J., Vodrážková, S., 2013. An acid-free method of microfossil extraction from clay-rich lithologies using the surfactant Rewoquat. Palaeontologia Electronica 16 (3), 1–16. doi: 10.26879/382.

Jolivet, L., Faccenna, C., Huet, B., Labrousse, L., Le Pourhiet, L., Lacombe, O., Lecomte, E., Burov, E., Denèle, Y., Brun, J.-P., Philippon, M., Paul, A., Salaün, G., Karabulut, H., Piromallo, C., Monié, P., Gueydan, F., Okay, A.I., Oberhänsli, R., Pourteau, A., Augier, R., Gadenne, L., Driussi, O., 2013. Aegean tectonics: Strain localisation, slab tearing and trench retreat. Tectonophysics 597-598, 1–33. doi: 10.1016/j.tecto.2012.06.011.

Jones, 2013. Foraminifera and their Applications. Cambridge University Press.

Jones, R.W., 1994. The Challenger foraminifera. Oxford University Press, Oxford, New York, Tokyo, 150 pp.

Jonkers, H.A., 1984. Pliocene benthonic foraminifera from homogeneous and laminated marls on Crete. Utrecht micropaleontological bulletins 31.

Jorissen, F.J., 1987. The distribution of benthic foraminifera in the Adriatic Sea. Marine Micropaleontology 12, 21–48. doi: 10.1016/0377-8398(87)90012-0.

Jorissen, F.J., 1999. Benthic foraminiferal successions across Late Quaternary Mediterranean sapropels. Marine Geology 153 (1-4), 91–101. doi: 10.1016/S0025-3227(98)00088-7.

Jorissen, F.J., de Stigter, H.C., Widmark, J.G., 1995. A conceptual model explaining benthic foraminiferal microhabitats. Marine Micropaleontology 26 (1-4), 3–15. doi: 10.1016/0377-8398(95)00047-X.

Jorissen, F.J., Fontanier, C., Thomas, E., 2007. Paleoceanographical proxies based on deep-sea benthic foraminiferal assemblage characteristics, in: Hillaire-Marcel, C., De Vernal, A. (Eds.), Proxies in late cenozoic paleoceanography, vol. 1. Elsevier, Amsterdam, 263–325. doi: 10.1016/S1572-5480(07)01012-3.

Jorissen, F.J., Wittling, I., Peypouquet, J.P., Rabouille, C., Relexans, J.C., 1998. Live benthic foraminiferal faunas off Cape Blanc, NW-Africa: Community structure and microhabitats.

Deep Sea Research Part I: Oceanographic Research Papers 45 (12), 2157–2188. doi: 10.1016/S0967-0637(98)00056-9.

Juggins, S., 2020-2022. rioja: Analysis of Quaternary Science Data: R package version 1.0-5. https://cran.r-project.org/package=rioja.

Juggins, S., Birks, H.J.B., 2012. Quantitative environmental reconstructions from biological data, in: Birks, H.J.B., Lotter, A.F., Juggins, S., Smol, J.P. (Eds.), Tracking Environmental Change Using Lake Sediments, vol. 5. Springer Netherlands, Dordrecht, 431–494. doi: 10.1007/978-94-007-2745-8_14

Kaiho, K., 1994. Benthic foraminiferal dissolved-oxygen index and dissolved-oxygen levels in the modern ocean. Geology 22 (8), 719. doi: 10.1130/0091-7613(1994)022<0719:BFDOIA>2.3.CO;2.

Kanzler, L., 2022. Neotectonic deformation of Pleistocene sedimentary deposits in the Lardos area, SE coast of Rhodes Island, Greece. Bachelor thesis, Hamburg.

Kawahata, H., Fujita, K., Iguchi, A., Inoue, M., Iwasaki, S., Kuroyanagi, A., Maeda, A., Manaka, T., Moriya, K., Takagi, H., Toyofuku, T., Yoshimura, T., Suzuki, A., 2019. Perspective on the response of marine calcifiers to global warming and ocean acidification—Behavior of corals and foraminifera in a high CO2 world "hot house". Progress in Earth and Planetary Science 6 (1). doi: 10.1186/s40645-018-0239-9.

Kaymakcı, N., Langereis, C., Özkaptan, M., Özacar, A.A., Gülyüz, E., Uzel, B., Sözbilir, H., 2018. Paleomagnetic evidence for upper plate response to a STEP fault, SW Anatolia. Earth and Planetary Science Letters 498, 101–115. doi: 10.1016/j.epsl.2018.06.022.

Kemp, A.C., Hawkes, A.D., Donnelly, J.P., Vane, C.H., Horton, B.P., Hill, T.D., Anisfeld, S.C., Parnell, A.C., Cahill, N., 2015. Relative sea-level change in Connecticut (USA) during the last 2200 yrs. Earth and Planetary Science Letters 428, 217–229. doi: 10.1016/j.epsl.2015.07.034.

Kemp, A.C., Horton, B.P., Culver, S.J., Corbett, D.R., van de Plassche, O., Gehrels, W.R., Douglas, B.C., Parnell, A.C., 2009. Timing and magnitude of recent accelerated sea-level rise (North Carolina, United States). Geology 37 (11), 1035–1038. doi: 10.1130/G30352A.1.

Kemp, A.C., Telford, R.J., 2015. Transfer functions, in: Shennan, I., Long, A., Horton, B.P. (Eds.), Handbook of sea-level research. Wiley, West Sussex, pp. 470–499. doi: 10.1002/9781118452547.ch31.

Khélifi, N., Sarnthein, M., Andersen, N., Blanz, T., Frank, M., Garbe-Schonberg, D., Haley, B.A., Stumpf, R., Weinelt, M., 2009. A major and long-term Pliocene intensification of the Mediterranean outflow, 3.5-3.3 Ma ago. Geology 37 (9), 811–814. doi: 10.1130/G30058A.1.

Kontogianni, V.A., Tsoulos, N., Stiros, S.C., 2002. Coastal uplift, earthquakes and active faulting of Rhodes Island (Aegean Arc): modeling based on geodetic inversion. Marine Geology 186 (3-4), 299–317. doi: 10.1016/S0025-3227(02)00334-1.

Kotthoff, U., Müller, U.C., Pross, J., Schmiedl, G., Lawson, I.T., van de Schootbrugge, B., Schulz, H., 2008a. Lateglacial and Holocene vegetation dynamics in the Aegean region: an integrated view based on pollen data from marine and terrestrial archives. The Holocene 18 (7), 1019–1032. doi: 10.1177/0959683608095573.

Kotthoff, U., Pross, J., Müller, U.C., Peyron, O., Schmiedl, G., Schulz, H., Bordon, A., 2008b. Climate dynamics in the borderlands of the Aegean Sea during formation of sapropel S1 deduced from a marine pollen record. Quaternary Science Reviews 27 (7-8), 832–845. doi: 10.1016/j.quascirev.2007.12.001.

Kranner, M., Harzhauser, M., Beer, C., Auer, G., Piller, W.E., 2022. Calculating dissolved marine oxygen values based on an enhanced Benthic Foraminifera Oxygen Index. Scientific reports 12 (1), 1376. doi: 10.1038/s41598-022-05295-8.

Kroon, D., Alexander, I., Little, M., Lourens, L.J., Matthewson, A., Robertson, A.H.F., Sakamoto, T., 1998. Oxygen isotope and sapropel stratigraphy in the Eastern Mediterranean during the last 3.2 million years, in: Robertson, A.H.F., Emeis, K.-C., Richter, C., Camerlenghi, A. (Eds.), Proceedings of the Ocean Drilling Program, Scientific Results, vol. 160, Chapter 14.

Kucera, M., 2007. Planktonic foraminifera as tracers of past oceanic environments, in: Hillaire-Marcel, C., De Vernal, A. (Eds.), Proxies in late cenozoic paleoceanography, vol. 1. Elsevier, Amsterdam, 213–262. doi: 10.1016/S1572-5480(07)01011-1.

Kuhnt, T., Schmiedl, G., Ehrmann, W., Hamann, Y., Andersen, N., 2008. Stable isotopic composition of Holocene benthic foraminifers from the Eastern Mediterranean Sea: Past changes in productivity and deep water oxygenation. Palaeogeography, Palaeoclimatology, Palaeoecology 268 (1-2), 106–115. doi: 10.1016/j.palaeo.2008.07.010.

Lascaratos, A., Roether, W., Nittis, K., Klein, B., 1999. Recent changes in deep water formation and spreading in the eastern Mediterranean Sea: a review. Progress in Oceanography 44 (1-3), 5–36. doi: 10.1016/S0079-6611(99)00019-1.

Laskar, J., Robutel, P., Joutel, F., Gastineau, M., Correia, A.C.M., Levrard, B., 2004. A long-term numerical solution for the insolation quantities of the Earth. Astronomy & Astrophysics 428 (1), 261–285. doi: 10.1051/0004-6361:20041335.

Lejzerowicz, F., Pawlowski, J., Fraissinet-Tachet, L., Marmeisse, R., 2010. Molecular evidence for widespread occurrence of Foraminifera in soils. Environmental microbiology 12 (9), 2518–2526. doi: 10.1111/j.1462-2920.2010.02225.x.

Lekkas, E., Papanikolaou, D., Sakellariou, D., 2000. Neotectonic Map of Greece, Rhodes Sheet, 1:100,000. Tectonic Committee of the Geological Society of Greece.

Leorri, E., Gehrels, W.R., Horton, B.P., Fatela, F., Cearreta, A., 2010. Distribution of foraminifera in salt marshes along the Atlantic coast of SW Europe: Tools to reconstruct past sea-level variations. Quaternary International 221 (1-2), 104–115. doi: 10.1016/j.quaint.2009.10.033.

Licari, L., Mackensen, A., 2005. Benthic foraminifera off West Africa (1°N to 32°S): Do live assemblages from the topmost sediment reliably record environmental variability? Marine Micropaleontology 55 (3-4), 205–233. doi: 10.1016/j.marmicro.2005.03.001.

Liddy, H.M., Feakins, S.J., Tierney, J.E., 2016. Cooling and drying in northeast Africa across the Pliocene. Earth and Planetary Science Letters 449, 430–438. doi: 10.1016/j.epsl.2016.05.005.

Lisiecki, L.E., Raymo, M.E., 2005. A Pliocene-Pleistocene stack of 57 globally distributed benthic $\delta^{18}O$ records. Paleoceanography 20 (1), PA1003. doi: 10.1029/2004PA001071.

Lolis, C.J., Bartzokas, A., Katsoulis, B.D., 2002. Spatial and temporal 850 hPa air temperature and sea-surface temperature covariances in the Mediterranean region and their connection to atmospheric circulation. International Journal of Climatology 22 (6), 663–676. doi: 10.1002/joc.759.

Loubere, P., Fariduddin, M., 1999. Quantitative estimation of global patterns of surface ocean biological productivity and its seasonal variation on timescales from centuries to millennia. Global Biogeochemical Cycles 13 (1), 115–133. doi: 10.1029/1998GB900001.

Lourens, L.J., Antonarakou, A., Hilgen, F.J., van Hoof, A.A.M., Vergnaud-Grazzini, C., Zachariasse, W.J., 1996a. Evaluation of the Plio-Pleistocene astronomical timescale. Paleoceanography 11 (4), 391–413. doi: 10.1029/96PA01125.

Lourens, L.J., Hilgen, F.J., 1997. Long-periodic variations in the earth's obliquity and their relation to third-order eustatic cycles and late Neogene glaciations. Quaternary International 40, 43–52. doi: 10.1016/S1040-6182(96)00060-2.

Lourens, L.J., Hilgen, F.J., Gudjonsson, L., Zachariasse, W.J., 1992. Late Pliocene to early Pleistocene astronomically forced sea surface productivity and temperature variations in the

Mediterranean. Marine Micropaleontology 19 (1-2), 49–78. doi: 10.1016/0377-8398(92)90021-B.

Lourens, L.J., Hilgen, F.J., Raffi, I., 1998. Base of large Gephyrocapsa and astronomical calibration of early Pleistocene sapropels in Site 967 and Hole 969D: solving the chronology of the Vrica section (Calabria, Italy), in: Robertson, A.H.F., Emeis, K.-C., Richter, C., Camerlenghi, A. (Eds.), Proceedings of the Ocean Drilling Program, Scientific Results, vol. 160, 191–197.

Lourens, L.J., Hilgen, F.J., Raffi, I., Vergnaud-Grazzini, C., 1996b. Early Pleistocene chronology of the Vrica Section (Calabria, Italy). Paleoceanography 11 (6), 797–812. doi: 10.1029/96PA02691.

Lourens, L.J., Hilgen, F.J., Shackleton, N.J., Laskar, J., Wilson, D., 2004. The Neogene period, in: Gradstein, F.M., Ogg, J.G., Smith, A. (Eds.), A Geologic Time Scale. Cambridge University Press, Cambridge UK, 409–440.

Løvlie, R., Støle, G., Spjeldnæs, N., 1989. Magnetic polarity stratigraphy of Pliocene-Pleistocene marine sediments from Rhodos, eastern Mediterranean. Physics of the Earth and Planetary Interiors 54 (3-4), 340–352. doi: 10.1016/0031-9201(89)90251-3.

Lutze, G.F., Coulbourn, W.T., 1984. Recent benthic foraminifera from the continental margin of northwest Africa: Community structure and distribution. Marine Micropaleontology 8 (5), 361–401. doi: 10.1016/0377-8398(84)90002-1.

Mackensen, A., Douglas, R.G., 1989. Down-core distribution of live and dead deep-water benthic foraminifera in box cores from the Weddell Sea and the California continental borderland. Deep Sea Research Part A. Oceanographic Research Papers 36 (6), 879–900. doi: 10.1016/0198-0149(89)90034-4.

Mackensen, A., Licari, L., 2004. Carbon isotopes of live benthic foraminifera from the south atlantic: sensitivity to bottom water carbonate saturation state and organic matter rain rates, in: Wefer, G., Mulitza, S., Ratmeyer, V. (Eds.), The South Atlantic in the Late Quaternary. Springer Berlin Heidelberg, 623–644. doi: 10.1007/978-3-642-18917-3_27.

Mackensen, A., Schmiedl, G., 2019. Stable carbon isotopes in paleoceanography: atmosphere, oceans, and sediments. Earth-Science Reviews 197, 102893. doi: 10.1016/j.earscirev.2019.102893.

Maheras, P., Xoplaki, E., Davies, T., Martin-Vide, J., Bariendos, M., Alcoforado, M.J., 1999. Warm and cold monthly anomalies across the Mediterranean basin and their relationship with circulation; 1860-1990. International Journal of Climatology 19 (15), 1697–1715. doi: 10.1002/(SICI)1097-0088(199912)19:15<1697::AID-JOC442>3.0.CO;2-S.

Marchitto, T.M., Curry, W.B., Lynch-Stieglitz, J., Bryan, S.P., Cobb, K.M., Lund, D.C., 2014. Improved oxygen isotope temperature calibrations for cosmopolitan benthic foraminifera. Geochimica et Cosmochimica Acta 130, 1–11. doi: 10.1016/j.gca.2013.12.034.

Marghany, M., 2022. Quantum cellular automata algorithm for automatic detection of hydrocarbon exploration zones, in: Marghany, M. (Ed.), Advanced Algorithms for Mineral and Hydrocarbon Exploration Using Synthetic Aperture Radar. Elsevier, 301–323. doi: 10.1016/B978-0-12-821796-2.00011-2.

Marino, G., 2008. Palaeoceanography of the interglacial eastern Mediterranean Sea. LPP Foundation, Utrecht, 145 pp.

Martini, E., 1971. Standard Tertiary and Quaternary calcareous nannoplankton zonation, in: Farinacci, A. (Ed.), Proceedings 2nd International Conference Planktonic Microfossils Roma: Rome (Ed. Tecnosci.), vol. 2, 739–785.

Maslin, M., 2016. In retrospect: Forty years of linking orbits to ice ages. Nature 540 (7632), 208–210. doi: 10.1038/540208a.

McCorkle, D.C., Emerson, S.R., 1988. The relationship between pore water carbon isotopic composition and bottom water oxygen concentration. Geochimica et Cosmochimica Acta 52 (5), 1169–1178. doi: 10.1016/0016-7037(88)90270-0.

McCorkle, D.C., Keigwin, L.D., Corliss, B.H., Emerson, S.R., 1990. The influence of microhabitats on the carbon isotopic composition of deep-sea benthic foraminifera. Paleoceanography 5 (2), 161–185. doi: 10.1029/PA005i002p00161.

McKay, C.L., Groeneveld, J., Filipsson, H.L., Gallego-Torres, D., Whitehouse, M.J., Toyofuku, T., Romero, O.E., 2015. A comparison of benthic foraminiferal Mn/Ca and sedimentary Mn/Al as proxies of relative bottom-water oxygenation in the low-latitude NE Atlantic upwelling system. Biogeosciences 12 (18), 5415–5428. doi: 10.5194/bg-12-5415-2015.

Meulenkamp, J.E., 1985. Aspects of the late Cenozoic evolution of the aegean region, in: Stanley, D.J., Wezel, F.-C. (Eds.), Geological evolution of the Mediterranean Basin. Springer New York, New York, 307–321. doi: 10.1007/978-1-4613-8572-1_15.

Meulenkamp, J.E., De Mulder, E.F.J., van de Weerd, A., 1972. Sedimentary history and paleogeography of the late Cenozoic of the Island of Rhodos. Zeitschrift der Deutschen Geologischen Gesellschaft 123 (2), 541–553. doi: 10.1127/zdgg/123/1972/541.

Meulenkamp, J.E., van der Zwaan, G.J., van Wamel, W.A., 1994. On late miocene to recent vertical motions in the Cretan segment of the Hellenic arc. Tectonophysics 234 (1-2), 53–72. doi: 10.1016/0040-1951(94)90204-6.

Meyers, P.A., Doose, H., 1999. Sources, preservation, and thermal maturity of organic matter in Pliocene–Pleistocene organic-carbon-rich sediments of the western Mediterranean Sea., in: Zahn, R., Comas, M.C., Klaus, A. (Eds.), Proceedings of the Ocean Drilling Program, Scientific Results, 383–390.

Milker, Y., Horton, B.P., Nelson, A.R., Engelhart, S.E., Witter, R.C., 2015a. Variability of intertidal foraminiferal assemblages in a salt marsh, Oregon, USA. Marine Micropaleontology 118, 1–16. doi: 10.1016/j.marmicro.2015.04.004.

Milker, Y., Horton, B.P., Vane, C.H., Engelhart, S.E., Nelson, A.R., Witter, R.C., Khan, N.S., Bridgeland, W.T., 2015b. Annual and seasonal distribution of intertidal foraminifera and stable carbon isotope geochemistry, Bandon Marsh, Oregon, USA. Journal of Foraminiferal Research 45 (2), 146–155. doi: 10.2113/gsjfr.45.2.146.

Milker, Y., Jorissen, F.J., Riller, U., Reicherter, K., Titschack, J., Weinkauf, M.F.G., Theodor, M., Schmiedl, G., 2019. Paleo-ecologic and neotectonic evolution of a marine depositional environment in SE Rhodes (Greece) during the early Pleistocene. Quaternary Science Reviews 213, 120–132. doi: 10.1016/j.quascirev.2019.04.021.

Milker, Y., Nelson, A.R., Horton, B.P., Engelhart, S.E., Bradley, L.-A., Witter, R.C., 2016. Differences in coastal subsidence in southern Oregon (USA) during at least six prehistoric megathrust earthquakes. Quaternary Science Reviews 142, 143–163. doi: 10.1016/j.quascirev.2016.04.017.

Milker, Y., Schmiedl, G., 2012. A taxonomic guide to modern benthic shelf foraminifera of the western Mediterranean Sea. Palaeontologia Electronica 15(2), 16A, 134p. doi: 10.26879/271.

Milker, Y., Schmiedl, G., Betzler, C., 2011. Paleobathymetric history of the Western Mediterranean Sea shelf during the latest glacial period and the Holocene: Quantitative reconstructions based on foraminiferal transfer functions. Palaeogeography, Palaeoclimatology, Palaeoecology 307 (1-4), 324–338. doi: 10.1016/j.palaeo.2011.05.031.

Milker, Y., Schmiedl, G., Betzler, C., Römer, M., Jaramillo-Vogel, D., Siccha, M., 2009. Distribution of recent benthic foraminifera in shelf carbonate environments of the Western Mediterranean Sea. Marine Micropaleontology 73 (3-4), 207–225. doi: 10.1016/j.marmicro.2009.10.003.

Milker, Y., Weinkauf, M.F.G., Titschack, J., Freiwald, A., Krüger, S., Jorissen, F.J., Schmiedl, G., 2017. Testing the applicability of a benthic foraminiferal-based transfer function for the reconstruction of paleowater depth changes in Rhodes (Greece) during the early Pleistocene. PloS one 12 (11), e0188447. doi: 10.1371/journal.pone.0188447.

Millot, C., Taupier-Letage, I., 2005. Circulation in the Mediterranean Sea, in: Saliot, A. (Ed.), The Mediterranean Sea, 5K. Springer Berlin Heidelberg, 29–66. doi: 10.1007/b107143.

Moissette, P., Quillévéré, F., Kontakiotis, G., Thivaiou, D., Koskeridou, E., Antonarakou, A., Drinia, H., Melinte-Dobrinescu, M., Cornée, J.-J., 2024. Early Pleistocene upper bathyal communities in fault-bounded paleovalleys of the island of Rhodes (Greece). Quaternary Research, 1–21. doi: 10.1017/qua.2024.19.

Moissette, P., Spjeldnæs, N., 1995. Plio-Pleistocene deep-water bryozonas from Rhodes, Greece. Palaeontology 38 (4), 771–799.

Mojtahid, M., Jorissen, F.J., Lansard, B., Fontanier, C., Bombled, B., Rabouille, C., 2009. Spatial distribution of live benthic foraminifera in the Rhône prodelta: Faunal response to a continental–marine organic matter gradient. Marine Micropaleontology 70 (3-4), 177–200. doi: 10.1016/j.marmicro.2008.12.006.

Morris, A., Robertson, A., 1993. Miocene remagnetisation of carbonate platform and Antalya Complex units within the Isparta angle, SW Turkey. Tectonophysics 220 (1-4), 243–266. doi: 10.1016/0040-1951(93)90234-B.

Murray, J.W., 1991. Ecology and palaeoecology of benthic foraminifera. Routledge, London, 397 pp.

Murray, J.W., 2001. The niche of benthic foraminifera, critical thresholds and proxies. Marine Micropaleontology 41 (1-2), 1–7. doi: 10.1016/S0377-8398(00)00057-8.

Murray, J.W., 2006. Ecology and applications of benthic foraminifera. Cambridge University Press, Cambridge, 426 pp.

Murray, J.W., 2007. Biodiversity of living benthic foraminifera: How many species are there? Marine Micropaleontology 64 (3-4), 163–176. doi: 10.1016/j.marmicro.2007.04.002.

Mutti, E., Orombelli, G., Pozzi, R., 1970. Geological studies on the Dodecanese Islands (Aegean Sea). IX. Geological map of the island of Rhodes (Greece); explanatory notes. Annales Géologiques des Pays Helléniques 22, 79–226.

Nelson, C.S., Freiwald, A., Titschack, J., List, S., 2001. Lithostratigraphy and sequence architecture of temperate mixed siliciclastic-carbonate facies in a new Plio-Pleistocene section at Plimiri, Rhodes Island (Greece). Department of Earth Sciences, University of Waikato, New Zealand, Occasional Report 25, 1–50.

Nguyen, T.M.P., Petrizzo, M.R., Speijer, R.P., 2009. Experimental dissolution of a fossil foraminiferal assemblage (Paleocene–Eocene Thermal Maximum, Dababiya, Egypt): Implications for paleoenvironmental reconstructions. Marine Micropaleontology 73 (3-4), 241–258. doi: 10.1016/j.marmicro.2009.10.005.

Ní Fhlaithearta, S., Reichart, G.-J., Jorissen, F.J., Fontanier, C., Rohling, E.J., Thomson, J., Lange, G.J. de, 2010. Reconstructing the seafloor environment during sapropel formation using benthic foraminiferal trace metals, stable isotopes, and sediment composition. Paleoceanography 25 (4), PA4225. doi: 10.1029/2009PA001869.

Nijenhuis, I.A., Lange, G. de, 2000. Geochemical constraints on Pliocene sapropel formation in the eastern Mediterranean. Marine Geology 163 (1-4), 41–63. doi: 10.1016/S0025-3227(99)00093-6.

Öğretmen, N., Cipollari, P., Frezza, V., Faranda, C., Karanika, K., Gliozzi, E., Radeff, G., Cosentino, D., 2018. Evidence for 1.5 km of uplift of the central anatolian plateau's southern

margin in the last 450 kyr and implications for Its multiphased uplift history. Tectonics 37 (1), 359–390. doi: 10.1002/2017TC004805.

Oksanen, J., Simpson, G.L., Blanchet, G.F., Kindt, R., Legendre, P., Minchin, P.R., O'Hara, R.B., Solymos, P., Stevens, M.H.H., Szoecs, E., Wagner, H., Barbour, M., Bedward, M., Bolker, B., Borcard, D., Carvalho, G., Chirico, M., De Caceres, M., Durand, S., Evangelista, H.B.A., FitzJohn, R., Friendly, M., Furneaux, B., Hannigan, G., Hill, M.O., Lahti, L., McGlinn, D., Ouellette, M.-H., Cunha, E.R., Smith, T., Stier, A., Ter Braak, C.J.F., Weedon, J., 2022. vegan: Community Ecology Package: R package version 2.6-2; 2.6-4. https://cran.r-project.org/web/packages/vegan/.

Paillard, D., Labeyrie, L., Yiou, P., 1996. Macintosh Program performs time-series analysis. Eos, Transactions American Geophysical Union 77 (39), 379. doi: 10.1029/96EO00259.

Papadopoulos, G.A., 1989. Seismic and volcanic activities and aseismic movements as plate motion components in the Aegean area. Tectonophysics 167 (1), 31–39. doi: 10.1016/0040-1951(89)90292-8.

Passier, H.F., Bosch, H.-J., Nijenhuis, I.A., Lourens, L.J., Böttcher, M.E., Leenders, A., Damsté, J.S.S., Lange, G.J. de, Leeuw, J.W., 1999. Sulphidic Mediterranean surface waters during Pliocene sapropel formation. Nature 397 (6715), 146–149. doi: 10.1038/16441.

Payne, A.S., Robertson, A., 1995. Neogene supra-subduction zone extension in the Polis graben system, west Cyprus. Journal of the Geological Society 152 (4), 613–628. doi: 10.1144/gsjgs.152.4.0613.

Payne, R.J., Babeshko, K.V., van Bellen, S., Blackford, J.J., Booth, R.K., Charman, D.J., Ellershaw, M.R., Gilbert, D., Hughes, P.D., Jassey, V.E., Lamentowicz, Ł., Lamentowicz, M., Malysheva, E.A., Mauquoy, D., Mazei, Y., Mitchell, E.A., Swindles, G.T., Tsyganov, A.N., Turner, T.E., Telford, R.J., 2016. Significance testing testate amoeba water table reconstructions. Quaternary Science Reviews 138, 131–135. doi: 10.1016/j.quascirev.2016.01.030.

Penaud, A., Eynaud, F., Etourneau, J., Bonnin, J., Vernal, A., Zaragosi, S., Kim, J.-H., Kang, S., Gal, J.-K., Oliveira, D., Waelbroeck, C., 2022. Ocean productivity in the Gulf of Cadiz over the last 50 kyr. Paleoceanography and Paleoclimatology 37 (2). doi: 10.1029/2021PA004316.

Perch-Nielsen, K., 1985. Cenozoic calcareous nannofossils, in: Bolli, H.M., Saunders, J.B., Perch-Nielsen, K. (Eds.), Plankton stratigraphy. Cambridge University Press, Cambridge UK, 427–555.

Perissoratis, C., Piper, D.J.W., 1992. Age, regional variation, and shallowest occurrence of S1 sapropel in the northern Aegean Sea. Geo-Marine Letters 12 (1), 49–53. doi: 10.1007/BF02092108.

Philippon, M., Brun, J.-P., Gueydan, F., Sokoutis, D., 2014. The interaction between Aegean back-arc extension and Anatolia escape since Middle Miocene. Tectonophysics 631, 176–188. doi: 10.1016/j.tecto.2014.04.039.

Pinardi, N., Zavatarelli, M., Adani, M., Coppini, G., Fratianni, C., Oddo, P., Simoncelli, S., Tonani, M., Lyubartsev, V., Dobricic, S., Bonaduce, A., 2015. Mediterranean Sea large-scale low-frequency ocean variability and water mass formation rates from 1987 to 2007: A retrospective analysis. Progress in Oceanography 132, 318–332. doi: 10.1016/j.pocean.2013.11.003.

Pirazzoli, P.A., Montaggioni, L.F., Saliège, J.F., Segonzac, G., Thommeret, Y., Vergnaud-Grazzini, C., 1989. Crustal block movements from Holocene shorelines: Rhodes Island (Greece). Tectonophysics 170 (1-2), 89–114. doi: 10.1016/0040-1951(89)90105-4.

Platt, J.P., 1986. Dynamics of orogenic wedges and the uplift of high-pressure metamorphic rocks. Geological Society of America Bulletin 97 (9), 1037. doi: 10.1130/0016-7606(1986)97<1037:DOOWAT>2.0.CO;2.

Poulos, S.E., Drakopoulos, P.G., Collins, M.B., 1997. Seasonal variability in sea surface oceanographic conditions in the Aegean Sea (Eastern Mediterranean): an overview. Journal of Marine Systems 13 (1-4), 225–244. doi: 10.1016/S0924-7963(96)00113-3.

Psarra, S., Tselepides, A., Ignatiades, L., 2000. Primary productivity in the oligotrophic Cretan Sea (NE Mediterranean): seasonal and interannual variability. Progress in Oceanography 46 (2-4), 187–204. doi: 10.1016/S0079-6611(00)00018-5.

Pujo-Pay, M., Conan, P., Oriol, L., Cornet-Barthaux, V., Falco, C., Ghiglione, J.-F., Goyet, C., Moutin, T., Prieur, L., 2011. Integrated survey of elemental stoichiometry (C, N, P) from the western to eastern Mediterranean Sea. Biogeosciences 8 (4), 883–899. doi: 10.5194/bg-8-883-2011.

Quillévéré, F., Cornée, J.-J., Moissette, P., López-Otálvaro, G.E., van Baak, C., Münch, P., Melinte-Dobrinescu, M.C., Krijgsman, W., 2016. Chronostratigraphy of uplifted Quaternary hemipelagic deposits from the Dodecanese island of Rhodes (Greece). Quaternary Research 86 (1), 79–94. doi: 10.1016/j.yqres.2016.05.002.

Quillévéré, F., Nouailhat, N., Joannin, S., Cornée, J.-J., Moissette, P., Lécuyer, C., Fourel, F., Agiadi, K., Koskeridou, E., Escarguel, G., 2019. An onshore bathyal record of tectonics and climate cycles at the onset of the Early-Middle Pleistocene Transition in the eastern Mediterranean. Quaternary Science Reviews 209, 23–39. doi: 10.1016/j.quascirev.2019.02.012.

R Core Team, 2022. R: A language and environment for statistical. R Foundation for Statistical Computing, Vienna, Austria.

R Core Team, 2023. R: A language and environment for statistical, R Foundation for Statistical Computing, Vienna, Austria.

Ragan, D.L., 2009. Structural Geology. An Introduction to Geometrical Techniques. Cambridge University Press.

Ramsay, J.G., Huber, M.I., Lisle, R.J., 1987. The techniques of modern structural geology: Volume 2: Folds and fractures. Academic Press, London, 700 pp.

Rasmussen, T.L., 2005. Systematic paleontology and ecology of benthic foraminifera from the Plio-Pleistocene Kallithea Bay section, Rhodes, Greece, in: Thomsen, E. (Ed.), Lagoon to deep-water foraminifera and ostracods from the plio-pleistocene Kallithea Bay section, Rhodes, Greece. Cushman Foundation for Foraminiferal Research 39, Washington, D.C., 53–157.

Rasmussen, T.L., Thomsen, E., 2005. Foraminifera and paleoenvironment of the Plio-Pleistocene Kallithea Bay section, Rhodes, Greece: evidence for cyclic sedimentation and shallow-water sapropels, in: Thomsen, E. (Ed.), Lagoon to deep-water foraminifera and ostracods from the plio-pleistocene Kallithea Bay section, Rhodes, Greece. Cushman Foundation for Foraminiferal Research 39, Washington, D.C., 15-51.

Rathburn, A.E., Corliss, B.H., 1994. The ecology of living (stained) deep-sea benthic foraminifera from the Sulu Sea. Paleoceanography 9 (1), 87–150. doi: 10.1029/93PA02327.

Revelante, N., Gilmartin, M., 1976. The effect of Po river discharge on phytoplankton dynamics in the Northern Adriatic Sea. Marine Biology 34 (3), 259–271. doi: 10.1007/BF00388803.

Rio, D., Channell, J., Bertoldi, R., Poli, M.S., Vergerio, P.P., Raffi, I., Sprovieri, R., Thunell, R.C., 1997. Pliocene sapropels in the northern Adriatic area: chronology and paleoenvironmental significance. Palaeogeography, Palaeoclimatology, Palaeoecology 135 (1-4), 1–25. doi: 10.1016/S0031-0182(97)00027-8.

Rio, D., Raffi, I., Villa, G., 1990. Pliocene-Pleistocene calcareous nannofossil distribution patterns in the Western Mediterranean, in: Proceedings of the Ocean Drilling Program, 107 Scientific Results. doi: 10.2973/odp.proc.sr.107.164.1990.

Robinson, A.R., Golnaraghi, M., Leslie, W.G., Artegiani, A., Hecht, A., Lazzoni, E., Michelato, A., Sansone, E., Theocharis, A., Ünlüata, Ü., 1991. The eastern Mediterranean general circulation: features, structure and variability. Dynamics of Atmospheres and Oceans 15 (3-5), 215–240. doi: 10.1016/0377-0265(91)90021-7.

Rodríguez-Tovar, F.J., Dorador, J., Grunert, P., Hodell, D., 2015. Deep-sea trace fossil and benthic foraminiferal assemblages across glacial Terminations 1, 2 and 4 at the "Shackleton Site" (IODP Expedition 339, Site U1385). Global and Planetary Change 133, 359–370. doi: 10.1016/j.gloplacha.2015.05.003.

Roether, W., Manca, B.B., Klein, B., Bregant, D., Georgopoulos, D., Beitzel, V., Kovačević, V., Luchetta, A., 1996. Recent changes in Eastern Mediterranean deep waters. Science (New York) 271 (5247), 333–335. doi: 10.1126/science.271.5247.333.

Rogerson, M., Cacho, I., Jimenez-Espejo, F., Reguera, M.I., Sierro, F.J., Martinez-Ruiz, F., Frigola, J., Canals, M., 2008. A dynamic explanation for the origin of the western Mediterranean organic-rich layers. Geochemistry, Geophysics, Geosystems 9 (7). doi: 10.1029/2007GC001936.

Rohling, E.J., 1991. Shoaling of the Eastern Mediterranean Pycnocline due to reduction of excess evaporation: Implications for sapropel formation. Paleoceanography 6 (6), 747–753. doi: 10.1029/91PA02455.

Rohling, E.J., 1994. Review and new aspects concerning the formation of eastern Mediterranean sapropels. Marine Geology 122 (1-2), 1–28. doi: 10.1016/0025-3227(94)90202-X.

Rohling, E.J., Cane, T.R., Cooke, S., Sprovieri, M., Bouloubassi, I., Emeis, K.C., Schiebel, R., Kroon, D., Jorissen, F.J., Lorre, A., Kemp, A., 2002. African monsoon variability during the previous interglacial maximum. Earth and Planetary Science Letters 202 (1), 61–75. doi: 10.1016/S0012-821X(02)00775-6.

Rohling, E.J., Cooke, S., 1999. Stable oxygen and carbon isotopes in foraminiferal carbonate shells, in: Sengupta, B. (Ed.), Modern Foraminifera. Kluwer Academic Publishers, Dordrecht, Boston, London, 239–258. doi: 10.1007/0-306-48104-9_14.

Rohling, E.J., Fenton, M., Jorissen, F.J., Bertrand, P., Ganssen, G., Caulet, J.P., 1998. Magnitudes of sea-level lowstands of the past 500,000 years. Nature 394 (6689), 162–165. doi: 10.1038/28134.

Rohling, E.J., Foster, G.L., Grant, K.M., Marino, G., Roberts, A.P., Tamisiea, M.E., Williams, F., 2014. Sea-level and deep-sea-temperature variability over the past 5.3 million years. Nature 508 (7497), 477–482. doi: 10.1038/nature13230.

Rohling, E.J., Hilgen, F.J., 1991. The eastern Mediterranean climate at times of sapropel formation: a review. Geologie en Mijnbouw 70, 253–264.

Rohling, E.J., Marino, G., Grant, K.M., 2015. Mediterranean climate and oceanography, and the periodic development of anoxic events (sapropels). Earth-Science Reviews 143, 62–97. doi: 10.1016/j.earscirev.2015.01.008.

Rossi, V., Horton, B.P., 2009. The application of subtidal foraminifera-based transfer function to reconstruct Holocene paleobathymetry of the Po Delta, northern Adriatic Sea. Journal of Foraminiferal Research 39 (3), 180–190. doi: 10.2113/gsjfr.39.3.180.

Rossignol-Strick, M., 1983. African monsoons, an immediate climate response to orbital insolation. Nature 304 (5921), 46–49. doi: 10.1038/304046a0.

Rossignol-Strick, M., 1987. Rainy periods and bottom water stagnation initiating brine accumulation and metal concentrations: 1. The Late Quaternary. Paleoceanography 2 (3), 333–360. doi: 10.1029/PA002i003p00333.

Rossignol-Strick, M., Nesteroff, W., Olive, P., Vergnaud-Grazzini, C., 1982. After the deluge: Mediterranean stagnation and sapropel formation. Nature 295 (5845), 105–110. doi: 10.1038/295105a0.

Rullkötter, J., Rinna, J., Bouloubassi, I., Scholz-Böttcher, B.M., Meyers, P.A., Johns, L., Rowland, S.J., 1998. Biological marker significance of organic matter origin and transformation in sapropels from the Pisano Plateau, Site 964, in: Robertson, A.H.F., Emeis, K.-C., Richter, C., Camerlenghi, A. (Eds.), Proceedings of the Ocean Drilling Program, Scientific Results.

Rutherford, S., D'Hondt, S., Prell, W., 1999. Environmental controls on the geographic distribution of zooplankton diversity. Nature 400 (6746), 749–753. doi: 10.1038/23449.

Saaroni, H., Bitan, A., Alpert, P., Ziv, B., 1996. Continental Polar outbreaks into the Levant and Eastern Mediterranean. International Journal of Climatology 16, 1175–1191.

Schiebel, R., Hemleben, C., 2017. Planktic foraminifers in the modern ocean. Springer Berlin Heidelberg. doi: 10.1007/978-3-662-50297-6.

Schmiedl, G., 2019. Use of foraminifera in climate science. Oxford Research Encyclopedia of Climate Science. Oxford University Press. doi: 10.1093/acrefore/9780190228620.013.735.

Schmiedl, G., De Bovée, F., Buscail, R., Charrière, B., Hemleben, C., Medernach, L., Picon, P., 2000. Trophic control of benthic foraminiferal abundance and microhabitat in the bathyal Gulf of Lions, western Mediterranean Sea. Marine Micropaleontology 40 (3), 167–188. doi: 10.1016/s0377-8398(00)00038-4.

Schmiedl, G., Kuhnt, T., Ehrmann, W., Emeis, K.-C., Hamann, Y., Kotthoff, U., Dulski, P., Pross, J., 2010. Climatic forcing of eastern Mediterranean deep-water formation and benthic ecosystems during the past 22000 years. Quaternary Science Reviews 29 (23-24), 3006–3020. doi: 10.1016/j.quascirev.2010.07.002.

Schmiedl, G., Mackensen, A., 2006. Multispecies stable isotopes of benthic foraminifers reveal past changes of organic matter decomposition and deepwater oxygenation in the Arabian Sea. Paleoceanography 21 (4). doi: 10.1029/2006PA001284.

Schmiedl, G., Mackensen, A., Müller, P.J., 1997. Recent benthic foraminifera from the eastern South Atlantic Ocean: Dependence on food supply and water masses. Marine Micropaleontology 32 (3-4), 249–287. doi: 10.1016/S0377-8398(97)00023-6.

Schmiedl, G., Milker, Y., Mackensen, A., 2023. Climate forcing of regional deep-sea biodiversity documented by benthic foraminifera. Earth-Science Reviews 244, 104540. doi: 10.1016/j.earscirev.2023.104540.

Schmiedl, G., Mitschele, A., Beck, S., Emeis, K.-C., Hemleben, C., Schulz, H., Sperling, M., Weldeab, S., 2003. Benthic foraminiferal record of ecosystem variability in the eastern Mediterranean Sea during times of sapropel S5 and S6 deposition. Palaeogeography, Palaeoclimatology, Palaeoecology 190, 139–164. doi: 10.1016/S0031-0182(02)00603-X

Schmiedl, G., Pfeilsticker, M., Hemleben, C., Mackensen, A., 2004. Environmental and biological effects on the stable isotope composition of recent deep-sea benthic foraminifera from the western Mediterranean Sea. Marine Micropaleontology 51 (1-2), 129–152. doi: 10.1016/j.marmicro.2003.10.001.

Schmittner, A., Bostock, H.C., Cartapanis, O., Curry, W.B., Filipsson, H.L., Galbraith, E.D., Gottschalk, J., Herguera, J.C., Hoogakker, B., Jaccard, S.L., Lisiecki, L.E., Lund, D.C., Martínez-Méndez, G., Lynch-Stieglitz, J., Mackensen, A., Michel, E., Mix, A.C., Oppo, D.W., Peterson, C.D., Repschläger, J., Sikes, E.L., Spero, H.J., Waelbroeck, C., 2017. Calibration of

the carbon isotope composition ($\delta^{13}C$) of benthic foraminifera. Paleoceanography 32 (6), 512–530. doi: 10.1002/2016PA003072.

Schneider, S., Linse, U., Stamatiadis, P., Falkenberg, J., Mutterlose, J., Weich, M., 2023. First record of Pliocene (Zanclean to mid Piacenzian) marine deposits on Rhodes (Greece): implications for eastern Mediterranean palaeo(bio)geography. Palaeobiodiversity and Palaeoenvironments 103 (1), 109–128. doi: 10.1007/s12549-022-00533-3.

Schönfeld, J., 2001. Benthic foraminifera and pore-water oxygen profiles: a re-assessment of species boundary conditions at the western Iberian margin. Journal of Foraminiferal Research 31 (2), 86–107. doi: 10.2113/0310086.

Schönfeld, J., 2002. A new benthic foraminiferal proxy for near-bottom current velocities in the Gulf of Cadiz, northeastern Atlantic Ocean. Deep Sea Research Part I: Oceanographic Research Papers 49 (10), 1853–1875. doi: 10.1016/S0967-0637(02)00088-2.

Schulz, M., Mudelsee, M., 2002. REDFIT: estimating red-noise spectra directly from unevenly spaced paleoclimatic time series. Computers & Geosciences 28 (3), 421–426. doi: 10.1016/S0098-3004(01)00044-9

Sen Gupta, B.K., 1999. Foraminifera in marginal marine environments, in: Sen Gupta, B.K. (Ed.), Modern Foraminifera. Springer Netherlands, Secaucus, 141–159. doi: 10.1007/0-306-48104-9_9.

Sen Gupta, B.K., Machain-Castillo, M.L., 1993. Benthic foraminifera in oxygen-poor habitats. Marine Micropaleontology 20 (3-4), 183–201. doi: 10.1016/0377-8398(93)90032-S.

Sgarrella, F., Moncharmont-Zei, M., 1993. Benthic foraminifera of the Gulf of Naples (Italy). Systematics and autecology. Bollettino della Società Paleontologica Italiana 32, 145–264.

Sgarrella, F., Di Donato, V., Sprovieri, R., 2012. Benthic foraminiferal assemblage turnover during intensification of the Northern Hemisphere glaciation in the Piacenzian Punta Piccola section (Southern Italy). Palaeogeography, Palaeoclimatology, Palaeoecology 333-334, 59–74. doi: 10.1016/j.palaeo.2012.03.009.

Shackleton, N.J., Opdyke, N.D., 1973. Oxygen isotope and palaeomagnetic stratigraphy of equatorial pacific core V28-238: oxygen isotope temperatures and ice volumes on a 105 year and 106 year scale. Quaternary Research 3 (1), 39–55. doi: 10.1016/0033-5894(73)90052-5.

Shannon, C.E., Weaver, W., 1949. The mathematical theory of communication. University of Illinois Press, Urbana.

Shaw, B., Ambraseys, N.N., England, P.C., Floyd, M.A., Gorman, G.J., Higham, T.F.G., Jackson, J.A., Nocquet, J.-M., Pain, C.C., Piggott, M.D., 2008. Eastern Mediterranean tectonics and tsunami hazard inferred from the AD 365 earthquake. Nature Geoscience 1 (4), 268–276. doi: 10.1038/ngeo151.

Shaw, B., Jackson, J., 2010. Earthquake mechanisms and active tectonics of the Hellenic subduction zone. Geophysical Journal International 181(2), 966-984. doi: 10.1111/j.1365-246X.2010.04551.x.

Shaw, H., Evans, G., 1984. The nature, distribution and origin of a sapropelic layer in sediments of the Silicia Basin, northeastern Mediterranean. Marine Geology 61 (1), 1–12. doi: 10.1016/0025-3227(84)90104-X.

Siddall, M., Rohling, E.J., Almogi-Labin, A., Hemleben, C., Meischner, D., Schmelzer, I., Smeed, D.A., 2003. Sea-level fluctuations during the last glacial cycle. Nature 423 (6942), 853–858. doi: 10.1038/nature01690.

Simpson, G.L., Hall, R.I., 2012. Human impacts: Applications of numerical methods to evaluate surface-water acidification and eutrophication, in: Birks, H., Lotter, A., Juggins, S., Smol, J.

(Eds.), Tracking environmental change using lake sediments. Springer, Dordrecht, 579–614. doi: 10.1007/978-94-007-2745-8_19.

Singh, R.K., Gupta, A.K., 2010. Deep-sea benthic foraminiferal changes in the eastern Indian Ocean (ODP Hole 757B): Their links to deep Indonesian (Pacific) flow and high latitude glaciation during the Neogene. Episodes 33 (2), 74–82. doi: 10.18814/epiiugs/2010/v33i2/001.

Spjeldnæs, N., Moissette, P., 1997. Celleporid (Bryozoan) thickets from the upper Pliocene of the island of Rhodes, Greece, in: James, N.P., Clarke, J. (Eds.), Cool-Water Carbonates. Society for Sedimentary Geology, 263–270. doi: 10.2110/pec.97.56.0263.

Sprovieri, R., Sprovieri, M., Caruso, A., Pelosi, N., Bonomo, S., Ferraro, L., 2006. Astronomic forcing on the planktonic foraminifera assemblage in the Piacenzian Punta Piccola section (southern Italy). Paleoceanography 21 (4), PA4204. doi: 10.1029/2006PA001268.

Steinthorsdottir, M., Lidgard, S., Håkansson, E., 2006. Fossils, sediments, tectonics. Facies 52 (3), 361–380. doi: 10.1007/s10347-006-0048-2.

Svetunkov, I., 2023. smooth: Forecasting Using State Space Models: R package version 3.2.0. https://CRAN.R-project.org/package=smooth.

Szuba, M.A., 2024. Basin formation caused by plate boundary-parallel extension, Island of Rhodes, Greece. Bachelor thesis, Hamburg.

Tanhua, T., Hainbucher, D., Schroeder, K., Cardin, V., Álvarez, M., Civitarese, G., 2013. The Mediterranean Sea system: a review and an introduction to the special issue. Ocean Science 9 (5), 789–803. doi: 10.5194/os-9-789-2013.

Telford, R.J., Birks, H., 2011. A novel method for assessing the statistical significance of quantitative reconstructions inferred from biotic assemblages. Quaternary Science Reviews 30 (9-10), 1272–1278. doi: 10.1016/j.quascirev.2011.03.002.

Telford, R.J., Trachsel, M., 2019. palaeoSig: Significance Tests for Palaeoenvironmental Reconstructions: R package version 2.0-3. https://cran.r-project.org/web/packages/palaeoSig/.

Telford, R.J., Trachsel, M., 2023. palaeoSig: Significance Tests of Quantitative Palaeoenvironmental Reconstructions: R package version 2.1-3. https://cran.r-project.org/package=palaeoSig.

ten Veen, J.H., 2004. Extension of Hellenic forearc shear zones in SW Turkey: the Pliocene–Quaternary deformation of the Eşen Çay Basin. Journal of Geodynamics 37 (2), 181–204. doi: 10.1016/j.jog.2004.02.001.

ten Veen, J.H., Kleinspehn, K.L., 2002. Geodynamics along an increasingly curved convergent plate margin: Late Miocene-Pleistocene Rhodes, Greece. Tectonics 21 (3), 8-1-8-21. doi: 10.1029/2001TC001287.

Ter Braak, C.J.F., 1986. Canonical correspondence analysis: a new eigenvector technique for multivariate direct gradient analysis. Ecology 67, 1167–1179.

Ter Braak, C.J.F., 1995. Non-linear methods for multivariate statistical calibration and their use in palaeoecology: a comparison of inverse (k-nearest neighbours, partial least squares and weighted averaging partial least squares) and classical approaches. Chemometrics and Intelligent Laboratory Systems 28 (1), 165–180. doi: 10.1016/0169-7439(95)80048-E.

Ter Braak, C.J.F., Juggins, S., 1993. Weighted averaging partial least squares regression (WA-PLS): an improved method for reconstructing environmental variables from species assemblages. Hydrobiologia 269-270, 485. doi: 10.1007/BF00028046.

Tetard, M., Ovsepyan, E., Licari, L., 2021. *Eubuliminella tenuata* as a new proxy for quantifying past bottom water oxygenation. Marine Micropaleontology 166, 102016. doi: 10.1016/j.marmicro.2021.102016.

Theodor, M., Schmiedl, G., Jorissen, F., Mackensen, A., 2016a. Stable carbon isotope gradients in benthic foraminifera as proxy for organic carbon fluxes in the Mediterranean Sea. Biogeosciences 13 (23), 6385–6404. doi: 10.5194/bg-13-6385-2016.

Theodor, M., Schmiedl, G., Mackensen, A., 2016b. Stable isotope composition of deep-sea benthic foraminifera under contrasting trophic conditions in the western Mediterranean Sea. Marine Micropaleontology 124, 16–28. doi: 10.1016/j.marmicro.2016.02.001.

Thomsen, E., Rasmussen, T.L., Hastrup, A., 2001. Calcareous nannofossil, ostracode and foraminifera biostratigraphy of Plio-Pleistocene deposits, Rhodes (Greece), with a correlation to the Vrica section (Italy). Journal of Micropalaeontology 20 (2), 143–154. doi: 10.1144/jm.20.2.143.

Tiberti, M.M., Basili, R., Vannoli, P., 2014. Ups and downs in western Crete (Hellenic subduction zone). Scientific reports 4, 5677. doi: 10.1038/srep05677.

Titschack, J., Joseph, N., Fietzke, J., Freiwald, A., Bromley, R.G., 2013. Record of a tectonically-controlled regression captured by changes in carbonate skeletal associations on a structured island shelf (mid-Pleistocene, Rhodes, Greece). Sedimentary Geology 283, 15–33. doi: 10.1016/j.sedgeo.2012.11.001.

Titschack, J., Nelson, C.S., Beck, T.I., Freiwald, A., Radtke, U., 2008. Sedimentary evolution of a Late Pleistocene temperate red algal reef (Coralligène) on Rhodes, Greece: correlation with global sea-level fluctuations. Sedimentology 55 (6), 1747–1776. doi: 10.1111/j.1365-3091.2008.00966.x.

Triantafyllou, I., Papadopoulos, G.A., 2022. Historical co-seismic uplift rates in the eastern Hellenic Subduction Zone: the case of Rhodes Island. Zeitschrift für Geomorphologie 63 (2-3), 201–217. doi: 10.1127/zfg/2021/0669.

Triantaphyllou, M.V., Antonarakou, A., Dimiza, M., Anagnostou, C., 2010. Calcareous nannofossil and planktonic foraminiferal distributional patterns during deposition of sapropels S6, S5 and S1 in the Libyan Sea (Eastern Mediterranean). Geo-Marine Letters 30 (1), 1–13. doi: 10.1007/s00367-009-0145-7.

Triantaphyllou, M.V., Gogou, A., Dimiza, M.D., Kostopoulou, S., Parinos, C., Roussakis, G., Geraga, M., Bouloubassi, I., Fleitmann, D., Zervakis, V., Velaoras, D., Diamantopoulou, A., Sampatakaki, A., Lykousis, V., 2016. Holocene climatic optimum centennial-scale paleoceanography in the NE Aegean (Mediterranean Sea). Geo-Marine Letters 36 (1), 51–66. doi: 10.1007/s00367-015-0426-2.

Triantaphyllou, M.V., Ziveri, P., Gogou, A., Marino, G., Lykousis, V., Bouloubassi, I., Emeis, K.-C., Kouli, K., Dimiza, M., Rosell-Melé, A., Papanikolaou, M., Katsouras, G., Nunez, N., 2009. Late Glacial–Holocene climate variability at the south-eastern margin of the Aegean Sea. Marine Geology 266 (1-4), 182–197. doi: 10.1016/j.margeo.2009.08.005.

Tsimplis, M., Velegrakis, A., Drakopoulos, P., Theocharis, A., Collins, M., 1999. Cretan deep water outflow into the Eastern Mediterranean. Progress in Oceanography 44 (4), 531–551. doi: 10.1016/S0079-6611(99)00042-7.

Tur, H., Yaltırak, C., Elitez, İ., Sarıkavak, K.T., 2015. Pliocene–Quaternary tectonic evolution of the Gulf of Gökova, southwest Turkey. Tectonophysics 638, 158–176. doi: 10.1016/j.tecto.2014.11.008.

van der Zwaan, G., Duijnstee, I., Dulk, M. den, Ernst, S., Jannink, N., Kouwenhoven, T., 1999. Benthic foraminifers: proxies or problems? Earth-Science Reviews 46 (1-4), 213–236. doi: 10.1016/S0012-8252(99)00011-2.

van der Zwaan, G.J., 1982. Paleoecology of late miocene mediterranean foraminifera. Utrecht micropaleontological bulletins 25, Utrecht University.

van der Zwaan, G.J., Jorissen, F.J., de Stigter, H.C., 1990. The depth dependency of planktonic/benthic foraminiferal ratios: Constraints and applications. Marine Geology 95 (1), 1–16. doi: 10.1016/0025-3227(90)90016-D.

van Hinsbergen, D., Langereis, C.G., Meulenkamp, J.E., 2005a. Revision of the timing, magnitude and distribution of Neogene rotations in the western Aegean region. Tectonophysics 396 (1-2), 1–34. doi: 10.1016/j.tecto.2004.10.001.

van Hinsbergen, D.J., Kouwenhoven, T.J., van der Zwaan, G.J., 2005b. Paleobathymetry in the backstripping procedure: Correction for oxygenation effects on depth estimates. Palaeogeography, Palaeoclimatology, Palaeoecology 221 (3-4), 245–265.

van Hinsbergen, D.J., Krijgsman, W., Langereis, C.G., Cornée, J.-J., Duermeijer, C.E., van Vugt, N., 2007. Discrete Plio-Pleistocene phases of tilting and counterclockwise rotation in the southeastern Aegean arc (Rhodos, Greece): early Pliocene formation of the south Aegean left-lateral strike-slip system. Journal of the Geological Society 164 (6), 1133–1144. doi: 10.1016/j.palaeo.2005.02.013.

van Hinsbergen, D.J.J., Schmid, S.M., 2012. Map view restoration of Aegean–West Anatolian accretion and extension since the Eocene. Tectonics 31 (5).

van Os, B.J.H., Lourens, L.J., Hilgen, F.J., Lange, G.J. de, Beaufort, L., 1994. The formation of Pliocene sapropels and carbonate cycles in the Mediterranean: Diagenesis, dilution, and productivity. Paleoceanography 9 (4), 601–617. doi: 10.1029/94PA00597.

Wagner, B., Vogel, H., Francke, A., Friedrich, T., Donders, T., Lacey, J.H., Leng, M.J., Regattieri, E., Sadori, L., Wilke, T., Zanchetta, G., Albrecht, C., Bertini, A., Combourieu-Nebout, N., Cvetkoska, A., Giaccio, B., Grazhdani, A., Hauffe, T., Holtvoeth, J., Joannin, S., Jovanovska, E., Just, J., Kouli, K., Kousis, I., Koutsodendris, A., Krastel, S., Lagos, M., Leicher, N., Levkov, Z., Lindhorst, K., Masi, A., Melles, M., Mercuri, A.M., Nomade, S., Nowaczyk, N., Panagiotopoulos, K., Peyron, O., Reed, J.M., Sagnotti, L., Sinopoli, G., Stelbrink, B., Sulpizio, R., Timmermann, A., Tofilovska, S., Torri, P., Wagner-Cremer, F., Wonik, T., Zhang, X., 2019. Mediterranean winter rainfall in phase with African monsoons during the past 1.36 million years. Nature 573 (7773), 256–260. doi: 10.1038/s41586-019-1529-0.

Weinkauf, M.F.G., Milker, Y., 2018. The effect of size fraction in analyses of benthic foraminiferal assemblages: A case study comparing assemblages from the >125 and >150 μm size fractions. Frontiers in Earth Science 6. doi: 10.3389/feart.2018.00037.

Wetzel, A., 2010. Deep-sea ichnology: observations in modern sediments to interpret fossil counterparts 60 (1), 125–138.

Wijmstra, T.A., Young, R., Witte, H., 1990. An evaluation of the climatic conditions during the Late Quaternary in northern Greece by means of multivariate analysis of palynological data and comparison with recent phytosociological and climatic data. Geologie en Mijnbouw 69, 243–251.

Wold, S., Ruhe, A., Wold, H., Dunn, I.W.J., 1984. The collinearity problem in linear regression. The Partial Least Squares (PLS) approach to generalized inverses. SIAM Journal on Scientific and Statistical Computing 5 (3), 735–743. doi: 10.1137/0905052.

Woodside, J., Mascle, J., Huguen, C., Volkonskaia, A., 2000. The Rhodes Basin, a post-Miocene tectonic trough. Marine Geology 165 (1-4), 1–12. doi: 10.1016/S0025-3227(99)00140-1.

WoRMS Editorial Board, 2024. World Register of Marine Species. Available from https://www.marinespecies.org at VLIZ. Last accessed 30-05-2024.

Wüst, G., 1961. On the vertical circulation of the Mediterranean Sea. Journal of Geophysical Research 66 (10), 3261–3271. doi: 10.1029/JZ066i010p03261.

Zahn, R., Winn, K., Sarnthein, M., 1986. Benthic foraminiferal $\delta^{13}C$ and accumulation rates of organic carbon: *Uvigerina peregrina* group and *Cibicidoides wuellerstorfi*. Paleoceanography 1 (1), 27–42. doi: 10.1029/PA001i001p00027.

Zijderveld, J., Hilgen, F.J., Langereis, C.G., Verhallen, P., Zachariasse, W.J., 1991. Integrated magnetostratigraphy and biostratigraphy of the upper Pliocene-lower Pleistocene from the Monte Singa and Crotone areas in Calabria, Italy. Earth and Planetary Science Letters 107 (3-4), 697–714. doi: 10.1016/0012-821X(91)90112-U.

Zirks, E., Krom, M.D., Zhu, D., Schmiedl, G., Goodman-Tchernov, B.N., 2019. Evidence for the presence of oxygen-depleted sapropel intermediate water across the Eastern Mediterranean during Sapropel S1. ACS Earth and Space Chemistry 3 (10), 2287–2297. doi: 10.1021/acsearthspacechem.9b00128.

Zitter, T.A.C., Woodside, J.M., Mascle, J., 2003. The Anaximander Mountains: a clue to the tectonics of southwest Anatolia. Geological Journal 38 (3-4), 375–394. doi: 10.1002/gj.961.

Appendix A | Systematic foraminiferal descriptions

For this doctoral thesis, a total of 271 benthic foraminifera have been identified on species level belonging to 117 genera and 3 planktic foraminifera species/genera that have been used as chronostratigraphic markers. Foraminifera identified to species level are systematically listed in alphabetical order in Appendix A and SEM photos of the most dominant species of this thesis are found in chapter 3-5. The systematic benthic foraminiferal description is following the Taxonomy of the World Register of Marine Species (WORMS; WoRMS Editorial Board, 2024) and unaccepted synonyms used in this work are additionally listed and marked in grey under the accepted name of the species.

Order *Astrorhizida* Lankester, 1885

Suborder *Saccamminina* Lankester, 1885
Superfamily *Psammosphaeroidea* Haeckel, 1894
Family *Psammosphaeridae* Haeckel, 1894
Subfamily *Psammosphaerinae* Haeckel, 1894

Genus *Psammosphaera* Schulze, 1875
Psammosphaera fusca Schulze, 1875

Order *Lituolida* Lankester, 1885

Suborder *Spiroplectamminina* Mikhalevich, 1992
Superfamily *Spiroplectamminoidea* Cushman, 1927
Family *Spiroplectamminidae* Cushman, 1927
Subfamily *Spiroplectammininae* Cushman, 1927

Genus *Spiroplectinella* Kisel'man, 1972
Spiroplectinella sepidua

Suborder *Verneuilinina* Kaminski & Mikhalevich 2004
Superfamily *Verneuilinoidea* Cushman, 1911
Family *Verneuilinidae* Cushman, 1911
Subfamily *Verneuilininae* Cushman, 1911

Genus *Gaudryina* d'Orbigny, 1839
Gaudryina siciliana Cushman, 1936

Order *Miliolida* Delage & Hérouard, 1896

Suborder *Miliolina* Delage & Herouard, 1896
Superfamily *Cornuspiroidea* Schultze, 1854
Family *Cornuspiroidea* Schultze, 1854
Subfamily *Cornuspirinae* Schultze, 1854

Genus *Cornuspira* Schultze, 1854
Cornuspira involvens Reuss, 1850

Superfamily *Milioloidea* Ehrenberg, 1839
Family *Cribrolinoididae* Haynes, 1981

Genus *Adelosina* d'Orbigny, 1826
Adelosina bicornis Walker & Jacob, 1798
Lachlanella bicornis (unaccepted)

Family *Hauerinidae* Schwager, 1876
Subfamily *Haueininae* Schwager, 1876

Genus *Cycloforina* Luczkowksa, 1972
Cycloforina villafranca Le Calvez & Le Calvez, 1958
Genus *Quinqueloculina* d'Orbigny, 1826
Quinqueloculina auberiana d'Orbigny, 1839
Quinqueloculina bosciana d'Orbigny, 1839
Quinqueloculina irregulari d'Orbigny, 1878
Quinqueloculina laevigata d'Orbigny, 1839
Quinqueloculina padana Perconig, 1954
Quinqueloculina parvula Schlumberger, 1894
Quinqueloculina schlumbergeri Wiesner, 1923
Quinqueloculina seminulum Linnaeus, 1758
Quinqueloculina venusta Karrer, 1868
Quinqueloculina viennensis Le Calvez & Le Calvez, 1958
Quinqueloculina stelligera (unaccepted)
Quniqueloculina berthelotiana d'Orbigny, 1839

Subfamily *Miliolinellinae* Vella, 1957

Genus *Biloculinella* Wiesner, 1931
Biloculinella globulus Bornemann, 1855
Biloculinella labiata Schlumberger, 1891
Genus *Miliolinella* Wiesner, 1931
Miliolinella semicostata Wiesner, 1923
Miliolinella subrotunda Montagu, 1803
Miliolinella webbiana d'Orbigny, 1839
Genus *Pseudotriloculina* Cherif, 1970
Pseudotriloculina limbata d'Orbigny, 1905
Quinqueloculina limbata (unaccepted)
Genus *Pyrgo* Defrance, 1824
Pyrgo depressa d'Orbigny, 1826
Pyrgo elongata d'Orbigny, 1826
Pyrgo inornata d'Orbigny, 1846
Pyrgo anomala (unaccepted)
Pyrgo lucernala Schwager, 1866
Genus *Triloculina* d'Orbigny, 1826
Triloculina adriatica Le Calvez & Le Calvez, 1958
Triloculina trigonula Lamarck, 1804
Triloculina oblonga Montagu, 1803
Triloculina tricarinata d'Orbigny, 1832

Subfamily *Sigmoilinitinae* Łuczkowska, 1974

Genus *Sigmoilina* Schlumberger, 1887
Sigmoilina costata Schlumberger, 1893
Sigmoilina distorta Phleger & Parker, 1951
Genus *Spirosigmoilina* Parr, 1942
Spirosigmoilina tenuis Čžjžek, 1848
Sigmoilinita tenuis (unaccepted)

Subfamily *Sigmoilopsinae* Vella, 1957

Genus *Sigmoilopsis* Finlay, 1947
Sigmoilopsis schlumbergeri Silvestri, 1904

Subfamily *Siphonapertinae* Saidova, 1975

Genus *Siphonaperta* Vella, 1957
Siphonaperta agglutinata Cushman, 1917
Quinqueloculina agglutinata (unaccepted)
Siphonaperta dilatata Le Calvez & Le Calvez, 1958
Siphonaperta irregularis (unaccepted)

Subfamily *Tubinellinae* Rhumbler, 1906

Genus *Articulina* d'Orbigny, 1826
Articulina mucronata d'Orbigny, 1839

Family *Spiroloculinidae* Wiesner, 1920

Genus *Spiroloculina* d'Orbigny, 1826
Spiroloculina dilatata d'Orbigny, 1846
Spiroloculina excavata d'Orbigny, 1846
Spiroloculina tensuiseptata Brady, 1884

Suborder *Nubeculariina* Saidova, 1981
Superfamily *Nubecularioidea* Jones, 1875
Family *Fischerinidae* Millett, 1898
Subfamily *Fischerininae* Millett, 1898

Genus *Trisegmentina* Wiesner, 1920
Trisegmentina compressa Wiesner, 1923
Fischerina compressa (unaccepted)

Order *Nodosariida* Calkins, 1926

Suborder *Nodosariina* Calkins, 1926

Superfamily *Nodosarioidea Ehrenberg, 1838*

Family *Glandulonodosariidae* Silvestri, 1901

Genus *Glandulonodosaria* Silvestri, 1900
Glandulonodosaria ambigua Neugeboren, 1856
Orthomorphina ambigua (unaccepted)
Genus *Orthomorphina* Stainforth, 1952
Orthomorphina perversa Schwager, 1866

Family *Lagenidae* Reuss, 1862

Genus *Hyalinonetrion* Patterson & Richardson, 1988
Hyalinonetrion gracillimum Seguenza, 1862
Procerolagena gracillima (unaccepted)
Genus *Lagena* Walker & Jacob, 1798
Lagena doveyensis Haynes, 1973
Lagena hispa Reuss, 1863
Lagena hispidula Cushman, 1913
Lagena nebulosa Cushman, 1923
Lagnea radiata Seguenza, 1862
Lagena striata d'Orbigny, 1839
Lagena strumosa Reuss, 1863
Lagena sulcata Walker & Jacob, 1798
Genus *Reussoolina* Colom, 1956
Reussoolina laevis Montagu, 1803
Lagena laevis (unaccepted)
Genus *Seguenzaella* Margerel, 2009
Seguenzaella lacunata Burrows & Holland, 1895
Fissurina lacunata (unaccepted)

Family *Nodosariidae* Ehrenberg, 1838

Subfamily *Frondicularinae* Reuss, 1860

Genus *Frondicularia* d'Orbigny, 1826

Subfamily *Nodosariinae* Ehrenberg, 1838

Genus *Laevidentalina* Loeblich & Tappan, 1986

Laevidentalina ariena Patterson & Pettis, 1986
Dentalina ariena (unaccepted)
Laevidentalina elegans d'Orbigny, 1846
Dentalina subemaciata (unaccepted)
Laevidentalina filiformis d'Orbigny, 1826
Dentalina filiformis (unaccepted)
Laevidentalina guttifera d'Orbigny, 1846
*Dentalina guttifera (*unaccepted)

Genus *Nodosaria* Lamarck, 1816
Genus *Pyramidulina* Fornasini, 1894
Pyramidulina catesbyi d'Orbigny, 1839

Superfamily *Stilostomelloidea* Finlay, 1947

Family *Stilostomellidae* Finlay, 1947

Genus *Siphonodosaria* Silvestri, 1924
Siphonodosaria lepidula Schwager, 1866 (Fig. 3.5)
Stilostomella lepidula (unaccepted)
Genus *Strictocostella* Patterson, 1987
Strictocostella advena Cushman & Laiming, 1931
Stilostomella advena (unaccepted)
Genus *Stilostomella* Guppy, 1894

Order *Polymorphinida* Mikhalevich, 1980

Suborder *Polymorphinina* Mikhalevich, 1980

Superfamily *Polymorphinoidea*

Family *Ellipsolagenidae* Silvestri, 1923

Subfamily *Ellipsolageninae* Silvestri, 1923

Genus *Fissurina* Reuss, 1850
Fissurina orbignyana Seguenza, 1862
Fissurina catanea Flint, 1899
Fissurina crebra Matthes, 1939
Fissurina faba Balkwill & Millett, 1884
Fissurina lucida Williamson, 1848
Fissurina marginata Montagu, 1803
Fissurina staphyllearia Schwager, 1866
Genus *Palliolatella* Patterson & Richardson, 1987
Palliolatella fasciata Egger, 1857
Fissurina fasciata (unaccepted)

Subfamily *Oolininae* Loeblich & Tappan, 1961

Genus *Favulina* Patterson & Richardson, 1988
Favulina foveolata Seguenza, 1862
Favulina hexagona Williamson, 1848
Oolina hexagona (unaccepted)
Favulina squamosa Montagu, 1803
Oolina squamosa (unaccepted)
Genus *Homalohedra* Patterson & Richardson, 1988
Homalohedra acuticosta Reuss, 1862
Genus *Oolina* d'Orbigny, 1839
Oolina ampulladistoma Jones, 1874
Oolina globosa Montagu, 1803

Subfamily *Parafissurininae* Jones, 1984

Genus *Parafissurina* Parr, 1947
Parafissurina felsinea Fornasini, 1894

Family *Glandulinidae* Reuss, 1860

Subfamily *Glandulininae* Reuss, 1860

Genus *Laryngosigma* Loeblich & Tappan, 1953
Laryngosigma lactea Walker & Jacob, 1798
Guttulina lactea (unaccepted)

Family *Polymorphinidae* d'Orbigny, 1839

Subfamily *Edithaellinae* Fuchs, 1967

Genus *Vasiglobulina* Poag, 1969
Vasiglobulina myristiformis Williamson, 1858

Subfamily *Polymorphininae* d'Orbigny, 1839

Genus *Globulina* d'Orbigny, 1839
Globulina gibba d'Orbigny, 1832
Genus *Guttulina* d'Orbigny, 1839
Guttulina communis d'Orbigny, 1826
Genus *Pyrulina* d'Orbigny, 1839
Pyrulina angulosa Egger, 1857
Genus *Sigmomorphina* Cushman & Ozawa, 1928
Sigmomorphina terquemiana Fornasini, 1900

Order *Robertinida* Loeblich & Tappan, 1984

Suborder *Robertinina* Loeblich & Tappan, 1984

Superfamily *Ceratobuliminoidea* Cushman, 1927

Family *Ceratobuliminidae* Cushman, 1927

Subfamily *Ceratobulimininae* Cushman, 1927

Genus *Lamarckina* Berthelin, 1881
Lamarckina scabra Brady, 1884

Family *Epistominidae* Wedekind, 1937

Genus *Hoeglundina* Brotzen, 1948
Hoeglundina elegans d'Orbigny, 1826

Superfamily *Robertinoidea* Reuss, 1850

Family *Robertinidae* Reuss, 1850

Subfamily *Robertininae* Reuss, 1850

Genus *Robertina* d'Orbigny, 1846
Robertina translucens Cushman & Parker, 1936

Order *Rotaliida* Lankester, 1885

Superfamily *Asterigerinoidea* d'Orbigny, 1839

Family *Asterigerinatidae* Reiss, 1963

Genus *Asterigerinata* Bermudez, 1949
Asterigerinata adriatica Haake, 1977
Asterigerinata mamilla Williamson, 1858
Astertigerinata mariae Sgarrella, 1990

Superfamily *Bolivinitoidea* Cushman, 1927

Family *Bolivinitidae* Cushman, 1927

Genus *Bolivina* d'Orbigny, 1839
Bolivina alata Seguenza, 1862
Bolivina antiqua d'Orbigny, 1846 (Fig. 4.3)
Bolivina difformis Williamson, 1858
Bolivina elongata Hantken, 1875
Bolivina pseudoplicata Kacharava, 1982
Bolivina spathulata Williamson, 1858 (Figs. 3.5, 4.3, 5.5)
Brizalina spathulata (unaccepted)
Bolivina subspinescens Cushman, 1922
Bolivina tongi var. filacostata Cushman & McCulloch, 1942
Bolivina variablis Williamson, 1858
Bolivina seminuda Cushman, 1911(Fig. 5.5)
Brizalina seminuda (unaccepted)
Brizalina striatula Cushman, 1922
Brizalina striatula (unaccepted)

Subfamily *Bolivinitinae* Cushman, 1927

Genus *Sigmavirgulina* Loeblich & Tappan, 1957
Sigmavirgulina tortuosa Brady, 1881

Subfamily *Fursenkoininae* Loeblich & Tappan, 1961

Genus *Fursenkoina* Loeblich & Tappan, 1961
Fursenkoina complanata Egger, 1893
Stainforthia complanata (unaccepted)
Fursenkoina subacuta d'Orbigny, 1852
Fursenkonia tenuis Seguenza, 1862

Subfamily *Parabrizalininae* Revets, 1996

Genus *Parabrizalina* Zweig-Strykowski & Reiss, 1976
Parabrizalina porrecta Brady, 1881

Superfamily *Buliminoidea* Jones, 1875

Family *Buliminidae* Jones, 1875

Genus *Bulimina* d'Orbigny, 1826
Bulimina aculeata d'Orbigny, 1826 (Fig. 3.5)
Bulimina elongata d'Orbigny, 1846 (Fig. 5.5)
Bulimina gibba Fornasini, 1902
Bulimina marginata d'Orbigny, 1826 (Figs. 3.5, 5.5)
Bulimina striata d'Orbigny 1832 (Fig. 3.5)

Genus *Praeglobobulimina* Hofker, 1951
Praeglobobulimina spinescens Brady, 1884

Genus *Protoglobobulimina* Hofker, 1951
Protoglobobulimina pupoides d'Orbigny, 1846

Globobulimina pupoides (unaccepted)

Genus *Rectuvigerina* Mathews, 1945

Rectuvigerina bononiensis Fornasini, 1888 (Fig. 4.3)

Rectuvigerina cylindrica Salvatorini, 1967

Rectuvigerina elongatastriata Colom, 1952

Uvigerina elongatastriata (unaccepted)

Rectuvigerina phlegeri Le Calvez, 1959 (Fig. 3.5)

Genus *Reussella* Galloway, 1933

Reusella spinulosa Reuss, 1850

Superfamily *Cassidulinoidea* d'Orbigny, 1839

Family *Cassidulinidae* d'Orbigny, 1839

Subfamily *Cassidulininae* d'Orbigny, 1839

Genus *Cassidulina* d'Orbigny, 1826

Cassidulina carinata Silvestri, 1896 (Figs. 3.5, 5.5)

Cassidulina leavigata d'Orbigny, 1826

Cassidulina obtusa Williamson, 1858 (Fig. 3.5)

Genus *Evolvocassidulina* Eade, 1967

Evolvocassidulina bradyi Norman, 1881

Cassidulinoides bradyi (unaccepted) (Fig. 5.5)

Genus *Globocassidulina* Voloshinova, 1960

Globocassidulina crassa d'Orbigny, 1839

Cassidulina crassa (unaccepted)

Globocassidulina oblonga Reuss, 1850

Cassidulina oblonga (unaccepted)

Globocassidulina subglobulosa Brady, 1881 (Fig. 3.5)

Subfamily *Ehrenbergininae* Cushman, 1927

Genus *Ehrenbergina* Reuss, 1850

Ehrenbergina pacifica Cushman, 1927

Ehrenbergina trigona Goës, 1896

Family *Globobuliminidae* Hofker, 1956

Genus *Globobulimina* Cushman, 1927

Globobulimina affinis d'Orbigny, 1839

Globobulimina pacifica Cushman, 1927

Family *Sphaeroidinidae* Cushman, 1927

Genus *Sphaeroidina* d'Orbigny, 1826

Sphaeroidina bulloides d'Orbigny, 1832 (Fig. 5.5)

Family *Uvigerinidae* Haeckel, 1894

Subfamily *Angulogerininae* Galloway, 1933

Genus *Trifarina* Cushman, 1923

Trifarina angulosa Williamson, 1858 (Fig. 3.5)

Angulogerina angulosa (unaccepted)

Trifarina fornasinii Selli, 1948

Subfamily *Uvigerininae* Haeckel, 1894

Genus *Siphouvigerina* Parr, 1950

Siphouvigerina ampullacea Brady, 1884

Uvigerina ampullaceal (unaccepted)

Genus *Uvigerina* d'Orbigny, 1826

Uvigerina auberiana d'Orbigny, 1839 (Fig. 3.5, 5.5)

Uvigerina bradyana Fornasini, 1900

Uvigerina longirostrata Daniels & Spiegler, 1978

Uvigerina mediterranea Hofker, 1932

Uvigerina peregrina Cushman, 1923 (Figs. 3.5, 4.3, 5.5)

Superfamily *Chilostomelloidea* Brady, 1881

Family *Alabaminidae* Hofker, 1951

Genus *Oridorsalis* Andersen, 1961

Oridorsalis umbonata Reuss, 1851 (Fig. 3.5)

Family *Chilostomellidae* Brady, 1881

Subfamily *Chilostomellinae* Brady, 1881

Genus *Chilostomella* Reuss, 1849

Chilostomella mediterranensis Cushman & Todd, 1949

Chilostomella oolina Schwager, 1878

Family *Gavelinellidae* Hofker, 1956

Subfamily *Gavelinellinae* Hofker, 1956

Genus *Gyroidina* d'Orbigny, 1826
Gyroidina umbonata Silvestri, 1898
Genus *Hansenisca* Loeblich & Tappan, 1987
Hansenisca soldanii d'Orbigny, 1826
Gyroidina soldanii (unaccepted)

Superfamily *Discorbinelloidea* Sigal, 1952

Family *Discorbinellidae* Sigal, 1952

Subfamily *Discorbinellinae* Sigal, 1952

Genus *Discorbinella* Cushman & Martin, 1935
Discorbinella bertheloti d'Orbigny, 1839

Family *Planulinoididae* Saidova, 1981

Genus *Planulinoides* Parr, 1941
Planulinoides bioconcavus Parker & Jones, 1862

Superfamily *Discorboidea* Ehrenberg, 1838

Family *Cancrisidae* Chapman, Parr & Collins, 1934

Genus *Cancris* De Montfort, 1808
Cancris auricula Fichtel & Moll, 1798
Genus *Valvulineria* Cushman, 1926
Valvulineria bradyana Fornasini, 1900 (Fig. 5.5)
Valvulineria copmplanata d'Orbigny, 1846
Valvulineria minuta Schubert, 1904
Valvulinera rugosa d'Orbigny, 1839

Family *Eponididae* Hofker, 1951

Subfamily *Eponidinae* Hofker, 1951

Genus *Alabaminella* Saidova, 1975
Alabaminella weddellensis Earland, 1936
Eponides weddellensis (unaccepted)
Genus *Eponides* De Montfort, 1808
Eponides concameratus Montagu, 1808

Family *Mississippinidae* Saidova, 1981

Subfamily *Stomatorbininae* Saidova, 1981

Genus *Stomatorbina* Dorreen, 1948
Stomatorbina concentrica Parker & Jones, 1864

Family *Rosalinidae* Reiss, 1963

Genus *Gavelinopsis* Hofker, 1951
Gavelinopsis praegeri Heron-Allen & Earland, 1913 (Fig. 3.5)
Genus *Neoconorbina* Hofker, 1951
Neoconorbina terquemi Rzehak, 1888
Genus *Rosalina* d'Orbigny, 1826
Rosalina anomala Terquem, 1875
Rosalina bradyi Cushman, 1915
Rosalina australis Parr, 1932
Rosalina macropora Hofker, 1951
Rosalina williamsoni Chapman & Parr, 1932
Discorbis williamsoni (unaccepted)
Genus *Tretomphaloides* Banner, Pereira & Desai, 1985
Tretomphaloides concinnus Brady, 1884

Superfamily *Glabratelloidea* Loeblich & Tappan, 1964

Family *Glabratellidae* Loeblich & Tappan, 1964

Genus *Conorbella* Hofker, 1951
Conorbella erecta Sidebottom, 1908
Conorbella pulvinata Brady, 1884,
Genus *Planoglabratella* Seiglie & Bermúdez, 1965
Planoglabratella opercularis d'Orbigny, 1839

Family *Heronalleniidae* Loeblich & Tappan, 1986

Genus *Heronallenia* Chapman & Parr, 1931
Heronallenia lingulata Burrows & Holland, 1895

Superfamily *Nonionoidea* Schultze, 1854

Family *Astrononionidae* Cushman & Edwards, 1937

Subfamily *Astrononioninae* Saidova, 1981

Genus *Astrononion* Cushman & Edwards, 1937
Astrononion stelligerum d'Orbigny, 1839

Family *Melonidae* Holzmann & Pawlowski, 2017

Genus *Melonis* De Montfort, 1808
Melonis affinis Reuss, 1851
Melonis barleeanum (unaccepted)

Family *Nonionidae* Schultze, 1854

Subfamily *Nonioninae* Schultze, 1854

Genus *Nonion* De Montfort, 1808
Nonion faba Fichtel & Moll, 1798
Nonion fabum (unaccepted)
Genus *Nonionoides* Saidova, 1975
Nonionoides turgidus Williamson, 1858
Nonionella turgida (unaccepted)
Genus *Pseudononion* Asano, 1936
Pseudononion japonicum Asano, 1936
Nonionella atlantica (unaccepted)

Family *Pulleniidae* Schwager, 1877

Subfamily *Pulleniinae* Schwager, 1877

Genus *Pullenia* Parker & Jones, 1862
Pullenia bulloides d'Orbigny, 1846
Pullenia quadriloba Reuss, 1867
Pullenia quinqueloba Reuss, 1851

Superfamily *Planorbulinoidea* Schwager, 1877

Family *Cibicididae* Cushman, 1927

Subfamily *Cibicidinae* Cushman, 1927

Genus *Cibicides* De Montfort, 1808
Cibicides pachyderma Rzehak, 1886 (Fig. 3.5)
Cibicidoides pachyderma (unaccepted)
Cibicides pseudolobatulus Perelis & Reiss, 1975 (Fig. 3.5)
Cibicides refulgens Montfort, 1808
Genus *Cibicidoides* Thalmann, 1939
Cibicidoides mundulus Brady, Parker & Jones, 1888 (Fig. 3.5)
Cibicidoides pseudoungerianus Cushman, 1922 (Figs. 3.5, 4.3, 5.5)
Cibicidoides variabilis d'Orbigny, 1826
Cibicidella variabilis (unaccepted)
Genus *Lobatula* Fleming, 1828
Lobatula lobatula Walker & Jacob, 1798
Cibicides lobatulus (unaccepted)
Lobatula wuellerstorfi Schwager, 1866
Cibicidoides wuellerstorfi (unaccepted)

Family *Planorbulinidae* Schwager, 1877

Subfamily *Planorbulininae* Schwager, 1877

Genus *Planorbulina* d'Orbigny, 1826
Planorbulina mediterranensis d'Orbigny, 1826

Family *Planulinidae* Bermudez, 1952

Genus *Hyalinea* Hofker, 1951
Hyalinea balthica Schröter, 1783 (Fig. 3.5)
Genus *Planulina* d'Orbigny, 1826
Planulina ariminensis d'Orbigny, 1826

Superfamily *Rotalioidea* Ehrenberg, 1839

Family *Ammoniidae* Saidova, 1981

Subfamily *Ammoniinae* Saidova, 1981

Genus *Ammonia* Bruennich, 1772
Ammonia beccarii Linnaeus, 1758 (Fig. 5.5)
Ammonia parkinsoniana d'Orbigny, 1839
Ammonia tepida Cushman, 1926

Family *Elphidiidae* Galloway, 1933

Subfamily *Elphidiinae* Galloway, 1933

Genus *Elphidium* De Montfort, 1808
Elphidium aculeatum d'Orbigny, 1846
Elphidium advena Cushman, 1922
Elphidium complanatum d'Orbigny, 1839
Elphidium complanatum thyrreanum Accordi, 1951
Elphidium crispum Linnaeus, 1758
Elphidium decipiens Costa, 1856
Elphidium macellum Fichtel & Moll, 1798
Elphidium margaritaceum Cushman, 1930
Elphidium translucens Natland, 1938
Genus *Porosononion* Putrya, 1958
Porosononion granosum d'Orbigny, 1846
Porosononion simplex Cushman, 1933

Family *Haynesinidae* Mikhalevich, 2013

Genus *Haynesina* Banner & Culver, 1978
Haynesina depressula Walker & Jacob, 1798 (Fig. 5.5)

Family *Notorotaliidae* Hornibrook, 1961

Genus *Buccella* Andersen, 1952
Buccella granulata di Napoli Alliata, 1952

Superfamily *Siphoninoidea*

Family *Siphoninidae* Cushman, 1927

Subfamily *Siphonininae* Cushman, 1927

Genus *Siphonina* Reuss, 1850
Siphonina reticulata Čžjžek, 1848

Superfamily *Turrilinoidea* Cushman, 1927

Family *Turrilinidae* Cushman, 1927

Genus *Eubuliminella* Revets, 1993
Eubuliminella exilis Brady, 1884 (Fig. 4.3)

Family *Stainforthiidae* Reiss, 1963

Genus *Stainforthia* Hofker, 1956
Stainforthia fusiformis Williamson, 1858

Suborder *Globigerinina* Delage & Hérouard, 1896

Superfamily *Globorotalioidea* Cushman, 1927

Family *Globorotaliidae* Cushman, 1927

Genus *Globoconella* Bandy, 1975
Globoconella puncticulata d'Orbigny, 1832 (Fig. 4.3)
Globorotalia puncticulata (unaccepted)
Genus *Neogloboquadrina* Bandy, Frerichs & Vincent, 1967
Neogloboquadrina pachyderma Ehrenberg, 1861
Neogloboquadrina pachyderma sinistral

Superfamily *Globigerinoidea* Carpenter et al., 1862

Family *Globigerinidae* Carpenter et al., 1862

Subfamily *Globigerininae* Carpenter et al., 1862

Genus *Sphaeroidinellopsis* Banner & Blow, 1959 (Fig. 4.3)

Order *Spirillinida* Hohenegger & Piller, 1975

Suborder *Spirillinina* Hohenegger & Piller, 1975

Family *Patellinidae* Rhumbler, 1906

Subfamily *Patellininae* Rhumbler, 1906

Genus *Patellina* Williamson, 1858
Patellina corrugata Williamson, 1858

Family *Spirillinidae* Reuss & Fritsch, 1861

Genus *Spirillina* Ehrenberg, 1843
Spirillina limbata Brady, 1879
Spirillina vivipara Ehrenberg, 1843
Spirillina wrigthi Heron-Allen & Earland, 1930

Order *Textulariida* Lankester, 1885

Suborder *Textulariina* Delage & Hérouard, 1896

Superfamily *Textularioidea* Ehrenberg, 1838

Family *Textulariidae* Ehrenberg, 1838

Subfamily *Textulariinae* Ehrenberg, 1838

Genus *Textularia* Defrance, 1824
Textularia agglutinans d'Orbigny, 1839
Textularia calcar Lalicker, 1935
Textularia gramen d'Orbigny, 1846
Textularia pala Čžjžek, 1848
Textularia pseudogramen Chapman & Parr, 1937
Textularia pseudorugosa Lacroix, 1931
Textularia conica (unaccepted)
Textularia sagittula Defrance, 1824
Spiroplectinella sagittula (unaccepted)
Genus *Bigenerina* d'Orbigny, 1826

Bigenerina nodosaria d'Orbigny, 1826

Genus *Sahulia* Loeblich & Tappan, 1985

Sahulia conica d'Orbigny, 1839

Siphotextularia conica d'Orbigny, 1839 (unaccepted)

Subfamily *Siphotextulariinae* Loeblich & Tappan, 1985

Genus *Karrerotextularia* Le Calvez, de Klasz & Brun, 1974

Karrerotextularia flintii Cushman, 1911

Siphotextularia flinitii (unaccepted)

Genus *Siphotextularia* Finlay, 1939

Siphotextularia concava Karrer, 1868

Superfamily *Eggerelloidea* Cushman, 1937

Family *Eggerellidae* Cushman, 1937

Subfamily *Eggerellinae* Cushman, 1937

Genus *Karreriella* Cushman, 1933

Karreriella bradyi Cushman, 1911

Genus *Martinottiella* Cushman, 1933

Martinottiella communis d'Orbigny, 1846

Family *Pseudogaudryinidae* Loeblich & Tappan, 1985

Subfamily *Pseudogaudryininae* Loeblich & Tappan, 1985

Genus *Connemarella* Loeblich & Tappan, 1989

Connemarella rudis Wright, 1900

Gaudryina rudis (unaccepted)

Genus *Pseudoclavulina* Cushman, 1936

Pseudoclavulina crostata Cushman, 1936

Order *Vaginulinida* Mikhalevich, 1993

Family *Vaginulinidae* Reuss, 1860

Subfamily *Lenticulininae* Chapman, Parr & Collins, 1934

Genus *Lenticulina* Lamarck, 1804

Lenticulina calcar Linnaeus, 1758

Lenticulina gibba d'Orbigny, 1839

Lenticulina orbicularis d'Orbigny, 1826

Genus *Marginulinopsis* Silvestri, 1904

Marginulinopsis costata Batsch, 1791

Marginulina costata (unaccepted)

Genus *Neolenticulina* McCulloch, 1977

Neolenticulina variabilis Reuss, 1850

Neolenticulina peregrina (unaccepted)

Genus *Saracenaria* Defrance, 1824

Saracenaria altifrons Parr, 1950

Subfamily *Marginulininae* Wedekind, 1937

Genus *Amphicoryna* Schlumberger, 1881

Amphicoryna hirsuta d'Orbigny, 1826

Amphicoryna scalaris Batsch, 1791

Appendix B | Stable isotope data

Table B1. Agathi Beach stable Isotope data of the epibenthic foraminifer *C. pseudoungerianus*.

Section heights [cm]	Picked individuals	$\delta^{13}C$ [‰ VPDB]	±	$\delta^{18}O$ [‰ VPDB]	±
470	3	-0.789	0.018	0.73	0.03
460	3	-1.03	0.015	0.551	0.03
450	3	0.259	0.018	1.065	0.04
440	3	0.211	0.015	0.89	0.02
430	3	0.353	0.008	0.864	0.03
420	3	-0.582	0.016	0.321	0.04
410	3	-0.12	0.015	0.794	0.03
403	3	0.832	0.016	1.148	0.04
400	3	-0.232	0.012	0.638	0.03
390	3	-0.508	0.019	0.707	0.04
380	3	-0.394	0.02	1.153	0.04
370	3	0.134	0.017	1.898	0.03
360	3	0.353	0.02	1.65	0.04
350	3	-0.146	0.018	1.524	0.05
340	3	0.657	0.022	1.383	0.04
330	3	0.56	0.02	1.229	0.05
320	3	0.601	0.019	1.066	0.03
310	3	0.787	0.014	1.255	0.04
300	3	0.222	0.019	0.93	0.04
290	3	0.429	0.017	1.149	0.03
280	3	-1.093	0.014	1.176	0.02
270	3	0.298	0.015	0.999	0.03
260	3	0.243	0.018	1.144	0.03
250	3	0.71	0.017	1.201	0.03
242	3	1.032	0.015	1.386	0.03
240	3	1.125	0.013	1.466	0.04
230	3	0.611	0.018	2.075	0.02
220	3	0.972	0.019	1.262	0.04
210	3	0.998	0.016	1.399	0.03
200	3	0.367	0.009	1.455	0.03
190	3	-0.035	0.026	1.529	0.03
180	3	0.384	0.017	1.227	0.03
170	3	-0.215	0.013	1.464	0.02
160	3	0.707	0.012	1.223	0.03
150	3	-0.261	0.018	1.248	0.04
140	4	0.533	0.017	1.14	0.03
130	3	-0.21	0.012	1.265	0.03
120	3	0.224	0.015	1.165	0.03
110	3	0.777	0.014	1.142	0.02
100	3	0.681	0.02	1.269	0.03
90	3	0.643	0.015	1.261	0.04
80	3	0.934	0.011	1.254	0.03
70	3	0.976	0.016	1.252	0.04
60	3	0.94	0.016	1.187	0.03
50	3	0.631	0.021	1.378	0.04
40	3	0.802	0.018	1.265	0.03
30	3	0.805	0.017	1.34	0.03
20	3	0.653	0.014	1.23	0.02

Table B2. Lardos stable Isotope data of the epibenthic foraminifer *C. pachyderma*.

Section height [cm]	$\delta^{13}C$ [‰ VPDB]	SD	$\delta^{18}O$ [‰ VPDB]	SD
931	-	-	-	-
921	-	-	-	-
911	-	-	-	-
901	-	-	-	-
891	-	-	-	-
881	-	-	-	-
871	0.596	0.046	0.718	0.078
861	-	-	-	-
851	-	-	-	-
841	-	-	-	-
831	-	-	-	-
821	-	-	-	-
811	-	-	-	-
801	1.206	0.011	1.699	0.016
791	0.982	0.011	1.63	0.012
781	0.745	0.014	1.455	0.008
771	-0.024	0.018	0.773	0.031
761	1.174	0.009	1.722	0.014
751	0.402	0.012	1.141	0.027
741	1.676	0.038	1.4	0.089
731	0.415	0.013	1.14	0.028
721	0.794	0.005	1.585	0.018
711	0.933	0.036	0.953	0.052
701	1.209	0.015	1.062	0.066
691	1.128	0.009	2.081	0.011
681	0.557	0.015	-0.31	0.064
671	0.409	0.013	1.28	0.027
661	1.633	0.009	1.859	0.025
651	0.443	0.013	1.33	0.026
641	0.402	0.014	1.674	0.02
631	0.675	0.013	1.549	0.009
621	0.997	0.043	1.494	0.07
611	0.851	0.007	1.649	0.019
601	0.968	0.008	1.753	0.022
591	0.888	0.013	2.067	0.024
581	1.072	0.009	1.928	0.025
571	1.602	0.012	1.732	0.024
561	1.081	0.005	2.108	0.039
551	1.458	0.016	2.083	0.021
541	-0.276	0.038	0.22	0.066
531	1.013	0.031	1.744	0.045
521	1.19	0.05	0.313	0.049
511	0.882	0.033	1.642	0.076

continued

Section height [cm]	$\delta^{13}C$ [‰ VPDB]	SD	$\delta^{18}O$ [‰ VPDB]	SD
501	1.199	0.006	1.75	0.026
491	1.116	0.016	2.219	0.018
481	1.412	0.014	1.932	0.025
471	0.302	0.014	1.492	0.029
461	1.021	0.011	1.876	0.029
451	1.125	0.013	2.017	0.019
441	1.104	0.014	2.018	0.04
431	0.619	0.008	1.823	0.018
421	0.561	0.016	1.59	0.021
411	1.306	0.005	1.262	0.015
401	1.365	0.007	1.159	0.025
391	1.019	0.005	2.089	0.012
381	1.535	0.015	1.696	0.021
371	1.488	0.011	1.531	0.05
361	0.817	0.006	1.614	0.028
351	1.331	0.011	2.034	0.013
341	1.561	0.008	2.807	0.037
331	1.255	0.017	2.35	0.017
321	1.238	0.006	2.468	0.014
311	1.306	0.004	2.493	0.015
301	1.306	0.006	2.281	0.011
291	1.48	0.012	1.796	0.031
281	1.186	0.014	2.222	0.025
271	1.261	0.008	2.157	0.023
261	1.321	0.014	1.79	0.038
251	1.386	0.005	2.384	0.033
241	1.108	0.013	1.963	0.013
231	1.117	0.006	2.065	0.023
221	1.276	0.011	2.143	0.034
211	0.996	0.013	1.366	0.018
201	1.166	0.008	1.965	0.018
191	1.203	0.005	1.447	0.031
181	1.103	0.01	1.663	0.015
171	0.242	0.01	1.049	0.023
157	0.744	0.026	1.44	0.063
141	0.926	0.014	1.401	0.012
131	1.309	0.011	1.4	0.017
121	0.528	0.011	1.524	0.026
111	-	-	-	-
101	1.689	0.02	1.822	0.02
91	1.514	0.035	1.311	0.054
81	1.159	0.012	1.58	0.02
71	1.596	0.01	1.974	0.012

continued				
61	1.44	0.011	2.019	0.018
51	1.471	0.009	1.515	0.012
41	1.6	0.01	1.637	0.03
31	1.208	0.012	1.482	0.008
21	1.146	0.011	1.788	0.01
11	0.911	0.011	2.01	0.026
1	1.007	0.01	1.778	0.023

Table B3. Plimiri 5 stable Isotope data of the epibenthic foraminifer *C. pseudoungerianus*.

Section heights [cm]	Picked individuals	δ13C [‰ VPDB]	±	δ18O [‰ VPDB]	±
20	3	0.296	0.013	0.268	0.028
30	3	0.136	0.017	0.361	0.03
40	3	-0.027	0.013	0.368	0.034
50	3	-0.062	0.012	0.133	0.023
60	3	0.591	0.011	0.678	0.013
70	3	0.122	0.006	0.666	0.012
80	-	-	-	-	-
90	-	-	-	-	-
100	-	-	-	-	-
110	-	-	-	-	-
120	-	-	-	-	-
130	-	-	-	-	-
140	-	-	-	-	-
150	-	-	-	-	-
160	-	-	-	-	-
170	-	-	-	-	-
180	-	-	-	-	-
190	-	-	-	-	-
200	-	-	-	-	-
210	3	0.45	0.017	0.232	0.028
220	3	0.943	0.01	0.515	0.026
230	3	0.549	0.013	0.348	0.022
240	3	0.513	0.014	0.338	0.022
250	3	0.621	0.011	0.665	0.018
260	3	0.415	0.009	0.39	0.02
270	4	0.234	0.021	0.651	0.035
280	3	0.351	0.013	0.568	0.026
290	3	-0.021	0.01	0.741	0.026
300	3	0.262	0.008	0.41	0.009
310	3	0.377	0.019	0.764	0.027
320	-	-	-	-	-
330	-	-	-	-	-
340	3	0.064	0.011	0.774	0.031
350	-	-	-	-	-
360	3	0.587	0.011	0.756	0.018
370	5	0.588	0.017	0.911	0.026
380	-	-	-	-	-
390	-	-	-	-	-

continued					
Section heights [cm]	Picked individuals	δ13C [‰ VPDB]	±	δ18O [‰ VPDB]	±
400	3	0.186	0.009	0.894	0.021
410	-	-	-	-	-
420	-	-	-	-	-
430	3	0.666	0.012	0.815	0.021
440	3	0.67	0.019	1.202	0.029
450	3	0.486	0.011	1.043	0.026
460	3	0.12	0.011	1.133	0.021
470	3	0.426	0.011	0.724	0.029
480	3	0.409	0.015	0.7	0.019
490	4	0.146	0.016	0.873	0.027
500	3	0.116	0.009	0.995	0.024
510	-	-	-	-	-
520	3	0.069	0.011	0.856	0.03
530	-	-	-	-	-
540	3	0.435	0.013	0.749	0.022
550	-	-	-	-	-
560	3	0.64	0.011	0.545	0.019
570	3	0.782	0.007	0.777	0.009
580	3	0.362	0.011	0.787	0.02
590	3	0.712	0.014	0.629	0.023
600	3	0.857	0.009	0.835	0.023
610	3	0.898	0.007	0.441	0.021
620	3	0.423	0.005	0.93	0.013
630	3	0.837	0.016	0.781	0.026
640	3	0.457	0.012	0.822	0.023
650	3	0.495	0.014	0.445	0.018
660	3	0.17	0.013	0.93	0.025
670	-	-	-	-	-

Table B4. Plimiri 5 stable Isotope data of the infaunal foraminifer *U. peregrina*.

Section heights [cm]	Picked individuals	δ13C [‰ VPDB]	±	δ18O [‰ VPDB]	±
20	6	-1.3	0.014	0.917	0.026
30	6	-1.286	0.011	0.914	0.026
40	5	-	-	-	-
50	5	-1.605	0.013	1.464	0.023
60	6	-1.515	0.01	0.38	0.027
70	5	-1.683	0.014	1.987	0.025
80	5	-1.911	0.016	1.761	0.026
90	5	-1.492	0.012	1.6	0.02
100	5	-1.442	0.013	1.593	0.027
110	5	-1.608	0.019	1.64	0.039
120	5	-1.061	0.015	1.553	0.03
130	5	-1.096	0.016	1.511	0.022
140	5	-1.171	0.011	1.591	0.03
150	5	-1.201	0.012	1.598	0.02
160	5	-0.619	0.009	0.352	0.011
170	5	-0.893	0.018	1.635	0.036
180	5	-1.11	0.013	1.413	0.016
190	5	-1.481	0.011	1.644	0.025
200	5	-1.449	0.013	1.436	0.021
210	5	-1.089	0.02	1.419	0.027
220	5	-1.48	0.014	1.154	0.025
230	5	-1.278	0.013	1.255	0.032
240	5	-1.372	0.015	0.964	0.022
250	5	-1.325	0.014	1.396	0.021
260	6	-1.361	0.006	1.7	0.011
270	5	-1.394	0.011	1.508	0.024
280	5	-1.172	0.016	1.234	0.03
290	5	-0.559	0.011	0.926	0.019
300	5	-1.085	0.014	1.279	0.021
310	5	-0.984	0.009	1.313	0.023
320	5	-1.382	0.012	1.572	0.02
330	6	-1.34	0.009	1.442	0.018
340	5	-0.947	0.026	1.662	0.049
350	5	-0.958	0.014	1.474	0.037
360	5	-0.816	0.011	1.746	0.02
370	7	-1.342	0.008	1.394	0.012
380	5	-1.24	0.015	1.475	0.028
390	7	-1.042	0.011	1.567	0.025
400	5	-1.171	0.012	1.615	0.027
410	6	-1.182	0.009	1.327	0.016
420	5	-1.257	0.01	1.424	0.024
430	5	-0.749	0.009	1.505	0.023
440	5	-1.14	0.012	1.62	0.028
450	5	-0.739	0.005	2.054	0.02
460	5	-0.948	0.014	1.49	0.028
470	5	-1.879	0.014	1.208	0.03
480	5	-0.824	0.018	1.662	0.037
490	5	-0.599	0.017	1.93	0.032
500	5	-0.951	0.015	2.263	0.014
510	5	-1.031	0.016	1.899	0.029
520	5	-1.062	0.012	1.833	0.022
530	6	-0.993	0.019	1.768	0.039
540	5	-0.735	0.011	1.529	0.019
550	5	-1.132	0.008	1.669	0.018
560	5	-0.781	0.008	1.614	0.016
570	5	-0.98	0.009	1.549	0.02
580	5	-0.6	0.01	1.772	0.009
590	5	-0.389	0.011	1.337	0.028
600	5	-0.372	0.013	1.359	0.024
610	5	-0.379	0.013	1.324	0.014
620	5	-0.462	0.011	1.413	0.019
630	6	-0.415	0.01	1.343	0.021
640	5	-0.23	0.014	1.315	0.032
650	5	-0.335	0.014	1.361	0.027
660	5	-0.697	0.015	1.405	0.03
670	5	-1.011	0.016	1.538	0.027

Table B5. Cape Vagia stable Isotope data of the epibenthic foraminifer *C. pseudoungerianus*.

Section depth [cm]	Picked individuals	δ13C [‰ VPDB]	±	δ18O [‰ VPDB]	±
4	3	-0.059	0.022	1.001	0.043
11	3	0.007	0.019	0.884	0.036
23	3	0.31	0.02	1.005	0.037
31	3	0.797	0.014	1.3	0.019
43	3	0.469	0.016	1.086	0.035
55	3	0.777	0.016	1.204	0.046
67	3	0.798	0.016	1.152	0.041
79	3	0.747	0.016	1.176	0.038
91	3	0.624	0.021	1.028	0.042
108	3	0.502	0.018	1.001	0.044
120	3	0.284	0.02	0.965	0.041
132	3	0.498	0.015	0.836	0.038
144	3	0.377	0.016	1.12	0.04
156	3	0.671	0.019	1.471	0.031
168	3	0.312	0.018	1.512	0.04
180	3	0.713	0.015	1.921	0.03
192	3	0.971	0.018	1.857	0.038
203	3	0.649	0.017	1.691	0.045
213	3	0.49	0.016	1.792	0.029
223	3	0.687	0.017	1.436	0.035
233	3	0.903	0.016	1.396	0.037
243	3	0.951	0.016	1.395	0.032
253	3	0.843	0.016	1.697	0.027
263	3	1.112	0.013	1.515	0.024
273	3	0.796	0.018	1.505	0.04
283	3	0.974	0.021	1.536	0.045
293	3	0.784	0.018	1.486	0.034
303	3	0.817	0.02	1.356	0.04
313	3	0.79	0.013	1.397	0.037
323	3	0.606	0.018	2.603	0.037
333	3	0.852	0.016	1.44	0.037
348	3	0.253	0.021	0.849	0.045
363	3	0.777	0.013	1.374	0.026
373	3	0.635	0.02	1.36	0.044
383	3	0.427	0.019	1.306	0.045
393	3	-0.007	0.015	1.353	0.038
403	3	-0.094	0.008	1.55	0.014
413	4	-0.512	0.014	1.371	0.033
423	3	-0.306	0.016	1.323	0.034
433	4	-0.206	0.017	1.498	0.04
443	6	0.552	0.017	1.697	0.043
453	4	0.672	0.017	1.216	0.036
463	3	0.853	0.023	1.192	0.047
473	4	0.832	0.014	1.164	0.036
483	3	0.995	0.018	1.147	0.03
493	-	-	-	-	-
503	4	0.705	0.016	1.281	0.037
513	4	0.724	0.012	1.435	0.024
523	3	-0.141	0.019	1.395	0.039
533	3	0.151	0.024	1.203	0.041

continued

Section depth [cm]	Picked individuals	δ13C [‰ VPDB]	±	δ18O [‰ VPDB]	±
543	3	0.627	0.015	1.311	0.029
553	3	0.717	0.017	1.291	0.026
563	3	0.93	0.015	1.318	0.03
573	3	1.038	0.021	1.348	0.049
583	3	0.859	0.021	1.068	0.045
593	3	1.107	0.017	1.192	0.034
603	3	1.159	0.019	1.156	0.038
613	3	0.942	0.015	0.885	0.04
623	3	1.07	0.015	0.927	0.033
633	3	1.204	0.012	1.054	0.023
643	3	0.885	0.016	1.107	0.032
653	3	0.961	0.022	1.047	0.043
663	3	0.948	0.013	1.097	0.028
673	3	0.651	0.02	1.064	0.044
683	3	0.572	0.01	0.708	0.026
693	-	-	-	-	-
703	-	-	-	-	-
713	-	-	-	-	-
733	4	-0.299	0.018	0.757	0.031
743	5	-0.169	0.016	0.773	0.031
772	4	-0.347	0.022	0.922	0.035
783	-	-	-	-	-
793	-	-	-	-	-
803	-	-	-	-	-
813	-	-	-	-	-
823	-	-	-	-	-
833	-	-	-	-	-
843	-	-	-	-	-
853	-	-	-	-	-
863	-	-	-	-	-
873	3	-1.114	0.021	1.094	0.036
883	3	-1.133	0.021	1.073	0.04
893	-	-	-	-	-
903	-	-	-	-	-
913	-	-	-	-	-
923	-	-	-	-	-
933	-	-	-	-	-
943	-	-	-	-	-
953	-	-	-	-	-
963	-	-	-	-	-
973	-	-	-	-	-
983	-	-	-	-	-
993	6	1.004	0.019	1.155	0.041
1003	-	-	-	-	-
1013	-	-	-	-	-
1023	-	-	-	-	-
1033	-	-	-	-	-
1043	-	-	-	-	-
1053	-	-	-	-	-
1063	-	-	-	-	-

continued					
1073	-	-	-	-	-
1083	-	-	-	-	-
1093	-	-	-	-	-
1103	-	-	-	-	-
1113	-	-	-	-	-
1123	-	-	-	-	-
1133	-	-	-	-	-
1143	-	-	-	-	-
1153	-	-	-	-	-
1163	-	-	-	-	-
1165	-	-	-	-	-
1167	-	-	-	-	-
1169	-	-	-	-	-
1171	-	-	-	-	-
1173	-	-	-	-	-
1175	-	-	-	-	-
1177	-	-	-	-	-
1179	-	-	-	-	-
1181	-	-	-	-	-
1183	-	-	-	-	-
1193	3	-0.277	0.018	0.991	0.04
1203	4	-0.405	0.016	1.016	0.026
1213	3	-0.184	0.019	0.944	0.039
1223	3	0.053	0.02	0.841	0.038
1233	6	0.126	0.02	0.888	0.037
1243	4	0.299	0.019	1.043	0.045
1253	3	0.373	0.017	1.289	0.042
1263	3	0.168	0.016	1.34	0.041
1273	3	0.501	0.023	1.302	0.044
1283	3	0.569	0.019	1.475	0.043
1293	3	0.47	0.018	1.544	0.042
1303	3	0.425	0.016	1.65	0.028
1313	3	0.434	0.016	1.567	0.036
1323	3	0.369	0.017	1.696	0.031
1333	3	0.407	0.019	1.596	0.037
1343	3	0.311	0.015	0.978	0.034
1353	3	0.241	0.016	1.365	0.037
1363	3	0.417	0.017	1.737	0.034
1373	3	0.556	0.015	1.518	0.033
1383	3	0.588	0.013	1.495	0.028
1393	3	0.39	0.011	1.661	0.021
1403	3	0.114	0.013	1.86	0.017
1413	3	-0.223	0.014	1.295	0.032
1423	3	-0.125	0.018	1.109	0.038
1433	3	0.315	0.018	1.15	0.033
1443	3	0.428	0.016	1.13	0.035
1453	3	0.415	0.017	1.717	0.04
1463	3	0.206	0.016	1.646	0.036
1473	3	0.351	0.012	2.014	0.022
1483	3	0.505	0.012	1.895	0.016
1493	3	0.245	0.02	1.618	0.037
1503	3	0.363	0.012	1.117	0.04
1513	3	0.49	0.017	1.443	0.038
1523	3	0.417	0.017	1.582	0.039

continued					
1533	3	0.95	0.023	1.478	0.043
1543	3	0.854	0.014	1.302	0.038
1553	3	0.897	0.015	1.151	0.034
1563	5	0.921	0.019	1.6	0.041
1573	3	1.201	0.016	1.345	0.026
1583	3	1.202	0.016	1.405	0.034
1593	3	0.94	0.016	1.074	0.042
1603	3	1.043	0.016	1.213	0.033
1613	3	1.156	0.018	1.255	0.038
1623	3	0.899	0.022	1.065	0.054
1633	3	0.761	0.019	1.041	0.038
1643	3	0.695	0.016	1.224	0.034
1653	3	0.763	0.019	1.057	0.031
1663	3	0.686	0.016	0.76	0.028
1673	3	0.759	0.016	0.89	0.03
1683	3	0.71	0.018	0.97	0.037
1693	3	1.01	0.011	1.526	0.023
1703	3	0.657	0.016	1.454	0.036
1713	3	0.527	0.019	1.147	0.029
1723	3	0.867	0.016	0.85	0.041
1733	3	1.062	0.019	1.03	0.039
1743	3	1.09	0.013	1.357	0.025
1753	3	0.964	0.016	1.438	0.037
1763	3	1.262	0.019	1.65	0.035
1773	6	1.006	0.018	1.732	0.034
1783	6	0.768	0.021	1.316	0.037
1793	-	-	-	-	-
1803	-	-	-	-	-
1813	-	-	-	-	-
1823	-	-	-	-	-
1833	-	-	-	-	-
1843	-	-	-	-	-
1853	-	-	-	-	-
1863	-	-	-	-	-
1873	-	-	-	-	-
1878	-	-	-	-	-
1883	-	-	-	-	-
1888	-	-	-	-	-
1893	-	-	-	-	-
1898	6	0.765	0.021	0.813	0.049
1903	5	0.609	0.018	1.065	0.041
1908	-	-	-	-	-
1918	3	0.066	0.013	1.31	0.026
1928	3	0.467	0.014	1.272	0.029
1938	3	0.93	0.018	0.778	0.028
1948	3	1.212	0.01	1.013	0.032
1958	3	1.285	0.025	1.189	0.044
1968	3	1.237	0.019	0.977	0.039
1978	3	1.56	0.025	1.045	0.051
1988	3	1.388	0.017	1.016	0.037

Table B6. Cape Vagia stable Isotope data of the infaunal foraminifer *U. peregrina*.

Section depth [cm]	Picked individuals	δ13C [‰ VPDB]	±	δ18O [‰ VPDB]	±
4	5	-1.395	0.017	1.257	0.037
11	5	-2.309	0.018	0.748	0.035
23	5	-1.583	0.019	1.092	0.040
31	5	-0.634	0.016	1.482	0.037
43	6	-0.841	0.016	1.546	0.041
55	5	-0.883	0.018	1.484	0.036
67	5	-0.416	0.014	1.764	0.045
79	5	-0.557	0.018	1.699	0.040
91	5	-0.349	0.02	1.705	0.034
108	5	-0.79	0.017	1.773	0.039
120	5	-0.676	0.018	1.92	0.038
132	5	-0.515	0.015	1.805	0.035
144	5	-0.727	0.016	1.831	0.038
156	5	-0.608	0.019	2.086	0.037
168	5	-0.982	0.022	1.945	0.040
180	5	-0.541	0.021	2.454	0.045
192	5	-0.699	0.021	2.277	0.038
203	5	-0.215	0.01	2.381	0.024
213	5	-0.495	0.022	2.187	0.042
223	5	-0.728	0.021	1.748	0.045
233	5	-0.66	0.021	1.653	0.038
243	4	-0.429	0.014	2.007	0.031
253	5	-0.118	0.019	2.19	0.039
263	5	-0.354	0.014	2.19	0.035
273	5	0.026	0.015	2.149	0.030
283	5	-0.296	0.017	2.265	0.041
293	5	-0.177	0.018	2.259	0.041
303	5	-0.005	0.018	2.408	0.038
313	5	-0.19	0.008	2.144	0.025
323	5	-0.214	0.018	2.388	0.035
333	5	-0.23	0.019	2.441	0.032
348	5	-0.33	0.019	2.207	0.037
363	5	-0.589	0.02	2.311	0.040
373	5	-0.254	0.015	2.474	0.026
383	5	-0.328	0.02	2.305	0.043
393	5	-0.637	0.014	2.259	0.032
403	5	-0.701	0.017	2.45	0.043
413	5	-1.074	0.016	2.485	0.036
423	5	-0.824	0.016	2.357	0.027
433	5	-1.328	0.008	2.145	0.016
443	5	-1.465	0.022	2.227	0.037
453	-	-	-	-	-
463	-	-	-	-	-
473	-	-	-	-	-
483	-	-	-	-	-
493	-	-	-	-	-
503	-	-	-	-	-
513	-	-	-	-	-
523	5	-0.848	0.017	2.049	0.036
533	5	-0.511	0.023	1.975	0.044

continued

Section depth [cm]	Picked individuals	δ13C [‰ VPDB]	±	δ18O [‰ VPDB]	±
543	5	-0.377	0.02	1.771	0.038
553	5	-0.181	0.019	1.853	0.043
563	5	-0.357	0.018	1.904	0.034
573	5	-0.357	0.017	1.704	0.041
583	5	-0.129	0.016	1.664	0.040
593	5	-0.122	0.018	1.865	0.036
603	5	-0.142	0.016	1.552	0.037
613	5	-0.049	0.015	1.697	0.034
623	5	-0.521	0.011	1.465	0.026
633	5	-0.126	0.02	1.494	0.037
643	5	-0.202	0.018	1.547	0.035
653	5	-0.19	0.022	1.508	0.035
663	5	0.11	0.012	1.713	0.019
673	5	-0.516	0.019	1.49	0.041
683	8	-1.205	0.017	1.137	0.038
693	-	-	-	-	-
703	-	-	-	-	-
713	-	-	-	-	-
733	-	-	-	-	-
743	-	-	-	-	-
772	-	-	-	-	-
783	-	-	-	-	-
793	-	-	-	-	-
803	-	-	-	-	-
813	-	-	-	-	-
823	-	-	-	-	-
833	-	-	-	-	-
843	-	-	-	-	-
853	-	-	-	-	-
863	-	-	-	-	-
873	5	-1.79	0.017	1.957	0.035
883	5	-1.835	0.017	2.057	0.037
893	5	-2.077	0.015	1.831	0.033
903	-	-	-	-	-
913	-	-	-	-	-
923	-	-	-	-	-
933	-	-	-	-	-
943	-	-	-	-	-
953	-	-	-	-	-
963	-	-	-	-	-
973	-	-	-	-	-
983	-	-	-	-	-
993	-	-	-	-	-
1003	-	-	-	-	-
1013	-	-	-	-	-
1023	-	-	-	-	-
1033	-	-	-	-	-
1043	4	-0.748	0.017	1.9	0.036
1053	-	-	-	-	-
1063	-	-	-	-	-

continued					
1073	-	-	-	-	-
1083	-	-	-	-	-
1093	-	-	-	-	-
1103	-	-	-	-	-
1113	-	-	-	-	-
1123	-	-	-	-	-
1133	-	-	-	-	-
1143	-	-	-	-	-
1153	-	-	-	-	-
1163	-	-	-	-	-
1165	-	-	-	-	-
1167	-	-	-	-	-
1169	-	-	-	-	-
1171	-	-	-	-	-
1173	-	-	-	-	-
1175	-	-	-	-	-
1177	-	-	-	-	-
1179	-	-	-	-	-
1181	-	-	-	-	-
1183	5	-1.423	0.019	1.875	0.033
1193	5	-1.384	0.013	1.809	0.035
1203	5	-1.111	0.02	1.939	0.040
1213	5	-0.961	0.018	1.856	0.037
1223	5	-0.856	0.015	1.84	0.032
1233	5	-0.746	0.023	1.675	0.034
1243	5	-0.791	0.021	1.893	0.035
1253	5	-0.397	0.022	2.17	0.039
1263	5	-0.625	0.024	2.244	0.042
1273	5	-0.613	0.017	2.405	0.034
1283	5	-0.473	0.016	2.263	0.037
1293	5	-0.674	0.016	2.255	0.028
1303	5	-0.388	0.011	2.442	0.028
1313	5	-0.407	0.017	2.284	0.039
1323	5	-0.429	0.018	2.316	0.043
1333	5	-0.424	0.019	2.278	0.039
1343	5	-0.387	0.013	2.398	0.026
1353	5	-0.554	0.019	2.43	0.031
1363	5	-0.512	0.018	2.564	0.037
1373	5	-0.583	0.019	2.466	0.041
1383	5	-0.334	0.017	2.433	0.045
1393	5	-0.32	0.01	2.54	0.033
1403	5	-0.395	0.024	2.673	0.054
1413	5	-0.76	0.017	2.41	0.042
1423	5	-0.614	0.021	2.224	0.047
1433	5	-0.82	0.017	2.061	0.043
1443	5	-0.61	0.017	2.164	0.038
1453	5	-0.444	0.02	2.375	0.039
1463	5	-0.751	0.017	2.684	0.039
1473	5	-1.086	0.014	2.817	0.029
1483	5	-0.567	0.021	2.51	0.044
1493	5	-0.623	0.015	2.627	0.037
1503	5	-1.163	0.024	2.796	0.044
1513	5	-0.946	0.022	2.536	0.035
1523	5	-0.662	0.021	2.354	0.040

continued					
1533	5	-0.281	0.016	2.305	0.036
1543	5	-0.324	0.019	2.188	0.040
1553	5	-0.259	0.019	2.29	0.045
1563	6	-0.213	0.013	2.139	0.029
1573	5	-0.007	0.02	1.918	0.048
1583	5	-0.222	0.022	1.822	0.039
1593	5	-0.38	0.022	1.718	0.042
1603	5	-0.366	0.019	1.744	0.041
1613	5	-0.187	0.012	1.824	0.024
1623	5	-0.37	0.021	1.771	0.043
1633	5	-0.352	0.017	1.63	0.035
1643	5	-0.065	0.017	1.906	0.036
1653	5	-0.224	0.013	2.04	0.030
1663	5	-0.288	0.018	1.822	0.038
1673	5	-0.501	0.016	1.773	0.039
1683	5	-0.606	0.017	1.775	0.039
1693	5	-0.08	0.02	1.943	0.036
1703	5	0.043	0.02	2.1	0.037
1713	5	-0.315	0.021	2.02	0.037
1723	5	-0.367	0.015	1.796	0.037
1733	5	-0.082	0.014	1.837	0.032
1743	5	-0.558	0.018	2.466	0.037
1753	5	-0.034	0.012	2.641	0.012
1763	5	-1.187	0.015	2.166	0.039
1773	5	-1.113	0.017	2.299	0.041
1783	6	-1.57	0.011	2.075	0.032
1793	-	-	-	-	-
1803	-	-	-	-	-
1813	-	-	-	-	-
1823	-	-	-	-	-
1833	-	-	-	-	-
1843	-	-	-	-	-
1853	-	-	-	-	-
1863	-	-	-	-	-
1873	-	-	-	-	-
1878	5	-0.898	0.017	1.789	0.041
1883	5	-0.7	0.022	1.794	0.037
1888	-	-	-	-	-
1893	5	-0.671	0.018	1.86	0.035
1898	5	-0.944	0.017	1.973	0.036
1903	5	-0.952	0.019	2.095	0.031
1908	5	-1.068	0.02	2.03	0.037
1918	5	-0.363	0.017	1.885	0.038
1928	5	-0.448	0.017	1.397	0.040
1938	5	-0.285	0.02	1.659	0.034
1948	8	-0.387	0.02	1.52	0.029
1958	5	-0.1	0.019	1.731	0.038
1968	5	-0.164	0.018	1.625	0.046
1978	5	-0.059	0.017	1.715	0.035
1988	3	0.141	0.019	1.469	0.029

Appendix C | Age Model Correlation

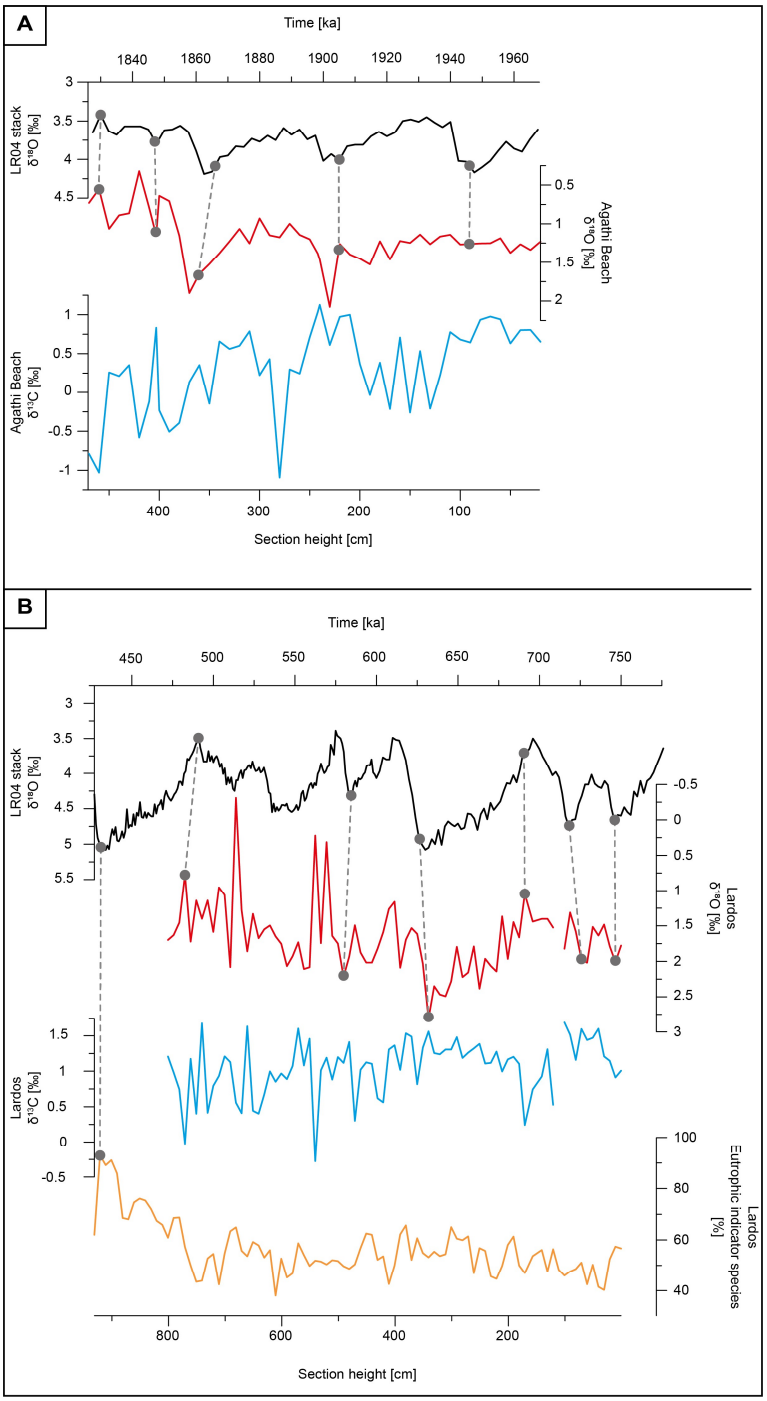

Figure C1. Correlation of $\delta^{18}O$ and $\delta^{13}C$ composition of A) Agathi Beach and B) Lardos with the benthic LR04 stack of Lisiecki and Raymo (2005). In addition to isotopic composition, the relative abundance of eutrophic/low oxygen tolerant indicator species was used for Lardos for the last fix point since no isotope data was available. Grey dots and dotted lines, indicate the position of the fix points used for the correlation.

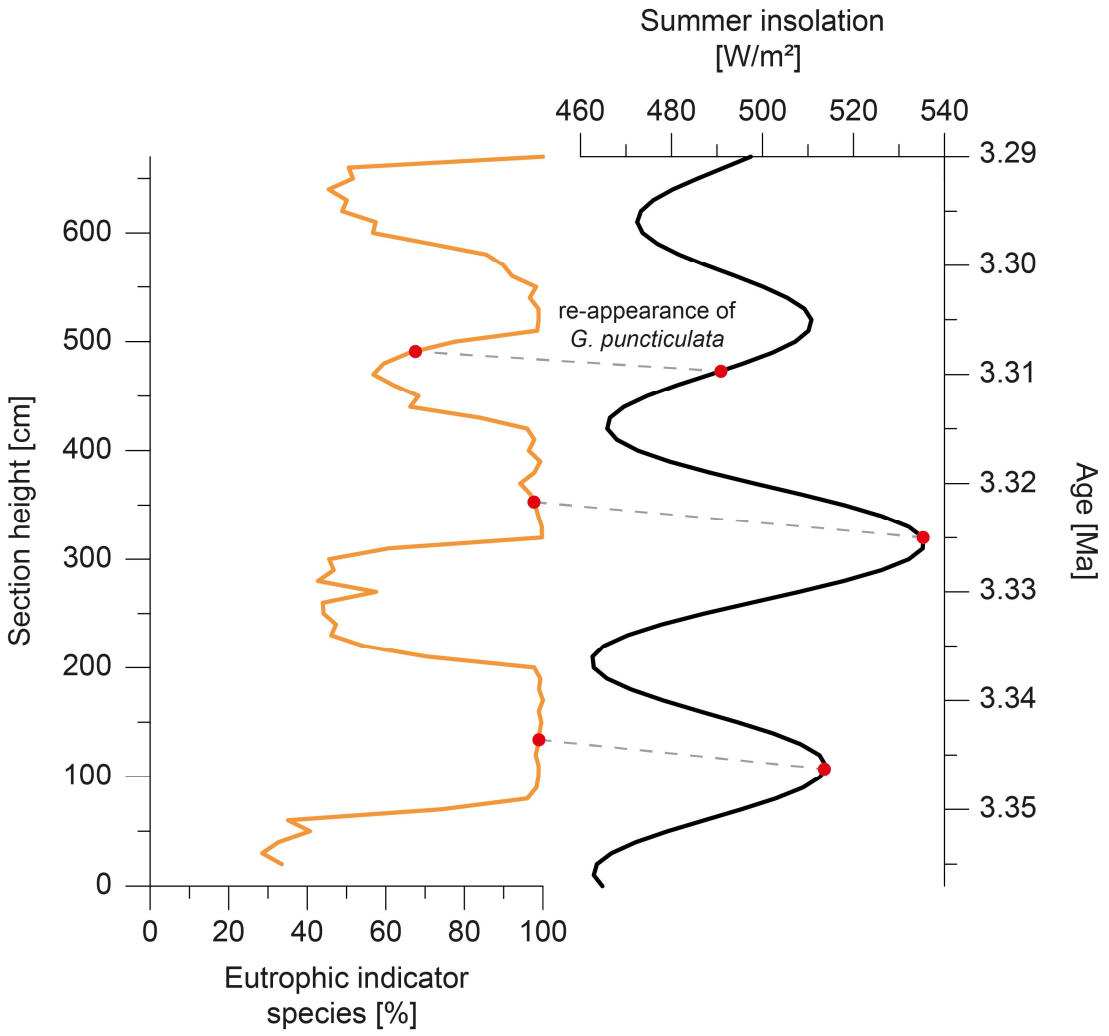

Figure C2. Graphical correlation of relative abundance of eutrophic indicator species in the Plimiri 5 section with the Northern Hemisphere summer insolation (after Laskar et al., 2004). Red dots indicate the points of correlation.

Table C1. Fixpoints used for the generation of the age model of the Plimiri 5 sediment sections. Age model development is mainly based on the graphical correlation of the relative abundance of eutrophic indicator species with the Northern Hemisphere summer insolation (after Laskar et al., 2004).

Section height [cm]	Age [ka]
178	3309.7
318	3325.1
537	3346.3

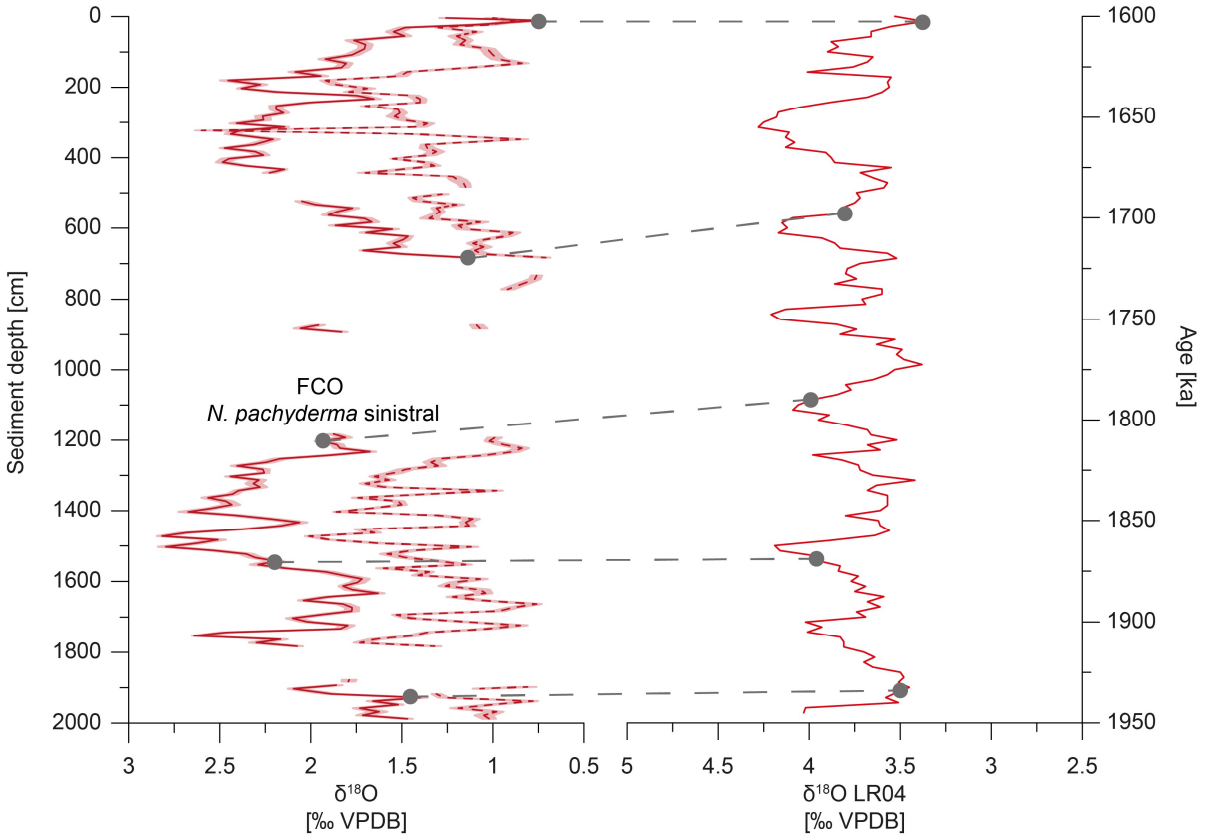

Figure C3. Correlation of $\delta^{18}O$ infaunal and epifaunal data of the Cape Vagia sediment section with the benthic LR04 stack of Lisiecki and Raymo (2005). Grey dots and dotted lines, indicate the position of the fix points used for the correlation.

Table C2. Fixpoints used for the generation of the age model of the Cape Vagia sediment section. Age model development is mainly based on the graphical correlation of the epibenthic $\delta^{13}C$ records of Cape Vagia with the LR04 stack (Lisiecki and Raymo, 2005).

Section depth [cm]	Age [ka]
14	1603.3
685	1697.8
1202	1790.1
1546	1869.0
1926	1934.3

Appendix D | Evaluation of transfer function

The paleo-water depth estimates for Agathi Beach, Lardos and Cape Vagia sections are not considered statistically significant at the 95% confidence level, tested with a randomization transfer function (randomTF) test (Telford and Birks, 2011) and a relatively low amount of variance in the fossil data sets of <30% is explained by paleo-water depth reconstructions (Table D1). Telford and Birks (2011) stated that transfer functions are prone to "false negative" (type II) errors if the transfer function poorly performs or is fitted, if the number of effective modern species, the number of fossil samples or the variability in the reconstruction is low. It is assumed that the transfer function itself works well since it has intensely and successfully been tested by Milker et al. (2017). However, only 29% of the fossil samples have a good fit to water depth in the Agathi Beach section while all other have a poor to extremely poor fit (Fig. D1). In the Lardos section 53% and in Cape Vagia section 18% of the fossil samples have a good fit to water depth, all other have a poor to extremely poor fit (Fig. D1). We assume the poor to extreme poor fit to water depth is the consequence of a lack of modern analogues for the fossil samples of the Agathi Bach, Lardos and Cape Vagia sections as earlier observed for the Pefka E section where the paleo-water depth reconstructions with the here used transfer function were significant on the 95th confidence level (Milker et al., 2017). Our assumption of the lack of modern analogues is supported by a coverage plot of the modern versus fossil foraminifera, where species such as *Cibicidoides pseudoungerianus, Uvigerina peregrina* and *Sphaeroidinia bulliodes* occur in higher abundance in the fossil record of the Agathi Beach section compared to the modern data set and many species of the modern data set are not present in the fossil data set (Fig. D2). Similarly, some species in the Lardos section (e.g., *Cassidulina carinata* s.l., *Bulimina costata, Bolivina spathulata, Gavelinopsis praegeri*) and in the Cape Vagia section (e.g., *C. pseudoungerianus*, *U. peregrina*, *B. sathulata*, *S. bulloides*) have a higher abundance in the fossil record compared to the modern data set and a number of modern species do not occur in the fossil data set (Fig. D2). Likewise, the test application of the Modern Analog Technique for paleo-water depth reconstructions shows little and unrealistic variability and paleo-water depths, particularly for the Agathi Beach section. For the Lardos section it shows more similar trends but somewhat shallower paleo-water depths (Fig. D3). Other studies have shown that the WA-PLS method, used to build the transfer function, performs well under mild non-analog situation (Ter Braak and Juggins, 1993; Ter Braak, 1995) and that the Weighted Averaging technique work most accurate under non-analog situations when compared to other methods (Hutson, 1977), so we have

any confidence to trust our reconstructions. Payne et al. (2016) showed that the majority of transfer function reconstructions for water table reconstructions using testate amoeba were non-significant. They suggest that such transfer function results should be critically evaluated and that the ecological preferences of the species used for the transfer function should be considered. In marine environments it is widely accepted that benthic foraminifera are not directly dependent on water depth but rather relay on other environmental factors, such as the substrate type and food availability (de Rijk et al., 2000; Milker et al., 2017). Additionally, the oxygen content at the sea bottom and pore waters also plays a major role in the distribution patterns of benthic foraminifera (e.g. Gooday, 1994; Bernhard and Sen Gupta, 1999; Schönfeld, 2001). The relatively high proportion of eutrophic/low oxygen tolerant taxa, as well as the changes in the ecosystem, described in chapter 3 and 5 additionally influence the distribution of benthic foraminifera. Furthermore, the transfer function reconstructions can be affected by orbital-driven and glacio-eustatic sea level changes, consequently leading to an overestimation of paleo-water depth estimates (Milker et al., 2019), which we consequently fitted out.

Table D1. Modern benthic foraminifera that also occur in the fossil data sets are marked with crosses.

benthic foraminifera in modern data set	Agathi Beach	Lardos	Cape Vagia
A.angulosa			x
A.mamilla		x	x
A.scalaris			
Adelosina spp.			
Ammonia spp.			x
B.costata	x	x	
B.elongata		x	x
B.granulata			
B.marginata s.l.	x		x
B.nodosaria	x		
B.spathulata		x	x
C.auriculus			x
C.carinata s.l.	x	x	x
C.obtusa	x	x	x
C.pachyderma s.l.		x	
C.pseudoungerianus	x	x	x
C.refulgens			
D.bertheloti	x	x	x
E.advenum			
E.complanatum	x		x
E.concameratus			
E.crispum s.l.	x		x
E.decipiens s.l.			x
E.granosum s.l.			
Elphidium sp.1	x		
G.altiformis			
G.oblonga			
G.orbicularis			
G.praegeri	x	x	x
G.rudis			
G.siciliana			
G.subglobosa	x	x	x
H.balthica		x	x
H.depressula			x
H.elegans			x
L.lobatula s.l.	x	x	x
L.orbicularis			x
M.barleeanum	x	x	x
Miliolinella spp.		x	
N.terquemi	x	x	x

continued

benthic foraminifera in modern data set	Agathi Beach	Lardos	Cape Vagia
N.turgida	x		x
P.ariminensis	x	x	x
P.crustata			
P.falsobeccarii			
P.irregularis			
P.mediterranensis			
P.opercularis			
Q.padana			
Q.seminula			
Q.stelligera			
Q.viennensis			
R.bradyi		x	
R.macropora			
R.spinulosa			x
Rosalina sp.1			x
S.bulloides	x		x
S.costata			
S.globula			
S.sagittula	x		x
S.schlumbergeri	x		x
Siphonaperta spp.			
T.agglutinans s.l.	x		
T.concinnus			
T.gramen		x	x
T.pseudorugosa			
T.trigonula			
Tretomphalus sp.1			
U.mediterranea			
U.peregrina	x	x	x
V.complanata		x	x

Table D2: Results of Paleo-water depth reconstruction of the Agathi Beach sediment section.

Section height [cm]	Estimated paleo-water depth after WA-PLS method [m]	Sample specific error [m]	Estimated paleo-water depth after MAT method [m]	overlap of the modern and fossil data set [%]
471	297.6	50.1	105.2	65
461	355.8	51.1	106.2	62
451	187.9	48.0	104.5	59
441	320.3	50.8	107.1	72
431	-	-	-	-
421	-	-	-	-
411	391.4	52.3	106.6	67
403.5	329.5	50.0	104.6	70
401	158.1	49.4	103.9	65
391	258.7	52.8	105.6	69
381	350.4	54.1	108.9	64
371	311.9	51.4	107.8	55
361	228.8	52.4	106.3	62
351	329.4	54.5	106.7	64
341	260.4	55.0	105.8	65
331	296.1	51.8	106.1	65
321	316.4	54.1	105.1	63
311	192.4	51.1	103.3	67
301	144.9	55.7	102.0	65
291	-	-	-	-
281	-	-	-	-
271	286.1	49.2	104.5	66
261	215.8	48.4	103.5	65
251	295.5	50.1	106.1	68
245	249.8	49.4	103.7	64
241	218.3	49.9	106.6	66
231	206.5	48.9	106.0	59
221	147.5	50.4	106.2	63
211	171.7	50.4	104.1	65
201	174.2	53.3	107.8	70
191	158.9	50.0	104.2	73
181	169.1	52.9	104.4	67
171	-	-	-	-
161	196.3	50.2	103.4	57
151	-	-	-	-
141	-	-	-	-
131	240.8	48.5	106.5	60

continued

Section height [cm]	Estimated paleo-water depth after WA-PLS method [m]	Sample specific error [m]	Estimated paleo-water depth after MAT method [m]	overlap of the modern and fossil data set [%]
121	186.9	48.7	98.8	70
111	219.9	49.8	103.5	73
101	233.4	48.8	103.6	73
91	163.0	49.1	104.4	80
81	110.3	49.3	102.8	73
71	117.5	48.7	106.0	67
61	221.6	49.5	107.5	67
51	272.1	49.3	105.3	67
41	277.5	49.4	106.0	61
31	217.4	48.1	105.8	68
21	342.6	51.5	108.4	68

Table D3. Interpolated and corrected paleo-water depth estimates of the Agathi Beach sediment section.

Age [ka]	corrected paleo-water depth estimates [m]
1827.0	286.7
1828.1	286.2
1829.2	286.7
1830.2	288.2
1831.3	290.2
1832.4	289.1
1833.5	285.0
1834.5	279.8
1835.6	277.0
1836.7	276.4
1837.8	277.2
1838.8	278.4
1839.9	280.0
1841.0	281.9
1842.1	284.3
1843.1	287.0
1844.2	290.1
1845.3	293.7
1846.4	297.6
1847.4	300.2
1848.5	301.4
1849.6	296.5
1850.7	289.2
1851.7	282.1
1852.8	275.5
1853.9	273.3
1855.0	275.1
1856.0	279.2
1857.1	281.9
1858.2	283.2
1859.3	283.9
1860.3	283.5
1861.4	281.9
1862.5	279.2
1863.6	275.3
1864.6	269.9
1865.7	263.0
1866.8	254.5

continued

Age [ka]	corrected paleo-water depth estimates [m]
1867.9	246.8
1868.9	242.5
1870.0	241.7
1871.1	246.2
1872.2	250.8
1873.2	253.8
1874.3	256.4
1875.4	258.5
1876.5	260.0
1877.5	261.1
1878.6	261.1
1879.7	257.8
1880.8	251.3
1881.8	244.0
1882.9	236.5
1884.0	228.8
1885.1	222.9
1886.1	218.8
1887.2	216.8
1888.3	216.8
1889.4	216.5
1890.4	215.1
1891.5	212.5
1892.6	211.8
1893.7	211.1
1894.7	209.3
1895.8	206.9
1896.9	205.2
1898.0	204.5
1899.0	202.2
1900.1	198.5
1901.2	195.9
1902.3	195.5
1903.3	196.4
1904.4	197.4
1905.5	198.3
1906.6	197.3
1907.6	195.7

continued

Age [ka]	corrected paleo-water depth estimates [m]
1908.7	193.6
1909.8	191.1
1910.9	187.8
1911.9	183.7
1913.0	178.8
1914.1	173.1
1915.2	168.5
1916.2	165.1
1917.3	162.0
1918.4	157.6
1919.5	152.0
1920.5	147.9
1921.6	145.7
1922.7	145.0
1923.8	144.8
1924.8	145.0
1925.9	146.3
1927.0	148.8
1928.1	152.6
1929.1	156.4
1930.2	159.9
1931.3	163.2
1932.4	166.6
1933.4	170.1
1934.5	173.8
1935.6	177.0
1936.7	179.5
1937.7	181.1
1938.8	182.8
1939.9	184.7
1941.0	187.0
1942.0	188.9
1943.1	190.5
1944.2	191.6
1945.3	191.1
1946.3	189.0
1947.4	185.3
1948.5	180.4

continued

Age [ka]	corrected paleo-water depth estimates [m]
1949.6	174.4
1950.6	167.5
1951.7	160.5
1952.8	153.5
1953.9	147.0
1954.9	142.2
1956.0	139.0
1957.1	138.1
1958.2	139.1
1959.2	142.0
1960.3	145.3
1961.4	148.3
1962.5	151.0
1963.5	153.3
1964.6	154.8
1965.7	155.6
1966.8	159.5
1967.8	166.9

Tabel D4. Results of paleo-water depth reconstruction of the Lardos sediment section.

Section height [cm]	Estimated paleo-water depth after WA-PLS method [m]	Sample specific error [m]	Estimated paleo-water depth after MAT method [m]	overlap of the modern and fossil data set [%]
931	-	-	-	-
921	-	-	-	-
911	-	-	-	-
901	-	-	-	-
891	-	-	-	-
881	-	-	-	-
871	-	-	-	-
861	-	-	-	-
851	-	-	-	-
841	-	-	-	-
831	-	-	-	-
821	-	-	-	-
811	98.8	57.5	128.5	74
801	156.7	54.2	115.7	68
791	203.0	56.1	120.0	65
781	271.4	63.4	129.9	75
771	303.4	55.4	130.9	69
761	297.2	53.4	128.6	69
751	-	-	-	-
741	144.0	47.8	106.0	64
731	245.0	50.5	115.3	72
721	182.7	52.0	130.9	71
711	234.1	48.7	103.1	62
701	157.1	59.7	107.9	61
691	232.9	55.4	111.1	66
681	-	-	-	68
671	248.5	62.7	114.1	63
661	102.9	53.7	113.3	66
651	166.5	61.3	115.9	68
641	91.3	55.2	125.1	64
631	93.6	57.7	132.1	63
621	216.1	56.4	110.5	69
611	75.2	49.4	122.7	51
601	130.9	52.9	144.0	52
591	151.8	52.1	131.1	56
581	208.0	52.0	131.9	66
571	181.2	54.2	134.9	73
561	236.4	52.7	141.5	66
551	231.3	53.6	136.7	55

continued

Section height [cm]	Estimated paleo-water depth after WA-PLS method [m]	Sample specific error [m]	Estimated paleo-water depth after MAT method [m]	overlap of the modern and fossil data set [%]
541	188.0	54.1	148.8	50
531	265.5	54.5	152.1	59
521	302.7	53.6	132.9	56
511	201.7	50.3	131.3	52
501	230.9	52.3	109.7	61
491	219.6	51.0	132.6	61
481	220.7	51.7	112.7	57
471	47.9	53.5	131.2	63
461	257.4	57.7	145.4	47
451	263.7	55.0	194.6	68
441	273.1	57.9	246.2	62
431	242.4	53.4	204.5	63
421	371.9	60.0	181.1	64
411	222.8	49.2	116.4	62
401	230.0	51.0	132.0	60
391	264.3	53.4	130.9	63
381	316.5	57.9	179.7	68
371	331.8	56.8	131.4	65
361	367.4	57.7	198.1	64
351	302.7	55.3	108.4	61
341	341.7	56.3	144.6	65
331	347.1	57.0	126.9	65
321	349.4	55.6	122.0	57
311	-	-	-	-
301	536.7	66.8	206.4	63
291	354.7	61.4	115.8	64
281	192.2	56.5	116.7	65
271	353.6	58.7	147.7	68
261	351.1	51.7	108.8	66
251	482.1	60.8	198.1	73
241	343.6	60.2	219.3	67
231	278.3	52.2	118.8	74
221	218.7	54.1	115.3	72
211	248.5	57.8	125.9	72
201	245.8	62.7	259.3	71
191	409.4	66.2	411.8	71
181	323.3	61.9	168.0	55
171	-	-	-	-
157	-	-	-	-

continued				
141	603.3	65.3	418.6	77
131	317.9	53.9	158.9	74
121	396.5	61.9	210.1	69
111	327.9	52.7	106.8	76
101	337.9	57.5	108.9	66
91	297.1	55.1	218.5	71
81	290.6	58.4	192.0	61
71	282.0	56.4	199.9	68
61	315.3	51.3	112.1	72
51	411.9	56.6	191.8	72
41	341.3	54.5	181.8	76
31	279.0	55.3	191.6	80
21	369.8	58.7	320.8	69
11	446.0	62.5	396.4	79
1	476.3	85.9	532.0	73

Table D5. Interpolated and corrected paleo-water depth estimates of the Lardos sediment section.

Age [ka]	corrected paleo-water depth estimates [m]
474.9	142.3
476.0	136.3
477.1	131.6
478.1	128.1
479.2	125.9
480.3	124.7
481.4	124.4
482.5	124.9
483.5	126.1
484.6	128.3
485.7	131.3
486.8	135.3
487.9	140.1
488.9	145.3
490.0	150.9
491.1	156.8
492.2	163.0
493.3	168.9
494.3	174.6
495.4	180.0
496.5	184.3
497.6	193.3
498.7	199.9

continued	
Age [ka]	corrected paleo-water depth estimates [m]
499.7	204.2
500.8	206.1
501.9	205.7
503.0	205.8
504.1	206.6
505.1	208.1
506.2	207.8
507.3	205.2
508.4	200.4
509.5	194.9
510.5	189.7
511.6	184.8
512.7	179.0
513.8	171.9
514.9	163.9
515.9	156.3
517.0	150.5
518.1	147.3
519.2	146.2
520.3	146.5
521.3	148.3
522.4	151.4
523.5	156.0

continued	
Age [ka]	corrected paleo-water depth estimates [m]
524.6	159.4
525.7	160.8
526.7	158.3
527.8	154.2
528.9	149.7
530.0	147.3
531.1	145.6
532.1	143.9
533.2	139.8
534.3	134.6
535.4	128.9
536.5	124.1
537.5	119.0
538.6	112.4
539.7	106.0
540.8	100.8
541.9	97.4
542.9	92.5
544.0	85.1
545.1	75.3
546.2	65.1
547.3	56.3
548.3	50.9

continued	
Age [ka]	corrected paleo-water depth estimates [m]
549.4	48.4
550.5	48.1
551.6	47.4
552.7	46.5
553.7	45.8
554.8	47.8
555.9	51.9
557.0	57.3
558.1	62.5
559.1	67.9
560.2	74.5
561.3	80.4
562.4	85.2
563.5	88.0
564.5	92.4
565.6	99.1
566.7	107.5
567.8	115.7
568.9	122.5
569.9	130.0
571.0	138.3
572.1	147.7
573.2	157.4

continued

Age [ka]	corrected paleo-water depth estimates [m]
574.3	167.1
575.3	176.5
576.4	183.6
577.5	188.4
578.6	191.8
579.7	195.0
580.7	198.0
581.8	199.9
582.9	200.6
584.0	200.0
585.1	198.9
586.1	197.6
587.2	196.4
588.3	195.8
589.4	192.9
590.5	187.2
591.5	179.3
592.6	174.1
593.7	171.5
594.8	169.5
595.9	167.0
596.9	164.1
598.0	162.5
599.1	162.9
600.2	164.9
601.3	166.8
602.3	168.2
603.4	172.2
604.5	179.0
605.6	186.8
606.7	192.1
607.7	194.7
608.8	196.7
609.9	198.7
611.0	204.0
612.1	213.0
613.1	223.5
614.2	230.6
615.3	234.3
616.4	237.8
617.5	241.1
618.5	244.2
619.6	247.2

continued

Age [ka]	corrected paleo-water depth estimates [m]
620.7	250.2
621.8	253.6
622.9	256.1
623.9	257.5
625.0	255.1
626.1	250.5
627.2	245.8
628.3	244.0
629.3	244.9
630.4	246.2
631.5	247.2
632.6	248.1
633.7	248.3
634.7	248.0
635.8	248.0
636.9	248.4
638.0	249.3
639.1	251.6
640.1	255.4
641.2	260.5
642.3	266.9
643.4	271.6
644.5	275.2
645.5	278.1
646.6	279.8
647.7	278.8
648.8	275.1
649.9	269.1
650.9	264.1
652.0	261.6
653.1	261.6
654.2	263.1
655.3	264.6
656.3	265.9
657.4	266.2
658.5	266.4
659.6	267.0
660.7	267.9
661.7	268.3
662.8	265.4
663.9	259.2
665.0	252.7
666.1	247.6

continued

Age [ka]	corrected paleo-water depth estimates [m]
667.1	244.3
668.2	242.5
669.3	242.2
670.4	243.4
671.5	246.1
672.5	246.9
673.6	245.6
674.7	242.4
675.8	237.8
676.9	233.5
677.9	229.3
679.0	225.2
680.1	219.9
681.2	215.0
682.3	210.9
683.3	208.4
684.4	209.0
685.5	210.4
686.6	212.8
687.7	215.2
688.7	219.5
689.8	225.8
690.9	234.3
692.0	244.9
693.1	257.6
694.1	272.5
695.2	288.3
696.3	305.1
697.4	322.7
698.5	341.2
699.5	361.0
700.6	377.1
701.7	387.5
702.8	390.7
703.9	392.7
704.9	393.5
706.0	393.0
707.1	392.1
708.2	390.6
709.3	390.3
710.3	389.0
711.4	386.0
712.5	380.6

continued

Age [ka]	corrected paleo-water depth estimates [m]
713.6	372.8
714.7	363.1
715.7	351.4
716.8	338.0
717.9	322.9
719.0	306.2
720.1	288.5
721.1	270.0
722.2	255.6
723.3	247.3
724.4	245.0
725.5	242.6
726.5	240.2
727.6	239.4
728.7	241.3
729.8	243.8
730.9	245.5
731.9	246.4
733.0	246.9
734.1	247.8
735.2	249.0
736.3	250.1
737.3	251.0
738.4	252.6
739.5	255.5
740.6	259.7
741.7	264.5
742.7	269.8
743.8	275.3
744.9	280.8
746.0	286.2
747.1	290.9
748.1	294.5
749.2	297.0
750.3	298.7

Table D6. Results of paleo-water depth reconstruction of the Cape Vagia sediment section.

Section height [cm]	Estimated paleo-water depth after WA-PLS method [m]	Sample specific error [m]	Estimated paleo-water depth after MAT method [m]	overlap of the modern and fossil data set [%]
31	134	27	115	75
55	146	29	110	78
79	196	33	110	78
108	230	36	118	80
132	238	38	116	78
156	349	53	110	73
180	256	38	111	67
203	304	44	111	70
223	195	32	110	71
243	138	28	112	79
263	153	28	111	68
283	236	36	116	78
303	378	55	111	76
323	345	50	114	79
348	366	52	112	82
373	264	40	111	81
393	359	51	111	79
413	467	77	218	55
433	-	-	-	-
453	57	30	110	75
473	-	-	-	-
493	63	28	110	76
513	30	35	111	79
533	473	79	111	81
553	379	59	116	81
573	237	37	114	78
593	188	31	110	77
613	203	34	115	72
633	261	40	116	81
653	247	38	117	78
673	402	60	113	83
693	-	-	-	-
713	-	-	-	-
743	-	-	-	-
783	-	-	-	-
803	-	-	-	-
823	-	-	-	-
843	-	-	-	-
863	-	-	-	-

continued

Section height [cm]	Estimated paleo-water depth after WA-PLS method [m]	Sample specific error [m]	Estimated paleo-water depth after MAT method [m]	overlap of the modern and fossil data set [%]
883	-	-	-	-
903	-	-	-	-
923	-	-	-	-
943	-	-	-	-
963	-	-	-	-
983	-	-	-	-
1003	-	-	-	-
1023	-	-	-	-
1043	-	-	-	-
1063	-	-	-	-
1083	-	-	-	-
1103	-	-	-	-
1123	-	-	-	-
1143	-	-	-	-
1163	-	-	-	-
1167	-	-	-	-
1171	-	-	-	-
1173	-	-	-	-
1175	-	-	-	-
1179	-	-	-	42
1183	-	-	-	21
1203	551	96	243	68
1223	544	89	289	87
1243	438	67	204	80
1263	-	-	-	-
1283	276	42	230	82
1303	224	34	130	87
1323	346	54	235	86
1343	258	38	204	90
1363	198	30	145	86
1383	325	50	235	83
1403	318	48	234	82
1423	276	42	116	85
1443	294	49	116	92
1463	141	27	139	78
1483	195	32	114	79
1503	250	36	114	74
1523	258	38	111	73
1543	198	31	111	66

continued				
1563	181	30	113	62
1583	167	30	115	66
1603	232	36	115	68
1623	212	34	119	76
1643	227	36	115	78
1663	283	50	123	82
1683	279	45	237	79
1703	302	44	125	67
1723	193	31	175	80
1743	413	62	114	68
1763	504	82	227	65
1783	102	32	181	67
1803	-	-	114	41
1823	110	29	105	66
1843	113	28	110	65
1863	116	30	112	55
1878	145	29	111	68
1888	239	37	112	60
1898	279	44	110	58
1908	-	-	115	46
1928	153	28	114	66
1948	85	26	107	59
1968	132	27	94	65
1988	155	28	112	68

Table D7. Interpolated and corrected paleo-water depth estimates of the Cape Vagia sediment section.

Age [ka]	corrected paleo-water depth estimates [m]	continued Age [ka]	corrected paleo-water depth estimates [m]	continued Age [ka]	corrected paleo-water depth estimates [m]	continued Age [ka]	corrected paleo-water depth estimates [m]
1606	158	1646	209	1687	164	1728	-
1607	155	1648	210	1688	172	1729	-
1608	153	1649	213	1689	180	1730	-
1609	150	1650	216	1691	189	1731	-
1610	148	1651	219	1692	200	1732	-
1611	147	1652	220	1693	209	1734	-
1612	146	1653	220	1694	219	1735	-
1613	146	1654	220	1695	230	1736	-
1614	147	1655	222	1696	245	1737	-
1615	148	1656	227	1697	256	1738	-
1616	149	1657	235	1698	258	1739	-
1617	151	1658	245	1699	255	1740	-
1619	153	1659	258	1700	-	1741	-
1620	155	1660	272	1701	-	1742	-
1621	158	1662	282	1702	-	1743	-
1622	161	1663	287	1703	-	1744	-
1623	167	1664	286	1705	-	1745	-
1624	174	1665	280	1706	-	1746	-
1625	181	1666	266	1707	-	1748	-
1626	186	1667	251	1708	-	1749	-
1627	190	1668	237	1709	-	1750	-
1628	196	1669	223	1710	-	1751	-
1629	203	1670	210	1711	-	1752	-
1630	210	1671	197	1712	-	1753	-
1631	217	1672	183	1713	-	1754	-
1633	222	1673	169	1714	-	1755	-
1634	223	1674	157	1715	-	1756	-
1635	223	1676	153	1716	-	1757	-
1636	221	1677	158	1717	-	1758	-
1637	217	1678	168	1719	-	1759	-
1638	214	1679	173	1720	-	1760	-
1639	210	1680	175	1721	-	1762	-
1640	208	1681	173	1722	-	1763	-
1641	206	1682	166	1723	-	1764	-
1642	206	1683	159	1724	-	1765	-
1643	206	1684	156	1725	-	1766	-
1644	208	1685	155	1726	-	1767	-
1645	209	1686	157	1727	-	1768	-

continued

Age [ka]	corrected paleo-water depth estimates [m]
1769	-
1770	-
1771	-
1772	-
1773	-
1774	-
1775	-
1777	-
1778	-
1779	-
1780	-
1781	-
1782	-
1783	-
1784	-
1785	-
1786	-
1787	-
1788	477
1789	479
1791	481
1792	482
1793	483
1794	485
1795	486
1796	487
1797	487
1798	486
1799	483
1800	480
1801	476
1802	470
1803	464
1805	457
1806	448
1807	439
1808	429
1809	418
1810	406
1811	394
1812	380
1813	366

continued

Age [ka]	corrected paleo-water depth estimates [m]
1814	351
1815	338
1816	325
1817	314
1818	306
1820	298
1821	291
1822	284
1823	276
1824	269
1825	262
1826	255
1827	249
1828	242
1829	238
1830	237
1831	237
1832	240
1834	244
1835	248
1836	253
1837	257
1838	259
1839	259
1840	257
1841	255
1842	254
1843	253
1844	254
1845	256
1846	259
1848	260
1849	261
1850	260
1851	257
1852	251
1853	245
1854	238
1855	231
1856	225
1857	219
1858	214

continued

Age [ka]	corrected paleo-water depth estimates [m]
1859	209
1860	206
1861	203
1863	200
1864	197
1865	195
1866	191
1867	187
1868	182
1869	179
1870	177
1871	176
1872	177
1873	178
1874	179
1875	178
1877	177
1878	176
1879	176
1880	176
1881	176
1882	175
1883	175
1884	174
1885	173
1886	173
1887	174
1888	176
1889	180
1891	184
1892	189
1893	194
1894	199
1895	204
1896	210
1897	216
1898	222
1899	224
1900	223
1901	223
1902	227
1903	234

continued

Age [ka]	corrected paleo-water depth estimates [m]
1904	244
1906	256
1907	269
1908	281
1909	286
1910	284
1911	275
1912	266
1913	257
1914	248
1915	240
1916	231
1917	222
1918	213
1920	206
1921	200
1922	196
1923	191
1924	182
1925	171
1926	157
1927	143
1928	129
1929	119
1930	116
1931	118
1932	125
1934	131
1935	135
1936	138
1937	140
1938	140
1939	139
1940	138
1941	138
1942	137
1943	137
1944	138

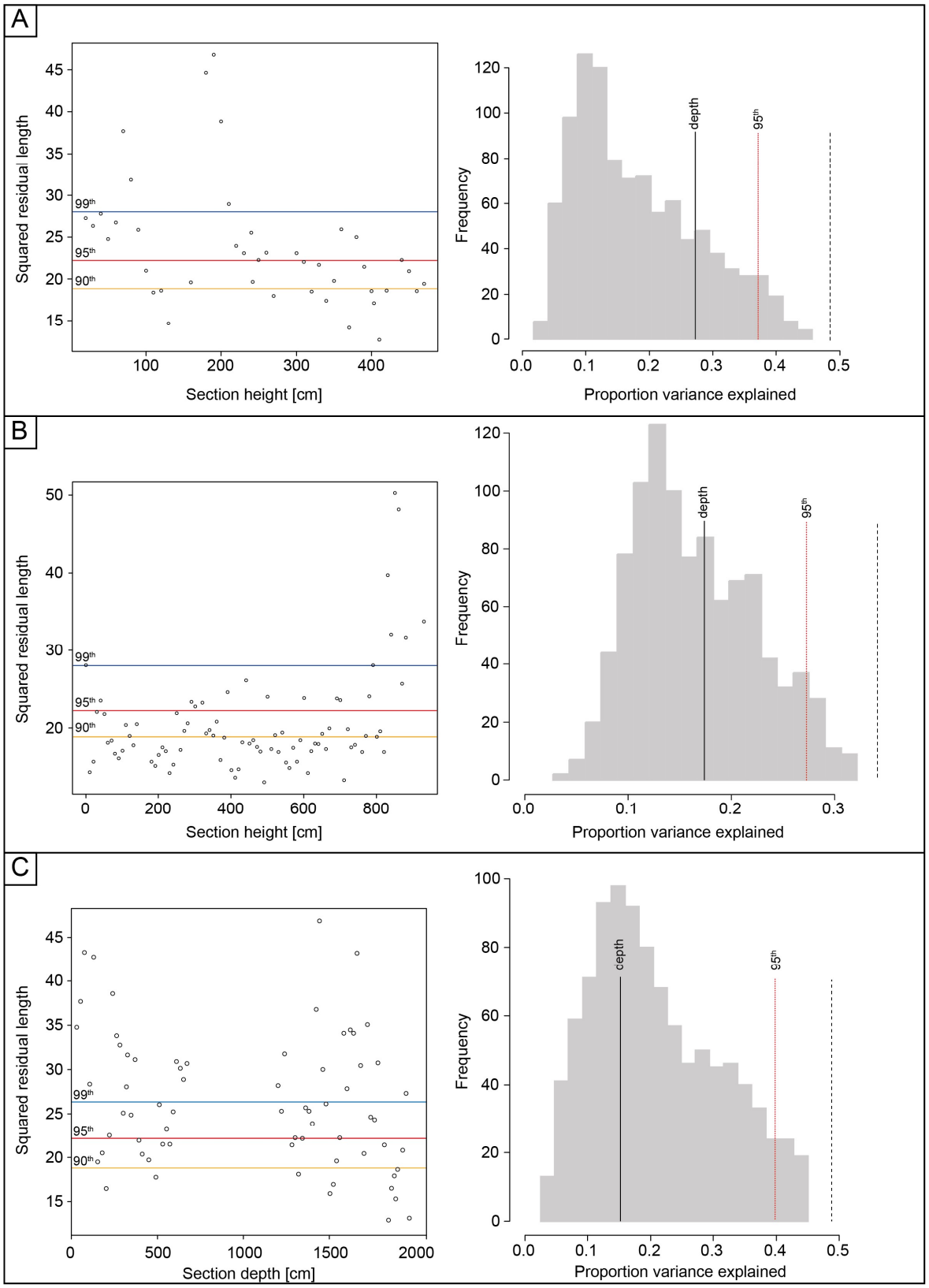

Figure D1. Right: Goodness-of-fit statistics shows the squared residual length of the fossil samples from **A.** Agathi Beach, **B.** Lardos and **C.** Cape Vagia versus section height/depth. Indicated with lines are the 90th (yellow), 95th (red) and 99th (blue) percentiles. Left: RandomTF test results are shown for **A.** Agathi Beach, **B.** Lardos and **C.** Cape Vagia. Proportion of variance in the fossil data set explained by 999 TFs trained with random data is displayed as histogram. Solid black line reflects the proportion of variance explained by the TF used in this study. Dotted black line shows the maximum variance in the fossil data set and dotted red line the 95%-confidence interval.

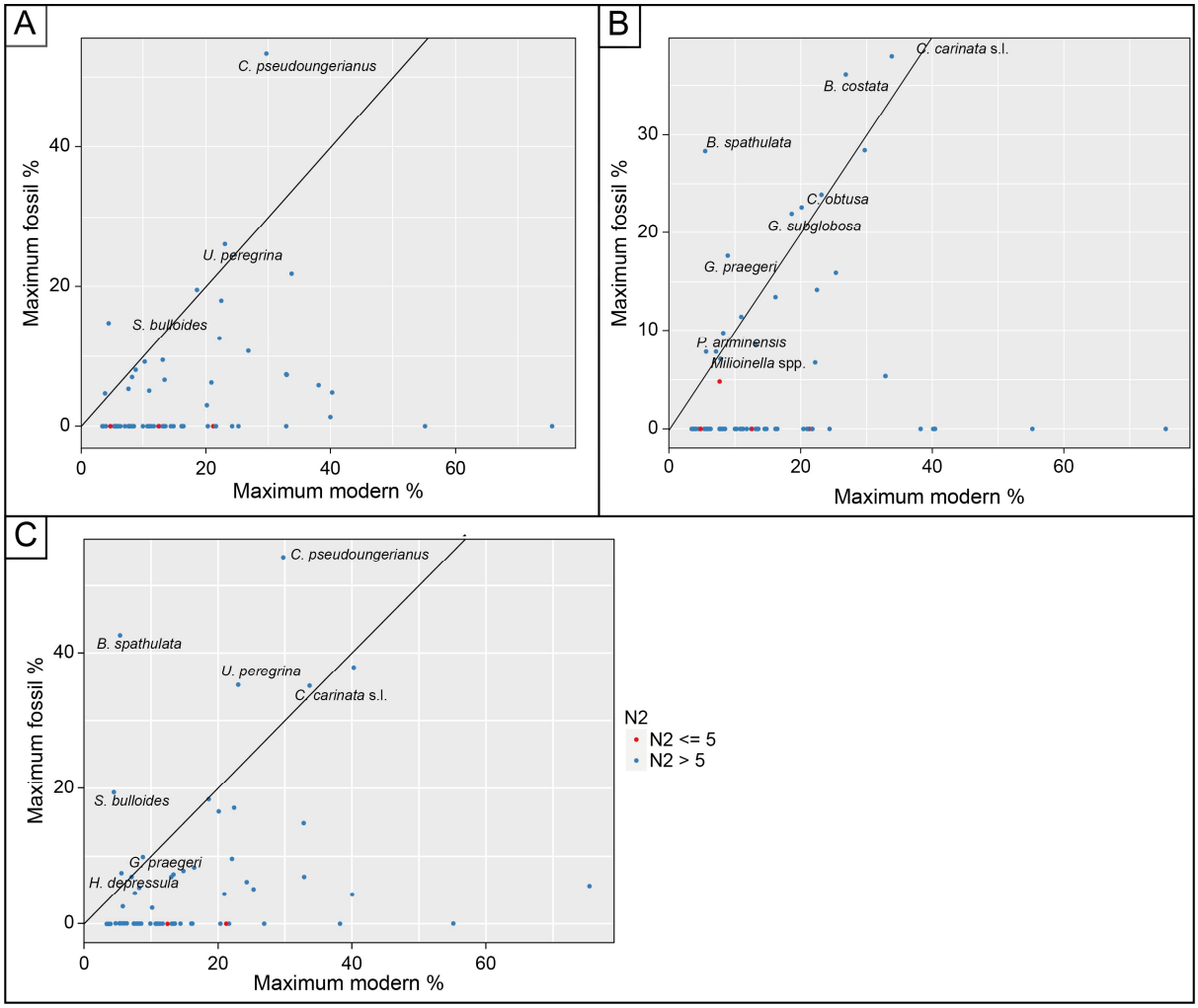

Figure D2. Coverage plots for **A.** Agathi Beach, **B.** Lardos and **C.** Cape Vagia showing the maximum species abundance of the modern data set versus the maximum abundance in the fossil data sets of Agathi Beach, Lardos and Cape Vagia.

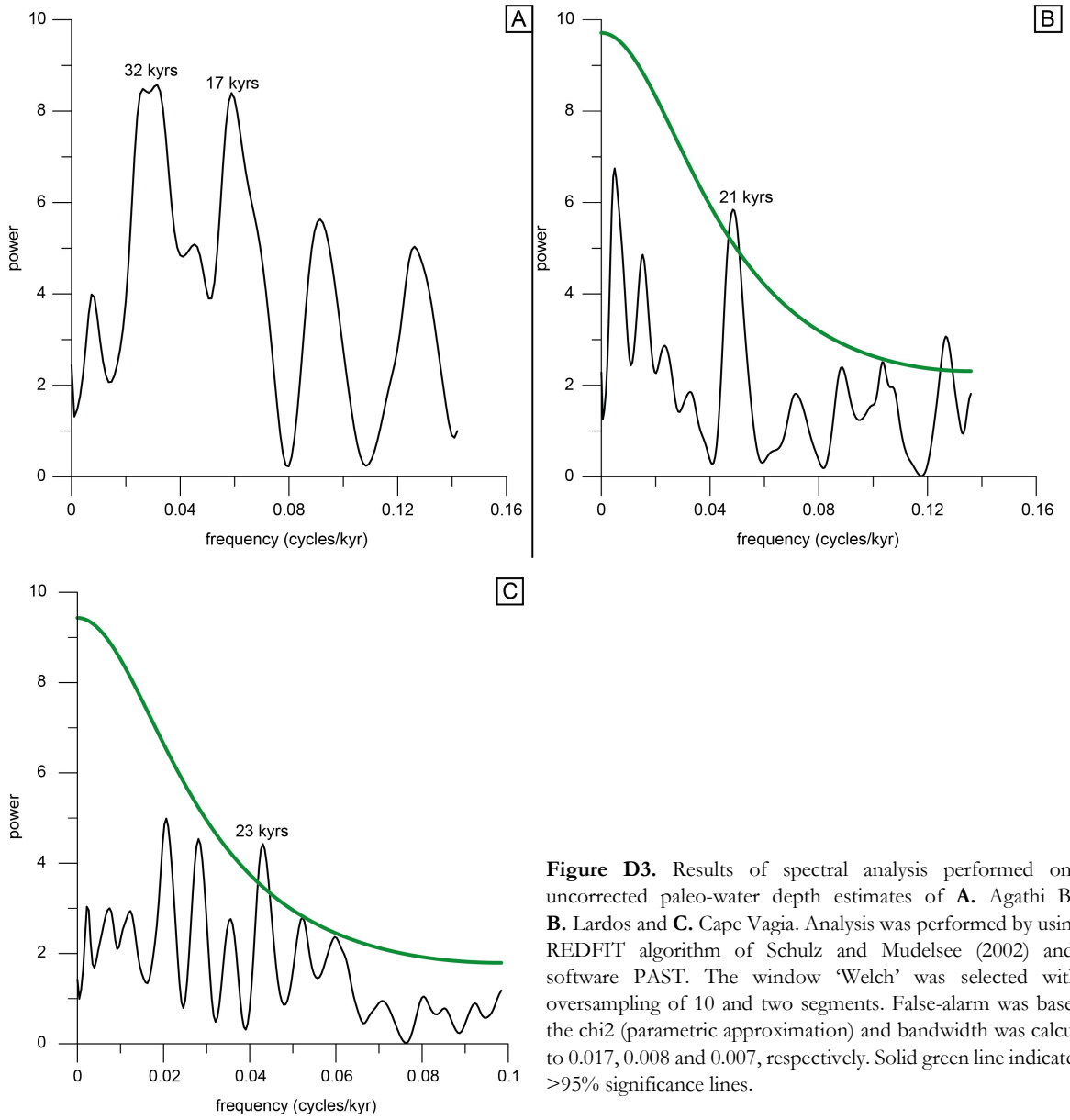

Figure D3. Results of spectral analysis performed on the uncorrected paleo-water depth estimates of **A.** Agathi Beach, **B.** Lardos and **C.** Cape Vagia. Analysis was performed by using the REDFIT algorithm of Schulz and Mudelsee (2002) and the software PAST. The window 'Welch' was selected with an oversampling of 10 and two segments. False-alarm was based on the chi2 (parametric approximation) and bandwidth was calculated to 0.017, 0.008 and 0.007, respectively. Solid green line indicates the >95% significance lines.

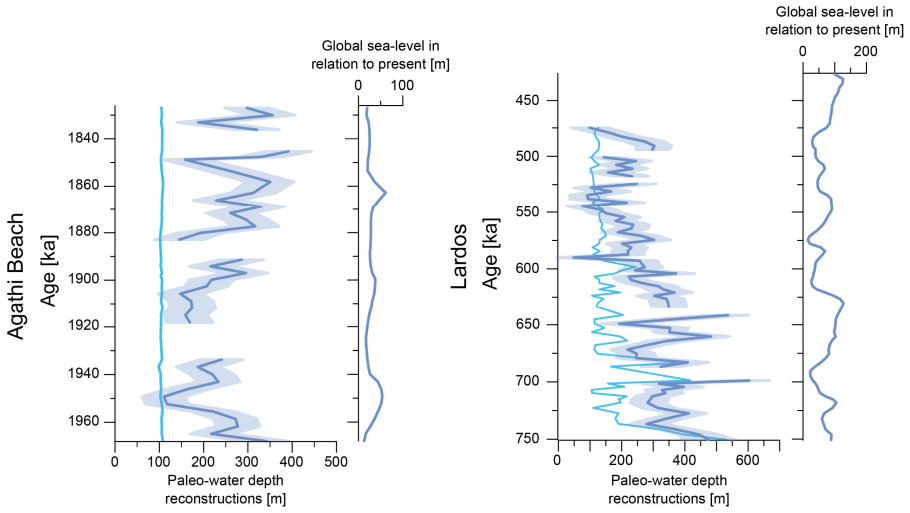

Figure D4. Comparison of paleo-water depth estimates calculated with Weighted Averaging-Partial Least Square (WA-PLS) shown in dark blue and Modern Analogue Technique (MAT), in pale blue. For reference, the global sea-level changes in relation to the present sea-level after Bintanja and van de Wal (2008) is also plotted.

Appendix E | Census counts

In Appendix E the census counts of the Cape Vagia sediment section are listed. For each sample the counts of both, the fraction >125 µm and >150 µm are listed below each other. Full census counts of the Agathi Beach, Lardos and Plimiri 5 sections are published as supplementary material in the corresponding publications.

Census counts of Agathi Beach and Lardos in:

Eichner D., Schmiedl G., Titschack J., Triantaphyllou M., Andersen N., Forster N., Milker Y., 2024. Impact of hydrological changes and vertical motions on Pleistocene marine environments of the eastern coast of the Island of Rhodes (Greece). Palaeogeography, Palaeoclimatology, Palaeoecology 636, 111980. https://doi.org/10.1016/j.palaeo.2023.111980

Census counts of Plimiri 5 section in:

Eichner D., Schmiedl G., Titschack J., Ferreira, M., Triantaphyllou M., Andersen N., Milker Y., 2024. Humid climate phases on the Island of Rhodes (Greece) during the Late Pliocene at times of sapropel formation. Marine Micropaleontology 187, 102341. https://doi.org/10.1016/j.marmicro.2024.102341

Table E1. Full census counts of the Cape Vagia sediment section.

fraction [µm]	Average depth [cm]	*Ammonia beccarii*	*Ammonia parkinsoniana*	*Ammonia* sp. 1	*Ammonia* spp.	*Asterigerinata mamilla*	*Asterigerinata* sp.1	*Asterigerinata* spp.	*Astrononion* sp.	*Astrononion stelligerum*	*Bigenerina nodosaria*	*Bolivina alata*	*Bolivina pseudoplicata*	*Bolivina subspinescens*	*Bolivina* spp.	*Bulimina aculeata*	*Bulimina gibba*	*Bulimina costata*	*Bulimina elongata*	*Bulimina marginata* s.l.	*Brizalina striatula*	*Bulimina / Globobulima* sp.	*Brizalina spathulata*	*Brizalina seminuda*	*Bolivina* cf. *antiqua*	*Caucris auriculus*	*Cassidulina carinata* s.l.	*Cassidulina obtusa*	*Cassidulina* sp.	*Cassidulinoides bradyi*	*Cibicides* cf. *locatulus*	*Cibicidoides pachyderma*	*Cibicides lobatulus*	*Cibicides pseudolobatulus*	*Cibicides refulgens*	*Cibicides variabilis*	*Cibicides* sp. 1	*Cibicides* spp.	*Cibicidoides mundulus*
125	31	6				2			6	1	1		1	3					1	3						2	44	2			6	14					1		7
150	31	3				0			4	1	1		0	1					0	2						0	28	2			6	6					0		3
125	55	7							6	1	1		1	1						6		1				6	59			1		7	17		2		1		9
150	55	2							2	0	1		0	1						3		0				5	31			0		7	12		2		0		8
125	79	1							8		2	1		2					1	40		1				1	32						5		2				9
150	79	1							3		2	0		1					1	29		0				1	16						2		1				7
125	108	3			4				1		5									28		1					16					4	7		1		3		6
150	108	0			4				1		5									20		0					8					4	6		1		0		6
125	132								5		5									26		2				1	36			4		1	4				2		16
150	132								0		3									15		1				1	17			2		1	2				0		11
125	156	5				2	2		2	1	2		4	1					3	26		5		2	1	1	59			1	1	6	18		8		1		15
150	156	2				1	1		1	1	2		0	1					2	18		0		0	1	1	40			1	1	6	15		4		0		14
125	180				1	2	2		9	3	4			2						7		16			1		67			1	2	1	11		2		9		3
150	180				0	1	0		5	1	4			1						5		2			1		36			0	2	1	7		2		2		3
125	203	1					2		3	2			2	6					3	15		7		1	2		35	1				4	11		5		7		
150	203	1					0		0	2			1	2					2	10		0		1	1		24	0				4	9		2		0		
125	223					4	1		3		2	2	1	2						1		5			1		36				1	3	18		5		5		6
150	223					0	0		0		2	0	0	1						1		1			0		18				1	3	12		3		1		2
125	243				1		1		3		1		1	2						1		7		1	3		57			2			24				6		5
150	243				0		0		1		1		0	0						1		1		0	3		43			1			15				0		4
125	263			2	3	2	1		5	4	1	1		6						5		14		1			69			1		3	15		4		1		7
150	263			0	3	2	0		3	2	1	1		2						4		4		0			46			1		3	7		4		1		4
125	283			2		1	1		1	3	1			2					1	3		14					70					1	12						10
150	283			1		0	0		0	2	1			0					1	1		5					43					1	8						8
125	303	1							3	2	1			1						3		5					56			1		1	9		1	1	2		14
150	303	0							2	1	1			0						2		2					42			0		1	9		1	1	1		12
125	323								1		3	12								8		3				1	36						7				1		18
150	323								0		3	7								6		0				1	31						1				0		13
125	348	2							5			8		1						4							56						1						19
150	348	1							1			4		0						3							42						0						13
125	373								1	1		12	1							15					1		53			3			4						16
150	373								0	1		7	0							13					1		47			0			3						10
125	393	2				1			3		3	4	1						1	23		5					41			9			4				4		15

150	393	2			0		0		3	3	0			0	17	3				37			7			4			0	12
125	413	1					3				2			2	58	14			2	41	3		3			3				17
150	413	1					2				1			1	30	6			1	19	3		0			1				15
125	433	4			1	4	1	2		5				3	19	93		4		50	2		5			8				1
150	433	2			1	0	1	0		4				1	16	54		1		35	1		2			5				1
125	453	21		19	11	33	10	2			1		5	28	20	138	12		7	165	8		1			46		4		1
150	453	13		10	7	2	2	2			1		1	20	9	76	4		5	115	7		1			32		2		1
125	473	22		1	10	15	1	5					1	13	5	100	8		1	86	6		1			35		3		1
150	473	12		0	2	0	0	2					0	5	4	80	6		1	59	5		0			22		0		1
125	493	9		13	5	5	3	5						17	15	49			2	80	2					18		4		
150	493	3		7	5	0	2	2						9	4	37			1	59	2					16		4		
125	513	12			4	1	4	1						22	13	83				19	4					20				2
150	513	8			2	0	2	1						20	9	69				11	4					15				2
125	533	2			9	1	3	3	2	1	1	1			9	9				60		15	3	2		7				9
150	533	1			4	0	2	0	2	1	0	0			6	4				37		11	1	1		5				7
125	553	1					4					1			27	35				79		6		1	1	9		1	3	9
150	553	0					2					0			18	9				39		3		0	1	8		0	0	8
125	573	2			1		9								7	12			2	38				5	1	19		6		5
150	573	1			1		7								6	3			1	22				3	1	14		4		5
125	593	3			3		3				1	1		2	3	12			2	47				7	1	22				4
150	593	1			1		1				1	0		1	3	1			2	27				4	1	18				3
125	613	2			1		2		5		5	1			2	9				33			1		6	20		3		
150	613	1			1		1		4		1	1			2	2				16			0		5	10		2		
125	633	4			2							3			5	9		1	1	18					7	22		1		5
150	633	2			2							1			3	6		0	1	12					7	9		1		5
125	653	1		1	3		5				3	1	1		7	26			1	27					1	23				3
150	653	0		0	3		1				0	0	0		6	15			1	20					1	16				2
125	673	1	1					6	3		2	1			9	16				72			2		5	10	1	1		8
150	673	1	1					3	3		0	0			7	4				43			1		5	7	1	1		5
125	693	2					33								6	5				13										1
150	693	2					20								6	4				10										1
125	713														27	42		1		165						3				
150	713														19	23		1		110						3				
125	743											1			143	33			1	227										3
150	743											1			110	8			1	169										3
125	783														36	10				162						1				
150	783														25	1				124						1				
125	803						2								24	61		6		335			3							
150	803						0								19	13		0		245			1							
125	823	2					1								31	111		1		411			1			1				
150	823	1					0								30	41		0		342			1			0				
125	843						3								44	12				254										
150	843						3								33	3				200										

125	863	1							1				1							49			61		1		414						2						
150	863	1							0				0							41			25		0		357						2						
125	883	8		12					11										12	57			131		1	1	6	1		12			2	4					6
150	883	8		8					6										9	20			40		0	1	2	0		0			2	2					5
125	903	3			5														9	21			18		1		15	10				4	9		2				
150	903	2			5														1	13			9		0		9	9				1	8		1				
125	923	2			1				6	4							4		4	26			1		5		32												
150	923	2			0				4	2							3		2	14			1		2		30												
125	943	24		6					8										26	15				3			36												
150	943	18		3					3										17	11				0			32												
125	963	5		2					2	4									18	12				2			104												
150	963	4		1					1	4									14	6				0			85												
125	983				7				1	3									37	36				13			65								1				
150	983				4				0	1									18	19				6			48								0				
125	1003	27		7					9	1									43	37				9			143												
150	1003	21		3					3	0									29	10				0			104												
125	1023	8		5					6	1									6	3			1		1		3						1						
150	1023	7		4					4	1									3	2			1		1		3						1						
125	1043	11		4					14	7	2								49	60			5		9	1	122						9		1				
150	1043	9		4					3	4	1								36	31			2		1	1	81						5		1				
125	1063	119	11	11					71	7									18	25							6												
150	1063	112	8	7					51	3									16	10							3												
125	1083	9	5							7										44					2		50						3						
150	1083	8	3							5										22					0		37						2						
125	1103	1			1												1		1	9					1		1												
150	1103	0			1												0		0	5					0		0												
125	1123	1			2							20					5			12				52			2												
150	1123	1			2							0					2			9				3			1												
125	1143				2												2			13				14	4		3	1											
150	1143				1												0			5				0	1		1	0											
125	1163				3			1									2		1	14				24	7		2	1					2				2		
150	1163				2			1									1		1	3				0	1		2	0					1				0		
125	1167	2				1				2			1						12	9				44	1	2	6						4						
150	1167	1				1				2			0						5	4				1	0	1	3						4						
125	1171	1				1											1		9	2			2	21			17	1		1			13						
150	1171	0				0											0		3	2			0	2			11	0		0			7						
125	1173				1														2					6			3	2					6						
150	1173				0														1					0			2	2					2						
125	1175																		1				1	10									4						
150	1175																		1				1	0									2						
125	1179	1			3																		186	392			9	9		1			27		3				
150	1179	0			2																		98	24			6	8		0			20		3				
125	1183				1					2		3					2			10			17	19	5		14						2		1				

150	1183		1				1		1			2			4	0	0	0		11				1	0			
125	1203				1		1		41	2		8		4	58	40				30		1		1	2			2
150	1203				0		0		23	0		7		4	45	3				26		0		0	2			2
125	1223			1			1		5			7		1	116	46				74		1		4			2	23
150	1223			0			0		3			6		0	92	4				48		1		3			0	16
125	1243		1						4			8		10	58	14				126					2			4
150	1243		0						4			6		9	41	3				89					2			4
125	1263		1						9			10		4	172	95				176		1		5	1		1	1
150	1263		1						7			7		1	128	27				118		0		1	0		0	1
125	1283						2		7	1				6	106	92				115		8		6				1
150	1283						2		7	1				6	88	37				78		6		4				1
125	1303						1		6	1				6	86	85			1	129		1		3				3
150	1303						0		5	0				5	59	34			1	86		1		2				3
125	1323			1			2	1	3	2					63	72				58		1				1		3
150	1323			1			1	1	1	0					49	19				40		1				1		3
125	1343								4	4				4	133	81				158		1		1	1			3
150	1343								3	0				4	107	23				107		0		0	0			3
125	1363	2		1			2		20					4	89	104				151		1		10				3
150	1363	1		0			1		11					2	75	26				95		1		7				3
125	1383		1	1					10						102	87				58				4				2
150	1383		0	0					10						73	29				39				4				1
125	1403	3					1		22	1					103	123				54		5		4	1			
150	1403	0					1		15	0					79	37				36		1		4	1			
125	1423														22	95				47		1		8			1	6
150	1423														14	21				33		0		6			0	4
125	1443	2		2			1								31	62		1		28				4	2			2
150	1443	1		1			0								26	17		0		17				2	2			2
125	1463						12		15	3		2	1		113	46		1		116		1		5	2			5
150	1463						8		12	1		2	1		78	11		0		69		0		4	2			5
125	1483	1		1	1	1	2		8		1		2		41	21		5	1	49	1			13	1			3
150	1483	0		0	1	1	1		7		0		2		31	8		1	0	31	1			9	1			3
125	1503		3						21	5	1		11		80	64		10	1	111		1		12	5	1	1	3
150	1503		3						17	3	1		10		59	26		0	1	74		0		7	4	1	1	2
125	1523	3				1		1		1	3	2	8		10	2		4		67				17	1			
150	1523	1				0		1		0	0	1	7		9	0		1		50				14	1			
125	1543		2	1		1		7			1		5		1	16			1	59	1	2	5	19		2	5	5
150	1543		2	1		1		6			0		2		1	6			1	37	0	0	4	16		2	1	5
125	1563			2		1		3		2	5		3		2	10		1		29			2	10	1			3
150	1563			1		1		3		1	2		2		2	5		1		20			2	6	0			1
125	1583	3			1			2		3		1	2		1	43				76		1	2	19	5			16
150	1583	2			0			2		0		1	2		1	9				36		0	2	14	4			15
125	1603	1		1				5		1			1		7	1				39				12	2			15
150	1603	0		1				4		1			1		3	1				29				6	2			12

125	1623				2				4							1		35			5				16				9		2	1		17
150	1623				1				3							1		24			0				12				5		1	1		16
125	1643					2			1									53			6		8		57	1	1		11		9			30
150	1643					0			1									43			0		0		36	0	1		8		7			24
125	1663				2				2						1			55			5		6	1	14				2					11
150	1663				1				1						1			41			1		1	1	6				2					9
125	1683				1		1		2									86			54		6	1	8				1					3
150	1683				0		1		2									75			15		2	1	4				1					1
125	1703				3				1									37			3		4		39	1	1		8		3			2
150	1703				2				1									28			2		0		27	1	0		7		2			2
125	1723				1													199			4		10		29	1		1	1		2			14
150	1723				0													182			0		2		20	1		1	1		1			11
125	1743	1			2	1	5	10		2					4			52			39		6		71	3	8	4	14					8
150	1743	0			0	0	4	0		2					3			31			8		1		56	2	2	4	9					7
125	1763	2			1			1		10					4	1		136			66	15	10	3	89		26		30		3			3
150	1763	0			0			1		9					3	1		85			21	6	2	3	53		4		24		2			2
125	1783				5			5			1				6		10	15			171	10	47		32	3	2		22		4	2		1
150	1783				1			3			0				5		6	9			81	1	10		18	3	0		20		3	2		1
125	1803	1			5	3		3			1			3	6		4	7	16		173	17	17	3	31	1	15		23		5			
150	1803	1			2	1		2			0			2	2		4	5	0		75	13	0	3	15	1	6		17		3			
125	1823	6			5	1		2			1			17	2		2	7			87				95	7	16		21		6			
150	1823	5			2	0		1			0			17	1		1	0			20				61	5	12		16		3			
125	1843	5	1	1	14			14			1				6		8	8			46			4	49	21	7	2	27		3			
150	1843	4	1	1	5			4			0				4		7	7			13			3	30	16	6	2	24		3			
125	1863	1			9			10		1	1						10	5			72	1	4	3	38	15	28			27	2			
150	1863	1			7			3		0	1						8	2			23	0	2	1	26	14	24			23	0			
125	1878	2			14			10			3				5		12	8			53		1	3	71	43	23		28		4			
150	1878	1			9			2			1				3		8	4			13		0	3	47	32	22		25		3			
125	1888	1			9			4						9			1	2			14	1	6	5	53	12	28		32		5		3	
150	1888	1			1			0						3			1	0			2	1	0	4	31	6	19		21		3		0	
125	1898	1			12			5			1	1						4			4	11	1	2	40	16	72		36		4		1	
150	1898	1			3			0			0	0						3			0	5	0	0	26	10	36		27		4		0	
125	1908				14			8				1						1		24	3	2	5	39	33	7	192		18		4		3	
150	1908				7			0				1						1		20	1	0	2	37	19	7	62		14		2		2	
125	1928		1	1	8			5			1			27		3		9			25				46	2			30		1		4	5
150	1928		1	0	5			0			0			21		3		7			8				28	2			17		0		0	5
125	1948			1	2			1				1	3	28				5			19				14	6			6		7		1	3
150	1948			0	1			0				0	1	19				5			4				9	4			3		5		1	2
125	1968			7	16			8	5		4			18		1		7			21	3			26	4	2		16	3	3		6	7
150	1968			6	4			0	5		1			9		1		5			3	1			13	2	0		12	3	1		2	4
125	1988	3	1	5	10			2	4		4	11				1		3			22				62	2		1	40	10	12		1	7
150	1988	3	1	2	2			2	4		0	0				1		0			18				35	1		1	18	7	7		0	7

continued

fraction [µm]	Average depth [cm]	*Cibicidoides pseudoungerianus*	*Cibicidoides* sp. 1	*Cibicidoides* spp.	*Chilostomella oolina*	*Discanomalina semipunctata*	*Discorbinella bertheloti*	*Hanzawaia rhodensis*	*Dentalina* sp.	*Dentalina arena*	*Dentalina guttifera*	*Ehrenbergina trigona*	*Elphidium aculeatum*	*Elphidium complanatum*	*Elphidium complanatum*	*Elphidium crispum*	*Elphidium decipiens*	*Elphidium macellum*	*Elphidium margaritaceum*	*Elphidium* sp. 1	*Elphidium* spp.	*Eponides pussilus*	*Favulina foveolata*	*Fursenkonia* sp.	*Fursenkonia complanata*	*Fissurina cataneа*	*Fissurina faba*	*Fissurina marginata*	*Fissurina orbigyana*	*Fissurina* c.f. *orbigyana*	*Fissurina staphyllearia*	*Fissurina lucida*	*Fissurina* spp.	*Frondicularia* sp.	*Gaudryina siciliana*	*Gavelinopsis praegeri*	*Globobulimina affinis*	*Globobulimina pacifica*	*Globobulimina pupoides*	*Globobulimina* sp.	*Globulina gibba*
125	31	164	7				15					3	1	4		6		4					3						2							7					
150	31	129	6				6					2	1	4		2		2					1						1							2					
125	55	207	1				20					9		2		3		1											3							18		3			
150	55	160	1				14					8		1		1		1											3							0		3			
125	79	235					21					3				6							2						2							16	2	6			
150	79	169					10					3				2							0						0							2	2	5			
125	108	149	1				12									2							3						1					2	10	4				
150	108	116	1				7									2							0						0					2	2	3				
125	132	190					24	1								2												2	1						10	28				
150	132	149					15	1								0												0	1						1	25				
125	156	108					9	1				4		1		5		2										3	2			1									
150	156	81					5	1				4		1		3		1										0	2			0									
125	180	77					15	3	2			11	1	3	3	3		3										3	6							12					
150	180	61					7	2	2			9	0	1	1	3		3										1	1							2					
125	203	75					12	2				7		1	2	2	3	3											6				1		1	19					1
150	203	57					6	1				5		0	0	0	1	2											5				0		1	2					1
125	223	128					23	1				6				5												3	1		1				13					
150	223	101					13	0				6				4												0	0		0				5					
125	243	194					15							1		4	2											1						1	16	1				
150	243	145					6							0		0	1											0						1	2	1				
125	263	146					13					1	1		3	4	1											5	5		3			3	14					
150	263	114					5					1	1		3	1	0											2	1		0			3	4					
125	283	158					13						2		4	1	2								2			1	2				2	2	14					
150	283	128					8						2		3	0	2								1			1	1				1	2	5					
125	303	84					7									1		2						1	1			1	2				1		8					
150	303	68					4									1		0						0	1			0	1				0		3					
125	323	116					8	1										1										1	4		1				12					
150	323	93					5	1										0										0	1		0				4					
125	348	97					5								2													2							9	1				
150	348	77					4								1													0							2	1				
125	373	108					8					1					1	1																		6	2				
150	373	89					5					1					1	1																		3	2				
125	393	99					9		2						1	2				1				1							1					8	4				

150	393	77			5		2					0	1			1			1				0				2	1			
125	413	28		15	11		3				1		4	4	1	2									4		7	23			
150	413	21		12	9		3				1		3	4	1	1									1		2	19			
125	433	3			1						1	1	8	7					1	1								11			
150	433	0			0						1	0	6	6					1	0								10			
125	453	18			8				4		7	7	30	22	4	16			9	7							5	1	2		
150	453	11			7				3		5	2	9	13	0	13			9	3							2	0	2		
125	473	7	6		7				3	1	6	3	22	10	17	12			8		1						7				
150	473	2	4		5				2	1	6	1	20	9	16	6			7		0						3				
125	493	10	12		3				3		10	1	2	21	8	6			6	2	4							1	1		
150	493	10	3		3				3		6	0	2	19	5	4			3	0	0							1	0		
125	513	20	2		6					1	2		3	6					6									1			
150	513	11	0		4					1	2		3	5					5									1			
125	533	94			22		3		3			1	2	7	3						1	1				1	4				
150	533	74			14		3		1			0	1	0	2						0	0				1	2				
125	553	118			22		4			1		3						2			1	1					13				1
150	553	103			11		4			1		1						0			0	0					3				0
125	573	104			12				6		3	3										2					3		1		
150	573	84			8				3		2	2										0					0		1		
125	593	119			16				5		1	3					1				5			1		1	3				1
150	593	88			13				2		1	2					1				2			0		1	1				1
125	613	122			17				2	1										2						1	7			1	
150	613	90			10				1	1										1						1	2			1	
125	633	117			17		1	1	1	1			1								1			1			5				
150	633	94			13		1	1	1	1			0								0			0			1				
125	653	130			14		1		2	2	2				1					3	1			2			1	1			
150	653	103			6		1		2	1	2				1					0	1			0			0	0			
125	673	180			10	1			4			2	1		1	1				2				3			2				1
150	673	137			5	0			3			1	1		0	1				1				0			0				0
125	693	8											3	45	11	4															
150	693	8											2	33	5	4															
125	713												2						1												
150	713												1						0												
125	743	13				2			1																		3				
150	743	9				0			1																		1				
125	783	3			1										1												1				
150	783	3			1										1												1				
125	803																		1												
150	803																		0												
125	823													2					1												
150	823													1					0												
125	843	1												3													1				
150	843	0												1													1				

125	863	1				1																
150	863	0				1																
125	883		2	6	1				1	2	3	3			1	5			1	7	5	
150	883		2	1	1				1	2	1	2			1	3			0	7	4	
125	903	4		4			1		2	5	8					2		1				
150	903	2		1			1		1	3	1					2		0				
125	923	1							1		7					1						
150	923	0							0		4					1						
125	943										8	1			1	1						
150	943										4	0			1	1						
125	963	1										1			11							
150	963	0										1			8							
125	983										4				1							
150	983										2				1							
125	1003							1			10		1		10							
150	1003							1			6		0		8							
125	1023										1				1							
150	1023										0				0							
125	1043	9		5		1			1		2		1	1	13				1			
150	1043	4		2		1			1		1		1	1	9				0			
125	1063										35				7							
150	1063										33				5							
125	1083	2							3			2			13				1			
150	1083	0							1			2			8				0			
125	1103	1										3			1							
150	1103	0										1			0							
125	1123									1		4			6							
150	1123									0		0			4							
125	1143										3	3			6							
150	1143										1	2			2							
125	1163									1	5	3			18							
150	1163									0	4	2			14							
125	1167			1				2	2	2	3	1			9							
150	1167			1				1	2	0	1	1			6							
125	1171	2		2		1		8	7	7	12				4			1				
150	1171	2		2		1		7	1	1	3				1			0				
125	1173							3			4	1										
150	1173							2			1	0										
125	1175									2	2											
150	1175									1	1											
125	1179					1	1	3	1		10	3					1			1		
150	1179					1	0	3	1		4	2					1			0		
125	1183	5							1	2		1				2	1		3	46		86

150	1183	5										0	0		1							2	0								1	46		82	
125	1203	38				3					3			3	3							27	2								5	32	14	3	
150	1203	27				2					2			1	1							16	0								3	28	11	3	
125	1223	67				22		1	1		5				1							7	1								14	1	12		
150	1223	54				16		1	1		3				1							4	0								6	0	11		
125	1243	24				4				2																		1			18		15		
150	1243	17				2				1																		0			7		14		
125	1263	34				3							1										2	3			1	1			27	2	15		
150	1263	32				3							1										0	1			1	0			11	2	14		
125	1283	67				9																		3				1			37	6	13		
150	1283	57				9																		0				1			20	4	12		
125	1303	65				5						1			1									4				2			41		6		
150	1303	55				4						1			1									0				0			23		5		
125	1323	37				9				1	1				1										2			3			65				
150	1323	35				6				1	1				1										1			2			27				
125	1343	65				3					2	1	1	1					1												72		2		1
150	1343	58				2					2	0	1	1					0												36		2		1
125	1363	94								2		2	3						2								1				5		7		
150	1363	83								2		0	3						2								0				2		7		
125	1383	90			1	2									1									1	1					1	5		4	2	
150	1383	78			1	1									0									1	0					1	0		3	1	
125	1403	110	2							1	3			2										2	1					3	5	6	17		
150	1403	84	1							1	2			0										0	1					3	1	6	15		
125	1423	175				7	1			1	4			3	1					1											9		5		
150	1423	146				5	0			1	4			0	1					0											3		4		
125	1443	235				5				1	1			1		1									1						12		2		
150	1443	193				3				1	1			0		0									0						6		2		
125	1463	88				8	2						1	4	1				1					2		1					24		20		
150	1463	72				4	1						1	4	1				1					0		1					9		19		
125	1483	84	3			4		5			2	1	1	1										1	1				3	1	15	3	3		
150	1483	69	1			3		4			2	1	0	1										0	1				3	1	3	2	2		
125	1503	47	2		4	15	2	10			1	6	3	2					2						1	1			2		14		5		1
150	1503	36	2		3	8	2	8			1	2	2	1					1						1	1			2		4		3		1
125	1523	59	1			8	2	17			4			1										1	1					3	11		1		
150	1523	48	1			7	2	16			1			1										0	1					2	6		1		
125	1543	103				28		21			6			1						1					3					3	6				
150	1543	78				17		13			5			0						0					2					3	2				
125	1563	71	8			13		15		1	8							1													3				
150	1563	52	8			6		9		0	7							0													1				
125	1583	182		1		19		15		2	3														3						13		2		
150	1583	146		1		11		12		2	0														3						1		1		
125	1603	122				9	1	7		2	2						1		1												5	4	1		
150	1603	98				8	1	5		1	1						1		0												2	4	1		

125	1623	130				8			1		1										1		2	1				8	4				
150	1623	100				4			0		1										1		1	1				1	4				
125	1643	224				17			4				1										2	2		2		13	9	7			
150	1643	190				13			3				1										0	2		0		6	6	7			
125	1663	158				4				2													1					8	5	17	7		
150	1663	141				1				2													1					2	5	14	1		
125	1683	101							1	1	1												1					5	7	29	4		
150	1683	88							1	0	0												0					1	7	28	0		
125	1703	69				9			6		1		1										4					9	7	4	2		
150	1703	60				3			6		1		0										3					5	7	4	0		
125	1723	164	1			5			1		1							1					1				1	24	11	17			
150	1723	141	0			4			1		1							1					0				1	9	11	15			
125	1743	169				17	1		6		3									1	1		3					18	7		4		
150	1743	126				9	0		3		1									1	1		1					5	7		1		
125	1763	54	2	3		12	1		6						2						3		1					2	34		29		
150	1763	34	0	3		11	1		5						2						2		1					1	34		27		
125	1783	11	4			6			2	1	7		3		1			2		2	1								11		6		
150	1783	10	4			5			2	1	6		2		0			1		0	0								9		6		
125	1803	2	12			7	2			1	17		2	2	2								3	1				3	98		39		
150	1803	1	8			4	1			0	10		1	0	1								0	1				2	90		31		
125	1823	5	12			7			4		12		3	2	3													3					
150	1823	3	8			6			4		8		3	2	3													2					
125	1843	4	8			8			1		14		2	8	3						6		3	3				1			1		
150	1843	3	3			6			0		10		4	5	2						4		0	1				0			0		
125	1863	1	20			6			2		11			7	6						1			3									
150	1863	0	15			3			1		6			5	4						0			1									
125	1878	6	11			6			2		12	4			7																		
150	1878	4	2			3			2		3	0			7																		
125	1888	10	15			6			5	3	32	9	2	10	8								2						6		10		
150	1888	10	6			6			4	2	20	5	2	2	8								0						6		8		
125	1898	5	15			17	1		1		20	1	4		18							1		2							1		
150	1898	3	12			11	1		1		13	1	1		16							1		0							1		
125	1908	2				6					4		8		5	1								4				1		3	1	2	2
150	1908	0				4					0		2		5	1								3				0		3	0	2	2
125	1928	99	5			30			16			6		1	4				5			1		1				12					
150	1928	75	5			10			12			3		0	4				5			1		1				6					
125	1948	71				19			10			2			2		5		2	1								2	2	2			
150	1948	57				8			6			0			2		4		2	0								0	2	2			
125	1968	72	12			28			20			12		1	2				9	1			1		1			10		2			
150	1968	49	7			14			17			8		0	1				9	0			0		1			5		2			
125	1988	112	18		2	39		1	46			23	1	8	1		10		14	1				2		2	4	12					
150	1988	70	10		2	25		0	36			17	1	0	1		5		13	1				1		2	4	4					

continued

fraction [µm]	Average depth [cm]	*Globobulimina myrsidiformis*	*Globocassidulina subglobosa*	*Globocassidulina oblonga*	*Gyroidina* spp.	*Guttulina communis*	*Guttulina lactea*	*Hoeglandina elegans*	*Haynesina* sp. 1	*Haynesina* sp.	*Haynesina depressula*	*Haynesina simplex*	*Homalohedra acuticosta*	*Karreriella bradyi*	*Lagena* spp.	*Lagena ampulla-distoma*	*Lagena laevis*	*Lagena sulcata*	*Lagena striata*	*Lagena stromosa*	*Lenticulina calcar*	*Lenticulina gibba*	*Lenticulina orbicularis*	*Lenticulina* (juvenile)	*Marginulina costata*	*Martinottiella communis*	*Melonis barleeanum*	*Neoconorbina terquemi*	*Nonion fabum*	*Nonionella atlantica*	*Nonionella turgida*	*Oridorsalis umbonatus*	*Orthomorphina ambigua*	*Orthomorphina perversa*	*Orthomorphia* sp.	*Oolina globosa*	*Oolina hexagona*	*Parabrizalina porreata*	*Parafissurina* c.f. *felsinea*	*Parafissurina* sp.
125	31		37		14						2	1			1								1	1		35	19				5							
150	31		23		11						2	0			1								0	1		27	12				3							
125	55		33		16			4													2						30	16				3	1						
150	55		26		12			4													2						18	8				2	0						
125	79		34		17			8													2		1		1		25	16				8							
150	79		7		9			8													2		1		1		15	6				7							
125	108		13		17			4																			23	12				13			1				
150	108		6		15			4																			17	9				11			0				
125	132		17		19																						10	2				15				1			
150	132		4		12																						9	1				10				0			
125	156		38		17			8			4	4							2			1	3				7	13				11			1				
150	156		27		8			8			1	2							2			0	1				5	7				6			1				
125	180		38		18						4								1	1			1				9	20	1			2			3	3			
150	180		22		11						0								1	1			1				6	11	0			2			1	0			
125	203		40		10						5											1					12	23				2			1				
150	203		18		8						2											0					7	13				2			0				
125	223		34		20			2			6																28	16				10							
150	223		14		14			2			2																23	9				8							
125	243		25		17						4	2									1						17	31	2			6				1			
150	243		7		10						4	0									1						8	17	0			4				1			
125	263		15		13			3				1											1				11	14				19							
150	263		6		10			3				0											0				7	7				12							
125	283		27		14						2						1										7	7				10				1			
150	283		18		11						2						0										4	3				6				1			
125	303		25		13						2	4					1										4	8				3	1			2			
150	303		13		11						1	1					0										3	4				3	0			2			
125	323		34		11						3																3	8				7							
150	323		17		6						1																3	8				6							
125	348		14		7						4	1					1										9	4				8							
150	348		10		6						2	0					0										6	4				6							
125	373		2		9						2	3					2										6	3	1			5							
150	373		1		8						2	0					1										4	2	1			5							
125	393		17		8						1	5					1			2							4	4				3							
150	393		9		7						0	2					0			1							4	4				2							

125	413	8	42		3	6	3			1	5		1				13	3		8	3			1			
150	413	4	35		1	1	0			1	2		1				8	0		3	3			1			
125	433		3			6	4			1							7			1					1		
150	433		2			3	3			1							5			0					1		
125	453	14	6			47	42						1			3	24	14	3	22	1				4		
150	453	5	3			27	17						0			1	13	7	2	9	0				0		
125	473	9	3			31	22									4	23	7		8					1		
150	473	4	1			14	11									1	11	2		7					0		
125	493	12	2			32	29	2								1	20	2		13	1				8		
150	493	8	1			17	15	1								0	14	1		10	1				4		
125	513	4	0			9	6	1								4	4	3							1		
150	513	2	0			5	6	0								0	4	0							1		
125	533	27	8			4	4					2		1		19	30	1			7	1					1
150	533	15	6			3	1					2		0		16	13	0			6	1					1
125	553	22	24		1	2						1	1	4		24	9				2	1	1		2		1
150	553	11	13		1	0						1	1	4		17	6				2	1	1		2		0
125	573	44	13		2	2						3		1		25	18				6						
150	573	32	11		2	0						3		1		21	13				5						
125	593	28	18			4		3				2		1		31	21	2			7						
150	593	21	14			1		1				2		1		23	9	1			7						
125	613	26	22	1	1	3	1		1		1	2				15	20	4		1	6						
150	613	12	14	1	1	1	0		1		0	1				11	9	1		0	5						
125	633	24	24				3									7	14				4	1					
150	633	16	13				2									4	10				4	1					
125	653	37	28			1	6					2				3	8				3				2		
150	653	27	19			1	1					2				1	7				2				1		
125	673	34	28			5	2							1	2	9	10			2	7	1					
150	673	18	20			2	1							1	2	7	1			1	5	1					
125	693		0			42	56													1							
150	693		0			36	50													0							
125	713	1	0						1								1				1						
150	713	0	0						0								0				1						
125	743		1													4					4						
150	743		1													1					3						
125	783		0			2							1	1		2											
150	783		0			1							1	1		2											
125	803	1	0			2	2																				
150	803	0	0			0	1																				
125	823		0			1																				1	
150	823		0			0																				0	
125	843		0										1														
150	843		0										0														
125	863		1				1																				

150	863		1		1																		
125	883	1	13	14	10					1	2	6	1			3			6	1			1
150	883	0	10	8	8					1	0	6	1			3			5	0			1
125	903	2	4	3		1								1	2		2	4					
150	903	1	4	0		0								1	1		0	3					
125	923		0	10	3									1									
150	923		0	3	2									0									
125	943		0	23	14																		
150	943		0	13	7																		
125	963		0	15	5										2								
150	963		0	7	1										1								
125	983		1	9	11																		
150	983		1	4	6																		
125	1003	1	0	15	8																		
150	1003	1	0	4	4																		
125	1023		0	7																			
150	1023		0	4																			
125	1043	2	6	6	4				1			1			2			3					
150	1043	1	6	1	3				0			1			1			2					
125	1063	1	0	20	10									5		1			1				
150	1063	0	0	10	9									2		0			1				
125	1083		0	8										7	4			1					1
150	1083		0	2										4	2			1					0
125	1103		1							1													
150	1103		0							1													
125	1123		0	2										2									5
150	1123		0	0										1									0
125	1143		0											1	2			1					
150	1143		0											1	1			0					
125	1163	3	0	7										1	3	1		1					1
150	1163	1	0	0										1	2	1		0					0
125	1167	1	0	12											1	2		6					
150	1167	0	0	5											1	2		4					
125	1171	6	0	10										1	3	4		7				2	
150	1171	2	0	2										0	1	2		1				1	
125	1173		0	1																			
150	1173		0	0																			
125	1175		0																				
150	1175		0																				
125	1179		168	6			2	1						1	4			2					36
150	1179		153	2			0	0						0	2			0					20
125	1183		51	3				3							3			1			1		98
150	1183		42	0				0							3			0			1		49

125	1203				3		3							1		1	3		5				8						
150	1203				1		3							0		0	3		2				7						
125	1223				5								1				4	2	3				9				7		1
150	1223				2								0				3	1	1				6				6		1
125	1243				1		1									1	1	1	1				3						
150	1243				0		1									0	1	1	1				2						
125	1263				4	1	1			1			1			1	1	9	1	1			8		2		1	2	
150	1263				3	1	1			0			1			0	0	6	1	1			5		2		1	2	
125	1283		1		10		7						3		1	1	2	5	6				10				1		
150	1283		0		8		6						1		1	0	1	2	5				9				0		
125	1303		3		10					1		1	1			1	3	5	2				5		5			1	
150	1303		2		6					0		0	0			1	3	3	2				4		1			1	
125	1323		1		9		1						3					2	3				9	1			4		
150	1323		1		7		1						2					2	3				7	0			2		
125	1343			4	1		1			2		1						8	6			1	10		1		4		
150	1343			1	0		1			1		1						6	3			0	6		1		3		
125	1363		2		6		1			2				7			1	9	4				7		2		4		
150	1363		0		4		1			1				4			1	4	3				5		2		3		
125	1383		4		21		1							9		1		10	2				8				7		
150	1383		0		16		1							7		0		6	0				8				5		
125	1403		3		13		1									3		1	4			1	3				4	1	
150	1403		1		12		1									2		1	4			0	1				4	1	
125	1423	1	3		4									1				5	8		1		4				3		
150	1423	0	2		4									1				3	2		0		4				3		
125	1443				0												1	3	4				3				3		
150	1443				0												1	2	2				0				2		
125	1463		5		2					1						1		5	1			1	4				4		
150	1463		0		0					0						1		3	1			0	1				3		
125	1483		14		3				1	1							1	6	5				1						
150	1483		8		1				1	0							1	3	3				1						
125	1503		56		25		2	4			1			1		1		17	25	1			2			1			
150	1503		36		19		2	0			1			1		0		7	16	0			1			0			
125	1523		38		9											1		16	10				1						
150	1523		24		6											0		11	9				1						
125	1543		28		15		2											33	7				4			1			
150	1543		10		12		2											20	5				4			0			
125	1563		17		4					1						1		10	14				5						
150	1563		8		1					1						0		3	7				2						
125	1583		33		20					2						2	3	27	13				15					3	
150	1583		12		13					1						1	2	14	7				9					1	
125	1603		31		20					1								25	10				13						
150	1603		20		13					1								13	4				7						
125	1623		16		8					1						1		20	5				11						

150	1623		9		5						0											1					15	3				9					
125	1643		6		12						1										1	1	1				30	13				16					
150	1643		3		11						0										1	1	1				20	7				9					
125	1663		4		9																						22	4				6					
150	1663		2		6																						18	3				4					
125	1683				3																						29	5				3					
150	1683				2																						17	2				2					
125	1703		4		2						1											1					26	12				9					
150	1703		1		1						0											1					20	8				6					
125	1723		2		23						1											4	1				8	4				9					
150	1723		1		17						0											3	1				6	2				8					
125	1743		17		60																1	1					3	13	4		2	19					
150	1743		4		37																1	1					1	5	3		1	13					
125	1763		12		49						2												4				6	8	6		6	18					
150	1763		4		36						2												4				6	4	2		2	12					
125	1783		4		24						3											3					5	12	3		10						
150	1783		2		19						3											3					2	7	2		7						
125	1803		10		18						9																	9	6		4	1					
150	1803		6		12						3																	7	3		1	1					
125	1823		32		17					1	7				2					1							2	9	6		2						
150	1823		25		13					1	2				0					1							0	6	1		1						
125	1843		10		26	1				1							1	1									5	21	3								2
150	1843		7		18	0				1							0	0									1	16	2								1
125	1863		40		10								1							1								25	2	1							
150	1863		21		7								1							1								11	2	1							
125	1878	1	24		6	2											1										1	22	1	2		1				1	3
150	1878	1	17		4	2											1										0	13	1	0		0				1	2
125	1888		26		9								1														2	29	5			2				1	1
150	1888		19		5								0														1	14	1			1				0	0
125	1898		39		11																	1					4	25			3					1	
150	1898		29		9																	1					3	15			1					1	
125	1908		27		66										1					2		2					1	9	1		1	2					1
150	1908		4		48										0					1		2					0	4	1		1	0					0
125	1928		34		10			2													2		2				19	31	4			8					
150	1928		13		8			2													2		2				6	18	1			4					
125	1948		20		13				4														2				21	15	1			11					
150	1948		10		12				1														2				12	8	1			6					
125	1968		30		8			1														1					29	50		1		8					
150	1968		18		7			0														1					17	36		0		7					
125	1988		50	2	17			3													1					2	34	91	4			11					1
150	1988		25	1	10			2													1					2	18	56	3			5					0

continued

fraction [µm]	Average depth [cm]	*Planorbulina mediterranensis*	*Planulina ariminensis*	*Planulinoides* sp.	*Pullenia bulloides*	*Pullenia quadriloba*	*Pullenia quinqueloba*	*Pyrgo anomala*	*Rosalina anomala*	*Rosalina bradyi*	*Rosalina* sp. 1	*Rosalina* sp. 2	*Rosalina* spp.	*Rectuvigerina bononiensis*	*Reussella spinulosa*	*Reussella* sp. 1	*Saracenaria altiformis*	*Stainforthia fusiformis*	*Siphonina reticulata*	*Siphonina* sp. 1	*Sigmoilopsis* sp.1	*Sigmoilinita distorta*	*Sigmoilinita tennis*	*Sigmoilopsis schlumbergeri*	*Sigmomorphina terquemiana*	*Sphaeroidina bulloides*	*Sphaeroidina* sp. 2	*Spiroloculina tenuiseptata*	*Spirotextularia concava*	*Spiroplectinella sagittula*	*Spirosigmoilinita* sp. 1	*Spirosigmoilinita tenuis*	*Stilostomella lepidula*	*Textularia agglutians*	*Textularia calcar*	*Textularia gramen*	*Triloculina* sp.	*Trifarina angulosa*	*Trifarina fornasinii*
125	31	2	3	5	1			2	10					0	2		2		1			2	8	6		9		3	1	4	3			3		9	8	7	1
150	31	2	3	3	0			1	7					0	2		0		1			0	8	4		5		3	0	4	0			3		8	4	3	1
125	55		2	5	5	1		1	11					0					3			1	3	14		19		3	4	10				2	2	3	6	7	2
150	55		1	1	3	0		1	4					0					3			1	0	13		18		1	3	5				2	2	2	5	2	2
125	79	4	4	13	6	2			4					0							2		4	5		23		7	1	16				1	1		4	2	
150	79	4	4	6	4	2			2					0							2		0	5		21		5	1	12				1	0		3	0	
125	108		6		7				2					0	1		6						2	14		30				12			1	2		10		3	
150	108		5		6				0					0	1		3						2	13		27				12			1	2		10		0	
125	132		3	7	3	3			2					0									1	17		48				4				1	1			1	
150	132		3	6	3	3			1					0									0	11		42				3				1	1			0	
125	156	1	9	1			1		8			1		0	7	3			1					1		29		1		11		1		9		3		5	
150	156	1	9	0			1		6			0		0	5	2			1					1		24		1		8		1		9		2		1	
125	180		6	3		2			3	5		1		0	1	1			2				3	4		17			1	6				6	4	1		6	
150	180		5	1		1			1	5		1		0	1	0			1				1	2		13			1	4				6	3	1		0	
125	203	1	10	3	3	2	3			4		3		0	2	2					1	3	1	4		25		2	8	8				2	3	7		5	
150	203	1	10	1	3	1	1			0		1		0	1	1					1	1	1	3		22		1	5	6				2	3	7		1	
125	223	3	12	20	2	5			7	9				1	1	6			1				6	6		26		2	2	14				6	1	20		11	
150	223	3	12	14	2	2			3	5				1	1	3			1				2	6		19		1	2	14				6	0	20		2	
125	243		2	13	2		5			7		1		1	5	6			1			5	6	3		19			5	11			1	5	1	15		12	
150	243		2	17	2		1			5		1		1	1	2			1			2	4	2		13			4	8			0	5	1	12		0	
125	263	1	3	14	3	8				11				0	2	5			1			3	1	4		17		2	3	11				2		4		31	
150	263	1	3	11	3	2				8				0	1	3			1			0	0	4		14		1	3	8				2		3		5	
125	283	1	7	19	2	1	1							3	4								3	1		30			1	5				2		3		3	
150	283	1	7	17	1	1	1							0	2								2	1		25			1	5				2		2		0	
125	303		4	18		3				3				3	3				1			2				34				5		1	1	2		2			
150	303		4	13		1				3				3	1				0			0				30				1		0	0	2		1			
125	323	1	13	12	1	3				4		1		0									1			34				4								4	
150	323	1	13	7	1	3				4		0		0									0			30				4								0	
125	348	1	9	20	3	1				3				0	5									1		54				12						1		1	
150	348	1	9	12	3	1				3				0	4									1		50				9						1		0	
125	373	2	3	14		2				1				0	1											50				8									
150	373	2	3	10		2				1				0	1											45				8									
125	393		11	15										6	2								3	1		48				10								1	

150	393		11	10										5	2								1	1		40				10								0	
125	413	1	1	2	4		2			2				27				25								16			1	3									
150	413	1	1	1	0		2			0				24				5								13			1	2									
125	433				5		1			6				8	2			1					1			3				1								2	
150	433				4		1			3				7	1			1					0			2				1								0	
125	453	2	4	2		1				19				4	2	4		1								6			2	14		7				1		7	
150	453	2	4	1		1				10				3	0	2		1								5			0	10		3				1		0	
125	473		1			2				16				0	3				1				7					1		5						1		14	
150	473		1			1				7				0	3				1				6					1		3						1		2	
125	493		1	3	1					6				1		1							2						1	2								9	
150	493		1	2	0					1				1		1							1						0	2								0	
125	513			4						2				0	1															3		2						25	
150	513			3						1				0	1															2		2						14	
125	533		6	4	3					3				0	4									2		26				13		2	1	1		3		7	6
150	533		6	3	2					1				0	4									1		22				12		1	1	1		3		2	6
125	553		1	14	8	2	1			3				0		2			2					9		36				2				5		4		3	
150	553		1	9	6	1	1			1				0		2			2					8		34				1				5		4		0	
125	573		3	9	1	1	1			6		2		0	1									3		21			1	2				3	1	2		10	
150	573		3	5	1	1	1			6		1		0	1									1		19			1	2				3	1	2		4	
125	593		4	8	5					8		3		0		1			4				4			11					1					2		3	
150	593		4	6	2					4		2		0		1			2				3			10					1					2		1	
125	613	5	4	10	7	1				9		2		0	4	2							6	2		13		2		12	1			3		4		9	
150	613	4	4	6	5	1				3		2		0	2	2							4	2		9		1		7	0			3		2		0	
125	633	3	7	2	2							2		0	2	4			1			2		2		29			2									9	
150	633	1	7	2	2							2		0	0	2			1			2		1		23			2									1	
125	653		3	10	6	7				3			1	0	2	3			2							29			1	1				1				3	
150	653		3	8	6	7				2			1	0	0	2			2							24			1	1				1				0	
125	673	1	10		11	4	2							1					2			2				56									1			17	
150	673	1	10		7	1	0							1					2			1				48									1			0	
125	693											1		0	2				1							2													
150	693											1		0	1				0							2													
125	713													0	1																							2	
150	713													0	1																							0	
125	743												3	0	1											14													
150	743												0	0	1											13													
125	783													0				1								3													
150	783													0				1								3													
125	803													0	2																								
150	803													0	2																								
125	823													0	1																							2	
150	823													0	0																							1	
125	843													0	1																								
150	843													0	1																								

125	863													0																									2
150	863													0																									0
125	883				6									1	3			1								3												3
150	883				4									1	2			0								3												0
125	903					2	2							0	2			1																				8
150	903					2	2							0	1			1																				2
125	923													0	1			1																				
150	923													0	0			1																				
125	943													0	5																							
150	943													0	2																							
125	963													0	3																							
150	963													0	2																							
125	983													0	3																							
150	983													0	1																							
125	1003													0	5																							
150	1003													0	5																							
125	1023													0	8																							
150	1023													0	3																							
125	1043	1		1	2							1		0	4			1				1				3			2	3								2
150	1043	1		1	2							1		0	3			1				1				1			2	1								0
125	1063				2									0	20											2												
150	1063				1									0	13											2												
125	1083				1		1							0	6	1																						
150	1083				1		1							0	5	1																						
125	1103													0												3												1
150	1103													0												2												0
125	1123													0																								
150	1123													0																								
125	1143													0																								
150	1143													0																								
125	1163													0	1																							
150	1163													0	1																							
125	1167													0	3	1		3																				
150	1167													0	2	1		1																				
125	1171													0		3								1														1
150	1171													0		3								1														0
125	1173													0		1																						
150	1173													0		1																						
125	1175		1											0		1																						
150	1175		1											0		1																						
125	1179									4				0	1											1				1								
150	1179									0				0	1											0				1								
125	1183									1				0	2							1				1												

150	1183									0		0	2						0			1												
125	1203		3	1						2		0	2	1					2	1		14				8					1			
150	1203		3	1						2		0	2	1					0	1		12				6					1			
125	1223		27	1	1				1			0	2			2			3	1	2	31				28					2		6	
150	1223		24	0	1				0			0	1			0			0	0	1	29				17					2		0	
125	1243		5	5						9		0							1		3	14				10								
150	1243		5	3						7		0							0		3	12				8								
125	1263	1	7		7	2				3		0							5		1	11				14						2	1	
150	1263	1	7		7	2				2		0							3		1	11				12						0	0	
125	1283		8	2						2		0							9	1		12			3	20						1	4	
150	1283		6	2						2		0							6	1		10			2	15						1	0	
125	1303		2	2	2			2				3	1	2					4		1	12				10							5	
150	1303		1	1	2			1				1	1	0					4		1	11				8							1	
125	1323		10	2	1							2							2		1	8			2	28					2		1	
150	1323		10	1	1							1							0		1	6			2	19					2		1	
125	1343		10		1		2	1		3		0	4	2							7	11			1	19						1	13	
150	1343		10		1		2	1		2		0	4	1							5	11			1	17						1	5	
125	1363	1	3	3	2			1		1		0									5	21			2	12							8	
150	1363	1	3	0	0			1		1		0									4	18			2	7							1	
125	1383		4		1	1				1		0				1						27				3							5	
150	1383		2		1	0				0		0				0						23				2							1	
125	1403	1	3	3	5					7		0	3			4						33			1	10								
150	1403	1	2	2	4					1		0	2			2						31			0	9								
125	1423	3	15	10		1		1		6		0	2	1							1	19			1	4				1			21	
150	1423	2	13	5		1		1		2		0	2	1							1	17			1	3				1			4	
125	1443		9	13				2		1		0	3	1							1	12			2	1					1		18	
150	1443		9	8				2		0		0	3	1							1	12			2	1					1		6	
125	1463		4	1	1	1	1			7		0	1	1		2				3		9		1	1		1			2			5	
150	1463		3	1	0	1	1			3		0	1	1		0				0		8		1	0		1			2			2	
125	1483			2	2	1				1		0	2				1	2			2	9			3	2	1			1			6	
150	1483			2	1	1				0		0	1				1	1			1	8			3	1	0			0			1	
125	1503	1	2	1	9	1			1	7	1	0	4	9	1	1		3		1	4	28	2	1	1	14		3	3				6	
150	1503	0	2	1	6	1			1	3	1	0	3	3	0	1		2		1	3	27	2	1	0	11		0	3				1	
125	1523		4	5	3		1	3	3	7		0		5							3	16		1	2	22		4	4	6	2		8	
150	1523		4	5	2		0	3	1	4		0		3							1	15		1	1	18		0	4	0	2		0	
125	1543	5	4	7	2	2	3	1		14		0	8	8			2		2	1	11	22		6		18		2	3		4		12	1
150	1543	4	4	5	2	0	3	1		4		0	5	4			2		2	0	8	18		3		16		0	3		0		1	1
125	1563	4	9				2		4			0	2	4						1	2	20		1		16		1	4		11		3	
150	1563	2	6				1		2			0	1	2						1	2	11		1		8		0	4		9		0	
125	1583	9		8	4	3	2		11			0	5	8							13	19		3		31	8		14	17			11	
150	1583	9		6	2	3	1		4			0	3	4							10	15		3		22	4		11	13			0	
125	1603	2	1	5	4	4	3		4			0					1			3	9	27		1		16		2	2		4		10	
150	1603	2	1	4	2	3	3		1			0					0			2	7	23		1		10		1	2		4		0	

125	1623	3	4	5	2				5				0		2				1		1	7		18	1		8				5		1	
150	1623	3	4	3	1				3				0		0				1		0	3		17	1		5				3		0	
125	1643	1	8	8	4	4	1		3				0	1	2							16		25	6		12	1	1		9		1	
150	1643	1	8	6	3	3	0		2				0	1	0							10		19	5		12	0	0		7		0	
125	1663				1	2			2				0								1	7		10	1		9		1	1				
150	1663				1	2			1				0								0	6		7	0		6		1	1				
125	1683	1	1	1	7	2							0	1	3							7		16			5						2	
150	1683	0	1	1	4	2							0	1	1							6		16			5						0	
125	1703	4		4	2	7			2	2			0	1	4									38			7		1		1		4	
150	1703	4		3	1	5			2	1			0	0	2									31			4		1		1		0	
125	1723	3	4	7	11	3	1		2				0					1				14		43			41			1	3		1	2
150	1723	3	4	5	9	3	0		1				0					1				12		39			32			1	2		1	2
125	1743	1	2		6	1	1			11			0		5		2	3			1	3		68		6	16		5		7		9	
150	1743	1	2		4	1	1			6			0		5		1	3			0	2		61		3	13		3		5		2	
125	1763	1	2	1	8		3		1	1			0	1	2		14							53				1	3	5	4		10	
150	1763	1	2	0	7		2		1	1			0	0	1		0							44				0	0	5	1		0	
125	1783		2				2				1		0		1		5				1			9						4			2	
150	1783		2				2				1		0		1		0				0			6						2			1	
125	1803				4	1	3			4		1	0		5		42											1			2		9	
150	1803				3	1	2			2		1	0		4		5											0			1		0	
125	1823	1	4		3	2	13			2		2	0		2						1			7			12				3		27	
150	1823	1	4		3	1	11			0		2	0		0						0			6			9				2		8	
125	1843	2	1		3		9			5			0		4					1	2			6			3				6		21	
150	1843	1	1		3		5			3			0		4					0	0			5			2				5		7	
125	1863				3		4			7			0		2					2	1	1		6			11				3		23	
150	1863				2		2			5			0		0					0	0	1		6			9				1		5	
125	1878	2			7	1	7			7			0	5	1		1					1	1	2			12				2		17	
150	1878	2			5	0	6			7			0	3			0					0	1	2			8				2		3	
125	1888	1	1	5	2	4	1			4			0	5			1							8							1		6	
150	1888	1	1	2	1	3	1			2			0	5			0							3							1		1	
125	1898				10		3			4			1		2									1							2		3	
150	1898				6		1			2			1		2									1							0		0	
125	1908	1			1	5	5			1			0	1							1		1	6	1						5		6	
150	1908	0			1	2	3			0			0	1							0		1	6	0						0		2	
125	1928	2	2	1	7	2			1	5			0	8	6			1		1		5		10	2	2	2	6	3	1	7		3	
150	1928	2	2	1	4	1			0	2			0	6	5			1		0		4		4	2	1	0	2	0	1	3		1	
125	1948	1	3	1	4	2			3	5			0	7	7							3					12	4		2	12		4	
150	1948	1	0	1	4	1			2	2			0	4	2							2					8	3		2	8		0	
125	1968	10	5		3	1	1		3	8	1		0	22	13	1		5				4		11	3	5	11	4	2		14	1	7	
150	1968	10	4		3	1	1		2	5	1		0	15	7	0		5				4		5	2	5	6	2	0		10	1	2	
125	1988	2	3		5	1		1	4	6	1		0	33	14			1				13		10	6	14	24	6			10		13	
150	1988	2	3		4	1		1	3	4	1		0	23	8			1				11		9	5	9	19	2			8		1	

fraction [µm]	Average depth [cm]	*Trifarina* sp. 1	*Uvigerina auberiana*	*Uvigerina peregrina*	*Uvigerina longimostrata*	*Valvulineria bradyana*	undefined	total	planktic	broken	splits
125	31	3	12	12		1	5	557	421	11	1/64+1/128
150	31	1	4	7		1	4	372	204	6	1/64+1/128
125	55	1	17	9		2	3	634	669	14	1/32
150	55	0	6	8		0	3	424	285	10	1/32
125	79		18	21		2	2	652	441	10	1/32
150	79		4	18		1	1	409	211	7	1/32
125	108		13	21		2		478	371	4	1/16+1/32
150	108		2	18		1		353	191	3	1/16+1/32
125	132		6	18		1		540	391	3	1/16
150	132		1	16		0		372	241	1	1/16
125	156		24	60		4	3	593	477	7	1/64
150	156		16	50		2	3	420	251	7	1/64
125	180		36	23			3	520	416	1	1/64
150	180		22	21			3	315	181	1	1/64
125	203		47	28		2	8	523	476	11	1/64
150	203		25	24		2	7	321	229	7	1/64
125	223	2	40	11		3		610	561	3	2/64
150	223	2	24	9		2		402	272	1	2/64
125	243		19	10		1		612	585	1	1/.32
150	243		9	7		1		379	241	1	1/32
125	263		44	10		2	1	604	449	2	1/32
150	263		27	7		1	1	377	205	2	1/32
125	283		20	28		2	2	532	364	2	2/32
150	283		16	22		1	2	379	207	0	2/32
125	303		17	49		2		422	272		1/32
150	303		9	39		2		300	153		1/32
125	323		15	38		1	1	433	214	1	1/16
150	323		11	31		0	1	313	117	0	1/16
125	348		7	34			1	413	254	3	1/16
150	348		5	31			1	314	156	0	1/16
125	1003					1	1	329	186		1
150	1003					1	1	201	128		1

continued

Average depth [cm]	*Trifarina* sp. 1	*Uvigerina auberiana*	*Uvigerina peregrina*	*Uvigerina longimostrata*	*Valvulineria bradyana*	undefined	total	planktic	broken	splits
373		2	18			1	369	175	1	1/32
373		2	14			1	297	143	1	1/32
393		24	46		1	1	458	411	2	1/16
393		13	35		0	1	336	268	0	1/16
413		9	61		3	4	510	1183	6	2/32
413		7	52		2	4	332	776	4	2/32
433			51		2	2	344	508		1/32
433			64		2	2	251	325		1/32
453		7	1		12	8	957	6620	4	1
453		4	1		8	8	537	5260	2	1
473		1	1		1	3	589	885	5	1
473		0	1		1	2	362	554	3	1
493		1	6		2	1	476	5622	3	1
493		1	4		2	1	299	4277	3	1
513		1	4		4		310	2356		1
513		1	3		4		224	2022		1
533	1	17	104		2	2	591	697	12	1/32
533	1	9	94		2	1	416	529	6	1/32
553		25	85		3	2	645	486	3	1/32
553		5	67		2	1	421	301	2	1/32
573		12	27		3		464	501	7	1/64
573		2	23		3		336	270	3	1/64
593	1	21	18				478	522	9	1/64+1/256
593	0	5	14				313	283	4	1/64+1/256
613		5	22	1	1	4	476	615	10	1/32
613		2	14	1	1	3	288	273	9	1/32
633		1	28		1		398	619		1/32
633		1	19		1		278	297		1/32
653		4	32		4		465	424	5	1/32
653		1	25		3		330	194	5	1/32
1303			41		3	3	578	226	1	1/8+1/16
1303			37		3	3	383	163	1	1/8+1/16

continued

Average depth [cm]	*Trifarina* sp. 1	*Uvigerina auberiana*	*Uvigerina peregrina*	*Uvigerina longimostrata*	*Valvulineria bradyana*	undefined	total	planktic	broken	splits
673		14	86		2	3	659	701	6	1/16
673		3	67		1	2	435	397	4	1/16
693					7	2	245	98		1
693					7	2	194	74		1
713					58		306	90		1
713					39		198	48		1
743			10		57		521	251		1
743			4		44		370	72		1
783			1		35	1	262	158		1
783			1		20	1	188	56		1
803					36	4	479	42		1
803					26	2	309	31		1
823					28		595	44		1
823					23		440	15		1
843					13		333	36		1
843					11		253	15		1
863					28	1	565	29		1
863					20	0	449	14		1
883		2	98		11	5	493	666		1/8
883		1	76		10	2	270	405		1/8
903			8		9		175	5682		1
903			4		4		95	4365		1
923							111	102		1
923							71	78		1
943					4		175	104		1
943					3		115	72		1
963							187	115		1
963							135	91		1
983					4		196	119		1
983					3		114	84		1
1703		75	34		2	6	463	159	7	1/16
1703		51	27		1	5	337	60	4	1/16

continued

125	1023			1	1	54	25		1
150	1023			1	1	36	23		1
125	1043	1	5	1		381	256		1
150	1043	0	0	1		229	168		1
125	1063					372	103		1
150	1063					286	83		1
125	1083					171	815		1
150	1083					105	560		1
125	1103	1	1			28	17		1
150	1103	0	0			10	11		1
125	1123	2				116	0		1
150	1123	2				25	0		1
125	1143	1				56	1		1
150	1143	0				15	0		1
125	1163	1				105	513		1
150	1163	0				38	408		1
125	1167			1	3	137	1358		1
150	1167			1	3	54	1188		1
125	1171			1		152	3523		1
150	1171			1		57	2991		1
125	1173				1	31	1517		1
150	1173				1	12	1128		1
125	1175					22	541		1
150	1175					8	405		1
125	1179			7	6	892	1763		1
150	1179			6	3	361	1572		1
125	1183			47	57	492	399	1	1/2
150	1183			42	49	347	295	1	1/2
125	1203			85	6	474	250		1/4+1/8
150	1203			81	5	337	117		1/4+1/8
125	1223			180	9	2 743	449	1	1/2
150	1223			136	6	0 507	338	0	1/2
125	1243	1	82		11	441	193		1/2
150	1243	1	64		7	315	99		1/2
125	1263			101	3	1 758	438		1/8
150	1263			85	3	0 514	281		1/8
125	1283			69	4	4 666	292		1/8
150	1283			58	4	4 477	214		1/8

continued

1323		56	4	2	480	221	3	1/8
1323		51	3	2	316	159	1	1/8
1343		67	14	3	737	239	2	1/4
1343		55	9	2	500	151	2	1/4
1363		32	6	2	647	282	5	2/8
1363		28	5	2	422	157	2	2/8
1383		58	7	3	547	60	1	1/8
1383		55	7	1	377	34	0	1/8
1403		65	1	2	641	131	7	2/16
1403		58	1	0	428	66	6	2/16
1423		44	11	11	569	200	2	1/4+1/8
1423		36	9	5	365	148	2	1/4+1/8
1443		64	4	3	543	100	4	1/4
1443		53	4	3	387	72	2	1/4
1463	3	11	3	4	560	153	6	2/8
1463	3	10	2	2	357	118	3	2/8
1483	6	19	3	3	378	143	3	1/16
1483	5	16	2	1	253	87	1	1/16
1503	29	54		1	772	480	12	1/32
1503	16	41		1	501	303	9	1/32
1523	28	30	3	11	475	240	11	1/64
1523	14	25	2	9	336	130	5	1/64
1543	47	17	4	16	617	151	12	2/128
1543	26	14	3	10	397	141	8	2/128
1563	47	5	3	7	392	207	10	1/64
1563	32	4	2	7	247	99	5	1/64
1583	61	22	1	8	791	452	14	1/32
1583	29	16	1	6	487	191	9	1/32
1603	56	21	6	6	527	224	12	1/32
1603	31	19	5	5	366	127	8	1/32
1623	12	15	1	4	405	140	5	1/16
1623	8	13	0	3	287	77	4	1/16
1643	14	58	12	4	732	273	3	1/8
1643	11	35	7	3	534	167	1	1/8
1663	7	48	9	3	448	126	7	1/16+1/32
1663	3	43	6	3	344	81	6	1/16+1/32
1683	21	43	4	3	470	94	9	1/16+1/32
1683	12	38	3	3	343	40	7	1/16+1/32

continued

1723	1	34	30		5	748	151	7	1/8
1723	0	17	24		4	601	85	2	1/8
1743		159	100	4	10	1000	672	15	1/32
1743		74	88	1	7	633	336	9	1/32
1763		90	145	8	4	1017	1030	22	1/8
1763		45	129	6	4	658	645	16	1/8
1783		4	13	1	3	505	1344	15	1/4+1/8
1783		2	11	0	3	285	750	12	1/4+1/8
1803			11	12	11	688	638	26	1/4
1803			10	8	8	380	342	18	1/4
1823		1	1	5	2	493	3329	15	1/2 + 1/4
1823		1	1	3	2	287	2173	9	1/2 + 1/4
1843		1	1	1	6	422	1681	13	1/4
1843		1	1	1	4	257	1107	8	1/4
1863			2	3	7	439	1704	5	1/2
1863			2	1	2	250	1071	0	1/2
1878		1	6	4	10	480	4297	9	2/4
1878		0	5	3	2	285	3396	5	2/4
1888			18	1	4	441	826	39	1
1888			17	0	4	255	448	24	1
1898			34	4	2	447	571	8	1/2
1898			23	0	1	272	310	7	1/2
1908			46	14	2	602	612	13	2/4
1908			38	10	0	322	388	12	2/4
1928	2	41	18	5	5	608		24	1/16+1/64
1928	0	15	11	3	2	346	206	15	1/16+1/64
1948		20		4	3	399	240	10	2/64
1948		8		2	3	242	125	6	2/64
1968		29	7	3	1	631	532	30	2/64
1968		7	5	0	1	375	292	16	2/64
1988		30	27	3	4	944	713	35	1/64
1988		15	19	0	2	575	393	25	1/64

Contribution to publications

Peer-reviewed publications

Impact of hydrological changes and vertical motions on Pleistocene marine environments of the eastern coast of the Island of Rhodes (Greece)

Field work: 0%

Laboratory pre-treatment: 50%

Foraminiferal data acquisition: 50%

Evaluation and interpretation: 80%

Publication authoring and composition: 80%

Humid climate phases on the Island of Rhodes (Greece) during the late Pliocene at times of sapropel formation

Field work: 0%

Laboratory pre-treatment: 0%

Foraminiferal data acquisition: 100%

Evaluation and interpretation: 80%

Publication authoring and composition: 80%

Prepared for publication in peer-reviewed journals

Tectonically induced vertical motions on the Island of Rhodes (Greece) during the Plio-Pleistocene

Field work: 50%

Laboratory pre-treatment: 80%

Foraminiferal data acquisition: 100%

Evaluation and interpretation: 80%

Publication authoring and composition: 90%

Declaration on oath

I hereby declare upon oath that I have written the present dissertation with the title: *Reconstruction of tectonically induced vertical motions and paleo-ecological evolution of the Island of Rhodes during the Plio-Pleistocene* independently and have not used further resources and aids than those stated. Passages that were taken literally or analogously from other publications are identified as such. I declare that this thesis has not been submitted to any other German or foreign examination board. I further declare that the submitted written version fully corresponds to the electronic version.

Eidesstattliche Versicherung

Hiermit erkläre ich an Eides statt, dass ich die vorliegende Dissertationsschrift mit dem Titel: *Reconstruction of tectonically induced vertical motions and paleo-ecological evolution of the Island of Rhodes during the Plio-Pleistocene* selbst verfasst und keine anderen als die angegebenen Quellen und Hilfsmittel benutzt habe. Stellen, welche wörtlich oder sinngemäß aus Veröffentlichungen entnommen wurden, sind als solche kenntlich gemacht. Ich versichere, dass ich die Dissertation nicht vorher im In- oder Ausland in einem anderen Prüfungsverfahren eingereicht habe. Ich versichere weiterhin, dass die eingereichte schriftliche und elektronische Fassung vollständig übereinstimmen.

Hamburg, 3 June 2024

D. Eichner

Daniela Eichner